FOURTH SEMIANNUAL TECHNICAL REPORT
1/1/72 - 6/30/72

Structural Effects on Electrical Properties
in Amorphous Semiconductors
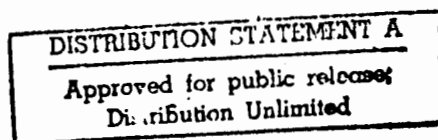
School of Engineering
Vanderbilt University
Nashville, Tennessee 37235

AD 748661

D D C
SEP 20 1972
RECEIVED
B

School of Engineering

VANDERBILT UNIVERSITY

Nashville, Tennessee 37203

247

DISCLAIMER NOTICE

THIS DOCUMENT IS THE BEST
QUALITY AVAILABLE.

COPY FURNISHED CONTAINED
A SIGNIFICANT NUMBER OF
PAGES WHICH DO NOT
REPRODUCE LEGIBLY.

FOURTH SEMIANNUAL TECHNICAL REPORT

1/1/72 - 6/30/72

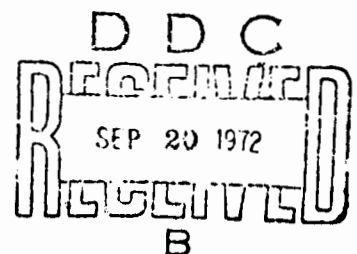Structural Effects on Electrical Properties
In Amorphous Semiconductors

School of Engineering
Vanderbilt University
Nashville, Tennessee 37235

D. L. Kinser, Co-Principal Investigator   615-322-2413

L. K. Wilson, Co-Principal Investigator   615-322-4742

Sponsored by

D D C

RECEIVED

SEP 20 1972

B
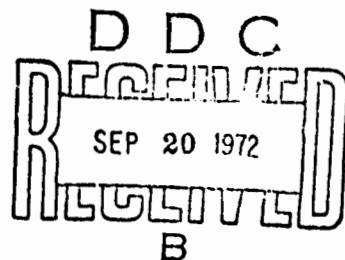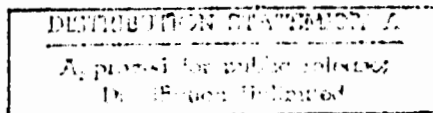
ABSTRACT

During this report period, work has continued on a survey of the structure, electrical and magnetic properties of transition metal oxide-phosphate glasses and glasses in the $As_2Te_3-As_2Se_3$ system which possess electrical or magnetic device potential. Results of magnetic and electrical observations in several transition metal-phosphate glasses have revealed a high degree of magnetic and structural order. The pronounced influence of glass-glass phase separation and compositional segregation has also been noted.

Examination of a series of $FeO-P_2O_5$ glasses has revealed a glass forming range which extends to 80 mole % FeO. Low temperature susceptibility and Mössbauer spectroscopy results on these glasses are reported herein. Low temperature susceptibility of the manganese, vanadium and iron glasses indicate that these glasses are all amorphous antiferromagnetic systems with a distinctive downward curvature of the reciprocal susceptibility versus temperature plot.

Detailed studies of the $As_2Te_3-As_2Se_3$ system has shown switching behavior which can be controlled with compositional variation. The compositional variation of the microstructure is noted in micrographs included in this report.

Statement of Problem

The device potential in amorphous semiconducting materials is a largely unexploited area, despite extensive research in this area. This is the result of a lack of systematic structure-property oriented research in these materials. A fundamental understanding of the structural features of this class of materials will allow rational interpretation and control of relationships between glass preparation variables and important electrical and magnetic properties.

Electronic conduction in amorphous solids has become the subject of interest to a number of theoreticians and has been reviewed by Mott[1],[2] Gubanov[3] and numerous others. Virtually all of these works have begun with an assumption that amorphous solids are uniformly random, even though they recognize glasses are generally heterogenous. These theoreticians have developed analytical descriptions of several systems which have been experimentally verified in some cases. Attempts to extend this approach to microscopically heterogenous systems have had notably little success. There remains a considerable body of experimental results, including Hall and Seebeck coefficients, which are not rationalized by present theory.

Pearson[4] has suggested that heterogenous structure in these materials may explain these anomalies if the separated phase is crystalline. It appears that heterogenous transport analysis similar to that of Volger[5] or Bube[6] is required to ascertain the transport behavior in each phase.

Another important anomaly between theory and observation concerns the theoretically predicted insensitivity of amorphous semiconductors to doping. Early experimental observations by Kolimets, et al.[7], conformed to the

theoretical predictions, but recent work by McKenzie[8] clearly conflicts
with the theory and the early work. It appears that the above anomalies
are the result of inadequate structural characterization, rather than
fundamental theoretical problems

Further evidence that structural heterogenities lie at the root of
these anomalies can be inferred from work by Kinser, et al.[9], in $K_2O-P_2O_5-V_2O_5$ glasses. This work has shown that marked changes in dielectric behavior
occur during thermal treatments customarily used to stress relieve glasses.
These changes have been shown to be the result of structural changes involving
precipitation of small amounts of crystals.

Wilson and Kinser[10] have observed similar, but somewhat more complex,
behavior in $FeO-P_2O_5$ glasses after thermal treatments corresponding to
annealing. Electron spin resonance (ESR) results have shown the onset of
structural changes during thermal treatment prior to their observation by
other commonly employed techniques[11,12].

It is thus apparent that homogenous glasses, semiconducting or otherwise,
are the exception rather than the rule.

General Methodology

The electrical and magnetic property changes accompanying structural
modifications during glass processing are of prime interest in the present
work. The above questions can only be answered with detailed structural
characterization of representative glasses from the oxide and chalcogenide
groups. The initial oxide glasses examined were the $FeO-P_2O_5$, $V_2O_5-P_2O_5$,
$CuO-P_2O_5$, $TiO_2-P_2O_5$ and $MnO-P_2O_5$ systems. The chalcogenide glasses are from
the $As_2Te_3-As_2Se_3$ system with Ag-As-S glasses in preliminary stages of study.

3.

ture over the range -80 to +100° C. These observations indicate that
the dielectric constant and loss tangent are essentially independent of
temperature over the frequency range 500 to 18,000 MHz. Far infrared
measurements conducted at 337 microns indicate further that the trans-
mission constant for the 80 arsenic tritelluride 20 arsenic trisenlenide
glass is independant of temperature over the range from 10 to 300°K. The
UHF dielectric properties are compositionally dependant but appear to be
temperature insensitive. These results are discussed in further detail
in the attached thesis of Mr. J. D. Pearson.

TRANSITION-METAL PHOSPHATE GLASSES

Manganese-phosphate glasses

Magnetic behavior of two-phase manganese phosphate glasses was studied
by means of variable temperature magnetic susceptibility and electron spin
resonance techniques. The high temperature magnetic susceptibility follows
a Curie-Weiss law. Figure one shows that the low temperature recipro-
cal susceptibility bends downward indicating considerable influence by para-
magnetic ions. The electrical conductivity of the glass is extremely low
suggesting that almost all of the manganese ions are in the divalent state.
It has been determined that the manganese divalent ions exist in the glass
in one of two distinct magnetic states-antiferromagnetically coupled pairs
in the manganese rich phase, or isolated ions in the phosphate rich phase.
Magnetic behavior was studied as a function of glass phase separation and
as a function of glass composition over the glass forming range. The
results were interpreted in terms of a model consisting of paired and isolated
divalent manganese ions. These results were reported at the May American
Ceramic Society meeting and the First International Amorphous Magnetism

Conference. A copy of the abstracts are appended.

Iron-phosphate glasses

A glass forming study of the iron oxide phosphate system has shown that the glass forming range extends to 80 mole percent ferric oxide when the glasses are melted in an oxidizing atmosphere and quenched in small quantities. Glasses above 80 mole percent ferric oxide spontaneously crystallized to alpha ferric oxide while intentionally devitrified glasses of lower iron content crystallized to iron phosphate. The magnetic susceptibility of glasses examined was described by a Curie-Weiss law over the range 100 to 525°K. Susceptibility studies indicated that the majority of the iron ions are antiferromagnetically ordered over the temperature and compositional ranges examined. Below 100°K, the reciprocal susceptibility bends downward and at approximately 10°K the susceptibility becomes constant as shown in Figure two. These results have been reported in two recent papers. Copies of the abstracts of these papers are appended.

The coordination and magnetic structure of the 55 mole percent ferric oxide glass containing various concentrations of ferrous and ferric ions were studied using Mössbauer effect spectroscopy at 77 and 300°K. Room temperature isomer shifts in the range 0.107-0.110 cm/sec and 0.023-0.047 cm/sec and quadrupole splittings of 0.217-0.265 cm/sec and 0.046-0.097 cm/sec for the ferrous and ferric ion, respectively, indicate tetrahedral coordination states.

Although no magnetic hyperfine structure was present at 300°K, splitting at 77°K was interpreted as evidence of either long relaxation times or limited magnetic ordering. Mössbauer spectroscopy of samples hear treated for intervals up to six hours at 600°C showed progressive precipitation of oxides in several crystalline phases. A detailed dis-

cussion of this work is presented in the attached thesis by Mr. H. L. Buchanan.

Vanadium-phosphate glasses

The electrical, thermal expansion and microstructural characteristics of vanadium phosphate glasses have been examined as a function of composition and oxidation state. These glasses exhibit liquid -- liquid immiscibility over a wide range of vanadium rich compositions at higher states of reduction. The presence of the miscibility is also reflected in the electrical and softening point observations. The compositional and oxidation dependance of the electrical properties and microstructure is best discussed in terms of a ternary diagram consisting of two different vanadium oxides and phosphorous pendoxide. When the system is analysed from this point of view the electrical conductivity behavior is seen to be clearly microstructurally dependant with a valley of minimum conductivity nearly corresponding to a spinodal composition across the ternary diagram. This work was presented at the May American Ceramic Society and is presently being prepared for publication.

CHALCOGENIDE GLASSES

The microstructure and DC and AC electrical properties of a series of arsenic triselenide-arsenic tritelluride glasses have been investigated. Electron microscopic observations indicate the presence of phase separation in these glasses. A metastable miscibility gap across the quasi-binary/ diagram is indicated. Variations in DC electrical properties may be due to structural changes, compositional changes or a combination of the two. Structural heterogenities due to phase separation appear to be responsible for Maxwell-Wagner-Sillars heterogeneous losses in these glasses. These results are discussed in further detail in the attached thesis of Mr. D. Hill and an abstract of a paper presented at the May American Ceramic Society meeting.

Extensive bulk switching studies have been performed on the same group of glasses mentioned above. Both threshold and memory switching have been observed in these glasses. Breakdown voltage was independant of sample thickness. Switching delay times at low over-voltages were in the hundreds of milliseconds range. Results of breakdown voltage vs temperature studies were computer fit to an approximate solution of the heat flow equation appropriate for the geometry, yielding experimental values of activation energy for conduction and thermal conductivity. These results clearly substantiate the thermal mechanism for electrical switching behavior in bulk samples of these glasses. A recently submitted paper detailing these experiments is attached with an abstract from a presentation at the May ceramic society meeting.

The UHF and microwave dielectric properties dielectric constant and loss tangent of these glasses have been examined as a function of tempera-

Structural characterization of these systems is being accomplished using electron microscopy, Guinier-DeWolff x-ray, electron spin resonance, spectroscopy, magnetic susceptibility, electron microprobe, dielectric relaxation, Mössbauer spectroscopy and differential thermal analysis techniques.

In conjunction with the structural tools, it is necessary that the conductivity, switching behavior and Seebeck coefficient by monitored to allow direct structure-property correlations.

RECOMMENDATIONS

1. Our principal recommendation is to continue the present program in its present direction to allow the synthesis of each of the results in a unified theory along the lines which are now clear in the chalcogenide system.

2. As in our previous recommendations, we continue to recommend the survey preparation of new glasses. We anticipate that the transition metal oxide-phosphate, silicate, borate and germanate survey presently in progress will be continued.

It is also anticipated that results on a new system Ag-As-S will be most helpful in developing switching models. A detailed ternary phase diagram was recently published (30) and our analyses should be simplified with this as a basis. It is further anticipated that Cu and Au substituted in the above system will be quite informative from an atomistic and microstructural model point of view.

3. The Mössbauer studies should be continued to examine 57 Fe and 127 Te in each of the systems presently under examination using other techniques. This will significantly aid in atomic structure model development in these systems as an addition to the present tools.

4. We recommend that the far infrared "conductivity loss spectra. This will allow the loss behavior to be explicitly attributed (31) to each mechanism thus reinforcing both atomic and microstructural analyses.

REFERENCES

1. N. F. Mott, "Conduction in Non-Crystalline Systems I & II," Phil. Mag. 17, 1259-1284 (1968)

2. N. F. Mott and E. A. Davis, Electronic Processes in Non-Crystalline Solids, Oxford, London, 1971.

3. A. Gubanov, "Quantum Theory of Amorphous Semiconductors," translated by A. Tybulewicz, Consultants Bureau, New York (1965)

4. A. D. Pearson, "The Hall Effect - Seebeck Effect Sign Anomaly in Semi-conducting Glasses," J. Electrochem. Soc. 111 (6) pp. 753-755, (1964).

5. J. Volger, "Note on Hall Potential Across an Inhomogeneous Conductor," Phys. Rev. 79, pp. 1023-1024 (1950).

6. R. Bube, "Interpretation of Hall and Photo-Hall Effects in Inhomogeneous Materials," Appl. Phys. Lett. 13 (4) pp. 136-139 (1968).

7. E. N. Kolimets, X. Mavrontova and T. F. Nazarova, "The Structure of Glass II, Consultants Bureau, New York (1960).

8. J. D. Mackenzie, "Electronic Conduction in Non-Crystalline Solids," J. Non-Crystalline Solids 2 pp. 16-26 1970).

9. D. L. Kinser, L. L. Hench and A. E. Clark, "Effect of Heterogenities on the Electrical Behavior of a Semiconducting Glass," to be submitted to Journal of Electrochemical Society.

10. L. K. Wilson and D. L. Kinser, "Structure Dependence of Electrical and Magnetic Properties of Iron-Phosphate Semiconductor Glasses," Proc. Region III IEEE Conference, November, 1969.

11. E. J. Friebele, L. K. Wilson, A. W. Dozier and D. L. Kinser, "Antiferro-magnetism in an Oxide Semiconducting Glass," Phys. Stat. Sol. (B) 45, 323 (1971).

12. E. J. Friebele, L. K. Wilson and D. L. Kinser, "Magnetic Behavior and Microstructure of Vanadium Phosphate Glass," J. American Ceramic Society, 55, 164 (1972).
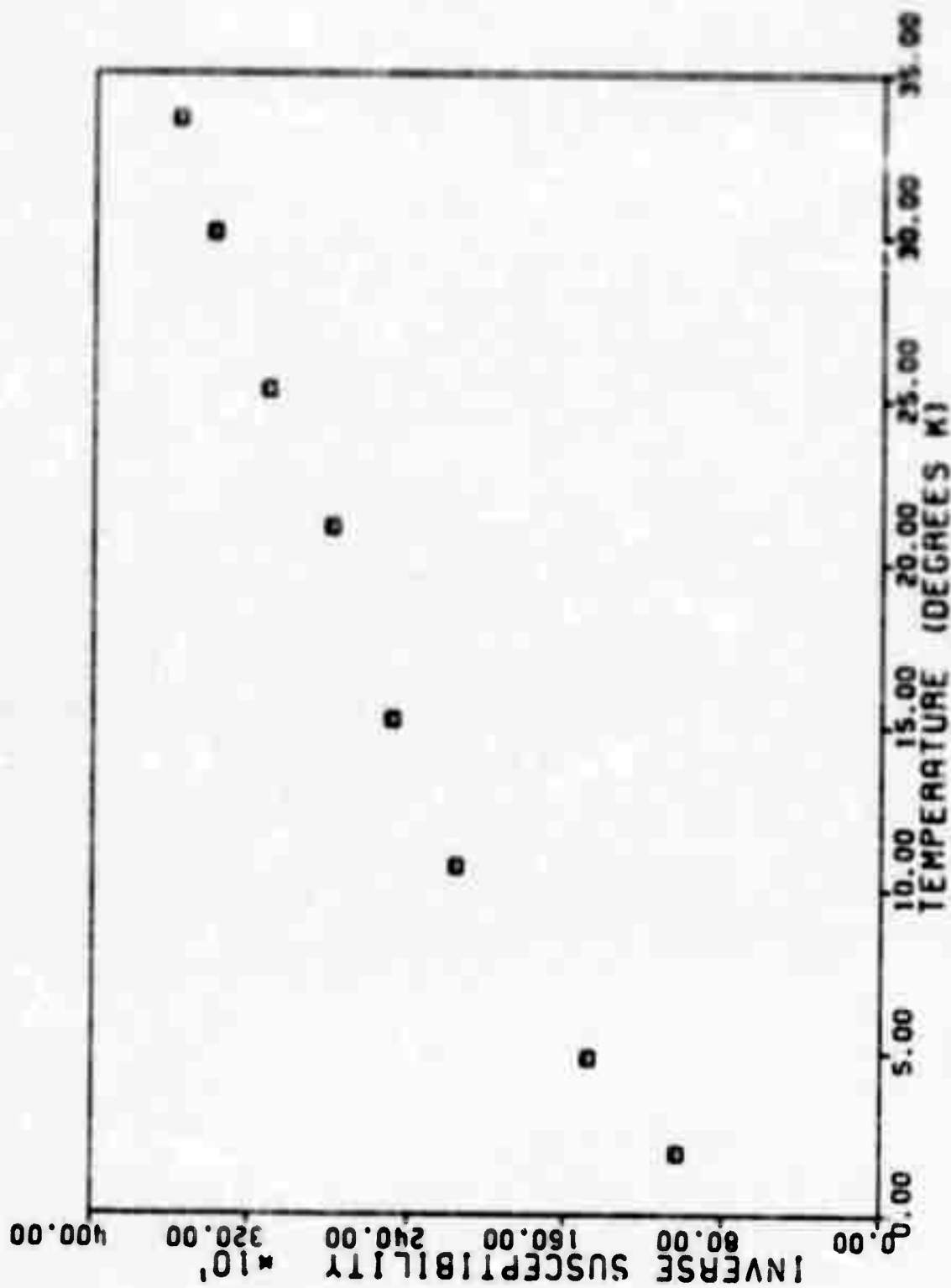
Fig. 1. Reciprocal Magnetic Susceptibility Versus Temperature for a 95 Mol % mol %
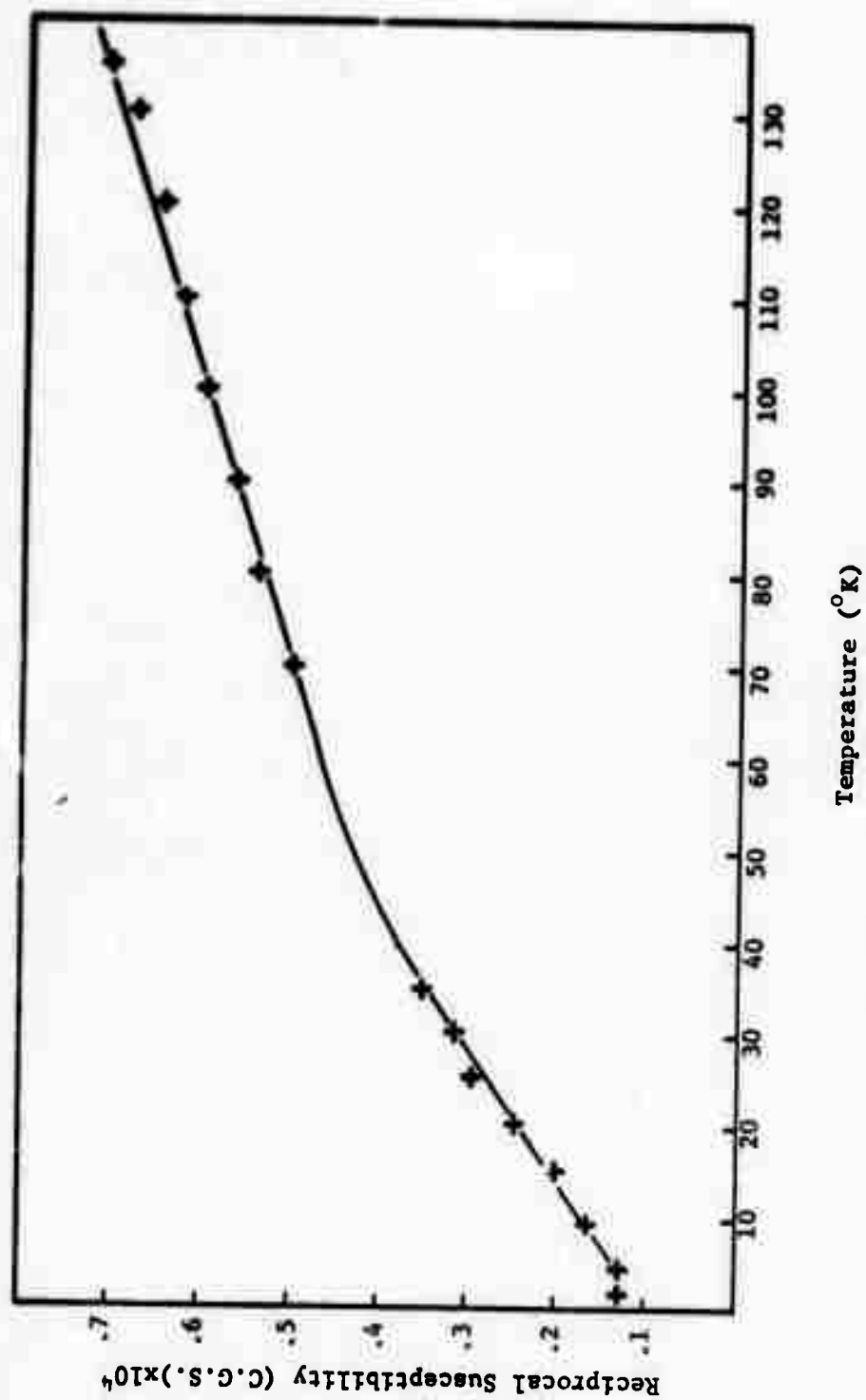Mol % P₂O₅ Glass

Fig. 2. (a) Reciprocal Magnetic Susceptibility Versus Temperature for a 55 Mol % Fe_2O 45 Mol % P_2O_5 Glass
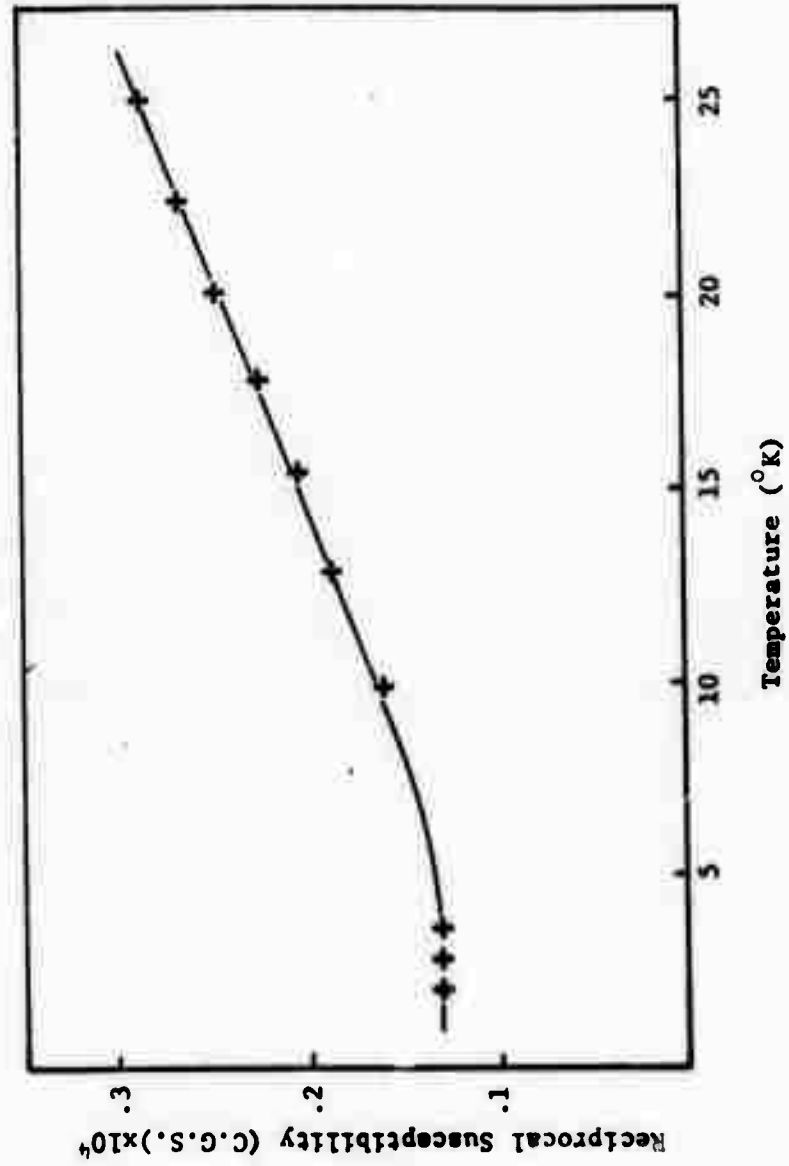
Fig. 2. (b) Low Temperature Behavior of the Magnetic Susceptibility
of 55 Mol % F_eO 45 Mol % P_2O_5 Glass

2:40–2:55 p.m.

3-G-72. Studies of the Fe₂O₃-P₂O₅ Glass System

J. H. DAYANI,* D. L. KINSER and L. K. WILSON, Vanderbilt University, Nashville, Tenn.

A glass forming study of the Fe_2O_3-P_2O_5 system has shown that the glass forming range extends up to 80 mole% Fe_2O_3 when the glasses are melted in an oxidizing atmosphere. All glasses were melted in air using a platinum ribbon furnace and rapidly quenched. Glasses above 80 mole% Fe_2O_3 spontaneously crystallized to α-Fe_2O_3 while intentionally devitrified glasses of composition below 80% crystallized to $FePO_4$. The magnetic susceptibility of all glasses examined was described by a Curie-Weiss law over the range 100° to 525°K. Susceptibility studies indicated that the majority of the iron ions are antiferromagnetically ordered over the temperature and compositional range examined. (Research sponsored by the U.S. Army Research Office-Durham).

2:20 - 2:35 p.m.

11-G-72. Magnetic and Structural Properties of Manganese Phosphate Glass

E. J. FRIEBELE,* D. L. KINSER and L. K. WILSON, Vanderbilt University, Nashville, Tenn.

Magnetic behavior of two-phase manganese phosphate glasses was studied by means of variable temperature magnetic susceptibility and electron spin resonance (ESR) techniques. The high temperature susceptibility follows a Curie-Weiss law. There is a magnetic transition in the glass at about 150°K, which is apparent both in the susceptibility and ESR data. The electrical conductivity of the glass is extremely low, indicating that almost all of the manganese ions are in the divalent state. It has been determined that the Mn^{2+} ions exist in the glass in one of two distinct magnetic states—antiferromagnetically coupled pairs in the manganese-rich phase, or isolated ions in the phosphate-rich phase. Magnetic behavior was studied as a function of liquid-liquid separation and as a function of glass composition over the glass forming region. The results were interpreted in terms of a model consisting of paired and isolated Mn^{2+} ions. (Research sponsored by the U.S. Army Research Office-Durham.)

10:15–10:30 a.m.

4-SS-72. Thermal and Compositional Dependence of Electrical Switching in As₂Te₃-As₂Se₃ Glasses

H. R. SANDERS,* L. K. WILSON, D. J. HILL and D. L. KINSER, Vanderbilt University, Nashville, Tenn.

Extensive bulk switching studies have been performed on the $xAs_2Te_3(1-x)As_2Se_3$ system as a function of composition. Both threshold and memory switching have been observed in all samples. Breakdown voltage and switching stability increase with increasing Se content. Breakdown voltage was essentially independent of sample thickness. Switching delay times at low overvoltage were in the hundreds of milliseconds range. Results of breakdown voltage vs temperature studies were computer fit to an approximate solution of the heat flow equation, yielding experimental values of activation energy for conduction. These results clearly substantiate the thermal mechanisms for electrical switching behavior in bulk samples of these glasses.

11:40–11:55 a.m.

8-SS-72. Microstructure Effects on Physical Properties in V₂O₅-P₂O₅ Glasses

A. W. DOZIER,* E. J. FRIEBELE, L. K. WILSON and D. L. KINSER, Vanderbilt University, Nashville, Tenn.

The electrical, thermal expansion, and microstructural characteristics of bulk V_2O_5-P_2O_5 glasses have been examined as a function of composition. These glasses exhibit liquid-liquid immiscibility over a wide range of V_2O_5 rich compositions. The presence of the miscibility gap is also reflected in the electrical and softening point observations. The effect of this structural segregation on the dc resistivity at constant temperature as a function of V^{4+}/V^{5+} in the glass is discussed. (Research sponsored by the U.S. Army Research Office-Durham.)

9:55–10:10 a.m.

3-SS-72. Microstructural and Electrical Properties of As₂Te₃-As₂Se₃ Glasses

D. J. HILL,* L. K. WILSON, H. R. SANDERS and D. L. KINSER, Vanderbilt University, Nashville, Tenn.

Electron microscopic, dc and ac conductivity observations have been conducted on a series of As_2Te_3-As_2Se_3 glasses. These results indicate the presence of extensive phase separation in all glasses examined, including the pure As_2Se_3 glass. The electrical properties of those glasses with microstructures which are sensitive to thermal history are different from previously published results. The present results indicate a clear need for thermal history characterization in physical property measurements in this glass system.

ABSTRACT

Submitted to

International Symposium on Amorphous Magnetism

ANTIFERROMAGNETISM IN THE VANADIUM, MANGANESE

AND IRON PHOSPHATE GLASS SYSTEMS

by

L. K. Wilson, E. J. Friebele and D. L. Kinser
Vanderbilt University
Nashville, Tennessee 37235

Variable temperature magnetic susceptibility and magnetic resonance measurements have been made on a series of concentrated vanadium, manganese and iron phosphate glasses. The high temperature magnetic susceptibility of all glasses studied obeyed a Curie-Weiss law with an antiferromagnetic Curie temperature. At low temperatures, the magnetic susceptibility data have been interpreted in terms of recent theoretical models of amorphous antiferromagnetism (1,2).

Measurements of magnetic resonance line intensity and line-width at 9.0 GHz as a function of temperature have shown the existence of extensive antiferromagnetic coupling between the transition metal ions (3,4). The resonance measurements have been shown to be sensitive to microstructural inhomogeneities (liquid-liquid phase separation and devitrification) in the glasses. Weak transitions at temperatures corresponding to the Neel temperatures of crystalline transition metal oxides have been observed.

1. A. W. Simpson, Phys. Stat. Sol. 40, 207 (1970)

2. S. Kobe and K. Handrich, Phys. Stat. Sol. 42, K69 (1970).

3. E. J. Friebele, L. K. Wilson, A. W. Dozier and D. L. Kinser, Phys. Stat. Sol.(b) 45, 323 (1971).

4. E. J. Friebele, L. K. Wilson and D. L. Kinser, J. Am. Cer. Soc. 55, 164 (1972).

ELECTRICAL SWITCHING PHENOMENA IN THE
As$_2$Te$_3$-As$_2$Se$_3$ GLASS SYSTEM

M. R. Sanders, Jr., L. K. Wilson and D. L. Kinser
School of Engineering
Vanderbilt University
Nashville, Tennessee
May, 1972

ELECTRICAL SWITCHING PHENOMENA IN THE
As_2Te_3-As_2Se_3 GLASS SYSTEM

This paper reports the results of electrical switching studies of a series of As_2Te_3-As_2Se_3 glasses. Kolomeits and Nagarova (1) and Rolios (2), and more recently Hill (3), have ⸺ reported electrical conductivity studies of this system. Kinser, et al. (4) have also reported electrical property studies in connection with a study of the microstructure of this system.

All of the glasses studied exhibit bulk threshold and memory switching with the critical voltage for switching (breakdown voltage V_{BR}) increasing with As_2Se_3 content. The switching process observed in these glasses has been found to occur by a thermal mechanism in agreement with studies previously reported by Warren (5) for a single composition of amorphous As_2Se_2Te and Tanaka and his co-workers (6-10) in the amorphous As-Te-Ge system. The thermal dependency of the breakdown voltage has been fitted to a thermal model in agreement with the theoretical work of Boer and Ovshinsky (11) and Sheng and Westgate (12). In these papers, an approximate solution of the heat flow equation is used to derive an equation for the temperature dependence of breakdown voltage:

$$V_{BR}(T) \exp\left[V_{BR}(T)/2V_o\right] = \left[\frac{2\kappa}{\sigma_o \Delta E}\right]^{1/2} T \exp\left[\frac{\Delta E}{2kT}\right] \tag{1}$$

where

κ = thermal conductivity

ΔE = activation energy of conduction and

$$\sigma = \sigma_o \exp\left[-\frac{\Delta E}{kT} + \frac{V}{V_o}\right]$$

where $\exp\left(\frac{V}{V_o}\right)$ expresses the field dependency of conductivity. The effect of the field dependent term is negligable for bulk samples although it becomes increasingly

16

more significant as the thickness of the sample decreases. Although the results of these studies agreed well in all cases with a thermal description, no attempt will be made to generalize these results to thin films, for which there is still controversy about the nature of the breakdown mechanism. Stocker (13) and Warren (14) have argued that the thermal description still applies for thin films, while others such as Boer and Ovshinsky (11) maintain that at least in some cases, other effects are predominant.

Experimental

All glasses examined in this study were prepared by fusing the appropriate materials in evacuated Vycor ampoules at 800°C in a rocking furnance. After heating for one hour, the ampoules were rapidly quenched in water. Reagent grade raw materials were employed after an initial study revealed essentially no impurity effects between reagent materials and 99.9999% materials. All samples were formed into small platelets by briefly remelting on a graphite plate and quenching with a second plate. Samples for all observations had a thickness of between 0.5 and 1.5 mm. Measurements were made on a sample by sandwiching it between brass electrodes in a holding device designed to maintain constant contact pressure. The samples studied covered the compositional range of 80:20 ($80As_2Te_3$: $20As_2Se_3$) to 40:60.

Variable temperature studies were performed by placing the sample holder in an thermostatically controlled oven. The sample temperature was monitored by a thermocouple mounted in one of the brass electrodes. Initial measurements were made as a function of heating rate in order to determine a sufficiently slow rate to insure thermal equilibrium. For temperature increments on the order of 10°C, it was found that a 20 minute interval between measurements was sufficient. Studies were performed over the range of 25°C to 140°C.

The I-V characteristics of the 80:20 and the 70:30 glass were obtained by using a closed-loop voltage-controlled constant current source whose DC output impedance was in excess of 15 megohms. The high source impedance was necessary in order to observe the

negative resistance region of the materials and was also useful in eliminating the tendency of some samples to switch at high rates between states of different current. The stability of the closed-loop system eliminated thermal hystersis caused by heating of the output transistors. The circuit was designed to provide output currents of 0-100 ma over a dynamic output voltage range of 0-250 V. The 60:40, 50:50 and 40:60 glasses had breakdown voltages too high to be measured with the constant-current source; their I-V characteristics were determined by connecting them to a manually controlled 0-1500 V power supply through a large series resistance. It was found experimentally that sweep rates of less than 10/sec were necessary in order to obtain an accurate representation of the I-V characteristics. A sweep cycle time on the order of 1 sec. was used for most of the measurements, with the results being displayed on a storage oscilloscope.

Switching delay time measurements were performed only on the 80:20 and 70:30 glasses because of the inordinately high voltages required to study the other samples. The delay time was measured by applying a voltage pulse across the sample through a 100K series resistor. The applied voltage and the voltage across the sample were simultaneously observed on a storage oscilloscope.

Results

The I-V characteristics shown in Fig. 1, are typical of all the samples studied. Virgin samples were initially found in the high resistance or "off" state as shown in Fig. 1a. Measured values of room temperature conductivity for this off state varied from 11×10^{-6} mho/cm for the 80:20 glass to 0.05×10^{-6} mho/cm for the 40:60 glass. If the samples were subjected to breakdown, the threshold switching behavior shown in Fig. 1b results, and the sample would generally cycle in this manner indefinitely. However, a sufficiently slow return sweep rate would lead to memory type behavior as shown in Fig. 1c and 1d, for which the sample remained in the low resistance state as current was reduced to zero. The sample remained in the low resistance state until

18

pulsed by a high current (20-50 ma) of several milliseconds duration.

Initial efforts to determine the breakdown voltages of the 80:20 glasses were unsuccessful. A given sample would exhibit breakdown voltages over a range of 5 to 200 volts, with a more or less random distribution within this range. To aid in the analysis of this inconsistency, a computer program was written which would plot a histogram of the number of breakdowns versus voltage and which was also able to produce the histogram with various degrees of statistical smoothing. The mean value and standard deviation of the original and smoothed histograms were calculated and were used as a measure of the validity of the smoothing technique. The program also calculated the mean and the standard deviation of the initial data set. The standard deviation of the data was taken as a measure of the data taking technique, with the assumption that a valid set of data should have a small standard deviation. The final program function was to produce a heavily smoothed time plot of the data. A highly erratic time plot was taken as an indication of poor data. Use of the program in conjunction with various data taking techniques produced a steady improvement in data until the point was reached where a consistent characterization of the device could be obtained. The improvement is evident in the fact that the initial data set has a mean of 48 volts with a standard deviation of 36.4 volts while a data set taken using improved techniques yielded a mean value of 100 volts with a standard deviation of 5.6. The breakdown voltage was found to be virtually independent of the sample thickness.

Fig. 2 shows the results of measurements of breakdown voltage versus composition. Although there is some scatter in breakdown voltages of different samples with the same composition, the compositional trend is obvious. It was also found that increasing Se content made the glass a more stable switch at the expense of much higher breakdown voltages. The 50-50 glass, for example, exhibited a very stable breakdown voltage over many breakdown cycles so long as the sample was not subjected to extremely high on-state currents.

Fig. 3 shows the results of switching delay time measurements on a 70:30 sample.

19

Two interesting results are apparent from this measurement. First, the threshold switching voltage for the pulsed case is nearly a factor of two higher than it is for the DC or steady state switching. Second, it is found that for values of applied voltage slightly greater than the threshold value, the switching delay time is extremely slow, ranging from 600 ms for the 70:30 sample to several seconds for some of the 80:20 glasses. The delay time was found to decrease sharply with increasing applied voltage, reaching the low millisecond region with over-voltages of several hundred volts. The delay time was also found to decrease when a given sample was subjected to repeated breakdown at the same applied voltage. Fig. 4 shows the results of the delay-time versus applied voltage measurements on the 80:20 glass. Curve 1 is for the virgin sample, which exhibits a very long initial switching delay time which then decreases sharply with increasing voltage. Above around 550 volts, the rate of decrease levels off. Curves 2 and 3 are subsequent runs taken on the same sample. It is seen that the behavior for low voltages is quite different for the three curves, but that at higher voltages, all the curves converge.

Fig. 5 shows the variation in I-V characteristics of a 50-50 sample as a function of temperature. The oscillogram 5(a), taken at room temperature, indicates a very high off state resistance and no breakdown with an applied voltage in excess of 1000 volts. Curves 5(b), 5(c) and 5(d), taken at 65°C, 102°C and 123°C, respectively, show successive decreases in the off-state resistance and breakdown voltage as the temperature rises. In Curve 5(e), taken at 140°C, the off-state and on-state resistance are approaching one another in magnitude and the breakdown voltage has fallen to below 100 volts. Finally, as the temperature is increased further, the sample crystallizes and switching ceases. The resistance of the crystalline state, shown in Curve 5(f) is extremely low. After crystallization, the sample remains in the low resistance state as the temperature decreases.

Fig. 6 shows a plot of breakdown voltage versus temperature for the 50-50 glass. If the field dependent term in Eq. 1 is neglected, a valid approximation for bulk samples, the equation can be restated as follows:

$$V_{BR} = \pi \left[\frac{k\kappa}{\sigma_o \Delta E} \right]^{1/2} T \exp\left(\Delta E / 2kT\right) \tag{2}$$

A nonlinear least-square fit computer program has been written to fit the V_{BR} versus T results to Eq. 2. ΔE and κ/σ_o were taken as the variable parameters of the fitting process. A very good fit to the above equation was obtained for all compositions. Table I shows the results of a least square fit of data from a 70:30 sample. V_{BR}(DATA) is the measured value of the breakdown voltage, V(FUNCTION) is the value predicted by the fitted equation, and the error is the difference between the two. It can be seen that the error is in all cases within the range of experimental error. Table II shows the values of ΔE and κ/σ_o obtained over the compositional range of 80:20 to 50:50.

TABLE I

Least Squares Fit of the V_{BR} Versus T Data for a 70-30 Glass
with $\kappa/\sigma_o = 3.156 \times 10^{-5}$ and $\Delta E = 0.40$ ev

Temperature	V(Function)	V(Data)	Error
295	188.7	190.0	1.3
308	141.7	137.0	-4.7
317	117.9	120.0	2.1
326	99.2	100.0	0.8
338	80.1	82.0	1.9
348	67.8	70.0	2.2
357	58.8	58.0	-0.8
364	53.0	50.0	-3.0

TABLE II

Activation Energy and κ/σ_o Ratio for a Series of

As_2Te_3-As_2Se_3 Compositions

Composition	ΔE(ev.)	$\kappa/\sigma_o (10^{-6})$
50-50	0.46	84.5
60-40	0.42	102.9
70-30	0.41	27.2
80-20	0.47	2.18

Discussion

As_2Se_3 is a glassy material and has a low tendency to crystallize when cooled from the liquid phase. Samples of As_2Se_3 have been subjected to voltages as high as 1.5 kilivolts without breakdown. Pure As_2Te_3, on the other hand, normally does not form a glass, and accordingly has a high conductivity. The system x $As_2Te_3:(1-x)As_2Se_3$ can be prepared in a glassy state, the presence of the selenium being sufficient to stabilize the glass for $x \geq 0.2$ (15). However, all evidence indicates that the As_2Se_3 is not actively involved in the switching process. Rather, by forming a glass with a high As_2Te_3 content, the As_2Se_3 sets up the conditions for the switching process to occur.

The initial breakdown mechanism is unquestionably thermal in nature. This fact is subtantiated here by the independence of breakdown voltage on thickness, the good agreement of the temperature data with Eq. 2, and, in a qualitative way, by the switching delay time behavior, which agrees well with that predicted by Warren (5) on the basis of his solution of the heat flow equation. When a voltage is first applied to a sample in the off state, current tends to become concentrated in small or filamentary paths through the material, probably because of local inhomogenities. As the voltage is increased, the power dissipation causes a localized heat build-up. Because of the low thermal conductivity of the glass, a point is soon reached for which the heat generated is greater than that which can be conducted away by the adjacent cooler material and thermal runaway occurs. This instability accounts for the negative resistance portion of the I-V characteristic. Once runaway occurs, the temperature of the conducting path increases rapidly, and if the current is allowed to increase sufficiently, phase separation and crystallization followed by liquification in the localized region will occur. As the current is reduced, the liquid material may return either to the glassy or crystalline state, depending on the rate of cooling. This statement is demonstrated by the DTA data obtained for the $As_2Te_3:As_2Se_3$ system. A typical thermogram

shows an exothermic reaction at some temperature T_1 which represents crystallization of the material and an endothermic reaction at some higher temperature T_2 which is the melting point. As the heating ratio increases, T_1 approaches T_2, and for very rapid heating rates, such as occurs in switching, the exothermic-crystallization reaction may not occur at all. However, the cooling rate in switching is controlled by the external sweep circuit and can be made as slow as desired. DTA observations indicate that upon cooling from the liquid state the material will become glassy if cooled rapidly, crystalline if cooled slowly. Thus, a rapid cooling or fast return sweep rate leads to threshold type switching, while a slow return sweep rate leads to memory behavior, where the conducting path is left in the crystalline conducting state.

The lack of consistency in the delay-time measurements of the 80:20 and 70:30 glasses prevented any quantative analysis of this data. The inconsistency appears to result from areas of remanent crystallization brought about by the relatively high currents associated with the pulsed switching. To a lesser degree, a similar problem had been observed in steady state switching of the 80:20 and 70:30 glasses and is not surprising in view of the relatively unstable nature of these glasses. The 60:40 and 50:50 glasses, which were considerably more stable under DC switching, would probably yield useful delay-time data, but unfortunately these measurements are unfeasible because of the extremely high voltages required.

Conclusions

1. Both threshold and memory switching are exhibited by the $As_2Te_3:As_2Se_3$ glass system.

2. Switching stability improves with increasing Se content at the expense of higher V_{BR}.

3. The switching mechanism in bulk $As_2Te_3:As_2Se_3$ glasses is thermal in nature.
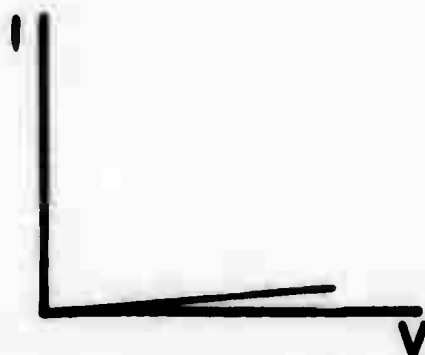
Acknowledgements

References

1. B. T. Kolomiets, T. N. Lamontova and T. F. Nazarova, "The Structure of Glass," Translated from Russian by E. B. Uvarov, Consultants Bureau, pp. 418-19, New York, 1960.

2. M. N. Roilos, "Conductivity and Hall Effect in Vitreous $As_2(se, Te)_3$," J. Non-Crystalline Solids, 6, 5-12 (1971).

3. D. J. Hill, "An Investigation of the Structural and Electrical Property Correlations in the Arsenic Triselenide-Arsenic Tritelluride Glass System," M.S. Thesis, Vanderbilt University, Nashville, Tennessee, 1972.

4. D. L. Kinser, L. K. Wilson H. R. Sanders and D. J. Hill, "Electrical, Thermal, and Structural Properties of As_2Te_3-As_2Se_3 Glasses," J. of Non-Crystalline Solids, to be published.

5. A. C. Warren, "Thermal Switching in Semiconducting Glasses," J. of Non-Crystalline Solids, 4, 613-16 (1970).

6. Kazunobu Tanaka, Sigeru Iizima, Michio Sugi, Yasumesa Okada and Makoto Kikuchi, "Thermal Effect on Switching Phenomenon in Chalcogenide Amorphous Semiconductors," Solid State Communications, 8, 387-9 (1970).

7. Sigeru Iizima, Michio Sugi, Makoto Kikuchi and K. Tanaka, "Electrical and Thermal Properties of Semiconducting Glasses As-Te-Ge," Solid State Communications, 8, 153-5 (1970).

8. Kazunobu Tanaka, Sigeru Iizima, Michio Sugi, Yasumasa Okada and Makoto Kikuchi, "Electrical and Calorimetrical Analysis of Memory Phenomenon in Amorphous Semiconductors," Solid State Communications, 8, 1333-36 (1970).

9. S. Iizima, M. Sugi, M. Kikuchi and K. Tanaka, "Effect of Stabilization on Electrical Conductivity in Chalcogenide Glass," Solid State Communications, 8, 1621-23 (1970).

10. Yasumasa Okada, Sigeru Iizima, Michio Sugi and Makoto Kikuchi, "Compositions and Structure of the Lock-on Filaments in As-Te-Ge Glasses," Journal of Applied Physics, 41 (13) 5341-44 (1970).

11. K. W. Boer and S. R. Ovshinsky, "Electrothermal Initiation of an Electronic Switching Mechanism in Semiconducting Glasses," Journal of Applied Physics, 41 (6) 2675-80 (1970).

12. W. W. Sheng and C. R. Westgate, "On the Preswitching Phenomena in Semiconducting Glasses," Solid State Communications, 9, 387-391 (1971).
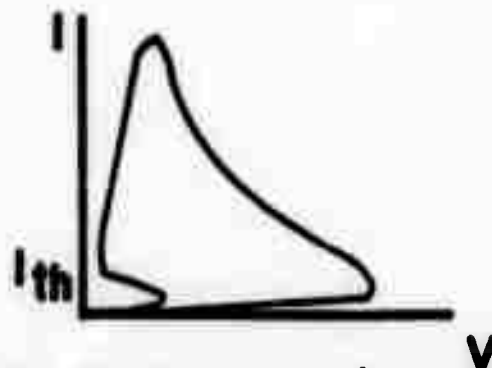
13. H. J. Stocker, "Bulk and Thin Film Switching and Memory Effects in Semiconducting Chalcogenide Glasses," Applied Physics Letters, 15 (2) 55-57 (1969).

14. A. C. Warren and J. C. Male, "Field Enhanced Conductivity Effects in Thin Chalcogenide-Glass Switches," Electronics Letters, 6 (18) (1970).

15. N. F. Mott and E. A. Davis, "Electronic Processes in Non-crystalline Materials," p. 561, Clarendon Press, Oxford, 1971.
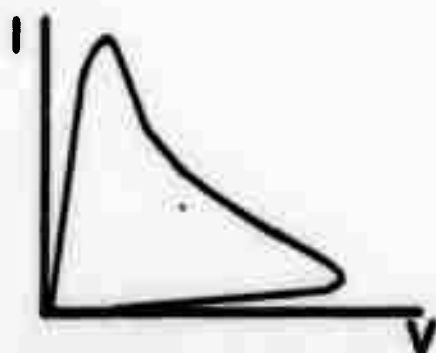
List of Figures

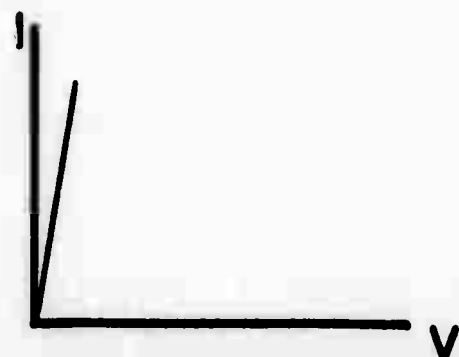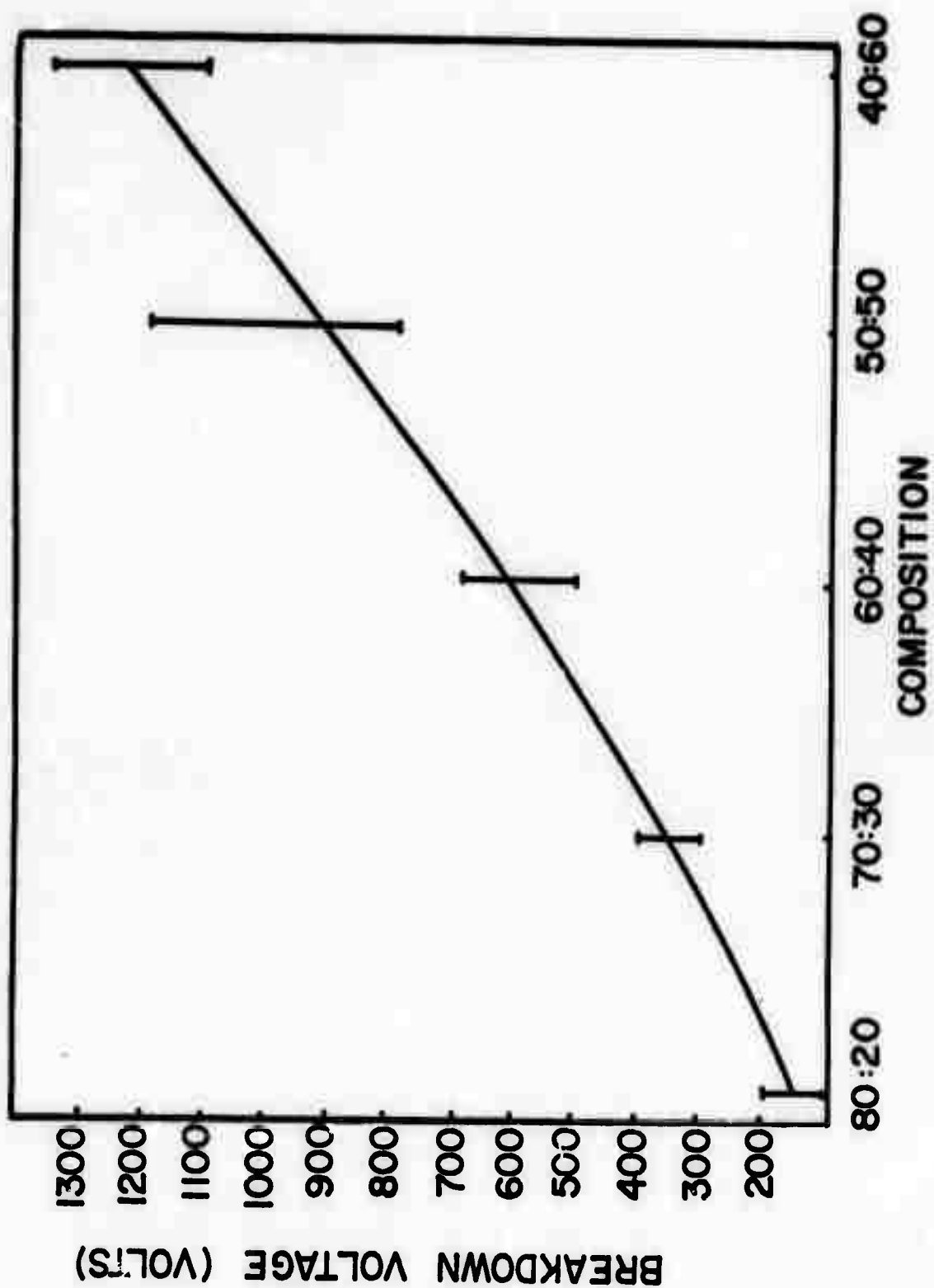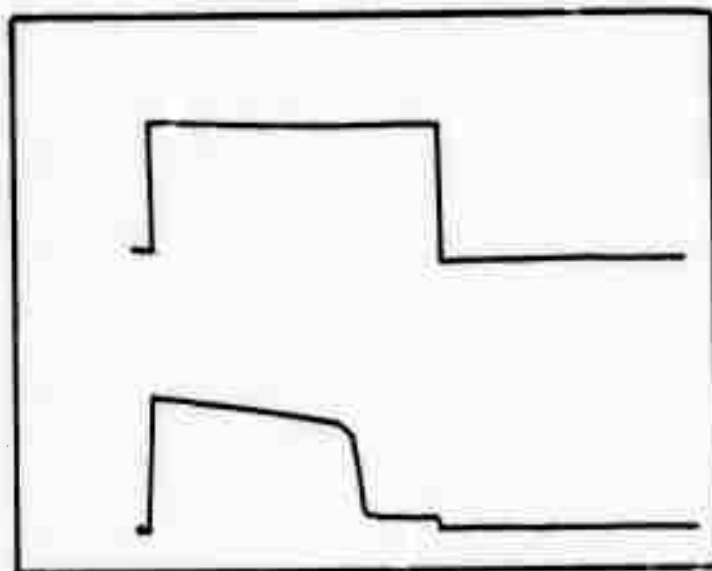A. HIGH RESISTANCE STATE

B. THRESHOLD SWITCHING

C. MEMORY CYCLE

D. LOW RESISTANCE STATE

FIG. 1
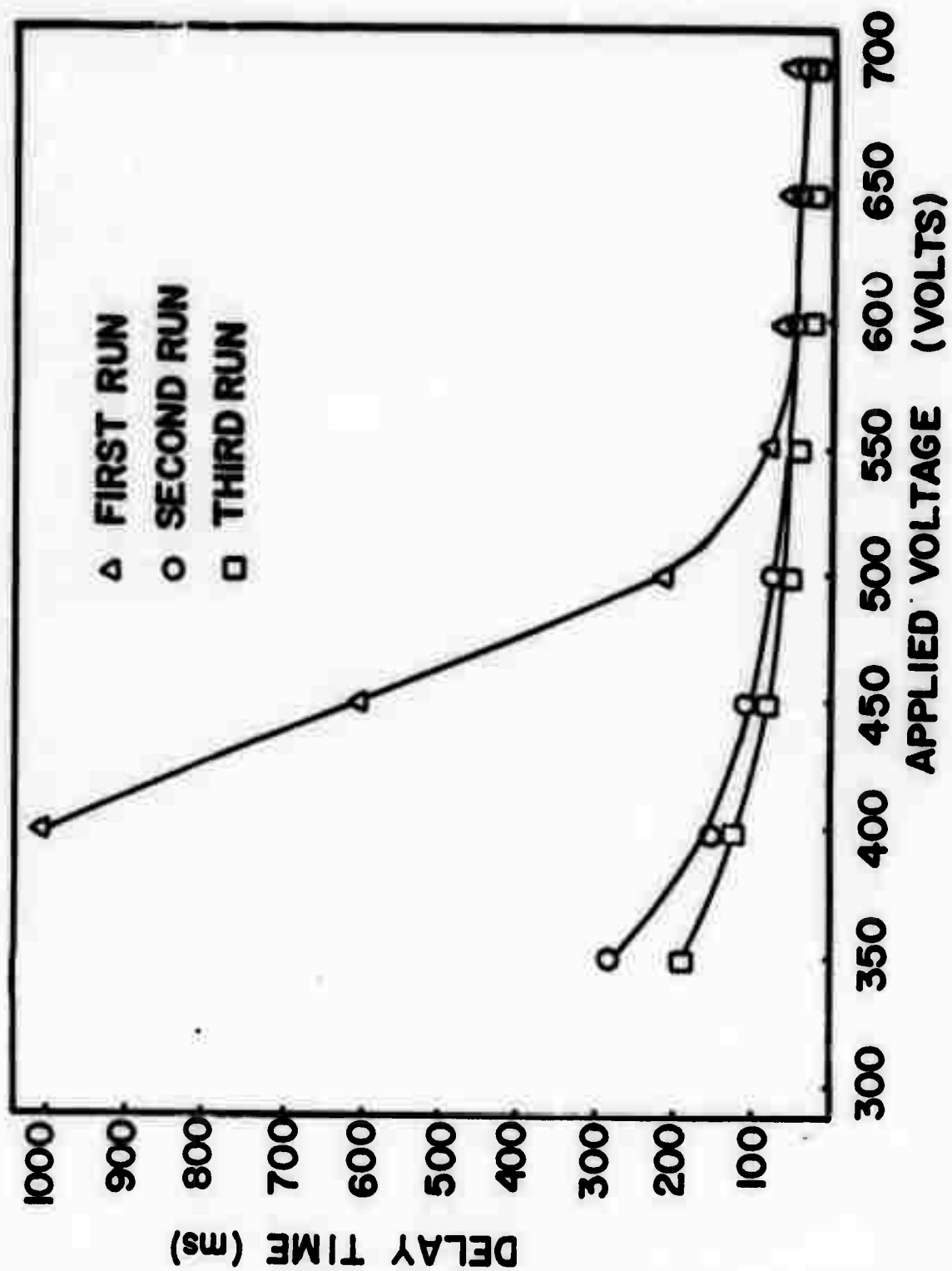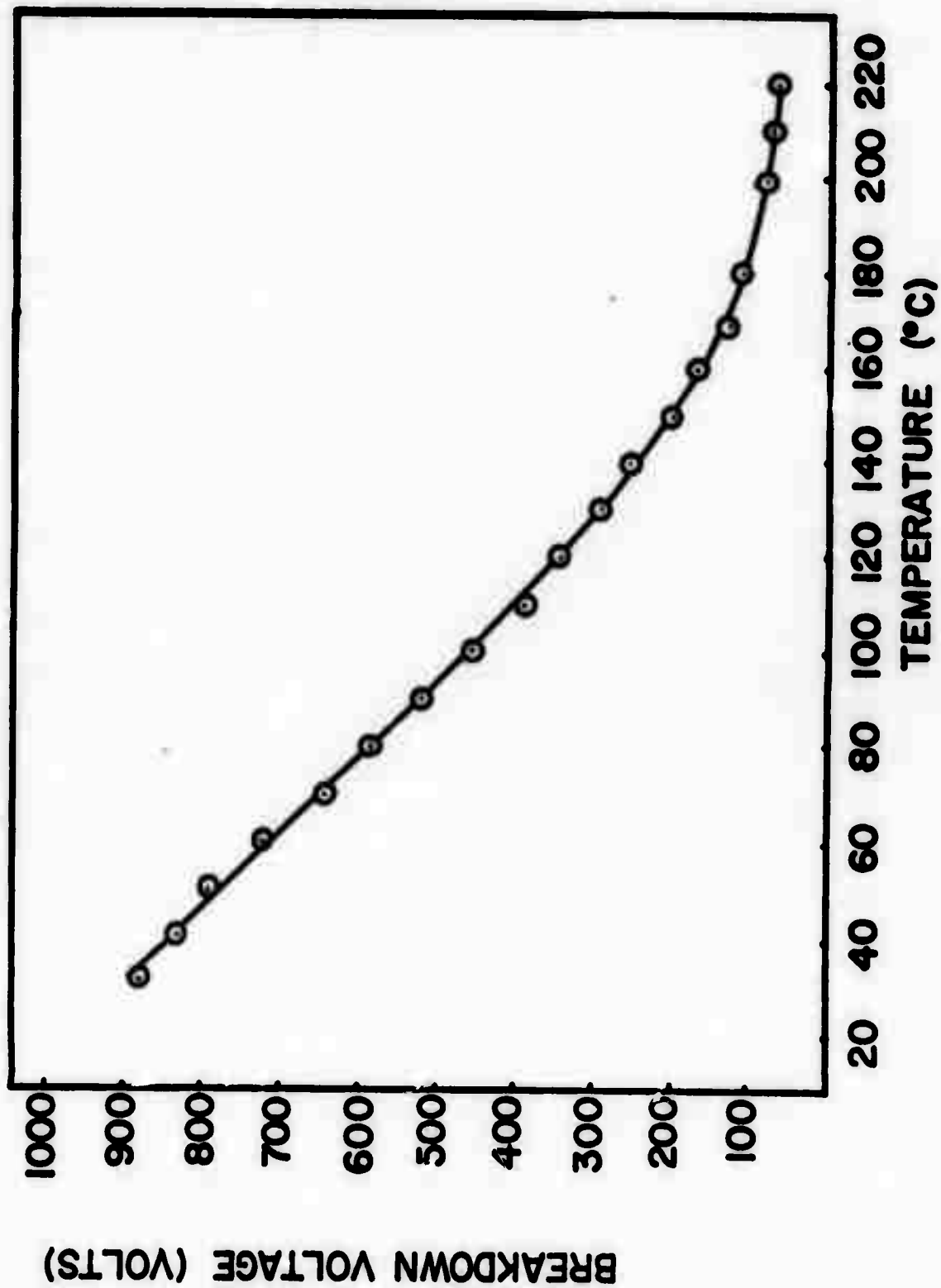
Fig. 2

29

30

F_ig. 3

FIG. 4

31

FIG. 5

32

A B C D E F

FIG. 6

33
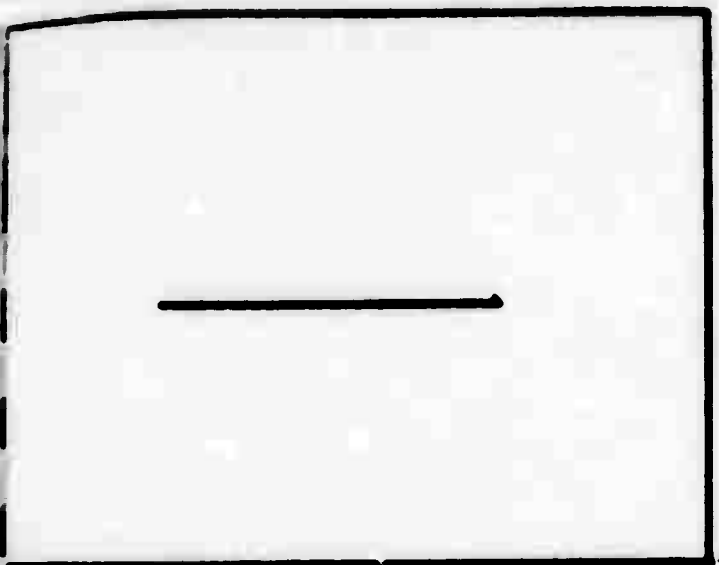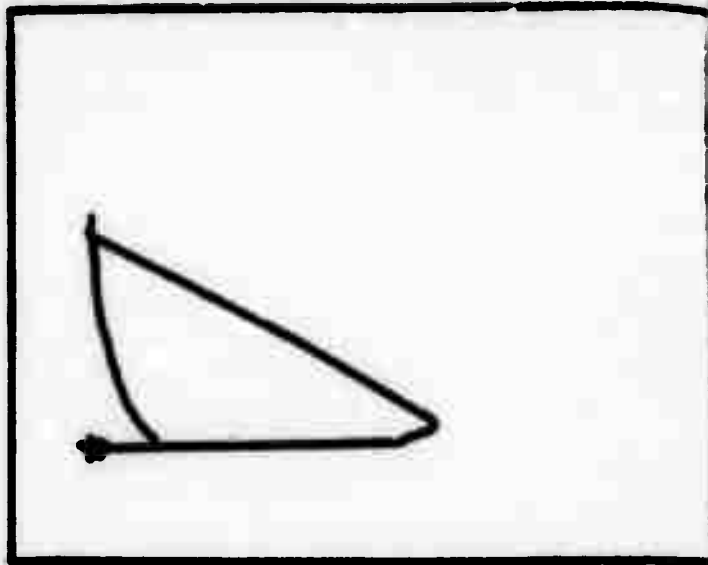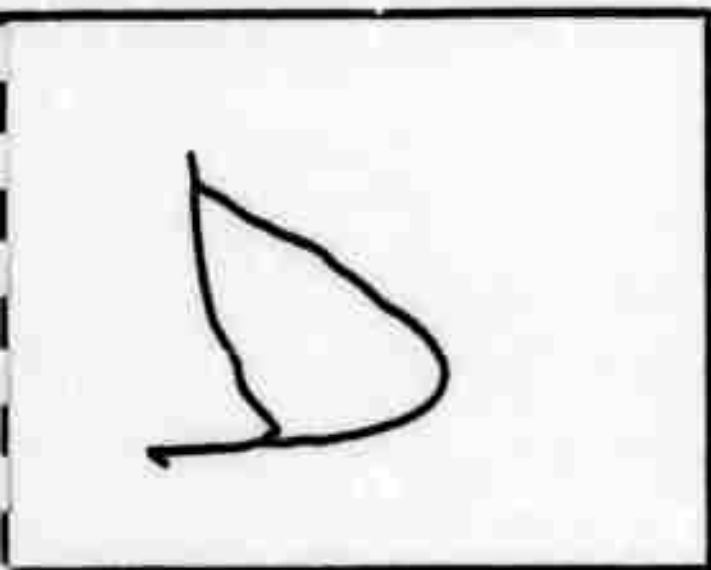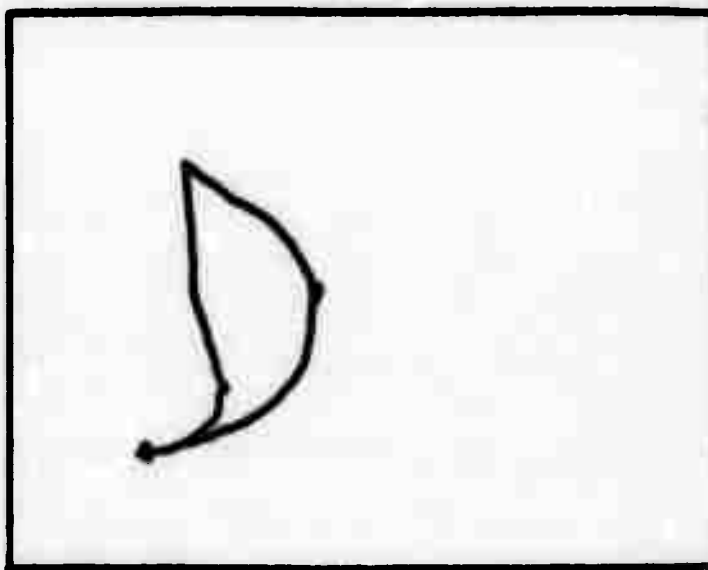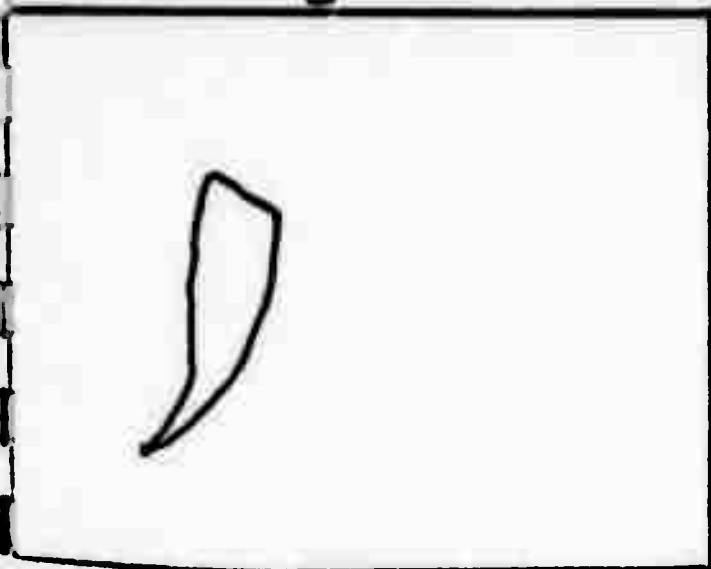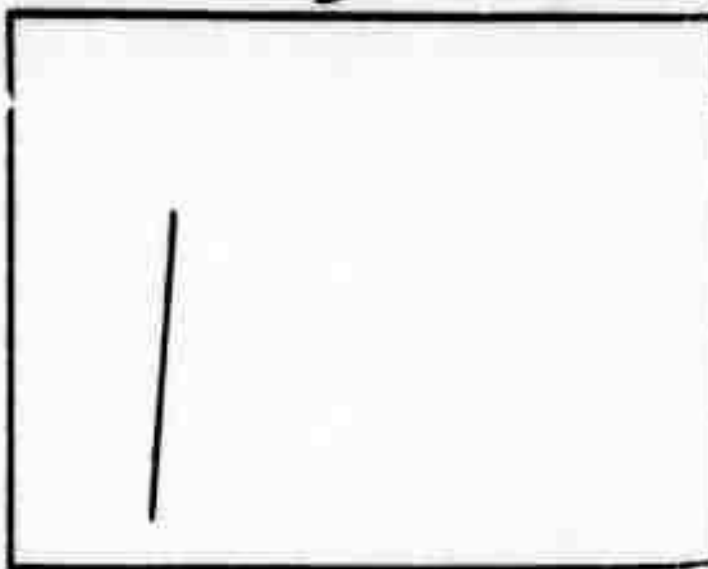
MÖSSBAUER EFFECT SPECTROSCOPY STUDIES OF
SOME IRON PHOSPHATE GLASSES

HERBERT LEE BUCHANAN III

Thesis under the direction of Professor Larry Wilson

The co-ordination states and magnetic structure of iron of a 55 mole % FeO-45 mole % P_2O_5 semiconducting glass containing various concentrations of Fe^{3+} and Fe^{2+} ions were studied using Mössbauer Effect Spectroscopy at $77^{\circ}K$ and $300^{\circ}K$. Room temperature isomer shifts in the range 0.107-0.110 cm/sec and 0.023-0.047 cm/sec and quadrupole splittings of 0.217-0.265 cm/sec and 0.046-0.097 cm/sec for the Fe^{2+} ion and Fe^{3+} ion, respectively, indicate tetrahedral co-ordination states. Although no magnetic hyperfine structure was present at $300^{\circ}K$, splitting at $77^{\circ}K$ was interpreted as evidence of either long relaxation times or limited magnetic ordering. MES spectra of samples of the 50% Fe^{3+}/Fe glass heat treated for intervals up to six hours at $600^{\circ}C$ showed progressive percipitation of oxides in several crystalline phases. The computer programmed curve fittings technique used throughout the analysis is presented and described.

Approved _____ Date _____
Adviser

34

MÖSSBAUER EFFECT SPECTROSCOPY STUDIES OF

SOME IRON PHOSPHATE GLASSES

by

Herbert Lee Buchanan III

Thesis

Submitted to the Faculty of the

Graduate School of Vanderbilt University

in partial fulfillment of the requirements

for the degree of

MASTER OF SCIENCE

in

Electrical Engineering

May, 1972

Nashville, Tennessee

Approved: Date

_____   _____

_____   _____

35

ACKNOWLEDGMENTS

Any merit to which the present work is entitled is the
result of help from many people to whom I am indebted. My special
thanks goes to Dr. L. K. Wilson who originally conceived the topic
and provided every type of interest and assistance throughout the
investigations. Some of the equipment was furnished through the kind
generosity of Dr. J. R. Van Wazer of the Department of Chemistry. A
great deal of technical expertise was obtained through conversations
with Dr. J. O. Thompson of the University of Tennessee and Dr. Felix
Obenshaing of the Oak Ridge National Laboratories. I would also like
to thank Mr. E. J. Friebele, Mr. J. H. Nelson, Mr. C. R. Phebus and
Dr. R. P. Manning for their vast patience and encouragement. I
would also like to thank Dr. C. V. Stephenson for his help in the
preparation of the thesis.

The final months used in the research were provided by the
United States Navy, whose generosity I shall shortly begin to repay.

TABLE OF CONTENTS

LIST OF TABLES

LIST OF FIGURES

CHAPTER I

THEORETICAL ASPECTS OF THE MÖSSBAUER EFFECT

In spite of new research tools and recent theoretical advances there is some confusion concerning the chemical and magnetic structure of the iron in iron-phosphate glasses. Recently Mössbauer Effect Spectroscopy, MES, has been successfully used to augment data obtained from the conventional optical and magnetic methods. This thesis describes the use of MES to obtain new structure and magnetic information on iron-phosphate glass systems. Although information obtained from MES is similar to that obtained by nuclear quadrupole resonance, NQR, and nuclear magnetic resonance, NMR, the importance difference lies in the fact that quadrupole moments of excited states as well as ground states may be observed, revealing valence and coordination information concerning isotopes such as Fe^{57} which has no ground state quadrupole moment.

The fact that a photon, emitted by the decay of an excited state, is characterized by the same energy as the incoming photon was demonstrated by Wood in 1904 in the resonant scattering of light. The finite lifetime of the excited state gives rise to a line-width, Γ, of the emitted radiation and is expressed by

$$\tau = \Gamma\hbar$$

The excitation probability $W(E)$ expressed as a function of the energy of radiation is given by the Breit-Wigner relation,

$$W(E) = \frac{1}{4} \cdot \frac{\Gamma^2}{(E-E_o)^2 + \frac{\Gamma^2}{4}}$$

which is more generally referred to as the Lorentzian shape function. It will be noticed that a resonance occurs only if the probability function of the source and that of the absorber overlap to an appreciable extent, that is, if

$$E_o - \frac{\Gamma}{2} \leq h\nu \leq E_o + \frac{\Gamma}{2}$$

The nuclear scattering process is characterized by a cross section parameter, σ, for photons of energy $E = h\nu$ by the relation

$$\sigma = \sigma_o W(E)$$

where

$$\sigma_o = \frac{2I_{ex} + 1}{2(I_{gr} + 1)} \cdot \pi\lambda_o^2$$

I_{ex} and I_{gr} are the spins of the excited and ground states respectively

42

and λ_o is the wavelength at resonance.[1]

The difficulty in the observation of gamma-ray resonance in nuclear systems arises from the fact that the law of the conservation of momentum requires a non-vanishing energy of recoil for the emitting system,

$$E_r = \frac{1}{2} Mv^2 = \frac{(h\nu)^2}{2Mc^2} \simeq \frac{(E_o)^2}{2Mc^2}$$

where M is the mass of the system and c is the velocity of light. In the case of atomic radiation, the emitted quanta of radiation is considerably smaller than the linewidth of the excited state. In nuclear transitions, however, the energy of the emitted and absorbed quanta is 3×10^4 larger with a proportional increase in the free recoil energy. Since the linewidths of both phenomena remain about the same, it is understood that the energy lost in recoil is enough to bring the entire nuclear system out of resonance. P. B. Moon, in 1955, showed that it was possible to add energy to the system, bringing the incident and emitted gamma ray back into coincidence.[2] He accomplished this by adding exactly twice the velocity of the recoil process to the source by placing it on a rapidly spinning wheel, thereby compensating for the velocity lost in both the source and the absorber.

In 1958, Rudolf Mössbauer discovered a different method of obtaining resonance scattering of high energy photons. He was investigating the resonance absorption of the 129 Kev transition of ^{191}Ir. This

line has a low recoil energy and is considerably broadened by the random Doppler shifting of velocities due to thermal agitations. In an effort to observe a decrease in the amount of resonance scattering, Mössbauer decreased the temperature to affect a decrease in the Doppler shift variations. Instead of a decrease in the resonant scattering, he observed an increase. At the apparent failure of the methods of classical mechanics, Mössbauer finally interpreted his results in terms of the Lamb theory (1939) for the resonant capture of thermal neutrons in crystals. Thus, instead of compensating for a recoil energy loss, Mössbauer had found a method by which the recoil energy is reduced to zero and the emitted photons are resonantly absorbed.

If the recoil energy, E_r, as calculated for the free atom case, is less than $h\nu$, the photon energy, and at the same time is less than the energy required to remove an atom from its lattice site, a fraction of the processes that occur will be recoilless according to,

$$f = 1 - \frac{E_r}{h\nu}$$

Application of x-ray or neutron scattering yields

$$f = \exp\left[-\frac{4\pi\langle x^2 \rangle}{\lambda^2}\right]$$

where $\langle x^2 \rangle$ is the mean square vibrational amplitude of the nuclear motion and λ is the wave length of the gamma ray. It is evident that

for a large effect to exist a small vibrational amplitude, such as that found in a crystal lattice, is desired. For a Debye solid,

$$f = \exp\left\{ -\frac{3}{2k} \frac{E_r}{\theta} \left[1 + 4\left(\frac{T}{\theta}\right)^2 \int_0^{\theta/T} \frac{x}{e^x} dx \right] \right\}$$

where θ = Debye temperature, T = absolute temperature, and k = Boltzmann's constant. Inspection of this equation will show how the reduction of the absolute temperature enabled Mössbauer to make the original observation of the recoilless emission of gamma radiation.

Due to the narrow linewidth of the nuclear transitions involved, the resonant absorption is quite sensitive to small energy variations in the gamma radiation. For this reason it is possible to observe directly the interactions between the nucleus and the orbital electron cloud. The manifestations of these interactions on the positions of the nuclear levels are what make Mössbauer Effect Spectroscope valuable in chemical and solid state applications.

Isomer Shift

In atomic spectroscopy one notices that the positions of the electronic levels are not fixed due to the interaction which exists between the levels. There do exist, analogous to these interactions, other interactions between electronic levels and nuclear levels. A change in the s-electron density due to a change in valence would directly affect the probability of finding that electron in the vicinity of the nucleus. As a result there is a Coulombic interaction which may

shift the positions of the nuclear levels. This effect, properly termed an "electronic monopole interaction" but more generally called the "isomer shift", arises from a difference in energy between an unperturbed state and an electrostatically affected version of that same state called the isomeric state. The effect of this monopole interaction is to shift the nuclear levels without removing their spin degeneracy. Thus, in the isomer shifting of these levels, the center of gravity of the entire Mössbauer spectra is seen to be displaced in velocity, usually in the positive direction. An expression for the expected isomer shift may be obtained by first expressing the electrostatic energy of the nucleus, δE, in terms of the nuclear radius, R, given a specific electronic configuration, $|\psi(o)|$, as,

$$\delta E = \frac{2\pi}{5} Ze^2 |\psi(o)|^2 R^2$$

It is recalled, however, that the nuclear transitions take place between levels so that the energy of the excited gamma ray becomes

$$E = \delta E_{ex} - \delta E_{gd} = \frac{2\pi}{5} Ze^2 |\psi(o)|^2 (R_{ex}^2 - R_{gd}^2)$$

At this point it is seen that the absolute value of the energy of a nuclear state is not as important as the energy of that state with respect to some arbitrary standard value. If this is the case then the isomer shift is given by the difference in the nuclear of two

identical materials caused by a variation in electron parameters. Thus
see Figure 1.

$$\text{I.S.} = \frac{2\pi Z e^2}{5} (R_{ex}^2 - R_{gd}^2)\{ |\psi_{abs}(o)|^2 - |\psi_{source}(o)|^2\}$$

or by separating nuclear and atomic parameters.

$$\text{I.S.} = \frac{4\pi}{5} Z e^2 R^2 (\frac{\delta R}{R}) \{ |\psi_{abs}(o)|^2 - |\psi_{source}|^2 \}$$

<u>nuclear</u>   <u>atomic</u>

where $\delta R = R_{ex} - R_{gd}$.

Of course the above expression does not include any correction
for relativistic considerations or distortions of the electronic wave
function at the origin. There have been more accurate expressions
developed as reported in summary form by D. A. Shirley.[3] As mentioned
previously, the electronic contribution to the isomer shift is attri-
butable directly to the activity of the s-electron density functions.
For an element such as iron, chemical bonding involves only a small
percentage of the total s-electron density, therefore one should expect
that for any appreciable shift to occur there must be a dependence of
the s-electron wave functions on the wave functions of the orbitals.
As will be discussed later, the study of iron reveals that the d-elec-
tron levels have the greatest influence of this type. As a result, the
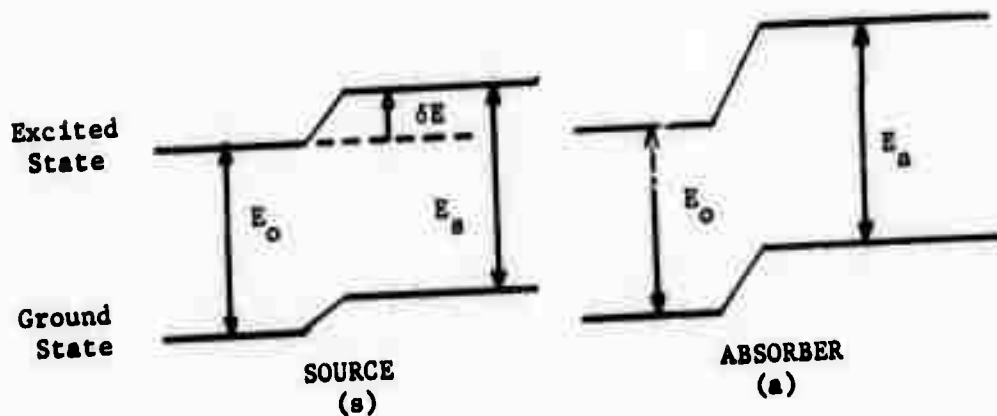
$$\delta E = \frac{2\pi}{5} Ze^2 |\Psi(0)|^2 R^2 \text{ (Relative to point nucleus)}$$

$$\text{Isomer Shift} = E_a - E_s$$

$$IS = \frac{2\pi}{5} Ze^2 [|\Psi_a(0)|^2 - |\Psi_s(0)|^2] [R_{ex}^2 - R_{gd}^2]$$

$$E_q(m_I) = eqQ \left[\frac{3m_I^2 - I(I+1)}{4I(2I-1)} \right]$$

$$\Delta E_q = E_q(3/2) - E_q(1/2) = \frac{eqQ}{2}$$
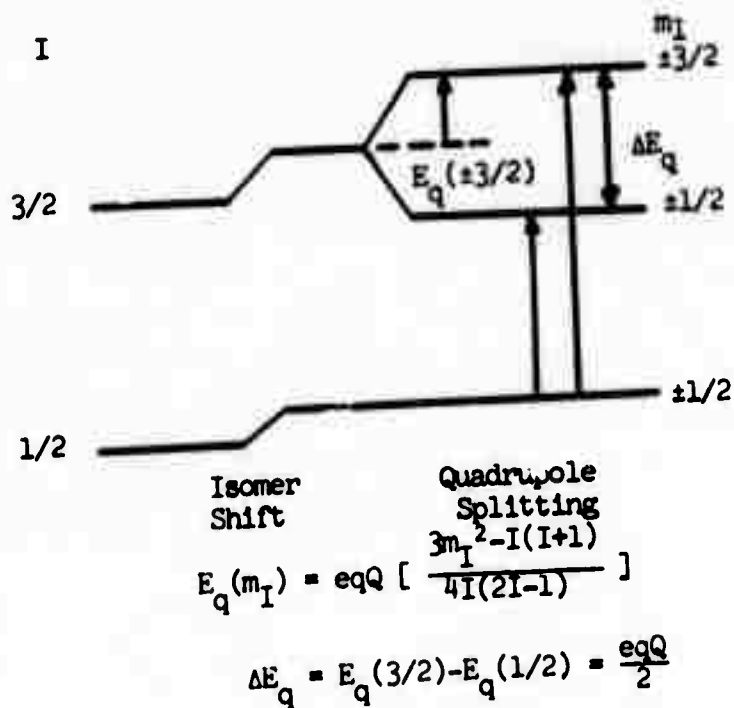
Fig. 1   Isomer shift and quadrupole splitting in Fe^{57}

values at the nucleus of the 1s, 2s, and 3s restricted Hartree-Fock
wave functions were calculated by R. E. Watson[4] for different d^n con-
figurations. The possible factors which influence the isomer shift
have been summarized by Shulman and Sugano[5] as either a direct contri-
bution from 4s bonding or an indirect contribution from 3d bonding.
The indirect contribution results from covalency effects between d-
electrons and either filled ligand orbitals or empty ligand orbitals.
Covalency involving filled ligand orbitals tends to increase d-electron
density thereby reducing s-electron density at the nucleus by means of
electrostatic shielding, whereas covalency involving empty ligand or-
bitals tends to reduce d-electron density in the target atom thus in-
creasing interaction between s-levels and nuclear fields. As far as
application is concerned, two quantities are determined from isomer
shift investigations. These are the nuclear radius dimensions, used
in verifications of nuclear models, and the electron density at the
nucleus, of interest in molecular structure and magnetic studies of the
solid state.

Quadrupole Splitting

So far, it has been assumed that the electron distributions are
spherically symmetric. If the more general case is considered in which
both prolate and oblate distortions are allowed, it is seen that the
$(2I + 1)$ degeneracy is the appearance in a Mössbauer spectra of two or
more lines separated by a difference in velocity representative of some
energy ΔE. This splitting is caused by an interaction between the nu-
clear quadrupole moment, Q, and the gradient of the electric field of

of the electron cloud and is given by

$$H = Z \cdot \nabla E$$

where $Q_{ij} = \int \rho X_i X_j d^3 x$, or

$$H = \frac{eqQ}{4I(2I-1)} \left[3I_z^2 - I(I + 1) + \frac{\eta}{2} (I_+^2 + I_-^2) \right]$$

where η is the assymetry parameter and I_+ and I_- are raising and lowering operators. The Hamiltonian in this form has the eigenvalues

$$E_Q = \frac{eqQ}{4I(2I-1)} \left[3m_I^2 - I(I + 1) \right] (1 + \frac{\eta^2}{3})^{\frac{1}{2}}$$

$$m_I = I, I-1, \ldots \ldots , -I$$

It is seen that the second power of the magnetic quantum number insures that states that differ only in the sign of m_I remain degenerate. Since work in iron involves transitions only between the ground and first excited states, it is seen that $m_I = 3/2, 1/2, -1/2, -3/2$ will result in a single doublet for each distinct value of the electric field gradient. An evaluation of the electrical field gradient tensor is a rather complex problem of solid state physics that has been dealt with to some extent with reference to iron compounds.[7,8]

In general, the factors affecting the electric field gradient are charges on distant ions and electrons in incomplete shells of the target atom itself. If the lattice parameters are known to good accuracy it is possible to determine the gradient of the electrical field at the site of the target atom but this may be quite different from the value of the same field at the target nucleus. An explanation of this is at hand when it is recalled that the electric field of some ligand charge configurations can lift the degeneracy of the five d-orbital states. Originally the states appear as illustrated (see Figure 2). The ligands are usually negative ions or neutral molecules with a prominent lone pair of electrons and affect the d-electrons of a transiton metal atom in two ways. One is through the electrostatic field of the negative charges and the other is covalent bonding with the d-orbitals. Those d-orbitals which have a large electron density in the direction of the ligand are repelled and have a higher energy. Those orbitals which avoid the directions of the ligands are not pushed up in energy so high. Therefore in the octahedral coordination the d_z^2 and $d_{x^2-y^2}$ are increased in energy by the same amount leaving d_{xy}, d_{xz} at a lower energy. The situation is exactly opposite in the tetrahedral coordination placing d_{xy}, d_{yz}, and d_{xz} in a higher energy state. The energy difference in the two orbital groups is called the ligand field splitting, Δ, generally denoted by 10Dq. If the coordination is distorted from either the octahedral or the tetrahedral then the degeneracy of the $d\epsilon$ and $d\sigma$ are lifted and there exists an energy, W, between each $d\epsilon$ or $d\sigma$ suborbital. The population of these suborbitals is now
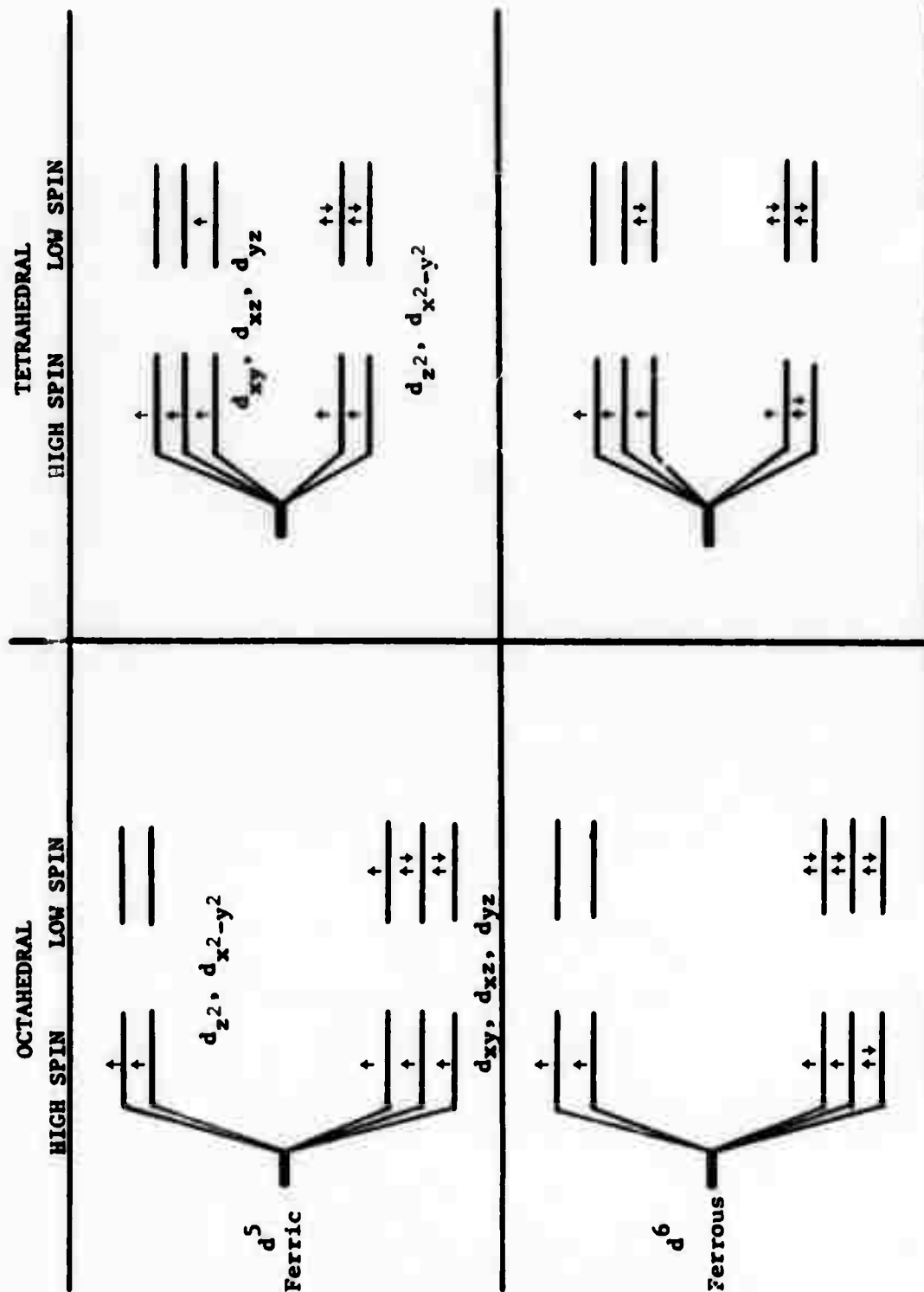
Fig. 2 Electron population of d orbitals for various electronic configurations of iron in the presence of octahedral and tetrahedral ligand fields.

determined by the Boltzmann factor, exp(- W/kT). It should be expected therefore that a considerable temperature dependence should be found for the quadrupole splitting. The details of this temperature dependence, from which the magnitude of the crystal field splitting may be deduced, have been found for a number of materials.[6]

The above discussion has ignored the relative intensities of the lines which do contain additional information. It will be noted that the radiation resulting from the two possible transitions of iron are anisotropic as shown below,[1]

Transition	Probability of Transition	Angular Dependence
$\pm 3/2 \to \pm 1/2$	1	$3/2(1+\cos^2\theta)$
$\pm 1/2 \to \mp 1/2$	1	$1+3/2\sin^2\theta$

where θ is the angle from the axis of symmetry. Note that there is no angle for which either line vanishes and the maximum difference in intensity occurs for $\theta = 0$ and is 3:1. This effect has been explored in some organic compounds of both tin[9] and iron[10].

Magnetic Hyperfine Splitting

The most noticeable part of the Mössbauer spectra results from the interaction of the nuclear magnetic dipole moment, $\bar{\mu}$, with the magnetic field of the electron cloud, $\bar{H}$. The Hamiltonian for this interaction may be written,

$$\bar{H}_m = -\bar{\mu} \cdot \bar{H} = -g\mu_n\bar{I} \cdot \bar{H}$$

where μ_n is the nuclear magneton and g is the gyromagnetic ratio. The eigenvalues may be written,

$$E_m \;=\; -\mu H m_I/I \;=\; -g\mu_n H m_I$$

$$m_I \;=\; I, \; I-1, \; \ldots \ldots, \; -I$$

indicating complete lifting of the $(2I + 1)$ levels with a splitting between adjacent levels of $g\mu_n\bar{H}$. For this reason, the spectra of metallic iron shows a six line pure nuclear Zeeman effect. It is at this point that the difference between the magnetic spectra from the Mössbauer experiment and those obtained in other nuclear resonance techniques becomes apparent. In NMR experiments, for example, nuclear transitions take place between the split levels of a nuclear state ($\Delta m_I = \pm 1$) whereas in the Mössbauer experiment transitions occur between nuclear levels themselves with the condition that the z-component of the angular momentum transferred to the emitted quanta of gamma radiation, L, must be conserved. The final selection rules may then be written,

$$|I_1 - I_2| \leq L \leq |I_1 + I_2| \qquad L \neq 0$$

$$\Delta m_I \;=\; 0, \; \pm 1$$

The appearance of hyperfine splitting makes possible the direct

computation of the transition probabilities. These are obtained from
the squares of the Clebsh-Gorden coefficients which are written

$$(I_1 I_2 m_1 m_2 | I_1 I_2 L m_1 - m_2)^2$$

It is also beneficial to consider the angular dependence of these trans-
itions. These are also given in terms of the angle between the mag-
netic field and the direction of propagation, θ. It is observed from
these expressions that the transition for $\Delta m = 0$ vanishes at $\theta = 0$ but
that the average over a sphere for each component angular dependence
gives a relative probability ratio of 3:2:1:1:2:3. The sum of the angu-
lar expressions is spherically symmetric.[1]

It has been shown that in some materials the magnetic field aris-
ing from the lattice itself is sufficient to cause magnetic hyperfine
splitting. Investigation of iron foil has yielded an internal field of
3.33×10^5 KOe at room temperature.[11] This value was derived from the
fact that the internal field is proportional to the total splitting in
the spectrum (the velocity difference between the two most distant
lines). The origin of this internal field is primarily due[12] to

a) The Fermi contact interaction (direct coupling between the
nucleus and unpaired electrons).

$$H_s = -\frac{16\pi}{3} \beta < \Sigma (\uparrow \psi_s^2(o) - \downarrow \psi_s^2(o))>$$

55

b) The orbital magnetic moment contribution

$$H_L = -2\beta < \frac{1}{r^2} > <L>$$

c) Dipolar interaction with electron spin

$$H_D = -2\beta < \frac{3\vec{r}(\vec{s} \cdot \vec{r})}{r^5} - \frac{s}{r^3} >$$

The appearance of these terms is based on the electron configuration.
A complete treatment is given by Freeman and Watson.[13]

It is necessary to point out that the three primary features of
the Mössbauer spectra isomer shift, quadrupole splitting, and magnetic
hyperfine splitting may occur simultaneously without regard to the mech-
anisms of their origin, see Figure 3. In order to split a spectra into
its separate components, some a priori knowledge of the system para-
meters in conjunction with computer fitting techniques must be used.
An interactive analysis program of this type was used by this author
and is described in Appendix II. In order to successfully predict a
spectra resulting from a number of interrelated parameters, it is nec-
essary to construct the Hamiltonian matrices for both the ground and ex-
cited states of the nucleus and then calculate the transition probabil-
ities from the resulting eigenvalues and eigenvectors.
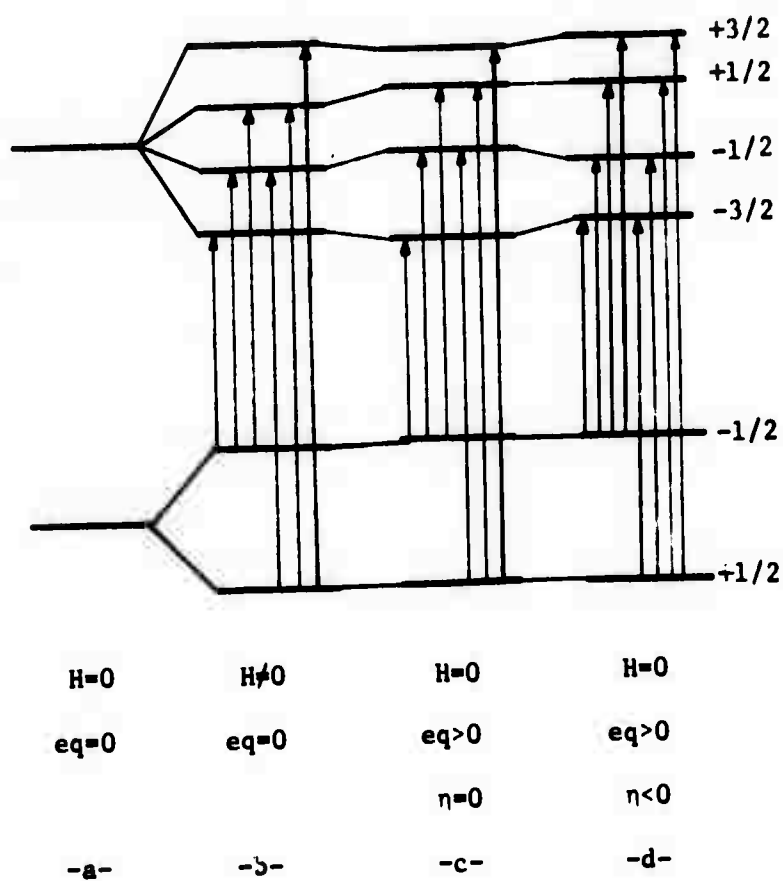
Fig. 3   Effect of combined magnetic and electric fields on
the two low levels of Fe^{57}

CHAPTER II

MÖSSBAUER EFFECT STUDIES OF AMORPHOUS MATERIALS

Before Mössbauer's discovery in 1958, the possibility of observing hyperfine structure of the nucleus had been all but discounted. However, the fact that gamma ray absorption of a material with thermal vibrations of the order of 10^5 cm/sec could be affected by the addition to the system of a velocity of 10^{-3} cm/sec gave new life to areas such as magnetism, lattice dynamics, chemical bonding, and nuclear physics. Although most of the early theoretical work approached the problem of a derivation of the expression of the absorption cross section area by assuming the nucleus was bound in a crystal lattice such as the work done by Maradudin,[14] several experiments were undertaken to investigate the possibility of a Mössbauer effect in glassy materials. Studies of this nature were reported by Gol'danskii[15] in 1963, who successfully used MES to study the chemical state of nuclei bound in both the crystalline and the vitreous states.

It is recalled from Chapter 1 that the recoil-free fraction in the resonant process may be written

$$f = \exp\left[-\frac{4\pi^2 \langle x^2 \rangle}{\lambda^2}\right)\right]$$

where $\langle x^2 \rangle$ is the mean square amplitude of the vibration in the direction

of the emission of the gamma ray averaged over the lifetime of the nuclear state involved.[1] It is seen that if $<x^2>$ is large, that is to say, if the nucleus is unbounded, the expression for the fraction would vanish and no effect would be observed. It would seem clear then that no Mössbauer effect could occur in a liquid as was demonstrated by E. Segre (1933).[16] Although no long range order occurs in a glass, the short range order is sufficient to bind a nucleus to suitably small dimensions and has been shown to give a substantial effect. In addition to the work of Gol'danskii, early demonstrations of this include ^{57}Fe in fused quartz and silicate glass,[17] iron pentacarbonyl frozen in an organic solvent,[18] and ^{119}Sn in polymethyl methacrylate.[19]

Although iron is not genrally a major constituent of inorganic glass, except as a bothersome impurity, its structural information may be very beneficial in deducing the overall structure of the compound. Because it is a transition metal, other magnetic and optical spectroscopic techniques in addition to Mössbauer spectroscopy make structural conclusions rather complete. For this reason, most of the recent studies favor iron as the doping element.[22,23,24,27]

As a result of investigations using several experimental methods it has been generally concluded[27] that iron in glass, in addition to the divalent and trivlanet states, may be present in various other coordination states:

a) It may replace the groups

$$[S_1 O_{3/2}] OM$$
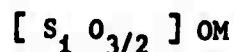
to give the structures

$$[\text{Fe}^{III} O_{4/2}]^- M^+$$

or

$$[\text{Fe}^{II} O_{4/2}]^{2-} 2M^+$$
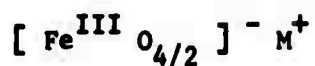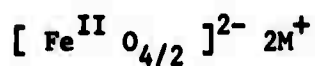
where the iron is the vitrifier with the coordination number 4 (M = Li, Na, K);

b) It may appear as a modifier in the composition of the groups

$$[\text{Fe}^{III} O_6]$$

and

$$[\text{Fe}^{II} O_6]$$
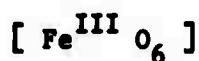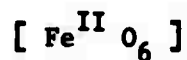
with a coordination number 6, or;

c) It may form oxides or alkaline ferrites in the colloid-disperse states.

If we assume that in the preparation of the glass, there exists some equilibrium distribution of the different forms of the ion, then a chemical expression may be written of the form[27]

$$[\ Fe^{III} \ O_{4/2} \ ] \ M \qquad Fe^{3+} \qquad Fe^{2+} \qquad [\ Fe^{II} \ O_{4/2} \ ] \ 2M$$

(group 2)   (group 3)

$$[\ Fe^{III} \ O \ ] \qquad\qquad\qquad [\ Fe^{II} \ O \ ]$$
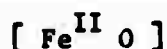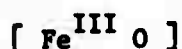
(group 4)   (group 5)

where groups 4 and 5 can be considered to consist of simply Fe^{3+} and Fe^{2+} ions respectively. The fact that the divalent and trivalent electron configurations result in substatually different electric and magnetic environments for the target nucleus should insure that the spectra resulting from these two states will be readily distinguishable.

As mentioned previously, the isomer shift arises in the fact that the electronic configuration in the source and absorber are not identical. This shift is principally attributable to a perturbation of the wave functions of the 3s orbitals in iron so that the difference in isomer shift between spectra of Fe^{3+} and Fe^{2+}, which differ only by one 3d electron, is not immediately understood. Since a single 3d electron should not appreciably affect the electronic charge density, $|\psi(o)|^2$, the shift must originate in the fact that the 3s electrons are spending some of their time farther from the nucleus than the 3d electrons. As a result, the electrostatic influence of the 3s electrons are directly affected by the screening effects of the lower 3d levels. The addition of a single 3d electron reduces the Coulombic attraction between the 3s

level and the nucleus allowing the 3s level to expand. The result is a substantial shift. Belyustin et al. found from a compilation of isomer shift data in five systems of glasses that in variable concentrations of Fe_2O_3 that the shift for each ion remained more or less constant in concentrations of more than 4 mole % at 0.037 ± 0.003 cm/sec. Along with other data indicating that the linewidths also remained constant, they concluded that a "short-range" order exists for iron atoms in both valence states. Work done on alkali silicate glasses[20] yielded values of 0.008 to 0.009 cm/sec for high spin Fe^{3+} and 0.083 cm/sec for high spin Fe^{2+}. Results of experiments done on silicate and phosphate glasses are shown in Figure 4 along with certain similar crystals.[24] While $Fe(PO_3)_3$, $Fe(PO_4) \cdot 2H_2O$, and $NaFeSi_2O_6$ are known to contain Fe^{3+} in octahedral coordination, crystalline $Fe(PO_4)$ and $KFeSi_3O_8$ are known to have the trivalent iron in tetrahedral coordination. The grouping in Figure 4 is evident and the results are generalized to show that while silicate glasses tend to have Fe^{3+} in 4-fold coordinated, the trivalent ion tends toward 6-fold coordination in phosphate glasses. This correlation between isomer shift and coordination number was shown by Walker et al.[33] by comparing the behavior of the ion in both coordination sites. Increased covalency in $3d^5$ and $3d^6$ compounds is generally the result of increases in 4s electron contribution.[34] Since isomer shifts are directly dependent on s-electron densities, it is expected that a change of coordination number from 6 to 4 for either the Fe^{3+} or Fe^{2+} would result in a decrease in the isomer shift. Kurkjian and E. A. Sigaty[24] found isomer shifts for tetrahedral sites of the order of 0.001
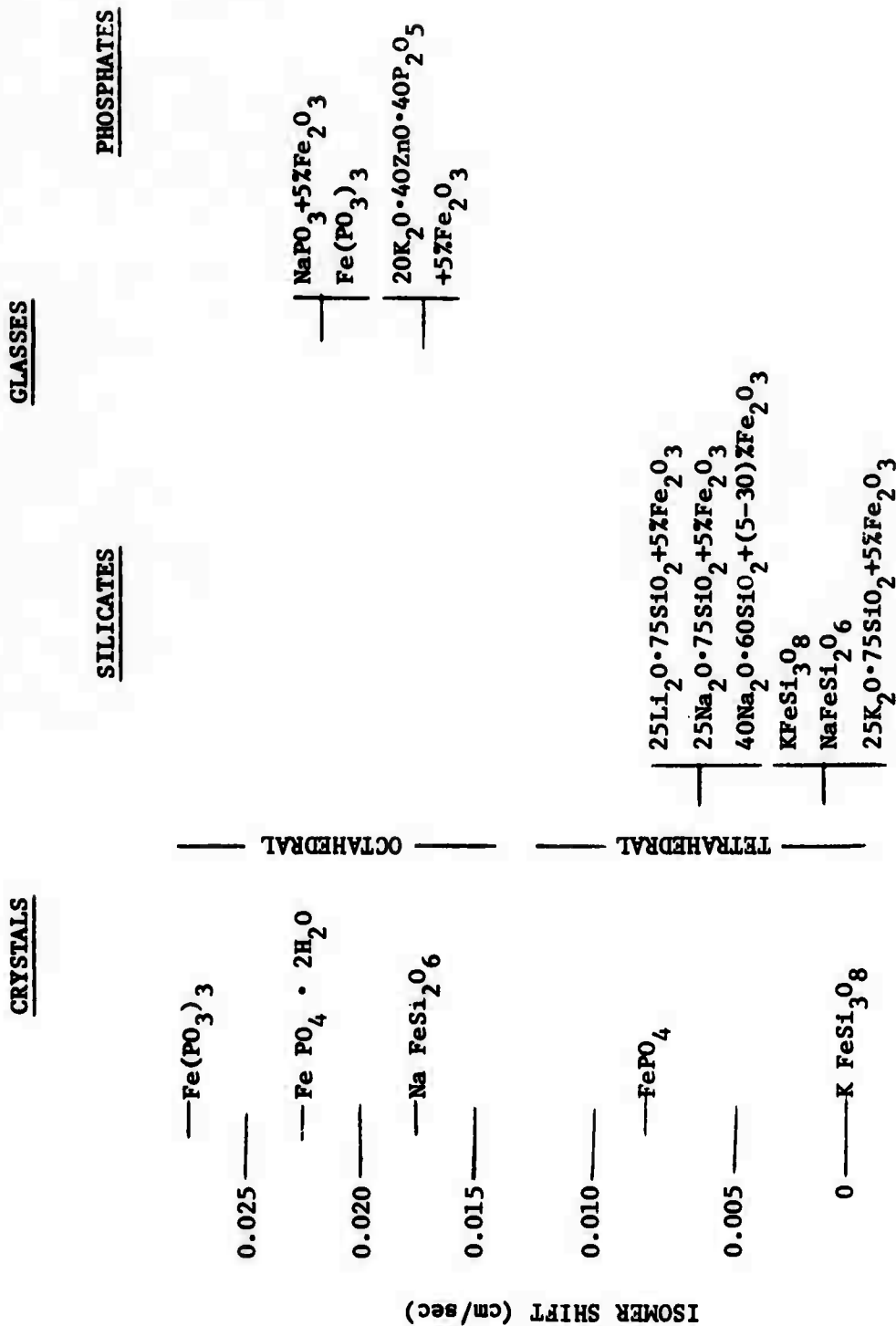
Figure 4. Comparison of Isomer Shifts in Typical Silicate and Phosphate Glasses (After Buchanan and Siegety)[24]

63

cm/sec while those for octahedral sites were substantially larger, of the order of 0.020 cm/sec. Although verification of this correlation for the divalent is less conclusive due to the small amount of work, some results are listed in Tables 1 and 2.

Since it is widely accepted that the structure of glasses is vastly distorted from cubic symmetry, one would expect that there would be some value for the electric field gradient at the nucleus from the d-shell electrons of the target atom as well as the electrostatic field of the ligand structure. It is, therefore, no surprise that in most glasses which contain iron quadrupole splitting is found for both ion states. The trivalent ion splitting in silicate glasses has been to have a range of 0.07-0.10 cm/sec which can therefore be considered indicative of tetrahedral coordination. The phosphate glasses show a somewhat wider range for the octahedral coordination of 0.032-0.088 cm/sec.[20] Splitting less than approximately 0.03 cm/sec or greater than 0.10 cm/sec would seem to indicate some combination of the two states. As with the isomer shift of the divalent ion, the quadrupole splitting has been incompletely explored, but reported values range from 0.200-0.229 cm/sec at 300 degrees Kelvin. There have been attempts to quantitatively analyze the substantial temperature dependence of the splitting values with respect to distorted octahedral symmetry by fitting the data to the values of the energy differences between the three-fold degenerate dε levels as published by Ingalls.[6,21,22]

Work done by A. Lerman, M. Stiller, and E. Hernon,[25] showed that the ratios of the areas under each of the two superimposed doublet spectra varied linearly with the relative proportion of each respective ion

TABLE 1

FE^{2+} PARAMETERS IN SILICATE MATERIALS

$(I.S.)_{Cu}$ (cm/sec)	C.N.
0.053	4(square planar)
0.060-0.077	4(tetrahedral)
0.081-0.101	6(octahedral)
0.110	8(distorted cube)

TABLE 2

FE^{2+} ISOMER SHIFT DATA FOR GLASSES AND REFERENCE

Glass Type	$(I.S.)_{Cu}$ (cm/sec)	Ref.
Phosphate	0.115	46
Phosphate	0.107	21
Phosphate	0.095-0.097	47
Silicate	0.089	48
Silicate	0.080	46
Silicate	0.067-0.089	27

in the material. Results of their experiments with mixtures of vivia-nite and amorphous ferric phosphate within 3% of conventional chemical methods were reported. At about the same time, Karyagin[35] showed that the intensities of the two peaks in the doublet should not be equal in the general case due to the anisotropy of the recoil free fraction re-gardless of the isotropy of the crystal. This "Gol'danskii-Karyagin Effect" may be employed to deduce the sign of V_{22} in both ^{57}Fe and ^{119m}Sn spectra.[36] This fact would make the separation of a composite spectra quite difficult. However, it has been determined that a mechan-ical mixture of two glasses, each of which contain only one ion and does give a symmetric doublet, yields an unresolved three line spectra that is quite similar to that obtained in most composite glasses.[27] There-fore, the assumptions that must be made for a glass under investigation to allow this type of analysis are that the absorber is thin enough to allow pure Lorentzian line shape,[28] both iron valence states undergo quadrupole splitting, and that there is no anisotropy in the reemission of gamma radiation.

One of the outstanding capabilities of the Mössbauer Effect is the opportunity for evaluating the magnetic behavior of the iron in glassy systems. Hyperfine splitting, hfs, has been observed in ferro- and antiferromagnetic materials as a result of the internal magnetic field.[29] In di- and paramagnetic substances, the ground state and ex-cited state degeneracy is removed by an external magnetic field,[30] how-ever it should be possible to observe hyperfine splitting without an external field provided that the electron spin relaxation time is large

compared to the reciprocal of the hyperfine interaction energy, that is, if $\tau > \frac{h}{2A}$ where A is the magnetic hfs energy.[26] In investigations of dilute concentrations of iron in sodium trisilicate glass, Kurkjian and Buchanan[26] have shown that as the temperature is lowered a fairly distinct six line spectra is evident with a large doublet completely obscurring the center two peaks. This could not be interpreted on the basis of a precipitation of an iron oxide since the hfs spectra decreased with an increase in iron concentration. The effect could only be explained in terms of a long spin relaxation time as discussed above since the glass was known to be paramagnetic at the low temperature. As the concentration is increased, the proximity of neighboring Fe^{3+} causes spin-spin coupling relaxation.

The "inverse spinel" effect was shown in work by Belyustin et al.[27] with various concentrations of Fe_2O_3 in sodium silicate glass. Two six line spectra overlapping on the last three lines with an intense trivalent doublet indicated eight Fe^{3+} on tetragonal A sites and eight Fe^{3+} and eight Fe^{2+} ions on octahedral B sites at room temperature. Shaw and Heasly[31] have investigated heat treatment on $Na_2O-Fe_2O_3-SiO_2$ and $Li_2O-MnO_2-SiO_2$ glasses and have interpreted their results on the basis of superparamagnetism.

Finally, it is understood that a combination of magnetic hfs and quadrupole coupling may exist simultaneously. Kurkjian and Buchanan[26] investigated the spectra of $Fe(PO_3)_3$ in both the vitreous and the crystalline states. While the crystal showed no quadrupole splitting, the value of the splitting for the divalent ion in the glass (20% of the

total iron present) indicated octahedral coordination. Below 10 degrees the glass showed the same quadrupole spectra superimposed on a six-line hyperfine structure. Although the hfs presumably resulted from a large fraction of the iron atoms in an internal magnetic environment, the fact that the proportions of the amplitudes were not 3:2:1:1:2:3 as found in metallic iron, seemed to indicate the possibility of other spin states of the trivalent ion that were not included in the hfs. It was postulated that although the glass was known to be paramagnetic, either some short range magnetic ordering is present or the degeneracies are lifted by a long relaxation time.

Finally, we notice that, just as in most other methods of spectroscopy, the linewidths are substantially increased in glassy materials. This broadening is usually explained as due to the variation in site parameters. For paramagnetic glasses this broadening is most likely due to incomplete relaxation of the magnetic hyperfine fields.[32] Belyustin et al.[27] concluded that the line broadening which occurs with a reduction in iron concentration may be explained by the formation of $Fe^{II}O_{4/2}^{2-}$ (group 3) in which the iron acts as a vitrifier. Although Fe^{3+} usually plays the role of a vitrifier due to its smaller atomic radius, the weak concentration may allow the divalent ion to appear in the network.[27] This suggestion has also been made by other authors, but the data is inconclusive since small concentrations give low effects and statistical errors are great. Due to a half-life of the excited nuclear state of about 100 ns., the theoretical minimum value of half-width is approximately 0.010 cm/sec in iron. The minimum observable half-width

is simply twice this due to the additive combination of source and absorber line widths. The instrumental linewidth obtained by Belyustin et al. was 0.040 cm/sec and the trivalent doublet was broadened by another 0.030 cm/sec. This may be due to the presence of the ion in both tetrahedral and octahedral coordination states. Since the quadrupole splitting for Fe^{3+} is of the order of the linewidth, the superposition of the two coordinations would be very difficult to resolve.

CHAPTER III

EXPERIMENTAL TECHNIQUES

Mössbauer spectra are obtained by irradiating the nucleus of certain isotopes with a narrow band of monoenergetic gamma radiation and tabulating the intensity of the emitted radiation with respect to some geometry of the system. Although detection of the gamma radiation is well accomplished through existing counting techniques, the problem of obtaining a swept range of gamma ray frequencies is a novel engineering problem. A workable solution is to use a radioactive source material which decays iso-energetically with the osotope contained in the absorber. A band of energies is the obtained by Doppler shifting the effective frequency of radiation at the absorber by adding a velocity to either the source or the absorber. An expression for this change in energy is given by $E = (v/c)E$, where E is the unshifted energy and v is the added velocity defined as positive when moving toward the nucleus. The resultant spectra is then given as absorption versus velocity.

Basically there are two methods which have been employed in Doppler shifting the source radiation. The simplest of these is the constant velocity method which Mössbauer used in his original experiments. In this method, a displacement is added to either the source or the absorber by means of mechanical cams, moving screws and gears,

rotating wheels piezoelectric crystals, or loudspeakers executing a constant velocity motion.[39] During a predetermined time interval the detected radiation is counted and recorded. The velocity is then altered by a small amount and the process is repeated. This is contin- ued until an entire spectra has been accumulated. An advantage of this method is that any part of a spectra may be examined in detail simply by reducing the increments of velocity and the limits to which it is altered.

The other method, the one used by the present author, applies motion to either the source or the absorber in such a way that all the velocities of interest are covered in one cycle. This motion is usu- ally applied by means of a loudspeaker coil upon which has been added a pick-up coil that indicates the actual movement being experienced. The coil is modulated with a triangular wave form and the pick-up coil gen- erates an error signal which is used by the drive unit in a feed-back control loop.[37,38] A multichannel analyzer having the same sweep rate as the drive unit samples each successive cycle in increments of time equal to the reciprocal of the product of the sweep frequency and the number of channels. The number of counts in each increment are the stored separately. The non-availability of a multichannel analyzer can be overcome by reducing all detected pulses to the same height and then modulating these pulses with the velocity drive signal. The result is then accumulated in a pulse height analyzer. This method provides an automatic cancellation of an non-linearities in the drive signal.[40]

The apparatus used in the current investigations employs the

addressing signal for the last bistable address register of a TMC
model 404 400 channel multichannel analyzer to drive a Nuclear Science
and Data Corporation model AM-1 velocity drive unit (see Figure 5).
The analyzer signal is a square wave with a period of 100 microseconds
corresponding to the period of sweep of the analyzer. The AM-1 drive
unit integrates this square wave to produce the triangular signal used
for the modulation of the drive coil. The feed-back control loop cor-
rection coil is also utilized. The drive signal is passed through a
D.C. power amplifier stage before driving the armature of the trans-
ducer and a velocity control potentiometer sets the peak value of this
driving waveform establishing the range of velocities to be scanned.
The linearity specifications cover only 95% of the waveform, introduc-
ing a 5% nonlinearity at the apex. Two bands of velocity are provided
0-10 cm/sec and 0-60 cm/sec, of which the former was utilized exclu-
sively.

Detection of the gamma radiation was accomplished by means of a
Reuter-Stokes 303PC331 proportional counter. The tube uses Krypton gas
at a pressure of 72 cm/Hg and a Berylium window 1" in diameter with a
thickness of 0.010". The applied voltage was 1900 volts. Output pulses
were amplified by a Tennelec model TC133 FET preamplifier and a Tennelec
model TC202 BLR linear amplifier with an intervening Tennelec model
TC441 single channel analyzer. The single channel is required to iso-
late the desired line of the source spectra.

There are at least 32 different elements in which the Mössbauer
effect has been found to exist in at least one of several isotopes. The
objective in any study is to find a single line decay of an unstable
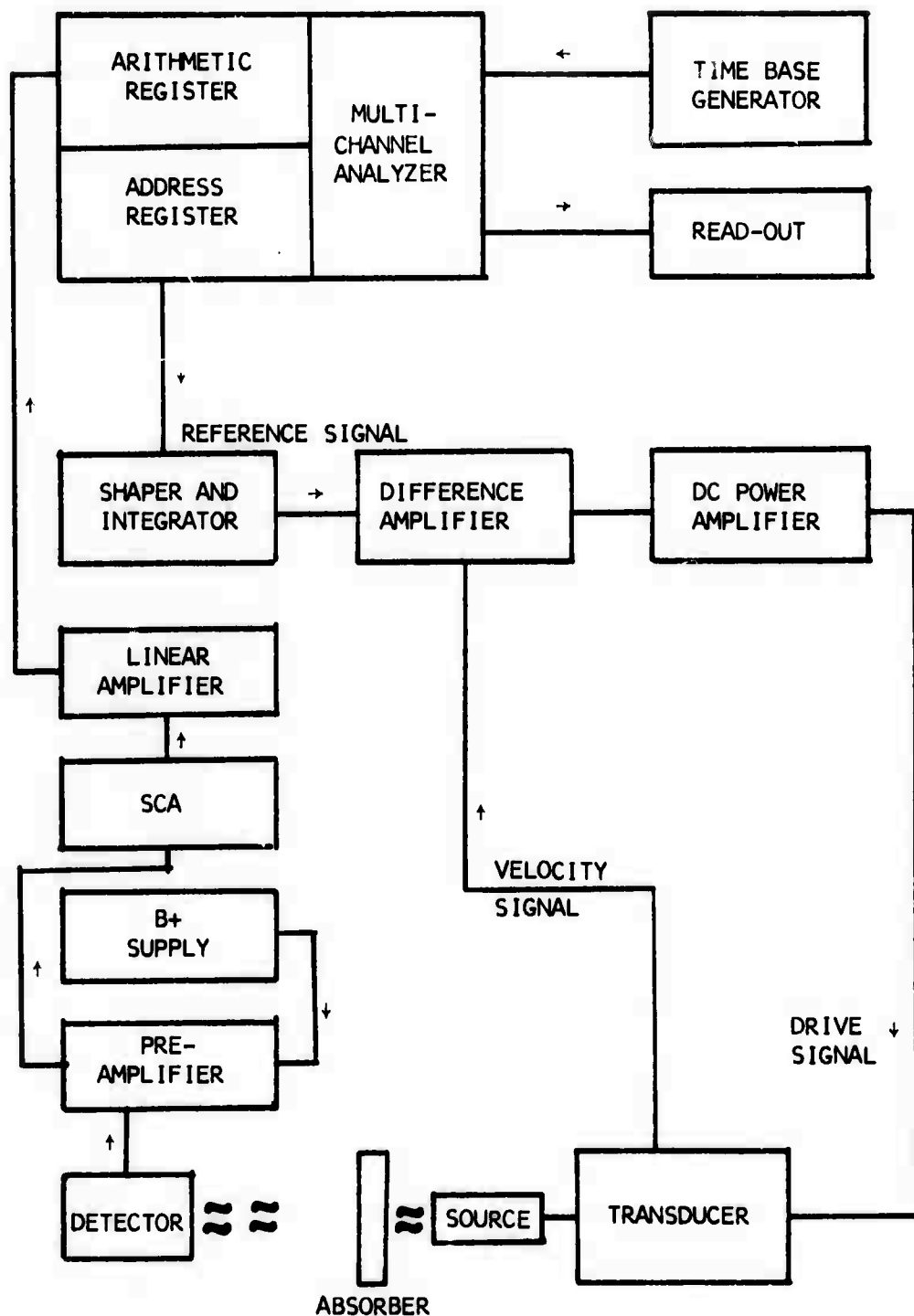
Fig. 5 logic diagram for the Mössbauer system

parent isotope which is iso-energetic with the nuclear transition to be observed. It is then generally desirable to diffuse the source material into a cubic host matrix in order to eliminate quadrupole coupling and magnetic splitting. The source used for the present work was Co^{57} diffused into the cubic environment of copper foil manufactured by New England Nuclear Corporation. After electroplating, the source was annealed for three hours at 1000 degrees centigrade in hydrogen and quenched. The width of the 14.4 Kev resonance line in a $K_4Fe(CN)_6 \cdot 3H_2O$ single line reference absorber with a thickness of 0.5 mg/cm was 0.036 cm/sec. In order to reduce the intensity of the 6.5 Kev x-ray present in the source spectra, a 3/8" thickness of lucite was inserted between the source and the absorber.

The calibration of the apparatus was accomplished by comparing the positions of the six spectral lines obtained from 0.001" iron foil, see Figure 6, with the reference splittings published in the literature.[41] The velocity difference between channels was assumed constant although examination of Figure 7 indicates that some non-linearity did exist. All measurements of isomer shift were made with reference to the single absorption line of stainless steel.

The accumulated data was extracted from the multichannel analyzer by means of an IBM typewriter which printed the total number of counts in each channel. The count totals were then transferred to punched cards at the expense of considerable time and effort. As one can imagine, the novelty and practicality of such a method diminishes very rapidly and an alternative would have been desirable.
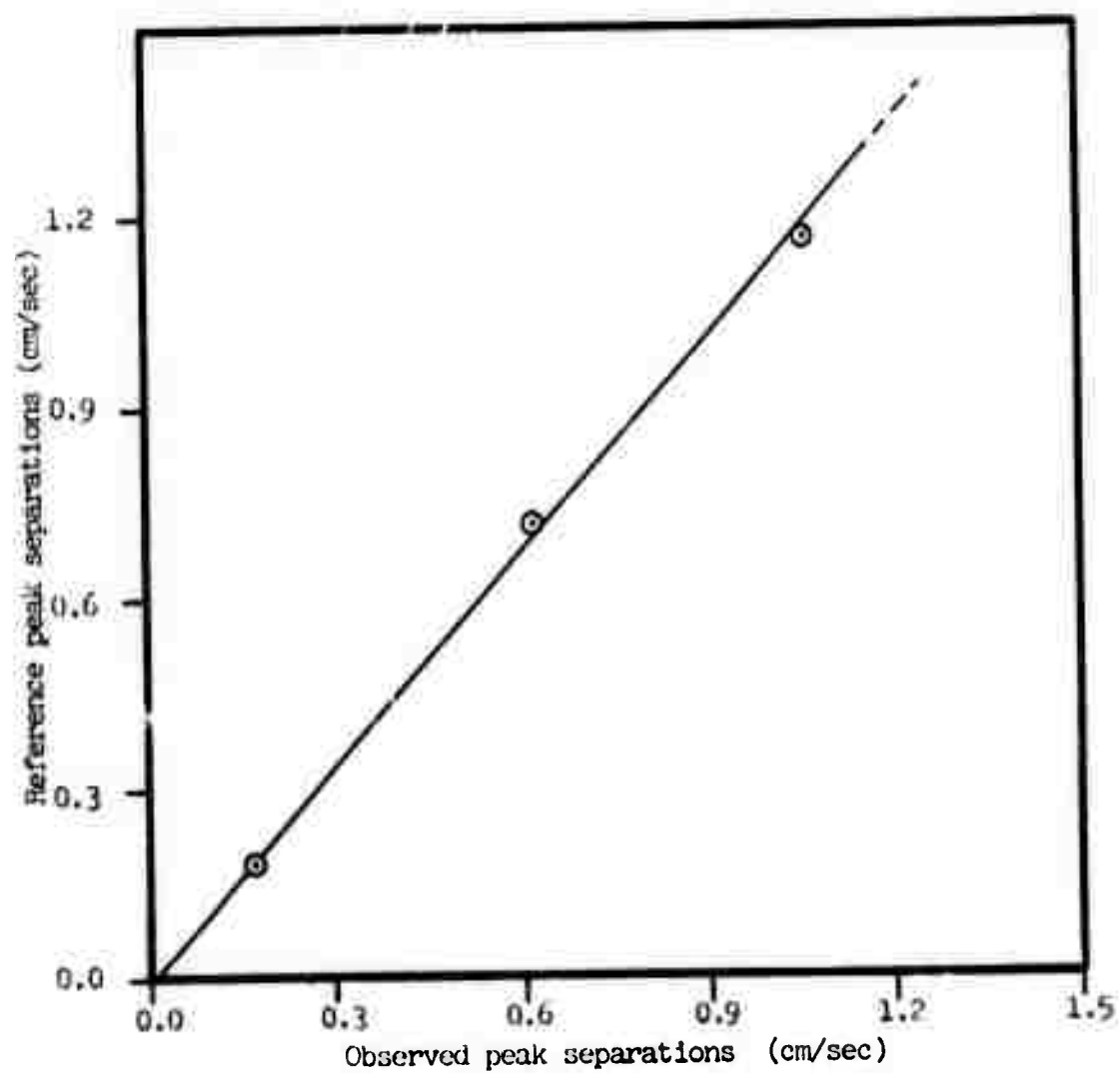
Fig. 6   Calibration curve for .001" iron foil

Except for the iron and stainless standard foils, all samples were finely powdered. A mixture of 400 mg of sample powder added to 2 grams of powdered urea was then placed between two solid brass cylinders and pressed in a hand vise. The result was an opaque disc 1-1/2" in diameter and 1/16 inch thick. This procedure produced an iron density of approximately 13 mg/cm^2. In order to determine the amount of broadening due to this heavy iron concentration,[28] the density was reduced to about 0.25 mg/cm^2 with only a 10% reduction in linewidth. Resolution at this concentration, however, was very poor.

After the discs had sintered, they were mounted in an aluminum holder which was then mounted to the bottom work surface of a Texas Instrument CLF 1 litre cryoflask with brass screws. In order to provide good thermal conduction from the disc, one face was coated with vacuum grease and pressed into contact with a thickness of aluminum foil which was then placed into contact with the aluminum mounting bracket. The only difficulty encountered with this arrangement was that when the system was brought to room temperature from 77 degrees K there was a tendency for the melting frost to dissolve the urea disc. This was remedied by allowing the evacuation pump to remain in operation during the warm-up period.

The glasses were prepared using a physical mixture of 55 mole % FeO and 45 mole % P_2O_5. The mixture was melted in air at 1300 degrees C for one hour and poured into buttons one cm thick and two cm in diameter. To vary the different relative concentrations Fe^{2+} and Fe^{3+} in the glass, dextrose (sample preparations I, II, and III, respectively) was added to the mixture to reduce Fe^{3+} to Fe^{2+} while in the melt. All

FIG. 7

FOLDED SPECTRA OF
.001 IRON FOIL AT ROOM TEMP

ABSORPTION (%)

VELOCITY (CM/SEC)
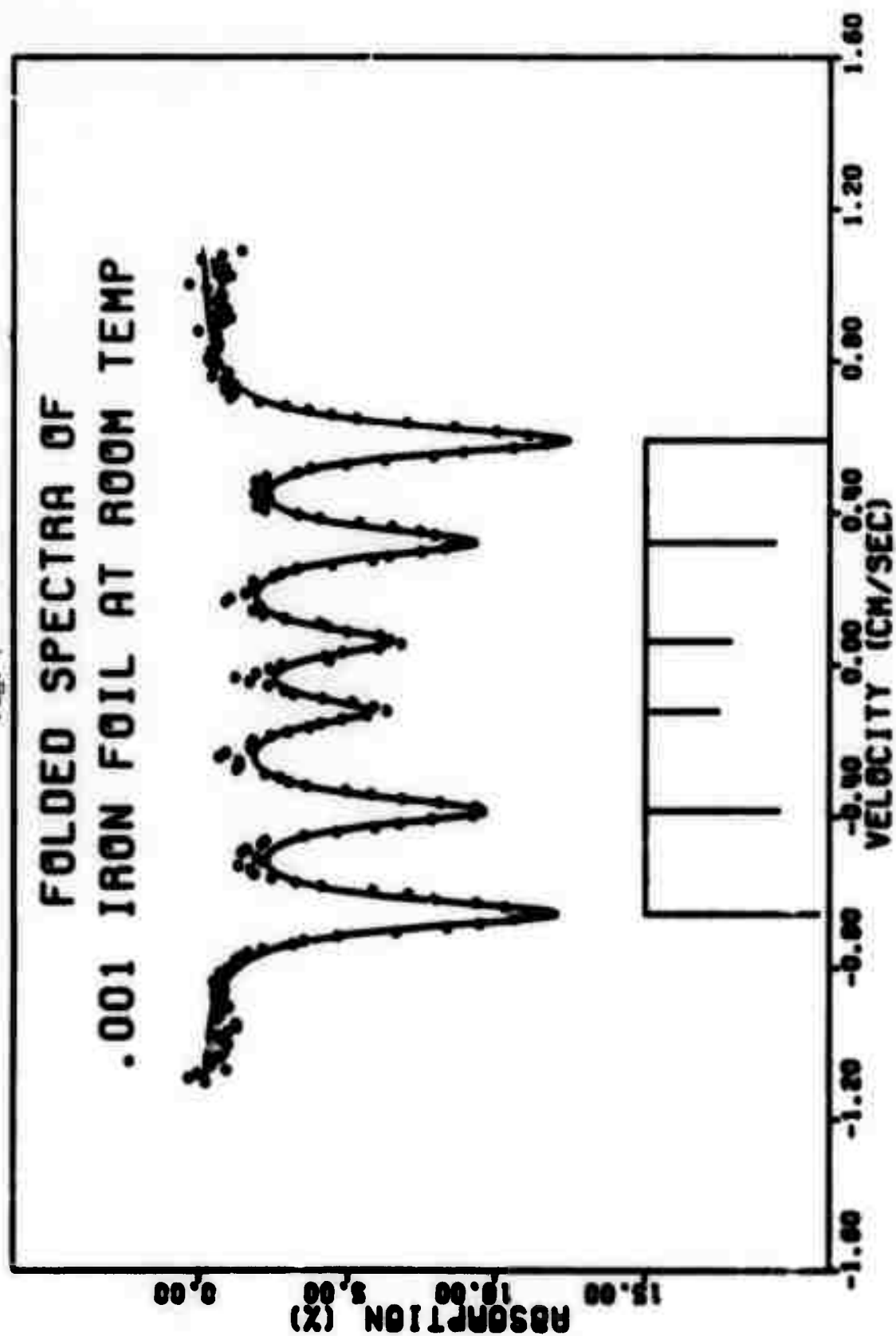
CHAPTER IV

RESULTS

General

The Mössbauer Effect Spectra of the 55-45 mole % $FeO-P_2O_5$
glasses at room temperature consist of three partially resolved lines
of unequal magnitudes. These lines are assumed to be the superposi-
tion of two independent doublets which result from the presence of the
two different ions. When the samples are cooled to 78^oK the observed
effect is substantially decreased. This is accompanied by an outward
migration of the line positions and an increase in their linewidths.
Heat treatment of the 50 % Fe^{3+}/Fe sample yielded additional lines
considerably displaced from zero velocity.

Room Temperature Data

Room temperature spectra for the three iron ratios were ob-
tained and are shown as Figures 8, 9, and 10. Since the dextrose
which was added to the melt in preparation of the samples served only
to change the oxidation state of a portion of the Fe^{3+} ion concentra-
tion to Fe^{2+}, one would expect that the overall iron concentration and
thus the amount of total affect observed in all three samples remains
the same. That this is indeed the case is demonstrated in the fac'
that the integral under the entire spectrum remains constant, regard-
less of the relative concentration. By employing a least-squares ap-
proximation procedure, two symmetric doublets were fit to the raw data,

FOLDED SPECTRA OF
15% Fe^{3+}/Fe SAMPLE AT 300 K

ABSORPTION (%)

VELOCITY (CM/SEC)

'79

Fig. 9

FOLDED SPECTRA OF
50% Fe^{3+}/Fe SAMPLE AT 300 K

FIG. 17

FOLDED SPECTRA OF
79% Fe^{3+}/Fe SAMPLE AT 300 K

VELOCITY (CM/SEC)

ABSORPTION (%)

81

41
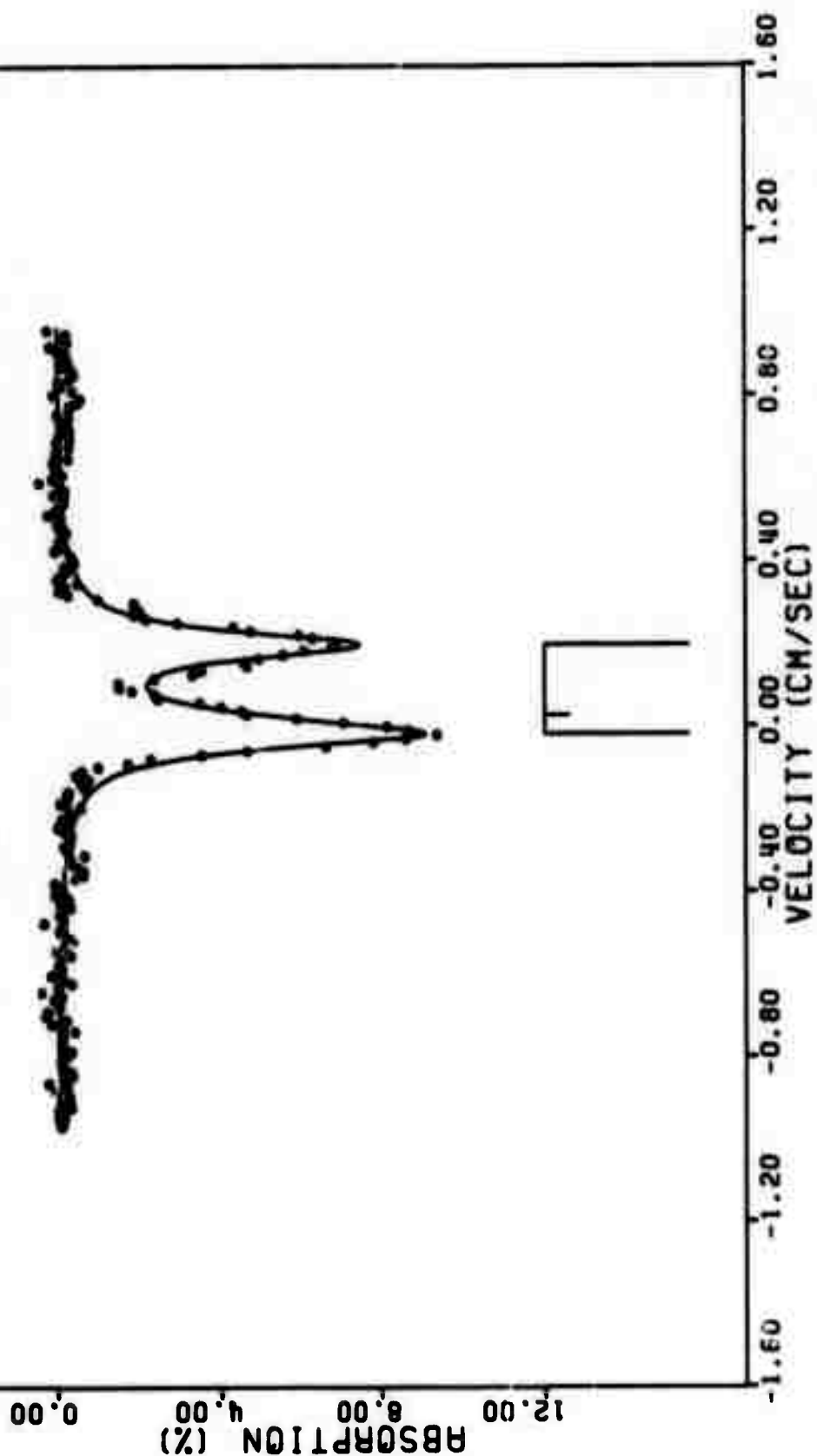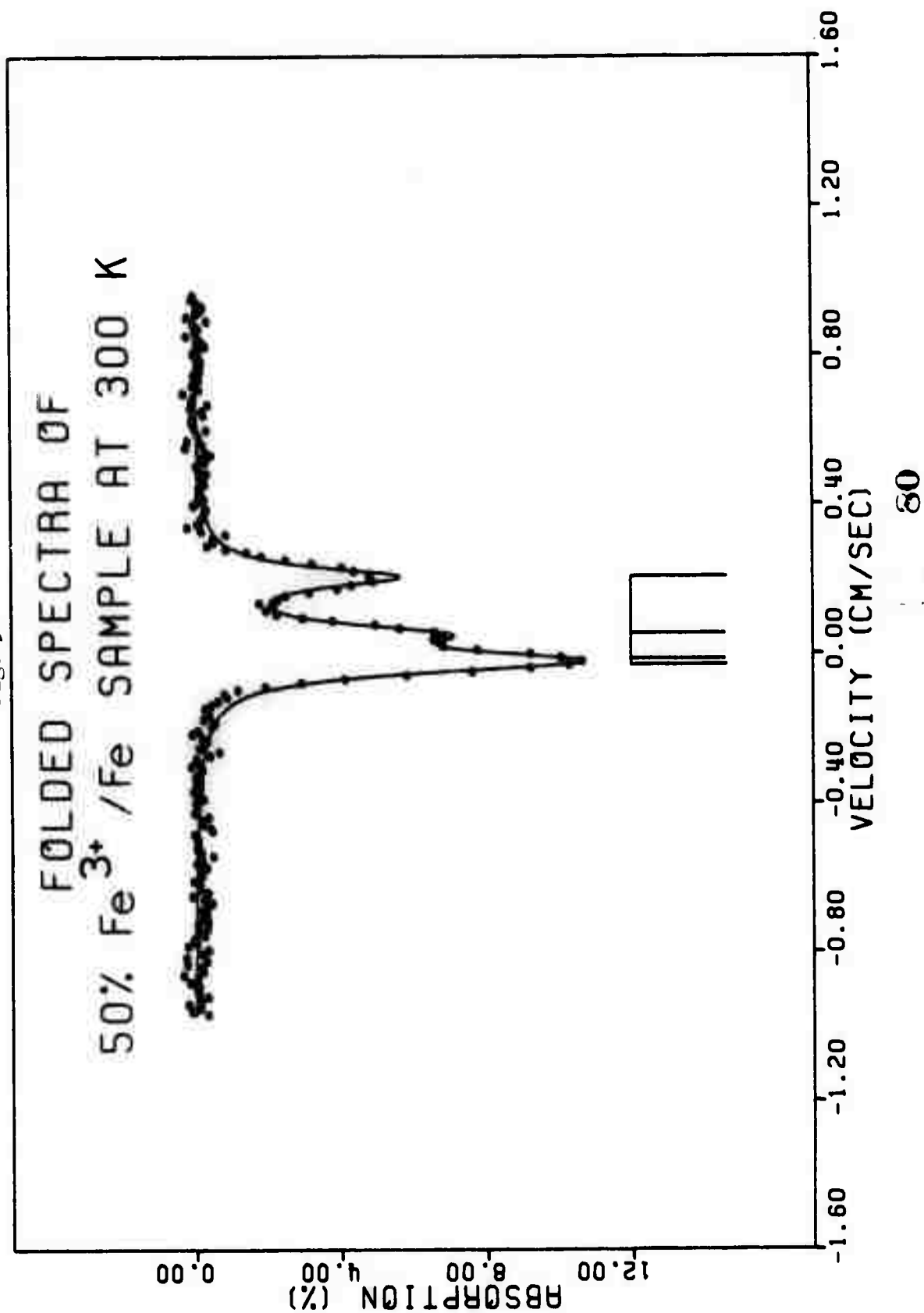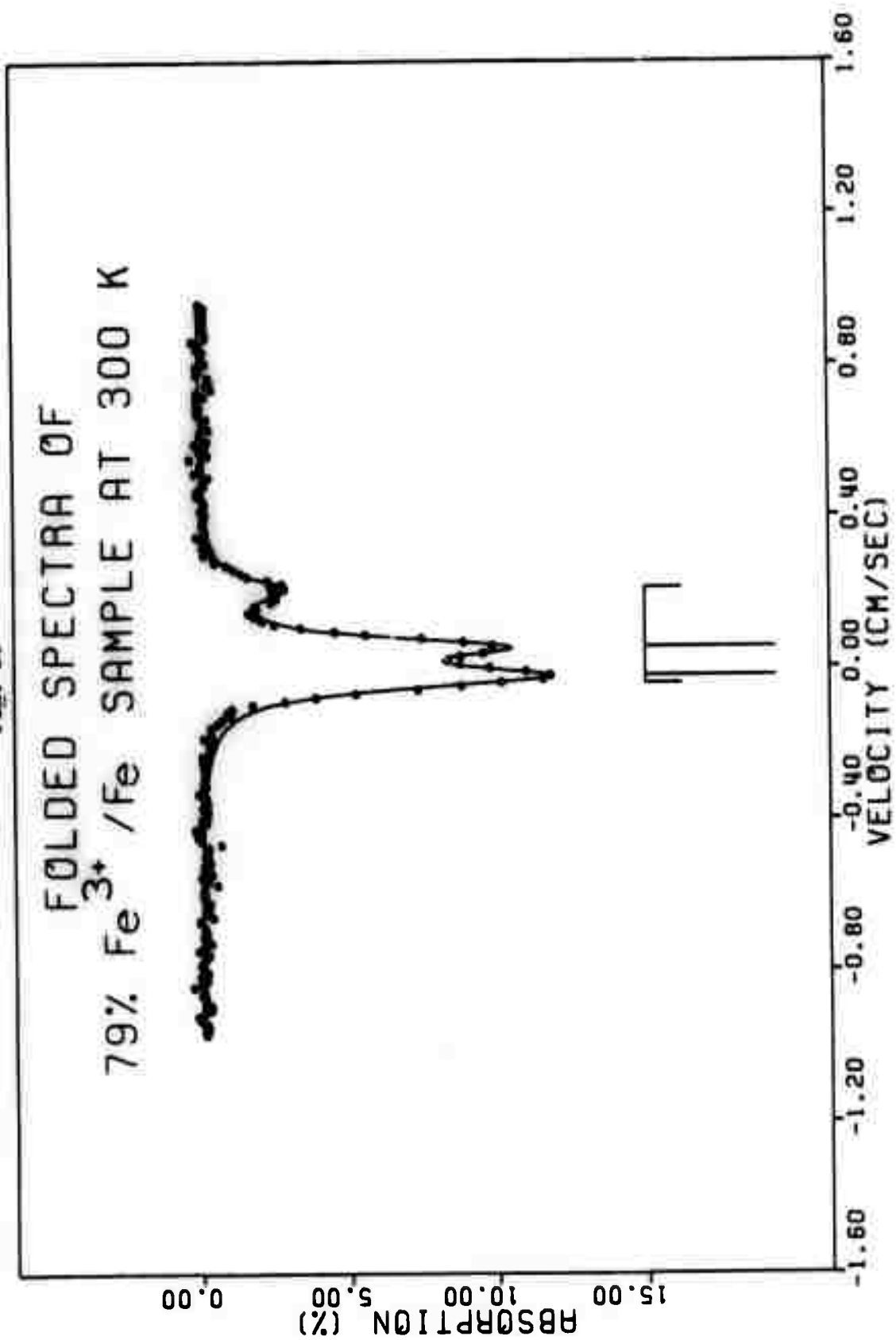
and the resulting line positions and relative amplitudes are shown
under each plot. The solid line passing through each set of experimen-
tal data points shows the total fitted spectra. The actual numerical
results for each fit calculation is given in tabular form with the same
title as the plot in Appendix II. In the case of each doublet, the
amplitudes of the two corresponding peaks were varied simultaneously
as one variable, whereas each position was varied independently. In
the case of the 15 % Fe^{3+}/Fe sample, it was found that the best fit
occurred for the case in which the negative peaks of both doublets were
made to have the same position.

Calculations of the relative ion concentrations present were made
using the ratios of the relative area values obtained in the computer-
analysis output (Appendix II). Quadrupole splittings were obtained as
the velocity difference between the two associated peaks and the isomer
shift values were obtained as the difference between the center of
gravity of the two peaks and zero velocity. The final results are shown
in Table III and Figures 11 and 12. In the case of both the di-valent
and the tri-valent ion, the quadrupole splitting increases with an in-
crease in the Fe^{3+}/Fe concentration. Although the magnitudes of the
tri-valent splittings are only about 30% of the di-valent values, the
two curves appear to have an almost identical second order dependence.

The similarity does not appear in the values for the isomer shift.
While the tri-valent shift increases with the Fe^{3+}/Fe ratio, the di-
valent shift seems to remain constant over the entire range of concen-
trations. A more complete picutre of isomer shift and quadrupole split-
ting activities could have been obtained using more data points in the
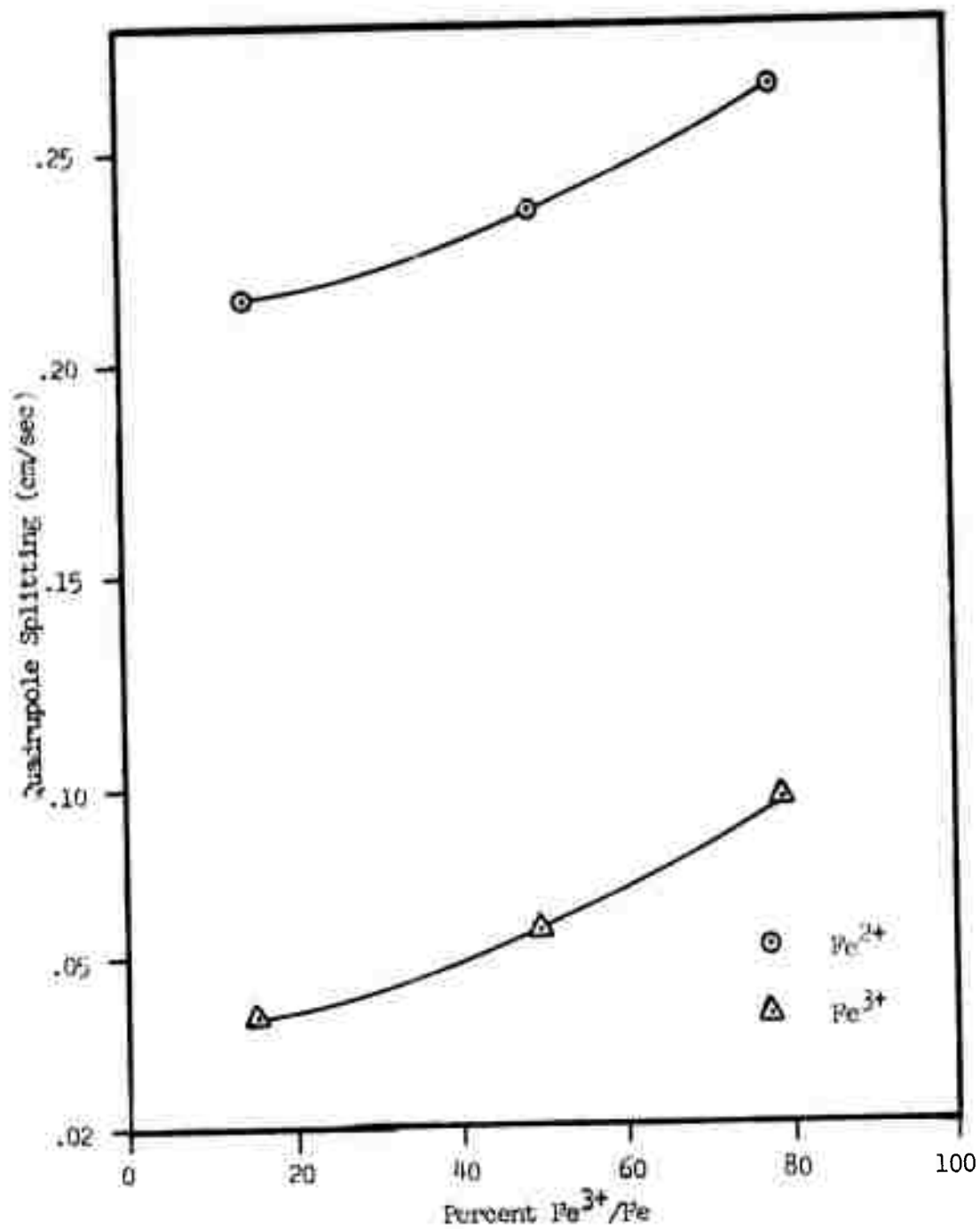
Fig. 11 Quadrupole splitting of the Fe^{3+} and Fe^{2+}_3 ion as a function of the concentration ratio, Fe^{3+}/Fe.

Fig. 12 Isomer shift of the Fe^{3+} and Fe^{2+} ion as a function of the concentration ratio, Fe^{3+}/Fe.

extreme high and low ends of the range of concentrations, however, these samples were not available and were omitted.

Low Temperature Data

A spectra was obtained for each of the concentrations at 78°K and are shown in Figures 13, 14, and 15. In each spectrum four independent Lorentzian line shapes were fitted to the data. The positions of these lines are plotted with respect to the concentration in Figure 16. As the tri-valent ion concentration is decreased, an almost linear migration of the four spectral lines away from a point slightly positive of zero velocity occurs. Accompanying this migration is a slightly non-linear increase in the line-width ranging from a value equal to that obtained in the room temperature observations for high Fe^{3+}/Fe concentrations to nearly six times as large in the low Fe^{3+}/Fe concentration (see Figure 17). As the line positions expand and the line widths increase, there is decrease in the amount of effect that is observed. This is expected since the integral under the spectrum is indicative of the total iron present, however, differences in this area and that obtained at room temperature would indicate a temperature dependence in the recoil-free fraction. The amount of effect that is observed becomes important when it is considered that the amount of noise present in all the data remains fairly constant at approximately 0.5% absorption while the amplitudes of the fitted peaks falls as low as 0.65% absorption. At this level lines are quite difficult to resolve and multiple lines are often completely obscured.

Fig. 13

FOLDED SPECTRA OF
Fe^{3+}/Fe SAMPLE AT 77 K
15%

ABSORPTION (%)

VELOCITY (CM/SEC)

Fig. 14

FOLDED SPECTRA OF
50% Fe^{3+}/Fe SAMPLE AT 77 K

ABSORPTION (%)

VELOCITY (CM/SEC)
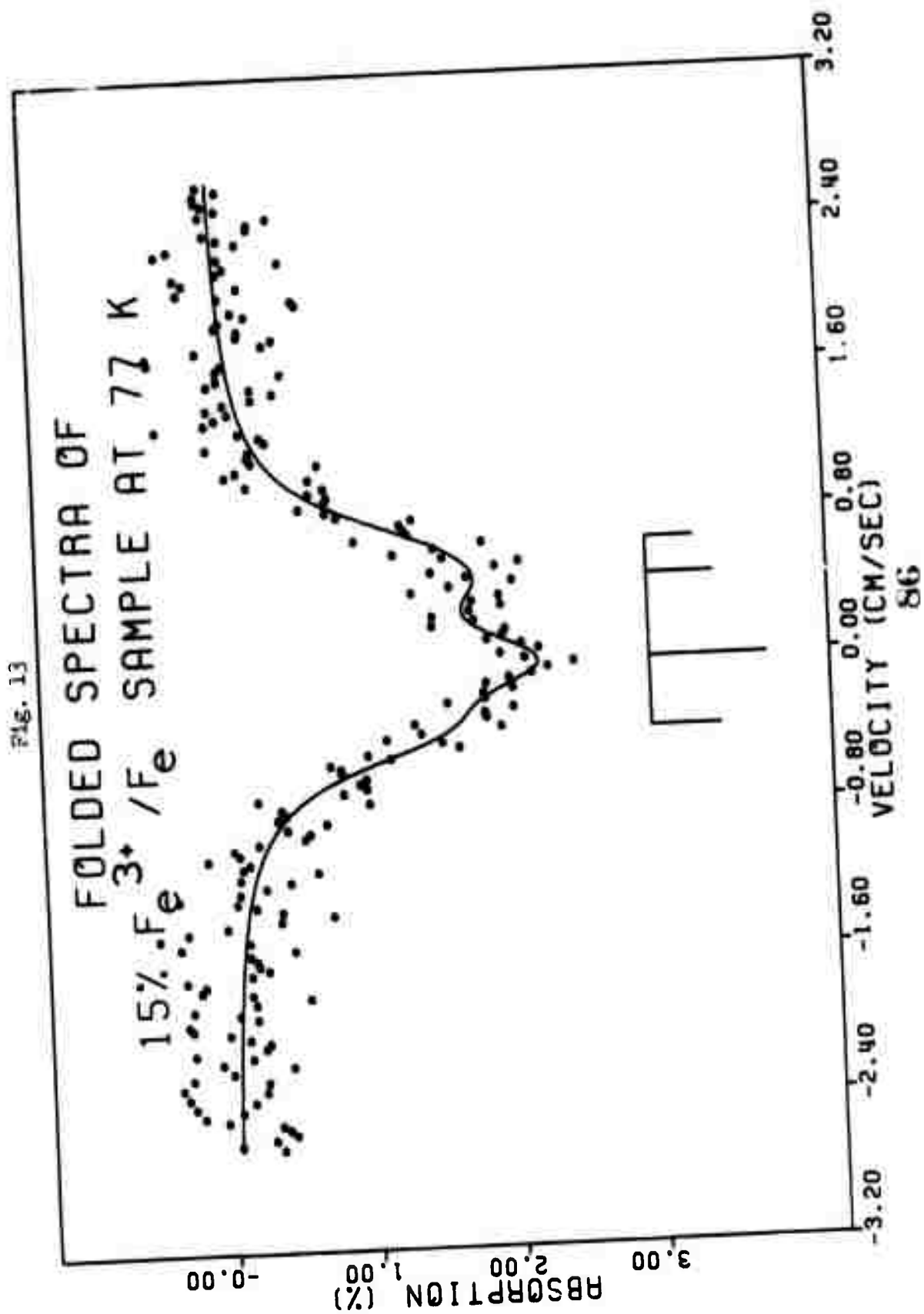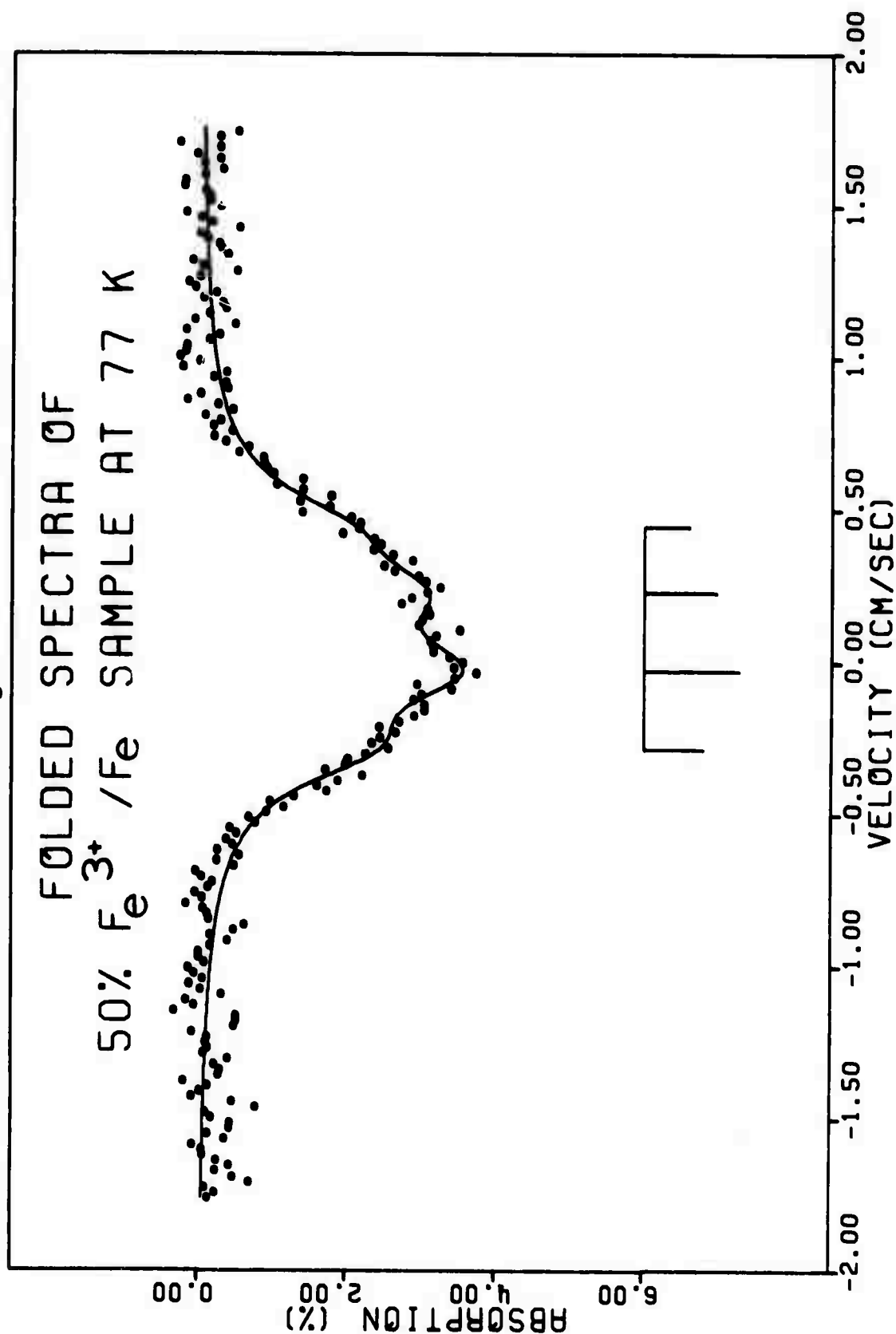
Fig. 15

FOLDED SPECTRA OF
79% Fe^{3+}/Fe SAMPLE AT 77 K
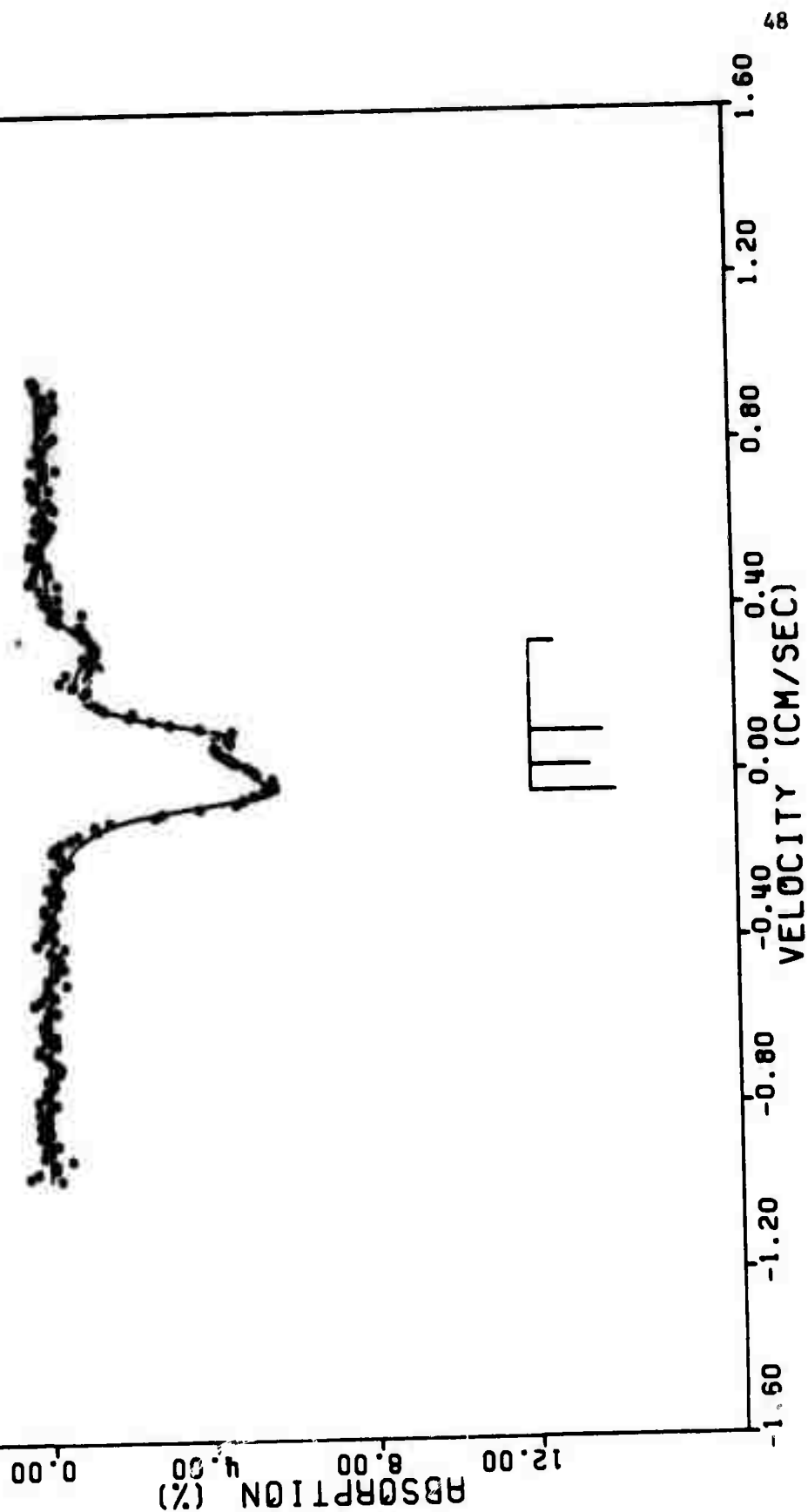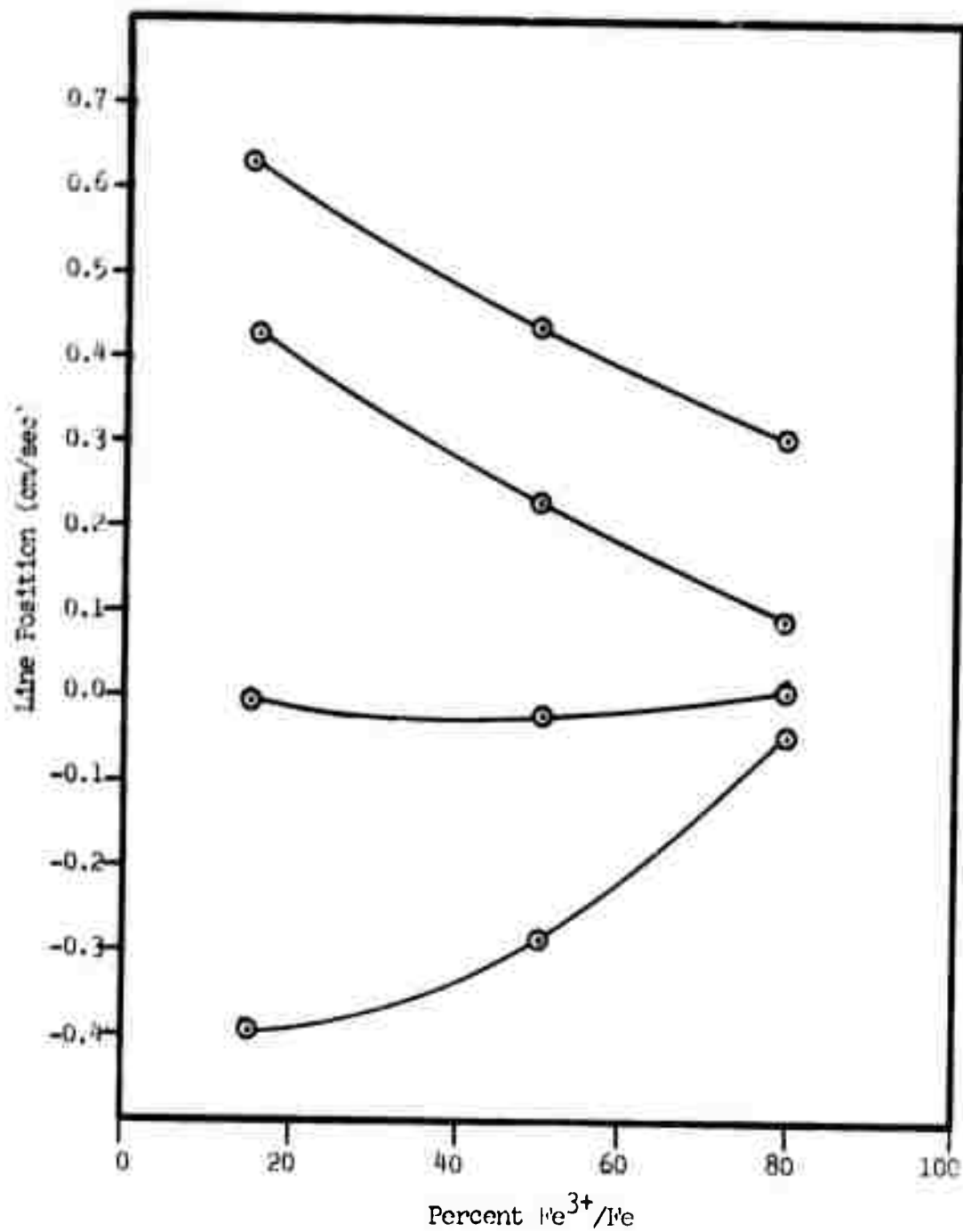
Fig. 16 Line positions as a function of the concentration ratio, Fe^{3+}/Fe, for the four lines of the $77°$ Kelvin samples.
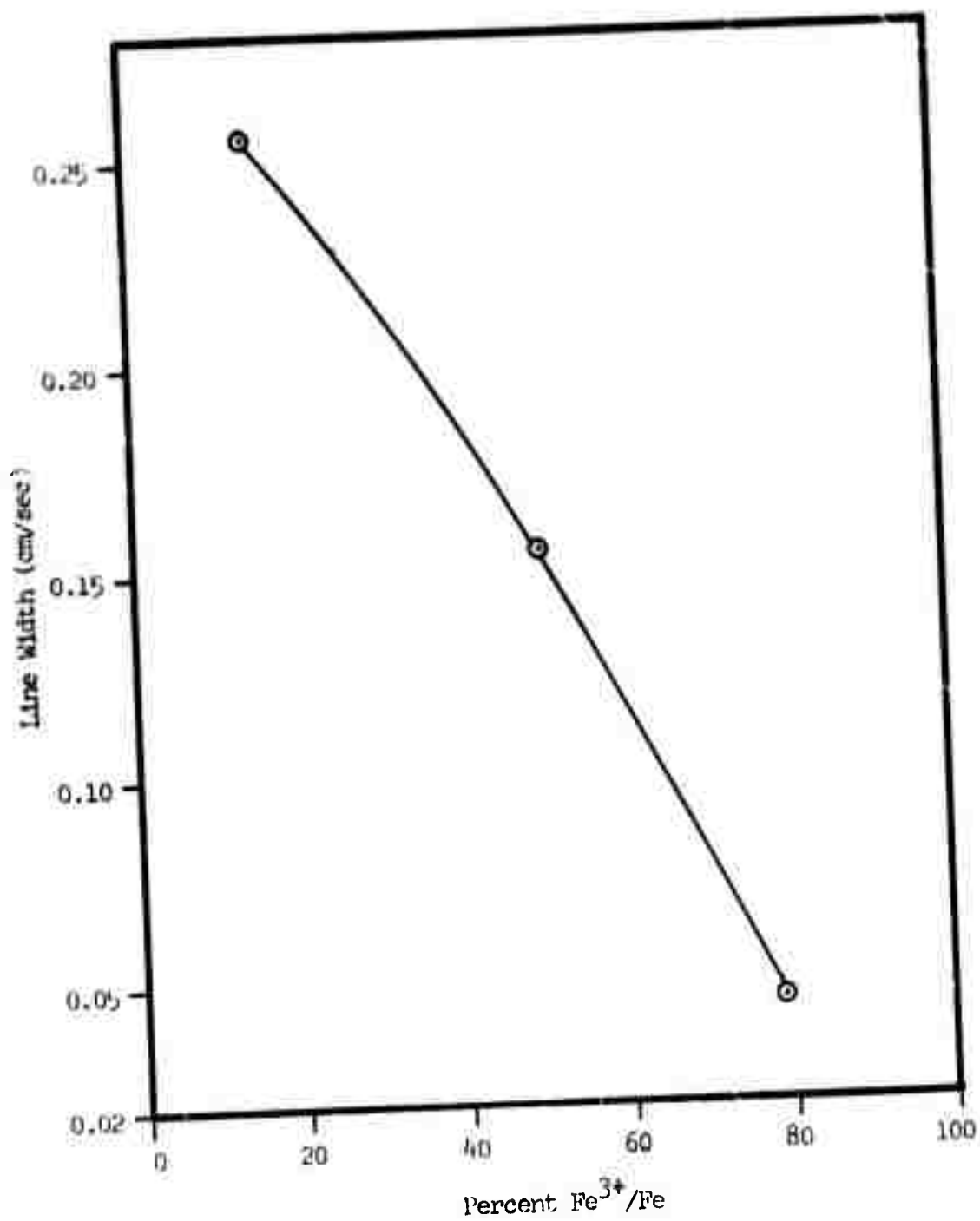
Fig. 17 Line width as a function of the concentration ratio, Fe^{3+}/Fe, for the $77°$ Kelvin samples.

Heat Treated Data

Mössbauer spectra were obtained at room temperature of samples
of the 50% Fe^{3+}/Fe concentration glass which were heat treated for 45,
90, 180, and 360 minutes at 600°C. These spectra are shown as Figures
18, 19, 20, and 21, respectively. The spectrum of the glass without
heat treatment was included previously as Figure 9. No attempt was made
to coordinate the variables associated with any two lines for the rea-
son that no clear cut trend was discovered. However, a graphic display
of the line positions and relative amplitudes is shown as Figure 22.
Lines are numbered in order of their appearance as the time of heat
treatment progresses. Examination of Figure 9 shows that line 1 was
initially considered to be a superposition of the two lines resulting
from the doublets of lines 2 and 3. While this probably remains true
for the heat treated samples, it is expected that lines 4 and 5 are due
to a different mechanism so that a redundancy in the fitting procedure
was not altogether necessary.

As in previous experiments, the line intensities must decrease as
more lines appear to conform to the fixed amount of iron present. This
is consistent with a chemical analysis which was completed on all heat
treated samples. It was found[42] that the heat treating did not affect
the Fe^{3+}/Fe ratio to within an experimental error of ± 0.5%. Also, it
is noticed that as new lines appear and become more completely resolved
the value of the fitted line half-width decreases. This would tend to
indicate that each of the initial lines is the sum of two or more small-
er lines in very close proximity. As the time of the heat treatment is

FOLDED SPECTRA OF
50% Fe^{3+}/F_e SAMPLE HEAT TREATED-45 MIN

Fig. 18

52

Fig. 19

FOLDED SPECTRA OF

50% Fe^{3+}/Fe SAMPLE HEAT TREATED-90 MIN

93

Fig. 20

FOLDED SPECTRA OF
50% Fe^{3+}/Fe SAMPLE HEAT TREATED-180 MIN

VELOCITY (CM/SEC)

ABSORPTION (%)

Fig. 21

FOLDED SPECTRA OF

50% Fe^{3+}/F_e SAMPLE HEAT TREATED-360 MIN

ABSORPTION (%)

VELOCITY (CM/SEC)

95

45 Min.

90 Min.

180 Min.

360 Min.

Velocity (cm/sec)
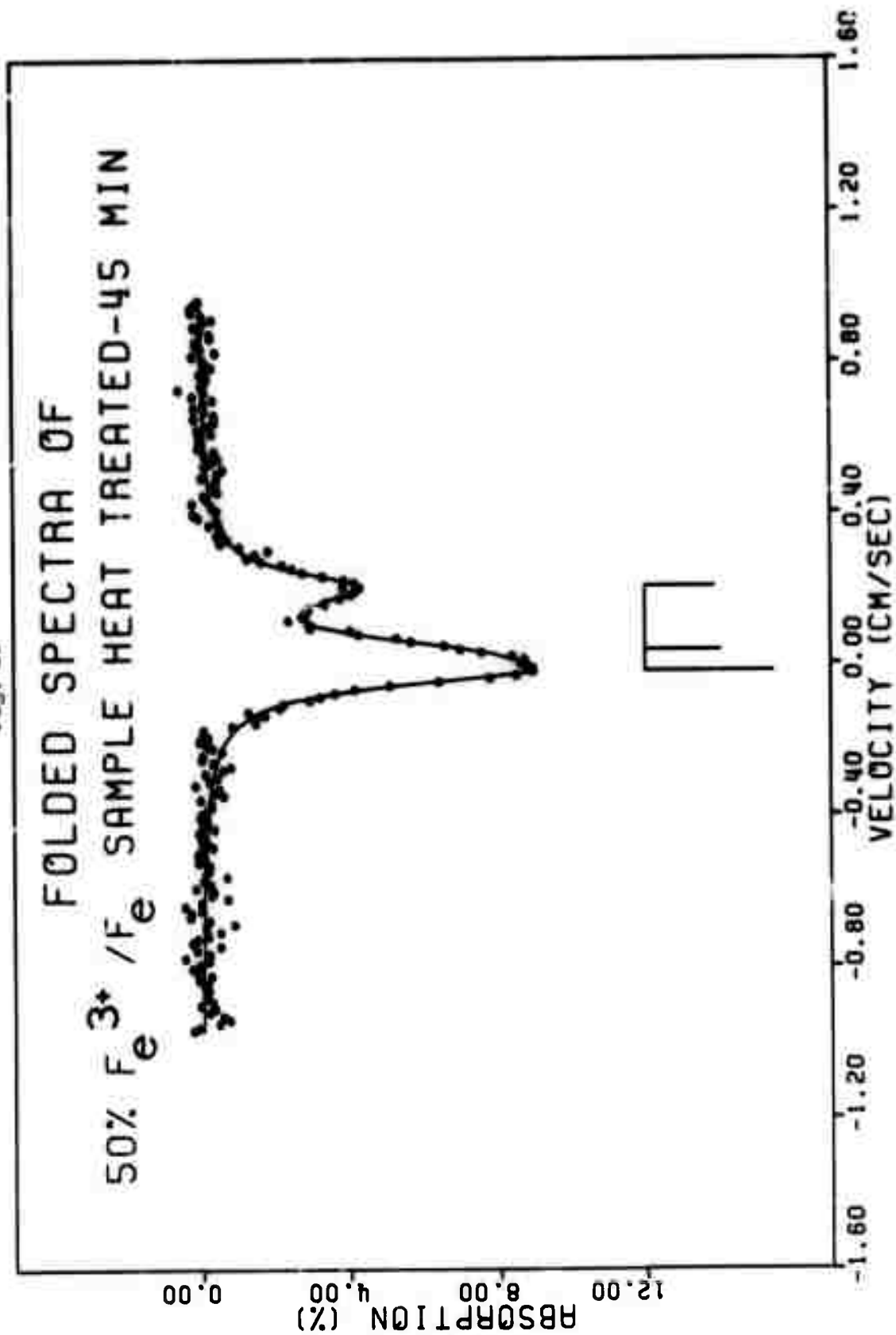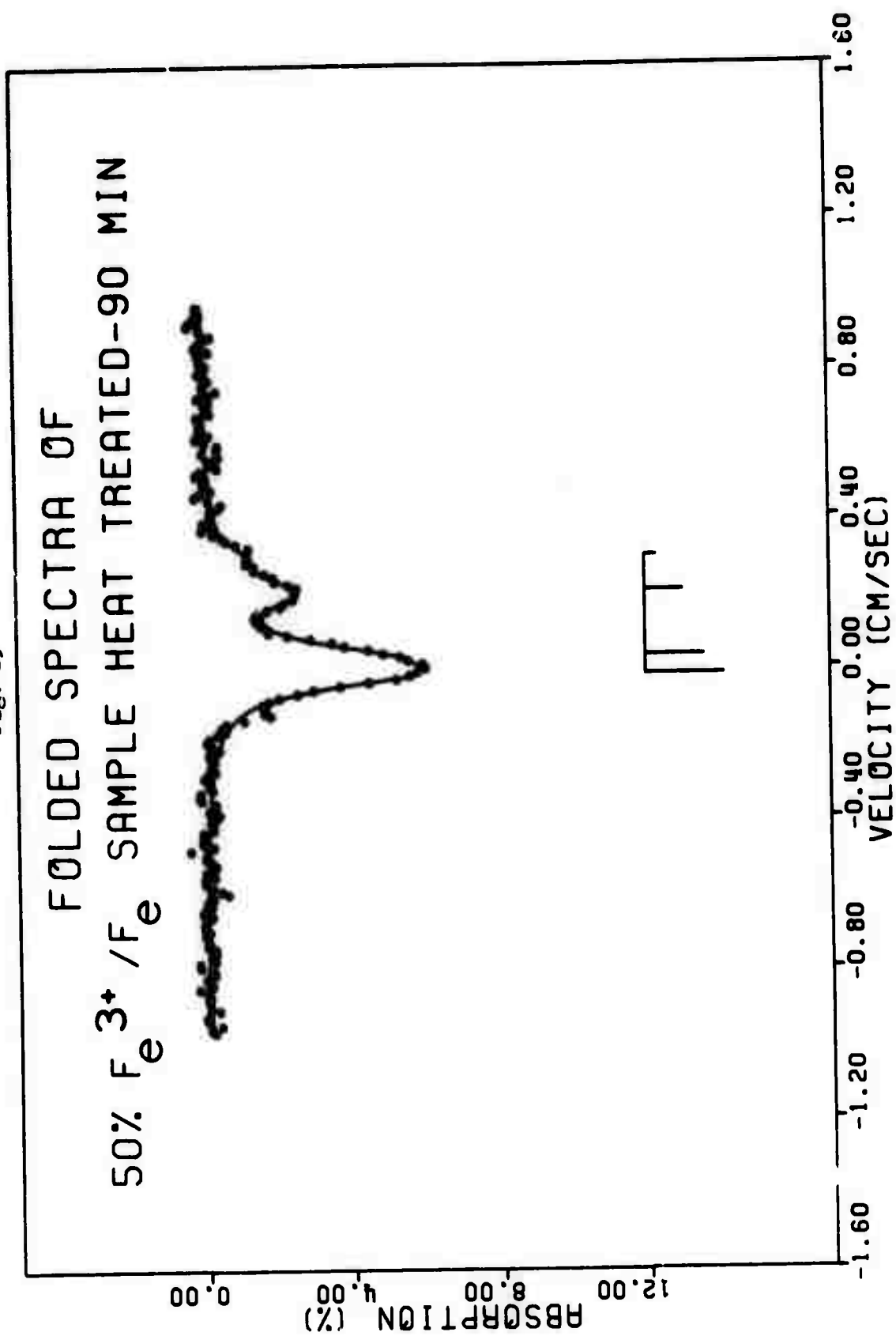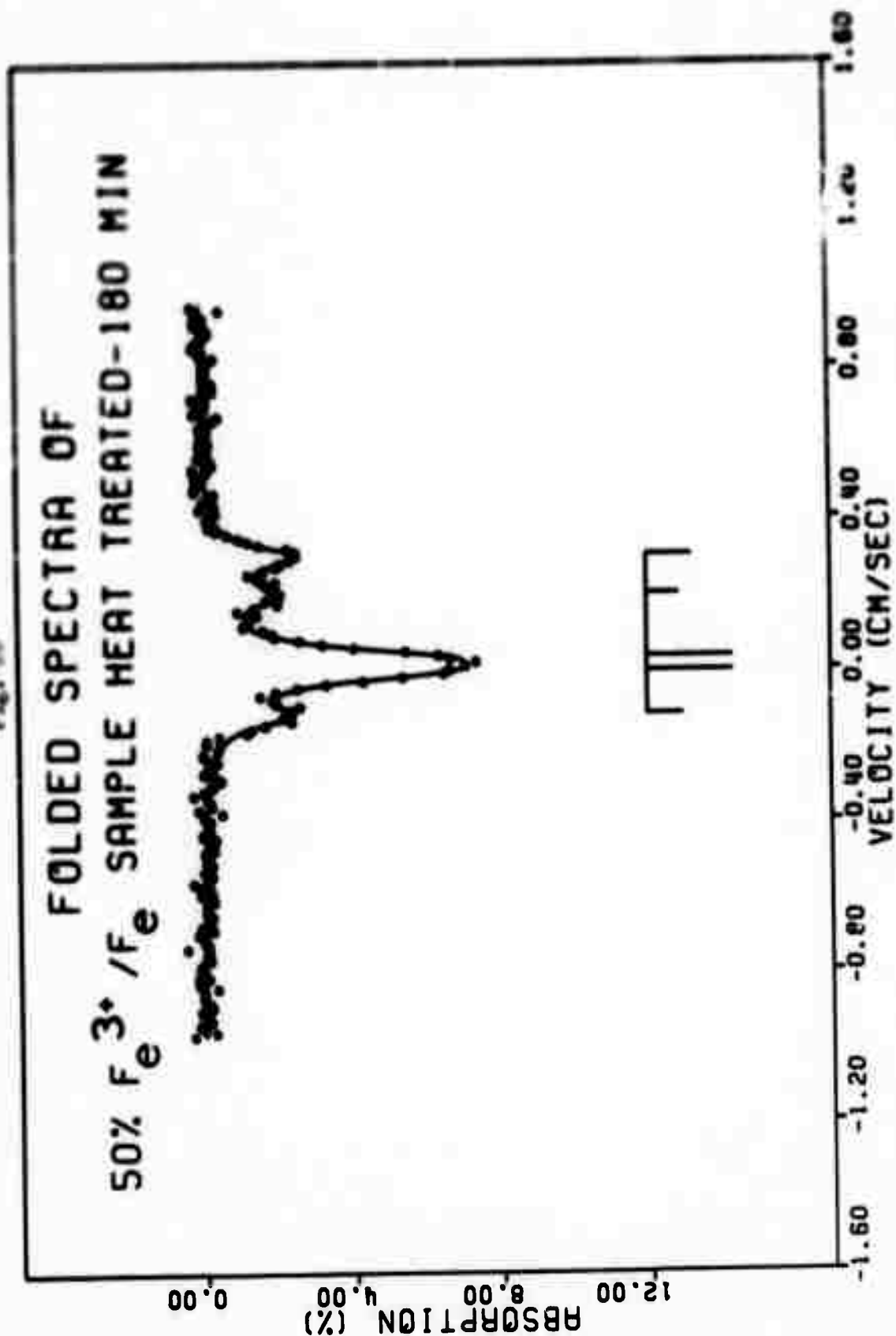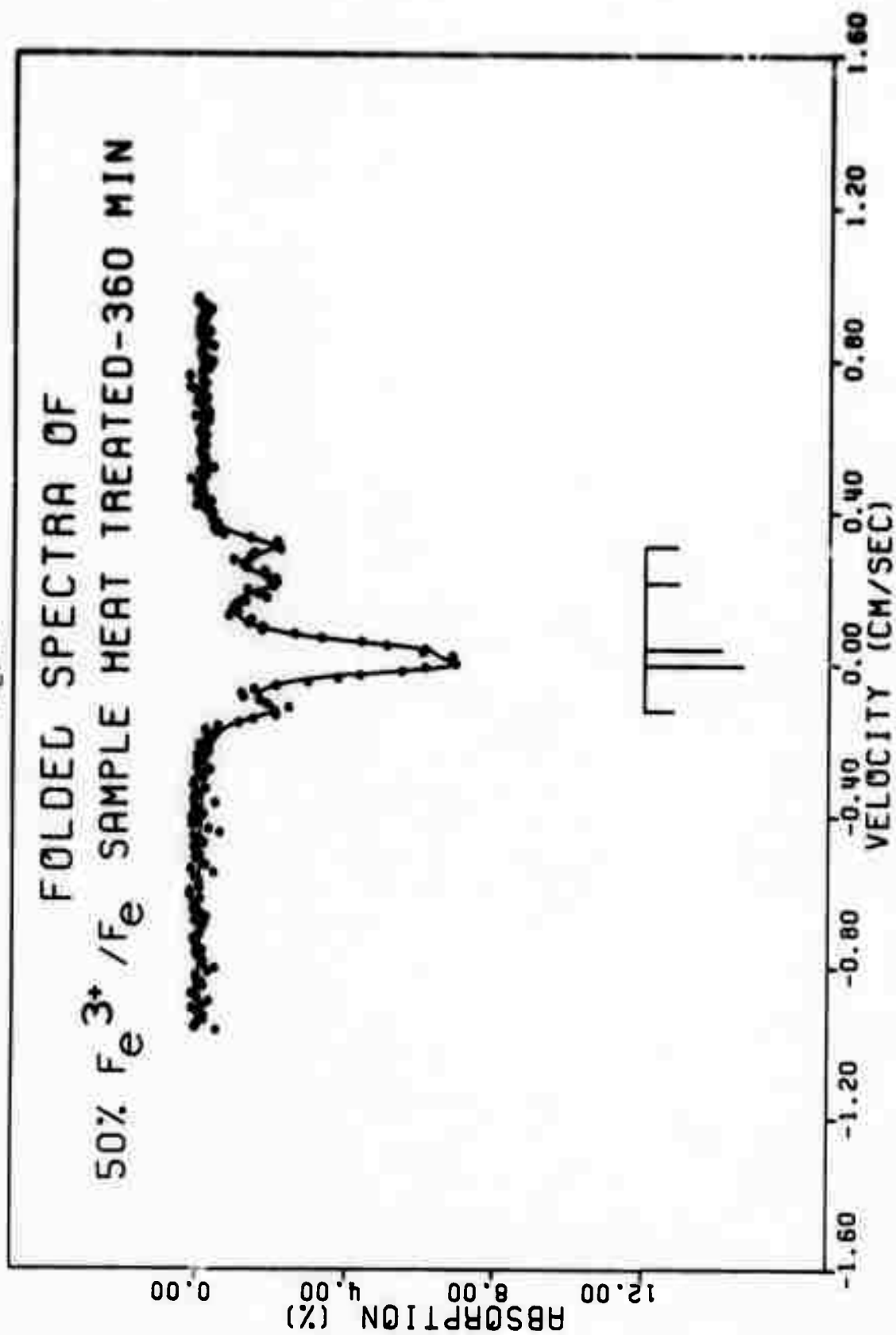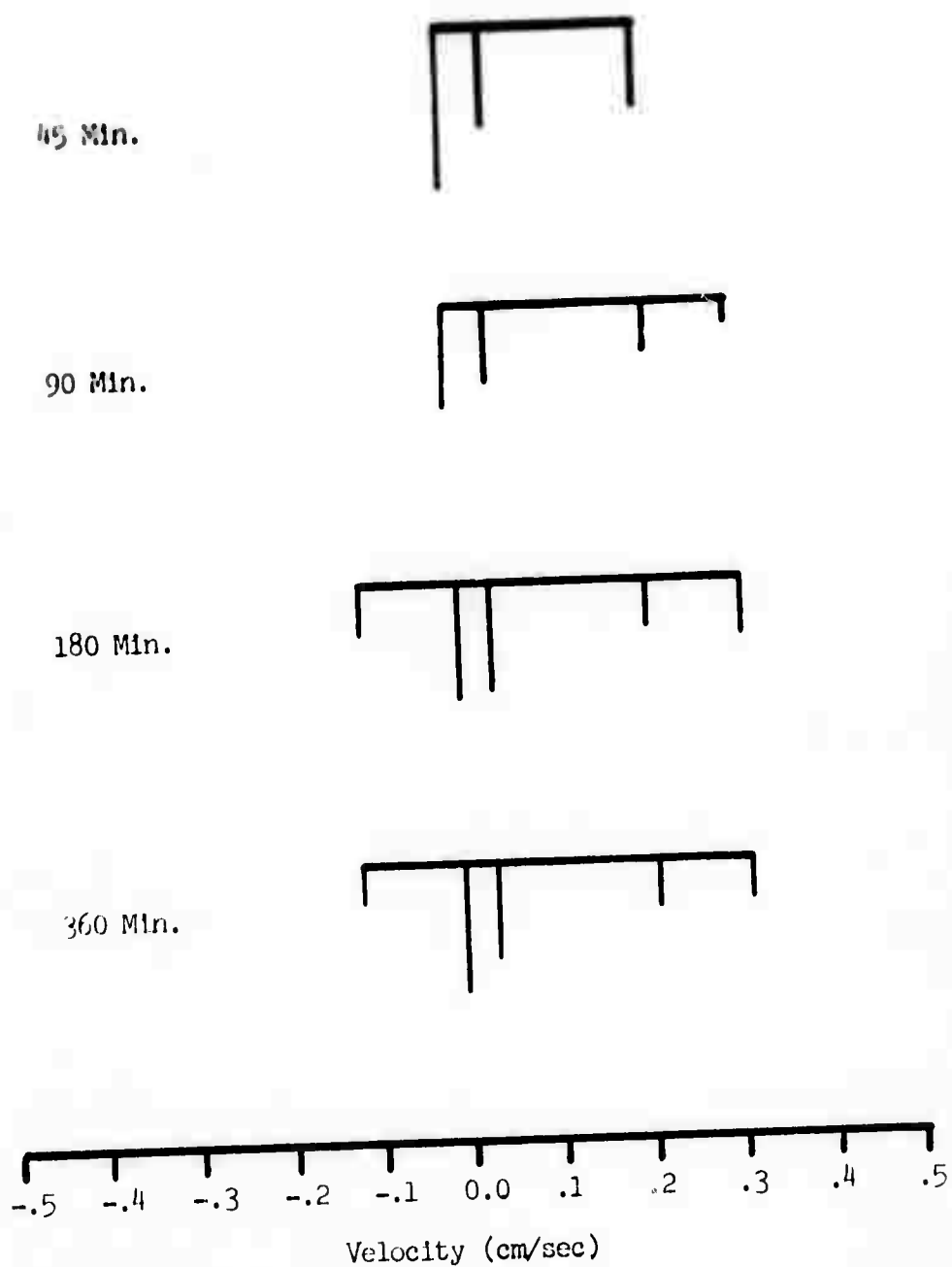
Fig. 22 Relative positions and amplitudes for the lines of the heat treated samples.

increased, the individual lines become more apparent and display the
natural line half-width. It is reasonable to assume that since the
final half-width value for the heat treated sample compares favorably
with the value before heat treating, that most of the superpositions
have been disclosed. However, a more drastic heat treatment using
larger amounts of the sample at a longer time and at the same tempera-
ture may yield other interesting information.

Chemical Analysis

As previously mentioned, the ratio, Fe^{3+}/Fe, may be obtained as
the ratio of the trivalent doublet area to the area of the entire spec-
trum. Since the accuracy of this method has been verified by quantita-
tive chemical analysis, it was decided to use the concentration value
obtained from the line area ratio throughout the analysis of all the
data.

CHAPTER V

DISCUSSION OF RESULTS AND CONCLUSIONS

In an amorphous sample with a high concentration of a paramag-
netic ions, as is present in the 55-45 mole % $FeO-P_2O_5$ glass, numerous
forms of Fe ions may be present simultaneously making interpretation
of the Mössbauer spectra quite difficult. Retaining the assumption
made in Chapter 4 that all of the ion states are in equilibrium, either
ion may act as the predominate vitrifier with the formation of stable
groups of either the divalent or the trivalent type, dependent on the
amount of Fe_2O present. Considering ligand field stabilization in $3d^6$
ions, Fe^{2+} might be expected to display octahedral coordination in
glasses. However, since it is known that Ni^{2+} occurs tetrahedrally co-
ordinated in some glasses, the possibility exists that Fe^{2+} may act
similarly. With regard to the high concentration of iron in the samples
subject to the present discussion, one could expect numerous interac-
tions between neighboring Fe^{3+} ions, between Fe^{3+} and Fe^{2+} ions, and be-
tween neighboring Fe^{2+} ions. Heat treatment could result in the perci-
pitation of several crystalline oxides as shown by Asm,[43] Bamford,[44] and
Belyustin et al.[27] Finally, it is recalled that these oxides may al-
ready be present in the colloid-disperse state. This state is most pro-
bable at high iron concentrations.[44]

Examination of Figures 8, 9, 10, 11, and 12 suggests that the
overall structure of the glass is not greatly affected by concentration

ratio of either ion present. Recalling Figure 4 and Tables I and II, the isomer shift values of approximately 0.10 and 0.020-0.045 for the divalent and trivalent doublets are consistent with other phosphate glasses and are characteristic of octahedral coordination for both ions. The fact that the divalent shift remains invariant with changes in concentration would tend to show that the electronic structure associated with these ions, particularly their 4s wave functions, are relatively free from co-valency changes due to the concentration of either ion. However, the decrease of isomer shift for the trivalent ion with a decrease in the Fe^{3+}/Fe ratio suggests an increase in the 4s electron density which would essentially amount to an increase in covalency associated with the Fe^{3+} ion. One might therefore surmise that any co-valency or coupling effects that are being observed would involve only neighboring trivalent ions. This is, however, an idea not completely consistent with the quadrupole splitting data.

The experimental ranges of quadrupole splitting values of 0.046-0.097 and 0.210-0.270 cm/sec for the Fe^{3+} and Fe^{2+} ions, respectively, are in good agreement with the values of Kurkjian and Sigety[24] of 0.032-0.088 and 0.200-0.229 cm/sec for octahedral coordination. This does verify the earlier conclusions concerning the coordination states of the two ions. However, it is noticed that both the curves of Figure 5-4 vary in a quite similar manner. It is recalled that the electric field gradient for the ferrous iron case is due to a ^5D electron configuration, whereas the field gradient in the ferric iron with a ^6S configuration is due primarily to nearby lattice contributions. The similarity

in the dependence of the quadrupole splitting on the Fe^{3+}/Fe ratio of the two ions might, then, be a result of a lesser interatomic distance in highly coupled ion pairs in a mixture rich with the smaller Fe^{3+} ion. One could then conclude that most of the ion pairs are antiferromagnetically complex Fe^{3+}-Fe^{2+}, in agreement with Friebele, Wilson, Dozier, and Kinser,[42] who studied these glasses by means of magnetic resonance technique. The spectra at 78° are more difficult to interpret. While work done on $Fe(PO_3)_3$ glass with 0.1-5.0 mole % Fe_2O_3(80% Fe^{3+}/Fe) by Kurkjian and Buchanan[26] showed little difference in spectra obtained at 78° and 300°K, the high iron concentrations yield definite changes at the two temperatures. In addition, it would appear that the differences are more precisely attributable to the increase in the concentration of the divalent ion (decrease in the Fe^{3+}/Fe ratio). While the curves of Figures 13, 14, and 15 were fitted with four lines with large values of half-widths, it is conceivable that the 50% and 15% Fe^{3+}/Fe spectra are rather a combination of central Fe^{3+} and Fe^{2+} doublets and a 6-line hyperfine set. Since the glass is known to be predominately paramagnetic this would resemble the results of Kurkjian and Buahanan[26] at 4°K which were explained in terms of either a short range magnetic alignment or a long electronic relaxation time which would remove the nuclear spin degeneracy and lead to Hfs. More experimentation with various other iron concentrations and other Fe^{3+}/Fe ratios at more temperatures would be valuable in resolving this question.

Heat treatment of the glasses showed the appearance of new lines which may be interpreted as a large central doublet superimposed on at

least one 6-line hyperfine structure. The similarity of this data to that obtained by Belyustin et al.[27] for the inverted spinel structure of Fe_3O_4 and the data for the crystal $FePO_4$ from Figure 4 indicates that a mixture of these two crystalline phases is being observed. This was also the conclusion of Friebele et al.[42] on the basis of x-ray diffraction measurements. Heat treatment of the 15% Fe^{3+}/Fe was not examined as this would probably produce other crystalline phases further complicating the spectra.

APPENDIX I

TABULATED COMPUTER ANALYSIS DATA

MOSSBAUER SPECTRUM PARAMETERS

TITLE: FOLDED SPECTRA OF .001 IRON FOIL AT ROOM TEMP

INITIAL ESTIMATES
(OBTAINED FROM "SEARCH" INPUT)

	VELOCITY(CM/SEC)	AMPLITUDE(%)
1:	-.6600	11.5442
2:	-.3850	9.6374
3:	-.1210	5.9226
4:	.0550	6.7412
5:	.3190	9.5457
6:	.5940	12.1306

USER ESTIMATE OF LINE HALF WIDTH=   .0400 CM/SEC
...ADDITIONAL CHANNEL CORRECTIONS ARE:
    10, 11, 32, 43, 45, 97,185,197,250,251,
269,271,272,314,316,322,335,

--NO VARIABLE CORRELATIONS REQUESTED--

AFTER ITERATION NO.   4

	VELOCITY(CM/SEC)	AMPLITUDE(%)	RELATIVE AREA
1:	-.6553	11.8303	2.4096
2:	-.3836	9.1199	1.8576
3:	-.1222	4.9096	1.0000
4:	.0614	5.7212	1.1653
5:	.3225	9.1054	1.8546
6:	.5928	12.1666	2.4781

FIT VALUE OF HALF WIDTH=   .0452 CM/SEC
MEAN SQUARED ERROR OF FIT PROCEDURE=   .4876 % ABSORPTION
DATA NOISE LEVEL=   .3440 % ABSORPTION

```
................................
MØSSBAUER SPECTRUM PARAMETERS
................................
```

TITLE: FOLDED SPECTRA OF 50% Fe^{3+}/β SAMPLE AT 300 K

INITIAL ESTIMATES
(OBTAINED FROM EXTERNAL INPUT)

	VELOCITY(CM/SEC)	AMPLITUDE(%)
1:	-.0465	6.8350
2:	-.0160	24.3370
3:	.0536	24.3370
4:	.2111	6.8350

USER ESTIMATE OF LINE HALF WIDTH=   .0400 CM/SEC
...ADDITIONAL CHANNEL CORRECTIONS ARE:
    188.

VARIABLE CORRELATIONS USED IN FIT PROCEDURE

DEPENDENT	INDEPENDENT	RATIO
AMP(1)	AMP(4)	1.000
AMP(2)	AMP(3)	1.000

AFTER ITERATION NØ.   5

	VELOCITY(CM/SEC)	AMPLITUDE(%)	RELATIVE AREA
1:	-.0307	5.2661	1.0216
2:	-.0134	5.1548	1.0000
3:	.0531	5.1548	1.0000
4:	.2063	5.2661	1.0216

FIT VALUE ØF HALF WIDTH=   .0327 CM/SEC
MEAN SQUARED ERRØR ØF FIT PRØCEDURE=   .2614 % ABSØRPTIØN
DATA NØISE LEVEL=   .3301 % ABSØRPTIØN

```
*******************************
MOSSBAUER SPECTRUM PARAMETERS
*******************************
```

TITLE: FOLDED SPECTRA OF 1%E Fe^{3+}/Fe SAMPLE AT 300 K

```
*INITIAL ESTIMATES*
(OBTAINED FROM EXTERNAL INPUT)
```

	VELOCITY(CM/SEC)	AMPLITUDE(%)
1:	-.0200	7.1460
2:	-.0200	1.0390
3:	.0053	1.0390
4:	.9064	7.1460

USER ESTIMATE OF LINE HALF WIDTH=   .0300 CM/SEC
...ADDITIONAL CHANNEL CORRECTIONS ARE:
113,115,117,129,131,133,

```
*VARIABLE CORRELATIONS USED IN FIT PROCEDURE*
```

DEPENDENT	INDEPENDENT	RATIO
AMP(1)	AMP(4)	1.000
VEL(2)	VEL(1)	1.000
AMP(2)	AMP(3)	1.000

```
*AFTER ITERATION NO.  40
```

	VELOCITY(CM/SEC)	AMPLITUDE(%)	RELATIVE AREA
1:	-.0184	7.1556	5.9345
2:	-.0184	1.2058	1.0000
3:	.0280	1.2058	1.0000
4:	.1987	7.1556	5.9345

FIT VALUE OF HALF WIDTH=   .0405 CM/SEC
MEAN SQUARED ERROR OF FIT PROCEDURE=   .3390 % ABSORPTION
DATA NOISE LEVEL=   .3932 % ABSORPTION

```
********************************
    MOSSBAUER SPECTRUM PARAMETERS
********************************
```

TITLE: FOLDED SPECTRA OF THE Fe^{3+}/Fe SAMPLE AT 300 K

```
        *INITIAL ESTIMATES*
    (OBTAINED FROM "SEARCH" INPUT)
```

	VELOCITY(CM/SEC)	AMPLITUDE(%)
1)	-.0441	9.5345
2)	-.0194	12.1000
3)	.0561	9.5907
4)	.2229	9.5958

USER ESTIMATE OF LINE HALF WIDTH= .0300 CM/SEC
...ADDITIONAL CHANNEL CORRECTIONS ARE:
384.

```
    *VARIABLE CORRELATIONS USED IN FIT PROCEDURE*
```

DEPENDENT	INDEPENDENT	RATIO
AMP(1)	AMP(4)	1.000
AMP(2)	AMP(3)	1.000

```
        *AFTER ITERATION NO.  5*
```

	VELOCITY(CM/SEC)	AMPLITUDE(%)	RELATIVE AREA
1)	-.0424	2.3932	1.0000
2)	-.0210	8.8085	3.6806
3)	.0547	8.8085	3.6806
4)	.2105	2.3932	1.0000

FIT VALUE OF HALF WIDTH=   .0398 CM/SEC
MEAN SQUARED ERROR OF FIT PROCEDURE=   .2345 % ABSORPTION
DATA NOISE LEVEL=   .2760 % ABSORPTION

```
...............................
MOSSBAUER SPECTRUM PARAMETERS
...............................
```

TITLE: FOLDED SPECTRA OF 50% Fe $^{3+}$/Fe$_0$ SAMPLE HEAT TREATED-45 MIN

INITIAL ESTIMATES
(OBTAINED FROM "SEARCH" INPUT)

	VELOCITY(CM/SEC)	AMPLITUDE(%)
1:	-.0194	9.4974
2:	.0484	5.5911
3:	.2132	4.4083

USER ESTIMATE OF LINE HALF WIDTH=   .0300 CM/SEC

--NO VARIABLE CORRELATIONS REQUESTED--

AFTER ITERATION NO. 4

	VELOCITY(CM/SEC)	AMPLITUDE(%)	RELATIVE AREA
1:	-.0202	4.9609	1.8496
2:	.0366	4.0757	1.0530
3:	.2040	3.7635	1.0000

FIT VALUE OF HALF WIDTH=   .0492 CM/SEC
MEAN SQUARED ERROR OF FIT PROCEDURE=   .2770 % ABSORPTION
DATA NOISE LEVEL=   .5609 % ABSORPTION

```
---------------------------------
MOSSBAUER SPECTRUM PARAMETERS
---------------------------------
```

TITLE: FOLDED SPECTRA OF 50% Fe^{3+}/Fe SAMPLE HEAT TREATED-90 MIN

INITIAL ESTIMATES
(OBTAINED FROM EXTERNAL INPUT)

	VELOCITY(CM/SEC)	AMPLITUDE(%)
1:	-.0146	7.2150
2:	.0312	4.9430
3:	.2133	1.8840
4:	.3028	5.0000

USER ESTIMATE OF LINE HALF WIDTH=   .0300 CM/SEC

--NO VARIABLE CORRELATIONS REQUESTED--

AFTER ITERATION NO.   4

	VELOCITY(CM/SEC)	AMPLITUDE(%)	RELATIVE AREA
1:	-.0176	4.2372	7.2340
2:	.0330	3.1865	5.4401
3:	.2045	2.0926	3.5725
4:	.2966	.5857	1.0000

FIT VALUE OF HALF WIDTH=   .0463 CM/SEC
MEAN SQUARED ERROR OF FIT PROCEDURE=   .1852 % ABSORPTION
DATA NOISE LEVEL=   .4035 % ABSORPTION

107

MØSSBAUER SPECTRUM PARAMETERS

TITLE: FØLDED SPECTRA ØF 50% Fe^{3+}/Fe SAMPLE HEAT TREATED-360 MIN

INITIAL ESTIMATES
(ØBTAINED FRØM "SEARCH" INPUT)

	VELØCITY(CM/SEC)	AMPLITUDE(%)
1:	-.1163	2.1064
2:	.0000	7.2136
3:	.0388	3.6660
4:	.2229	1.7933
5:	.3004	2.3393

USER ESTIMATE ØF LINE HALF WIDTH=   .0300 CM/SEC
...ADDITIØNAL CHANNEL CØRRECTIØNS ARE:
    299,

--NØ VARIABLE CØRRELATIONS REQUESTED--

AFTER ITERATIØN NØ.   4

	VELØCITY(CM/SEC)	AMPLITUDE(%)	RELATIVE AREA
1:	-.1235	1.5153	1.0000
2:	-.0046	5.2796	3.4842
3:	.0388	4.0952	2.7026
4:	.2128	1.7647	1.1646
5:	.3074	1.6838	1.1112

FIT VALUE ØF HALF WIDTH=   .0316 CM/SEC
MEAN SQUARED ERRØR ØF FIT PRØCEDURE= .1993 % ABSØRPTION
DATA NØISE LEVEL=   .2722 % ABSØRPTION

```
----------------------------------
MØSSBAUER SPECTRUM PARAMETERS
----------------------------------
```

TITLE: FOLDED SPECTRA OF 50% Fe $^{3+}$/Fe SAMPLE HEAT TREATED-180 MIN

INITIAL ESTIMATES
(OBTAINED FROM EXTERNAL INPUT)

	VELOCITY(CM/SEC)	AMPLITUDE(%)
1:	-.1203	3.6620
2:	-.0034	9.2060
3:	.0359	8.5930
4:	.2013	3.2370
5:	.3017	4.2070

USER ESTIMATE OF LINE HALF WIDTH=   .0300 CM/SEC
...ADDITIONAL CHANNEL CORRECTIONS ARE:
    107,188,

--NO VARIABLE CORRELATIONS REQUESTED--

AFTER ITERATION NO.   4

	VELOCITY(CM/SEC)	AMPLITUDE(%)	RELATIVE AREA
1:	-.1188	1.8757	1.1177
2:	-.0040	4.6088	2.7464
3:	.0340	4.6060	2.7447
4:	.2005	1.6781	1.0000
5:	.3011	2.3581	1.4052

FIT VALUE OF HALF WIDTH=   .0329 CM/SEC
MEAN SQUARED ERROR OF FIT PROCEDURE=   .1971 % ABSORPTION
DATA NOISE LEVEL=   .4727 % ABSORPTION

```
------------------------------------
    MOSSBAUER SPECTRUM PARAMETERS
------------------------------------
```

TITLE: FOLDED SPECTRA OF 1% Fe^{3+}/Fe SAMPLE AT 77 K

INITIAL ESTIMATES
(OBTAINED FROM "SEARCH" INPUT)

	VELOCITY(CM/SEC)	AMPLITUDE(%)
1:	-.2642	2.4687
2:	-.0264	2.9533
3:	.2907	2.3783
4:	.5285	2.5774

USER ESTIMATE OF LINE HALF WIDTH=   .0300 CM/SEC
...ADDITIONAL CHANNEL CORRECTIONS ARE:
      38, 46, 47, 50, 51, 56, 99,107,145,146,
     155,156,163,308,309,352,398,

--NO VARIABLE CORRELATIONS REQUESTED--

AFTER ITERATION NO. 7

	VELOCITY(CM/SEC)	AMPLITUDE(%)	RELATIVE AREA
1:	-.3942	.9476	1.4559
2:	-.0183	1.6095	2.4729
3:	.4320	.8987	1.3809
4:	.6873	.6508	1.0000

FIT VALUE OF HALF WIDTH=   .2561 CM/SEC
MEAN SQUARED ERROR OF FIT PROCEDURE=   .2448 % ABSORPTION
DATA NOISE LEVEL=   .4833 % ABSORPTION

MOSSBAUER SPECTRUM PARAMETERS

TITLE: FOLDED SPECTRA OF 50% Fe $^{3+}$/Fe SAMPLE AT 77 K

INITIAL ESTIMATES
(OBTAINED FROM EXTERNAL INPUT)

	VELOCITY(CM/SEC)	AMPLITUDE(%)
1:	-.2836	2.0000
2:	-.0263	2.0000
3:	.2379	2.0000
4:	.4433	2.0000

USER ESTIMATE OF LINE HALF WIDTH= .0300 CM/SEC
...ADDITIONAL CHANNEL CORRECTIONS ARE:
77,273,274,326,343,344,

--NO VARIABLE CORRELATIONS REQUESTED--

AFTER ITERATION NO. 8

	VELOCITY(CM/SEC)	AMPLITUDE(%)	RELATIVE AREA
1:	-.2844	1.5606	1.3332
2:	-.0277	2.5282	2.1599
3:	.2312	1.2012	1.6242
4:	.4438	1.1705	1.0000

FIT VALUE OF HALF WIDTH= .1536 CM/SEC
MEAN SQUARED ERROR OF FIT PROCEDURE= .2339 % ABSORPTION
DATA NOISE LEVEL= .3174 % ABSORPTION

```
----------------------------------
MOSSBAUER SPECTRUM PARAMETERS
----------------------------------
```

TITLE: FOLDED SPECTRA OF 79% Fe $^{3+}$/Fe SAMPLE AT 77 K

INITIAL ESTIMATES
(OBTAINED FROM EXTERNAL INPUT)

	VELOCITY(CM/SEC)	AMPLITUDE(%)
1:	-.0454	1.0000
2:	.0154	5.2870
3:	.0979	4.5000
4:	.3140	1.4400

USER ESTIMATE OF LINE HALF WIDTH=   .0300 CM/SEC
...ADDITIONAL CHANNEL CORRECTIONS ARE:
      54,109,121,152,189,198,304,355,396,

--NO VARIABLE CORRELATIONS REQUESTED--

AFTER ITERATION NO. 6

	VELOCITY(CM/SEC)	AMPLITUDE(%)	RELATIVE AREA
1:	-.0455	4.1762	3.4245
2:	.0152	2.9273	2.4004
3:	.0978	3.5774	2.9335
4:	.3140	1.2195	1.0000

FIT VALUE OF HALF WIDTH=   .0449 CM/SEC
MEAN SQUARED ERROR OF FIT PROCEDURE=   .2228 % ABSORPTION
DATA NOISE LEVEL=   .4938 % ABSORPTION

112

APPENDIX II

MÖSSBAUER SPECTRUM ANALYSIS PROGRAM

The computer program listed in this appendix was used to analyse all of the data obtained in the present investigations. It is written in Fortran IV to be used with the XDS Sigma 7 computer. With the exception of several READ and WRITE statements in which arithmetic operations are performed, the program is compatible with any computer equipped with a standard USASI Fortran IV compiler and at least 45,000 words of high speed memory. Typical running times are two minutes for compilation and 1.5 minutes for execution. All input is read on the F:5 DCB and all output is written on the F:6 DCB. If a Calcompu plot of the problem is desired, it is obtained by assigning the F:PLOT DCB to the drum plotter.

A solution is obtained by correcting the initial estimates for the parameters of up to 10 separate spectral lines to give a least-square best fit approximation to the experimental data. Initial estimates may be supplied either internal or external to the program and the output is in the form of Appendix I. Additionally, the line parameters may be made interdependent. Use of the program requires the following input cards:

      1st card - (Format I1) plotter option

            (a) 0, no plot desired

            (b) 1, plot on device assigned to F:PLOT

2nd card - (Format I2, 15A4) number of characters in the title string (no more than 20), title string

3rd card - (Format 2I5, 2F10.5, I1) number of points in raw data (no more than 400), number of peaks to be fit (no more than 10), approximation of line half-width (in cm/sec, if negative then not varied in fit procedure), velocity scale (in cm/sec, positive or negative), option code:

 (a) 0, no options requested

 (b) 1, options requested as listed on next card

4th card - (if option code is 1) - (Format 6I2, F10.5) options in order left to right are marked with 1 is requested 0 or blank if not requested, or as specified below:

 (a) number of bad channels to be corrected (default to 0)

 (b) printing of each iteration of fit procedure (default prints only last iteration)

 (c) folding code: -1 for data in left half, + 1 for data in right half, 0 if data is to be folded about middle channel (default to 0)

 (d) search procedure which generates initial parameters for the number of spectral lines specified previously (default requires estimates to be input separately)

 (e) parameter correlation option, input no. of

correlations desired. Actual correlations listed
below (default is no correlations)

(f) maximum number of iterations allowed (default
is 99)

(g) convergence criterion (default is 0.0001)

The following cards supply additional information for the execution of
options (a), (d), (e). The additional data cards for an option must
appear if that option is requested and in the order listed below:

(i) channels which are to be corrected are listed on
successive cards (Format 10I5). The count value for a corrected
channel is made equal to the mean count value of the two adjac-
ent channels. Adjacent bad channels may not be corrected.

(ii) this card must appear regardless of the number of
options requested. It defines the Format in which the raw data
is to appear later. The Format appears as a legal FORTRAN IV
statement with enclosing parentheses.

(iii) Correlations are expressed in terms of an inde-
pendent variable, a dependent variable, and a multiplicitive
ratio which relates them. A spectral line is specified by two
parameters, position and amplitude. Considering (N) lines or-
dered by ascending velocity, the line parameters are numbered
from 1 through (2N) such that the odd numbers represent velocity
parameters and the even numbers represent amplitude parameters.
Each correlation is placed on a separate card, (Format 2I5,
F10.5), giving the dependent parameter number, the independent

parameter number, and the desired ratio (dependent/independent). For example, constraining the amplitude of the third line to be twice the amplitude of the fifth line would be written as,

$$6 \; . \; . \; . \; 10 \; . \; . \; . \; . \; . \; 2.0$$

Three parameters may be correlated together by correlating any two with the third.

      (iv) the initial estimates are input using a separate card for each spectral line. The position (cm/sec) and amplitude (0.01 x percentage absorption) are written using a Format (2F10.5).

In all cases the number of extra data values or cards must coincide with the values found on the option card. Immediately following the last of the extra data cards, the raw data is added, written to the Format that was previously specified.

```
      DIMENSIØNX(202),Y(202),C(22),NAME(15),IBUF(1000),DATA(
     $500),KIND(15
     &),ICR(200),IFØRMT(10),CMAT(22,22)
      CØMMØNNAME,M,IPT,MVAR,CMAT
      CØMMØN/FI/X,Y,C,DEL,N,MAX,GAMMA
      DATAKIND/'1ST ','HALF',' FØ','LDED','2ND ','HALF',' S
     SPF',
     &'CTRA',' ØF ','"SEA','RCH"','EXTE','RNAL','VEL(','AMP(
     $'/
      CALLAUTØEX
      READ(5,1180)IPLØT
      IF(IPLØT.EQ.1)CALLPLØTS(IBUF,1000,1)
      NAME(3)=KIND(7)
      NAME(4)=KIND(8)
      NAME(5)=KIND(9)
 1000 READ(5,1270,END=1170)NCHAR,(NAME(I),I=6,15)
      READ(5,1290)NPTS,NPK,GAMMA,VEL,ØPTION
      C(2*NPK+1)=ABS(GAMMA)
      C(2*NPK+2)=0.
      M=2*NPK+2
      DØ1010II=1,M
      DØ1010JJ=1,M
      IF(II.NE.JJ)CMAT(II,JJ)=0.
 1010 IF(II.EQ.JJ)CMAT(II,JJ)=1.
      NBAD=0
      IPT=0
      IFØLD=0
      MAX=99
      DEL=.0001
      ISERCH=0
      IF(ØPTION.GT.0)READ(5,1300)NBAD,IPT,IFØLD,ISERCH,ICØRR
     $,MAX,DEL
      IF(NBAD.NE.0)READ(5,1310)(ICR(II),II=1,NBAD)
      READ(5,1280)IFØRMT
      IF(ISERCH.NE.0)READ(5,1190)(C(2*II-1),C(2*II),II=1,NPK
     $)
      IF(ICØRR.EQ.0.)GØTØ1030
      DØ1020IC=1,ICØRR
      READ(5,1200)JDEP,INDEP,RATIØ
      CMAT(JDEP,JDEP)=0.
      CMAT(JDEP,INDEP)=RATIØ
 1020 CMAT(INDEP,JDEP)=RATIØ
 1030 READ(5,IFØRMT)(DATA(I),I=1,NPTS)
      IF(NBAD.EQ.0)GØTØ1070
 1040 DØ1060I=1,NBAD
      IF(ICR(I).EQ.1.ØR.ICR(I).EQ.NPTS)GØTØ1050
C     IF(ICR(I).EQ.ICR(I+1)-1)GØ TO 50
```

```
      DATA(ICB(I))=(DATA(ICB(I)-1)+DATA(ICB(I)+1))*.5
      GØTØ1060
1050  IF(ICB(I).EQ.1)DATA(1)=(DATA(2)+DATA(3))*.5
      IF(ICB(I).EQ.NPTS)DATA(NPTS)=(DATA(NPTS-1)+DATA(NPTS-2
     $))*.5
1060  CØNTINUE
1070  CØNTINUE
      NBAD=0
      NX=NPTS-1
      DØ1080NY=2,NX
      AVGE=(DATA(NY-1)+DATA(NY+1))*.5
      IF(ABS(DATA(NY)-AVGE).LT.AVGE*.01)GØTØ1080
      NBAD=NBAD+1
      NBADC=NBAD
      ICB(NBAD)=NY
1080  CØNTINUE
      IF(NBAD.GT.0)GØTØ1040
      DV=.5
      CL=1.
      CR=1.
      IF(IFØLD.LT.0)CR=0.
      IF(IFØLD.GT.0)CL=0.
      IF(IFØLD.NE.0)DV=1.
      N=(NPTS+1)/2
      DØ1090I=1,N
      JP=NPTS+1-I
1090  Y(I)=DV*(CL*DATA(I)+CR*DATA(JP))
      JO=(IFØLD+1)*2+1
      NAME(1)=KIND(JO)
      NAME(2)=KIND(JO+1)
      DELV=2*ABS(VEL)/N
      X(1)=-(ABS(VEL))
      DØ1100I=2,N
1100  X(I)=X(I-1)+DELV
      YMAX=Y(1)
      DØ1110I=1,N
1110  IF(Y(I).GT.YMAX)YMAX=Y(I)
      DØ1120I=1,N
1120  Y(I)=1.-Y(I)/YMAX
      IF(ISERCH.EQ.0)CALLSEARCH(X,Y,C,N,NPK)
      ISERCH=ISERCH*2
      WRITE(6,1210)(NAME(I),I=1,15),KIND(ISERCH+10),KIND(ISE
     SRCH+11),(JK,
     &C(2*JK-1),100.*C(2*JK),JK=1,NPK)
      WRITE(6,1220)C(2*NPK+1)
      IF(NBADC.GT.0)WRITE(6,1230)(ICB(IY),IY=1,NBADC)
      IF(ICØRR.NE.0)GØTØ1130
```

118

```
         WRITE(6,1240)
         GOTO1160
1130  WRITE(6,1250)
         DO1150IC=1,M
         IF(CMAT(IC,IC).EQ.1)GOTO1150
         DO1140IJ=1,M
         IF(CMAT(IC,IJ).EQ.0.)GOTO1140
         IP1=0
         IP2=0
         IF(MOD(IC,2).EQ.0.)IP1=1
         IF(MOD(IJ,2).EQ.0.)IP2=1
         IC1=(IC+1)/2
         IJ1=(IJ+1)/2
         WRITE(6,1260)KIND(14+IP1),IC1,KIND(14+IP2),IJ1,CMAT(IC
      S,IJ)
1140  CONTINUE
1150  CONTINUE
1160  CALLFIT
         IF(IPLOT.EQ.1)CALLGRAPH(Y,X,C,NAME,N,NPK,IBUF,NCHAR)
         GOTO1000
1170  IF(IPLOT.EQ.1)CALLPLOT(0.,0.,999)
         CALLEXIT
1180  FORMAT(I1)
1190  FORMAT(2F10.5)
1200  FORMAT(2I5,F10.5)
1210  FORMAT(////////22X,29('-')//,22X,'MOSSBAUER SPECTRUM PAR
      SAMETERS'//,22
      &X,29('-')//,5X,'TITLE: ',15A4///,28X,'*INITIAL ESTIMAT
      SES*'/,23X,'(
      &OBTAINED FROM ',2A4,' INPUT)'//,16X,'VELOCITY(CM/SEC)'
      S,14X,
      &'AMPLITUDE(%)'/,16X,16('-'),14X,12('-')/,(12X,I2,':',4
      SX,F8.4,21X,
      &F8.4))
1220  FORMAT(/5X,'USER ESTIMATE OF LINE HALF WIDTH=',3X,F7.4
      S,' CM/SEC')
1230  FORMAT(5X,'...ADDITIONAL CHANNEL CORRECTIONS ARE:'/(10
      SX,10(I3,',')
      &))
1240  FORMAT(///17X,'--NO VARIABLE CORRELATIONS REQUESTED--')
1250  FORMAT(///12X,'*VARIABLE CORRELATIONS USED IN FIT PROC
      SEDURE*'//,13X
      &,'DEPENDENT',8X,'INDEPENDENT',10X,'RATIO'//,13X,9('-'),
      S8X,11('-'),1
      &0X,5('-'))
1260  FORMAT(14X,A4,I2,')',11X,A4,I2,')',10X,F7.3)
1270  FORMAT(I2,15A4)
```

```
1280 FØRMAT(10A4)
1290 FØRMAT(2I5,2F10.5,I1)
1300 FØRMAT(6I2,F10.5)
1310 FØRMAT(10I5)
     END
C
C
     SUBRØUTINESEARCH(X,Y,C,N,NPK)
     DIMENSIØNX(202),Y(202),C(22),DUM(202)
     DO2000I=1,N
2000 DUM(I)=Y(I)
     NVAR=2*NPK
     DO2020I=2,NVAR,2
     C(I)=0.
     DO2010J=1,N
     IF(C(I).GT.DUM(J))GØTO2010
     C(I)=DUM(J)
     C(I-1)=X(J)
2010 CØNTINUE
     DO2020J=1,N
2020 DUM(J)=DUM(J)-RNTZ(X(J),C(I),C(I-1),C(NVAR+1))
     DO2050K=2,NVAR,2
     IF(NPK-1)2030,2060,2030
2030 DO2050L=4,NVAR,2
     IF(C(L-1).GE.C(L-3))GØTO2040
     CP=C(L-3)
     CA=C(L-2)
     C(L-3)=C(L-1)
     C(L-2)=C(L)
     C(L-1)=CP
     C(L)=CA
2040 CØNTINUE
2050 CØNTINUE
2060 RETURN
     END
C
C
     SUBRØUTINEFIT
     DIMENSIØNA(22,22),B(22),C(22),P(202,22),R(202),X(202),
    $Y(202),NAME(
    &15),AREA(10),CMAT(22,22)
     CØMMØNNAME,M,IPT,MVAR,CMAT
     CØMMØN/FI/X,Y,C,DEL,N,MAX,GAMMA
     CØMMØN/SØ/A,B,MA
     AR=0.
     MA=1
     IT=0
```

```
3000 EL=AR
     CALLCORRECT(CMAT,C,MVAR,M)
     AR=0.
     DO30101I=1,N
3010 AR=AR+(Y(I)-VAL(I))**2
     IF(IPT.GE.1.AND.IT.NE.0)WRITE(6,3170)IT,AR,(I,C(I),I=1
    $,M)
     IF(IT.LE.0)GOTO3020
     IF(ABS(AR-EL)/AR.LE.DEL)GOTO3110
     IF(IT.GE.MAX)GOTO3100
3020 IT=IT+1
     DO30301I=1,N
     R(I)=VAL(I)-Y(I)
     DO3030J=1,MVAR
     P(I,J)=PART(I,J)
3030 CONTINUE
     DO30401I=1,MVAR
     B(I)=0.0
     DO3040J=1,MVAR
3040 A(I,J)=0.0
     DO30601I=1,MVAR
     DO3060J=1,N
     DO3050K=1,MVAR
3050 A(I,K)=A(I,K)+P(J,I)*P(J,K)
3060 B(I)=B(I)-P(J,I)*R(J)
3070 CALLSOLVE(I,IK)
     GOTO(3080,3110),IJK
3080 IPOINT=1
     DO30901I=1,M
     IF(CMAT(I,I).NE.1)GOTO3090
     C(I)=B(IPOINT)+C(I)
     IPOINT=IPOINT+1
3090 CONTINUE
     IF(GAMMA.LT.0)C(M-1)=ABS(GAMMA)
     GOTO3000
3100 WRITE(6,3180)MAX
     RETURN
3110 MHALF=(M-2)/2
     DO3120IAREA=1,MHALF
3120 AREA(IAREA)=C(M-1)*C(2*IAREA)*(ATAN((100.-C(2*IAREA-1)
    $)/C(M-1))-AT
    &AN((-100.-C(2*IAREA-1))/C(M-1)))
     ARMIN=AREA(1)
     DO31301IR=2,MHALF
3130 IF(AREA(IR).LT.ARMIN)ARMIN=AREA(IR)
     DO31401IR=1,MHALF
3140 AREA(IR)=AREA(IR)/ARMIN
```

```
      WRITE(6,3150)IT,(JK,C(2*JK-1),100.*C(2*JK),AREA(JK),JK
     S=1,MHALF)
      WRITE(6,3160)C(M-1),SORT(AR/N)*100.,C(M)*100.
      RETURN
3150  FORMAT(///24X,'*AFTER ITERATION NO. ',I2,'*'///,10X,'VE
     SLOCITY(CM/SE
     6C)',4X,'AMPLITUDE(%)',6X,'RELATIVE AREA'/,10X,16('-'),
     S4X,12('-'),
     &4X,13('-')/(6X,I2,'S',2X,F8.4,11X,F8.4,10X,F9.4))
3160  FORMAT(/5X,'FIT VALUE OF HALF WIDTH=',12X,F7.4,' CM/SE
     SC'/,5X,'MEAN
     & SQUARED ERROR OF FIT PROCEDURE=',F7.4,' % ABSORPTION'
     S,/5X,'DATA N
     4OISE LEVEL=',19X,F7.4,' % ABSORPTION')
3170  FORMAT(//'ITERATION'I3/12('-')/'SUM SQUARED ERROR ='1P
     SD15.8/
     &//(10X'C('0PI2,')='1PD15.7))
3180  FORMAT(//'****NO CONVERGENCE IN'I3,' ITERATIONS****')
      END
C
C
      SUBROUTINESOLVE(IJK)
      DIMENSIONA(22,22),B(22),C(22,22),NAME(15),L(22),MM(22)
     S,E(450),CMAT
     &(22,22)
      COMMONNAME,N,IPT,MVAR,CMAT
      COMMON/SO/A,B,M
      DOUBLEPRECISIONE,D,C,X
      IJK=1
      ICOUNT=1
      DO4000I=1,MVAR
      DO4000J=1,MVAR
      E(ICOUNT)=A(J,I)
 4000 ICOUNT=ICOUNT+1
      CALLMINV(E,MVAR,D,L,MM)
      ICOUNT=1
      DO4010I=1,MVAR
      DO4010J=1,MVAR
      C(J,I)=E(ICOUNT)
 4010 ICOUNT=ICOUNT+1
      IF(D.EQ.0)IJK=2
      IF(D.EQ.0)WRITE(6,4060)
      Z=0.0
      DO4030I=1,MVAR
      X=0.
      DO4020J=1,MVAR
 4020 X=C(I,J)*A(J,I)+X
```

```
4030  Z=Z+ABS(X-1.0)
      IF(Z.GT.1.E-03)WRITE(6,4070)Z
      IF(Z.GT.1.E-03)IJK=2
      DO4040I=1,MVAR
      A(I,1)=0.0
      DO4040J=1,MVAR
4040  A(I,1)=A(I,1)+C(I,J)+B(J)
      DO4050I=1,MVAR
4050  B(I)=A(I,1)
      RETURN
4060  FORMAT('INVERSE DOES NOT EXIST')
4070  FORMAT(2X,'INVALID INVERSE Z=',F8.5)
      END
C
C
C****  THE FOLLOWING SUBROUTINE SHOULD CALCULATE THE VALUE
C****  OF THE APPROXIMATING FUNCTION EVALUATED AT THE I-TH
C****  DATA POINT.
      FUNCTIONVAL(I)
      DIMENSIONNAME(15),X(202),Y(202),C(22),CMAT(22,22)
      COMMONNAME,M,IPT,MVAR,CMAT
      COMMON/FI/X,Y,C,DEL,N,MAX,GAMMA
      L=M-2
      VAL=0.
      DO5000J=1,L,2
      DX=(X(I)-C(J))/C(M-1)
      B=1./(1.+DX+DX)
5000  VAL=VAL+C(J+1)+B
      VAL=VAL+C(M)
      RETURN
      END
C
C
C****  THE FOLLOWING SUBROUTINE SHOULD CALCULATE THE VALUE
C****  OF THE PARTIAL OF THE APPROXIMATING FUNCTION WITH
C****  RESPECT TO THE J-TH VARIABLE, EVALUATED AT THE
C****  I-TH DATA POINT.
      FUNCTIONPART(I,J)
      DIMENSIONNAME(15),X(202),Y(202),C(22),CMAT(22,22)
      COMMON/FI/X,Y,C,DEL,N,MAX,GAMMA
      COMMONNAME,M,IPT,MVAR,CMAT
      PART=0.
      IMX=0
      DO6000JREAL=1,M
      IMX=IMX+CMAT(JREAL,JREAL)
      IF(IMX.EQ.J)GOTO6010
6000  CONTINUE
```

```
6010  IF(JREAL.EQ.M)GOTO6050
      IF(JREAL.EQ.M-1)GOTO6060
      IF(MOD(JREAL,2).EQ.0)GOTO6030
      DO6020IROW=1,M,2
      IF(CMAT(IROW,JREAL).EQ.0)GOTO6020
      DX=(X(I)-C(IROW))/C(M-1)
      B=1./(1.+DX*DX)
      PART=PART+2.*C(IROW+1)*DX*B*B/C(M-1)
6020  CONTINUE
      RETURN
6030  DO6040IROW=2,M,2
      IF(CMAT(IROW,JREAL).EQ.0)GOTO6040
      DX=(X(I)-C(IROW-1))/C(M-1)
      PART=PART+CMAT(IROW,JREAL)/(1.+DX*DX)
6040  CONTINUE
      RETURN
6050  PART=1.
      RETURN
6060  L=M-2
      DO6070K=1,L,2
      DX=(X(I)-C(K))/C(M-1)
      B=DX/(1.+DX*DX)
6070  PART=PART+C(K+1)*B*B
      PART=2.*PART/C(M-1)
      RETURN
      END
C
C
      SUBROUTINECORRECT(CMAT,C,MVAR,M)
      DIMENSIONCMAT(22,22),C(22)
      MVAR=M
      DO7010I=1,M
      IF(CMAT(I,I).EQ.1.)GOTO7010
      C(I)=0.
      DO7000J=1,M
      IF(CMAT(I,J).EQ.0)GOTO7000
      C(I)=C(I)+CMAT(I,J)*C(J)
7000  CONTINUE
      MVAR=MVAR-1
7010  CONTINUE
      RETURN
      END
C
C
C        SUBROUTINE MINV
C
C     PURPOSE
```

```
C           INVERT A MATRIX
C
C        USAGE
C           CALL MINV(A,N,D,L,M)
C
C        DESCRIPTION OF PARAMETERS
C           A-INPUT MATRIX, DESTROYED IN COMPUTATION AND REPLAC
SED BY
C              RESULTANT INVERSE
C           N-ORDER OF MATRIX A
C           D-RESULTANT DETERMINANT
C           L-WORK VECTOR OF LENGTH N
C           M-WORK VECTOR OF LENGTH N
C
C        REMARKS
C           MATRIX A MUST BE A GENERAL MATRIX
C
C        SUBROUTINES AND FUNCTION SUBPROGRAMS NEEDED
C           NONE
C
C        METHOD
C           THE STANDARD GAUSS-JORDAN METHOD IS USED.  THE DETE
SRMINANT
C           IS ALSO CALCUATED. A DETERMINANT OF ZERO INDICATES
STHAT
C           THE MATRIX IS SINGULAR.
C
C     ........................................................
S....
C
        SUBROUTINEMINV(A,N,D,L,M)
        DIMENSIONA(1),L(1),M(1)
C
C     ........................................................
S....
C
C        IF A DOUBLE PRECISION VERSION OF THIS ROUTINE IS DESIR
SED, THE
C        C IN COLUMN 1 SHOULD BE REMOVED FROM THE DOUBLE PPRECI
SSION
C        STATEMENT THAT FOLLOWS
C        DOUBLEPRECISIONA,D,BIGA,HOLD
C        THE DOUBLE PRECISION VERSION OF THIS ROUTINE MUST ALSO
C        CONTAIN DOUBLE PRECISION FORTRAN FUNCTIONS. ABS IN STA
STEMENT
C        10 MUST BE CHANGED TO DABS
C
```

```
C      ...............................................................
       S...
C
C        SEARCH FOR THE LARGEST ELEMENT
C
       D=1.0
       NK=-N
       D08180K=1,N
       NK=NK+N
       L(K)=K
       M(K)=K
       KK=NK+K
       BIGA=A(KK)
       D08020J=K,N
       IZ=N*(J-1)
       D08020I=K,N
       IJ=IZ+I
 8000 IF(DABS(BIGA)-DABS(A(IJ)))8010,8020,8020
 8010 BIGA=A(IJ)
       L(K)=I
       M(K)=J
 8020 CONTINUE
C
C          INTERCHANGE ROWS
C
       J=L(K)
       IF(J-K)8050,8050,8030
 8030 KI=K-N
       D08040I=1,N
       KI=KI+N
       HOLD=-A(KI)
       JI=KI-K+J
       A(KI)=A(JI)
 8040 A(JI)=HOLD
C
C          INTERCHANGE COLUMNS
C
 8050 I=M(K)
       IF(I-K)8080,8080,8060
 8060 JP=N*(I-1)
       D08070J=1,N
       JK=NK+J
       JI=JP+J
       HOLD=-A(JK)
       A(JK)=A(JI)
 8070 A(JI)=HOLD
C
```

```
C          DIVIDE COLUMN BY MINUS PIVOT (VALUE OF PIVOT ELEMEN
      ST IS
C          CONTAINED IN BIGA)
C
 8080 IF(BIGA)8100,8090,8100
 8090 D=0.0
      RETURN
 8100 DO8120I=1,N
      IF(I-K)8110,8120,8110
 8110 IK=NK+I
      A(IK)=A(IK)/(-BIGA)
 8120 CONTINUE
C
C          REDUCE MATRIX
C
      DO8150I=1,N
      IK=NK+I
      HOLD=A(IK)
      IJ=I-N
      DO8150J=1,N
      IJ=IJ+N
      IF(I-K)8130,8150,8130
 8130 IF(J-K)8140,8150,8140
 8140 KJ=IJ-I+K
      A(IJ)=HOLD*A(KJ)+A(IJ)
 8150 CONTINUE
C
C          DIVIDE ROW BY PIVOT
C
      KJ=K-N
      DO8170J=1,N
      KJ=KJ+N
      IF(J-K)8160,8170,8160
 8160 A(KJ)=A(KJ)/BIGA
 8170 CONTINUE
C
C          PRODUCT OF PIVOTS
C
      D=D*BIGA
C
C          REPLACE PIVOT BY RECIPROCAL
C
      A(KK)=1.0/BIGA
 8180 CONTINUE
C
C          FINAL ROW AND COLUMN INTERCHANGE
C
```

```
      K=N
8190  K=(K-1)
      IF(K)8260,8260,8200
8200  I=L(K)
      IF(I-K)8230,8230,8210
8210  JQ=N*(K-1)
      JR=N*(I-1)
      D08220J=1,N
      JK=JQ+J
      HOLD=A(JK)
      JI=JR+J
      A(JK)=-A(JI)
8220  A(JI)=HOLD
8230  J=M(K)
      IF(J-K)8190,8190,8240
8240  KI=K-N
      D08250I=1,N
      KI=KI+N
      HOLD=A(KI)
      JI=KI-K+J
      A(KI)=-A(JI)
8250  A(JI)=HOLD
      GOTO8190
8260  RETURN
      END
C
C
C
      SUBROUTINEGRAPH(C,V,CST,NAME,NP,NC,IBUF,NCHAR)
      DIMENSION Y(202),C(202),V(202),IBUF(1000),NAME(15),CST(
     $22),D1(10),D
     42(10),YSM(502),XSM(502)
      NC2=NC*2
      D09000I=1,NC
      D1(I)=CST(2*I-1)
9000  D2(I)=CST(2*I)*100./2
      D09010I=1,NP
      Y(I)=100.*VAL(I)
9010  C(I)=100.*C(I)
      XSM(1)=V(1)
      DELX=2*ABS(V(1))/500.
      D09020IS=2,500
9020  XSM(IS)=XSM(IS-1)+DELX
      D09030IS=1,500
      YSM(IS)=0.
      D09030JI=2,NC2,2
9030  YSM(IS)=YSM(IS)+RNTZ(XSM(IS),CST(JI),CST(JI-1),CST(NC2
     $+1))*100.
```

```
      CALLPLØT(2.,4.,-3)
      CALLSCALE(V,8.0,NP,1)
      CALLSCALE(C,3.0,NP,-1)
      Y(NP+1)=C(NP+1)
      Y(NP+2)=C(NP+2)
      CALLAXIS(0.,-1.25,17HVELØCITY(CM/SEC),-17,8.,0.,V(NP+1
     S),V(NP+2))
      CALLAXIS(0.,0.,14HABSØRPTION(Z),14,3.,90.,Y(NP+1),Y(NP
     S+2))
      CALLPLØT(0.,-1.25,3)
      CALLPLØT(0.,0.,2)
      CALLPLØT(0.,3.,3)
      CALLPLØT(0.,4.25,2)
      CALLPLØT(8.,4.25,2)
      CALLPLØT(8.,-1.25,2)
      CALLLABEL(0.5,3.75,7.5,3.75,NAME(1),20,0.2,2,0.1,0.,0)
      CALLLABEL(0.5,3.75,7.5,3.75,NAME(6),NCHAR,0.2,1,0.1,0.
     S,0)
      DØ9040I=1,NP
      C(I)=C(I)-CST(NC2+2)*100.
 9040 Y(I)=Y(I)-CST(NC2+2)*100.
      DØ9050I=1,NP
 9050 CALLSYMBØL((V(I)-V(NP+1))/V(NP+2),(C(I)-Y(NP+1))/Y(NP+
     S2),0.04,1,0.
     &0,-1)
      XSM(501)=V(NP+1)
      XSM(502)=V(NP+2)
      YSM(501)=Y(NP+1)
      YSM(502)=Y(NP+2)
      CALLFLINE(XSM,YSM,500,1,0,0)
      ALNMAX=D1(1)
      ALNMIN=D1(1)
      DØ9060I=1,NC
      IF(D1(I).LT.ALNMIN)ALNMIN=D1(I)
 9060 IF(D1(I).GT.ALNMAX)ALNMAX=D1(I)
      CALLPLØT((ALNMIN-V(NP+1))/V(NP+2),0.,3)
      CALLPLØT((ALNMAX-V(NP+1))/V(NP+2),0.,2)
      DØ9070I=1,NC
      CALLPLØT((D1(I)-V(NP+1))/V(NP+2),(D2(I)-Y(NP+1))/Y(NP+
     S2)-3.,3)
 9070 CALLPLØT((D1(I)-V(NP+1))/V(NP+2),0.,2)
      CALLPLØT(12.,-4.,-3)
      RETURN
      END
C
C
      FUNCTIØNRNTZ(X,AMP,PØS,GAMMA)
```

```
      CALLPLOT(2.,4.,-3)
      CALLSCALE(V,8.0,NP,1)
      CALLSCALE(C,3.0,NP,-1)
      Y(NP+1)=C(NP+1)
      Y(NP+2)=C(NP+2)
      CALLAXIS(0.,-1.25,17HVELOCITY(CM/SEC),-17,8.,0.,V(NP+1
     S),V(NP+2))
      CALLAXIS(0.,0.,14HABSORPTION(Z),14,3.,90.,Y(NP+1),Y(NP
     S+2))
      CALLPLOT(0.,-1.25,3)
      CALLPLOT(0.,0.,2)
      CALLPLOT(0.,3.,3)
      CALLPLOT(0.,4.25,2)
      CALLPLOT(8.,4.25,2)
      CALLPLOT(8.,-1.25,2)
      CALLLABEL(0.5,3.75,7.5,3.75,NAME(1),20,0.2,2,0.1,0.,0)
      CALLLABEL(0.5,3.75,7.5,3.75,NAME(6),NCHAR,0.2,1,0.1,0.
     S,0)
      DO9040I=1,NP
      C(I)=C(I)-CST(NC2+2)*100.
 9040 Y(I)=Y(I)-CST(NC2+2)*100.
      DO9050I=1,NP
 9050 CALLSYMBOL((V(I)-V(NP+1))/V(NP+2),(C(I)-Y(NP+1))/Y(NP+
     S2),0.04,1,0.
     S0,-1)
      XSM(501)=V(NP+1)
      XSM(502)=V(NP+2)
      YSM(501)=Y(NP+1)
      YSM(502)=Y(NP+2)
      CALLFLINE(XSM,YSM,500,1,0,0)
      ALNMAX=D1(1)
      ALNMIN=D1(1)
      DO9060I=1,NC
      IF(D1(I).LT.ALNMIN)ALNMIN=D1(I)
 9060 IF(D1(I).GT.ALNMAX)ALNMAX=D1(I)
      CALLPLOT((ALNMIN-V(NP+1))/V(NP+2),0.,3)
      CALLPLOT((ALNMAX-V(NP+1))/V(NP+2),0.,2)
      DO9070I=1,NC
      CALLPLOT((D1(I)-V(NP+1))/V(NP+2),(D2(I)-Y(NP+1))/Y(NP+
     S2)-3.,3)
 9070 CALLPLOT((D1(I)-V(NP+1))/V(NP+2),0.,2)
      CALLPLOT(12.,-4.,-3)
      RETURN
      END
C
C
      FUNCTIONRNTZ(X,AMP,POS,GAMMA)
```

```
DX=(X-POS)/GAMMA
RNTZ=AMP*(1./(1.+DX*DX))
RETURN
END
```

LIST OF REFERENCES

1. G. K. Werthheim, Mössbauer Effect: Principles and Applications, New York: Academic Press, 1964.

2. F. R. Metzger, Prog. Nucl. Phys. 7, 53 (1959).

3. D. A. Shirley, Rev. Mod. Phys. 36, 339 (1964).

4. R. E. Watson, Phys. Rev. 119, 1934 (1960).

5. R. G. Shulman and S. Sugano, J. Chem. Phys. 42, 39 (1965).

6. R. Ingalls, Phys. Rev. 133, A787 (1964).

7. N. L. Costa, J. Danon, R. Moreira Xaxier, J. Phys. Chem. Sol. 23, 1783 (1962).

8. S. De Benedetti, G. Lang, R. Ingalls, Phys. Rev. Lett. 6, 60 (1961).

9. V. I. Gol'danski, E. F. Makarov, and V. V. Khrapov, Soviet Phys. JETP (English Translation) 17, 508 (1963).

10. R. B. King, R. H. Herber and G. K. Wertheim, Inorg. Chem. 3, 101 (1964).

11. S. S. Hanna, J. Heberle, C. Littlejohn, G. J. Perlow, R. S. Preston and P. H. Vincent, Phys. Rev. Lett. 4, 177 (1960).

12. J. Danon, Lectures on the Mössbauer Effect, New York: Gordon and Breach, 1968.

13. A. J. Freeman and R. E. Watson, "Hyperfine Interaction in Magnetic Materials," in G. T. Rado and H. Shul (eds.) Magnetism Vol. IIA, Academic Press, New York and London, 1965, p.167.

14. A. A. Maradudin, Rev. Mod. Phys. 36, 417 (1964).

15. V. I. Gol'danskii, The Mössbauer Effect and Its Applications to Chemistry, (Academy of Sciences Press, USSR, Moscow, 1963).

16. E. Fermi and E. Segre, Z. Physik 82, 729 (1933).

17. H. Pollak, M. de Coster and S. Amelinckx, Proceedings of the 2nd International Conference on Mössbauer Effect, Saclay France, 1961, p.298, Wiley, New York, 1962.

18. W. Kerler, Z. Physik, 173, 321 (1963).

19. V. A. Bryukhanov, V. I. Gol'danskii, N. N. Delyagin, E. F. Markarov and V. S. Shipinel, Soviet Phys., JETP 15, 443 (1962).

20. C. R. Kurkjian and Sigety in Proceedings of the 7th International Congress on Glass, Brussels, 1965.

21. P. L. Mattern, Ph.D. Thesis, Cornell University, 1965.

22. J. P. Gosselin, U. Shimony, L. Grodzins and A. R. Cooper, Phys. Chem. Glasses 8, 56 (1967).

23. G. Tomandl, G. H. Frischat and H. J. Oel, Glastech. Ber. 40, 293 (1967).

24. C. R. Kurkjian and E. A. Sigety, Phys. Chem. Glasses 9, 73 (1968).

25. A. Lerman, M. Stiller, E. Hernion, Earth and Planetary Science Letters, (Netherlands) Vol. 3, No. 5, 409-16.

26. C. R. Kurkjian and D. N. E. Buchanan, Phys. and Chem. of Glasses 5, 3 (June, 1964).

27. A. A. Belyustin, Y. M. Ostaneirch, A. M. Pisarevskii, S. B. Tomilov, U. Bai-shi, and L. Cher, Soviet Physics-Solid State 7, 5, p.1163.

28. S. L. Ruby and J. M. Hicks, Rev. of Sci. Instr. 33, 1 (1962).

29. S. S. Hanna, J. Herberle, C. Littlejohn, G. J. Perlow, R. S. Preston, and D. H. Vincent, Phys. Rev. Lett. 9, 12 (1960).

30. N. Blum, L. Grodzins (1962) Bull. Amer. Phys. Soc. 7, 39; with P. P. Craig et al. (1962) Phys. Rev. Lett. 9, 12.

31. R. R. Shaw and J. H. Heasly, J. Amer. Cer. Soc. 50, 297 (1967).

32. J. W. G. Wignall, J. Chem. Phys. 44, 2462 (1966).

33. L. R. Walker, G. K. Wertheim, and V. Jaccarino, Phys. Rev. Lett. 6, 98 (1961).

34. G. K. Wertheim and R. H. Herber, J. Chem. Phys. 36, 2497 (1962).

35. S. V. Karyagin, Proceedings of the Academic Society, USSR, Phys. Chem. Soc. 148, 110 (1964).

36. L. May, An Introduction to Mössbauer Spectroscopy, New York: Plenum Press, 1971, p.98.

37. F. C. Ruegg, J. J. Spikerman and J. R. DeVoe, Rev. Sci. Instr. 36, 356 (1965).

38. F. W. D. Woodhams, J. Sci. Instr. 44, 285 (1967).

39. K. Cassel and A. H. Jiggins, J. Sci. Instr. 44, 212 (1967).

40. H. H. Wicheman, Ph.D. Thesis, University of California, August, 1964).

41. "Mossbauer Effect Data Index," 3rd ed. North Am. Aviation, 1966.

42. E. J. Friebele, L. K. Wilson, A. W. Dozier, D. L. Kinser, Phys. Stat. Sol. (b) 45, 323 (1971).

43. Abou-el-Azm, A-E-M, J. Soc. Glass Tech. 38, 101 (1954).

44. C. R. Bamford, Phys. Chem. Glasses 1, 159 (1960); 2, 163 (1964);

$\underline{3}$, 54 (1962).

45. M. G. Clark, G. M. Bancroft and A. J. Stone, <u>J. Chem. Phys</u>. <u>47</u>, 4250 (1967).

46. G. K. Lewis and H. G. Drickamer, <u>J. Chem. Phys</u>. <u>49</u>, 3785 (1968).

47. C. Hirayama, J. G. Castle and M. Kuriyama, <u>Phys. Chem. Glasses</u> <u>9</u>, 109 (1968).

48. W. A. Weyl, <u>Coloured Glasses</u> (Society of Glass Technology, Sheffield, 1951).

49. I. J. Gruverman, <u>Mössbauer Effect Methodology</u>, <u>Vol. 1</u>, New York: Plenum Press, 1965.

50. A. Abragam, <u>L'Effet Mössbauer</u>, New York: Gordon and Breach, 1964.

51. L. V. Azaroff, <u>Introduction to Solids</u>, New York: McGraw-Hill Book Co., Inc., 1960.

52. H. Frauenfelder, <u>The Mössbauer Effect</u>, New York: W. A. Benjamin, Inc., 1962.

53. L. May (ed.), <u>An Introduction to Mössbauer Spectroscopy</u>, New York: Plenum Press, 1971.

54. C. R. Kurkjian, <u>J. Non-Crys. Sol</u>. <u>3</u>, 157 (1970).

55. C. R. Kurkjian and E. A. Sigety, <u>Phys. Chem. Glasses</u>, Vol. <u>9</u>, No. 3, June, 1968).

56. C. Hirayama, J. G. Castle, Jnr., and M. Kuriyama, <u>Phys. Chem. Glasses</u>, Vol. <u>9</u>, No. 4, August, 1968.

AN INVESTIGATION OF THE STRUCTURAL AND ELECTRICAL PROPERTY CORRELATIONS IN THE ARSENIC TRISELINIDE-ARSENIC TRITELLURIDE GLASS SYSTEM

DAVID JOSEPH HILL

Thesis under the direction of Professor Donald L. Kinser

The microstructure and D.C. and A.C. electrical properties of a series of arsenic triselinide-arsenic tritelluride glasses have been investigated. Electron microscopic observations indicate the presence of phase separation in these glasses. A miscibility gap across the ternary phase diagram is indicated. Variations in D.C. electrical properties may be due to structural changes, compositional changes or a combination of both. Structural inhomogeneities due to phase separation appear to be responsible for Maxwell-Wagner-Sillars heterogeneous losses in these glasses.

Approved _____ Date _____

AN INVESTIGATION OF THE STRUCTURAL AND ELECTRICAL PROPERTY

CORRELATIONS IN THE ARSENIC TRISELINIDE-ARSENIC TRITELLURIDE

GLASS SYSTEM

By

David Joseph Hill

Thesis

Submitted to the Faculty of the

Graduate School of Vanderbilt University

in partial fulfillment of the requirements

for the degree of

MASTER OF SCIENCE

in

MATERIALS SCIENCE AND ENGINEERING

May, 1972

Nashville, Tennessee

Approved: Date:

_____   _____

_____   _____

ACKNOWLEDGMENTS

TABLE OF CONTENTS

LIST OF TABLES

LIST OF FIGURES

CHAPTER I

INTRODUCTION

Amorphous semiconductors have been known to the scientific community for many years. One system of these materials, chalcogenide glasses, which consist of a combination of a metal with the heavier elements of the oxygen group of the periodic table, were thought to behave similarly to intrinsic crystalline semiconductors. Kolimiets et al.[1] in 1955, investigated several amorphous materials made from various combinations of antimony, arsenic, selenium, sulfur, tellurium and thallium. They reported high room temperature electrical conductivities. Some theoretical theories[2] were advanced and some additional experimental work was done,[3] but in the most part, these glasses remained a laboratory curiosity for the ten years after Kolimiets' investigations. With the discovery[4] in the early sixties of an electrical switching phenomenon in a chalcogenide glass, much interest has been shown to the development of these and associated glasses for use as solid state devices. Characterization of the thermal, electrical, structural, and optical properties has been undertaken at numerous industrial and university laboratories.

The majority of the work done in these systems has been an attempt to create stable and reproducible devices which exhibit switching and/or memory characteristics. Attempts to explain these unusual phenomenon observed in terms of conventional band and transport

theories[5,6] have not been universally accepted.[7,8,9,10]

Many of the assumptions of the band theory presuppose a homogeneous material. An important property of glasses that seems to be ignored by proponents of the above theories is the possibility of formation of a metastable immiscibility in most glass systems. Haller, et al.[11] have reported an explanation of this phase separation as it occurs in a sodium borosilicate system. Consideration of this phenomenon could lead to explanations of the inconsistencies in these theories. It would also support the filamentary conduction hypothesis,[10] which is based on an electro-thermal process. Pearson[12] has reported phase separation in several switching and memory glasses and Stocker, et al.[9] have done theoretical calculations supporting the thermal theories.

This author chose to investigate one of the chalcogenide systems which exhibits memory and switching characteristics to determine if structural inhomogeneities are indeed present and if they have any effect on other properties. The system arsenic triselenide-arsenic tritelluride was chosen since no work has been done on the structural characterization of these glasses. It was decided to study the electrical properties of the system for evidence of possible correlations with microstructure.

Thus the purpose of this investigation was to measure the A.C. and D.C. electrical properties and examine the microstructure of glasses in the As_2Te_3-As_2Se_3 system to determine if any correlation exists between these properties. This paper presents a report of this investigation.

CHAPTER II

EXPERIMENTAL PROCEDURE

Six glasses were studied from the arsenic-selenium-tellurium system. The compositions were $xAs_2Te_3-(100-x)As_2Se_3$ with x equal to 80, 70, 60, 50, 40, and 0. All compositions lie on the $As_2Te_3-As_2Se_3$ join of the ternary phase diagram, Figure 1. Throughout this paper, compositions will be denoted as a ratio of mole per cent As_2Te_3 to mole per cent As_2Se_3. Thus 80/20 indicates a composition consisting of 80 mole per cent As_2Te_3 and 20 mole per cent As_2Se_3.

The glasses were made by sealing reagent grade materials of the proper proportions in evacuated Vycor ampules and heating for one hour at 800°C. The melting was done in a rocking furnace specially designed to assure complete mixing of the components. The furnace was a tube furnace with a sample ampule holder mounted such that it would pivot under the action of a motor driven cam. This caused the liquid sample to be rocked back and forth in the ampule as one end was alternately raised and lowered with respect to the other end. The melts, still in the Vycor capsules, were quenched in room temperature water. All samples for the studies were made from these bulk glasses.

A preliminary investigation using high purity (at least 99.999%) materials handled under an inert gas atmosphere and sealed under vacuum in fused silica ampules was conducted. The specific materials used are listed in Table 1. These samples were given the same melting treatment
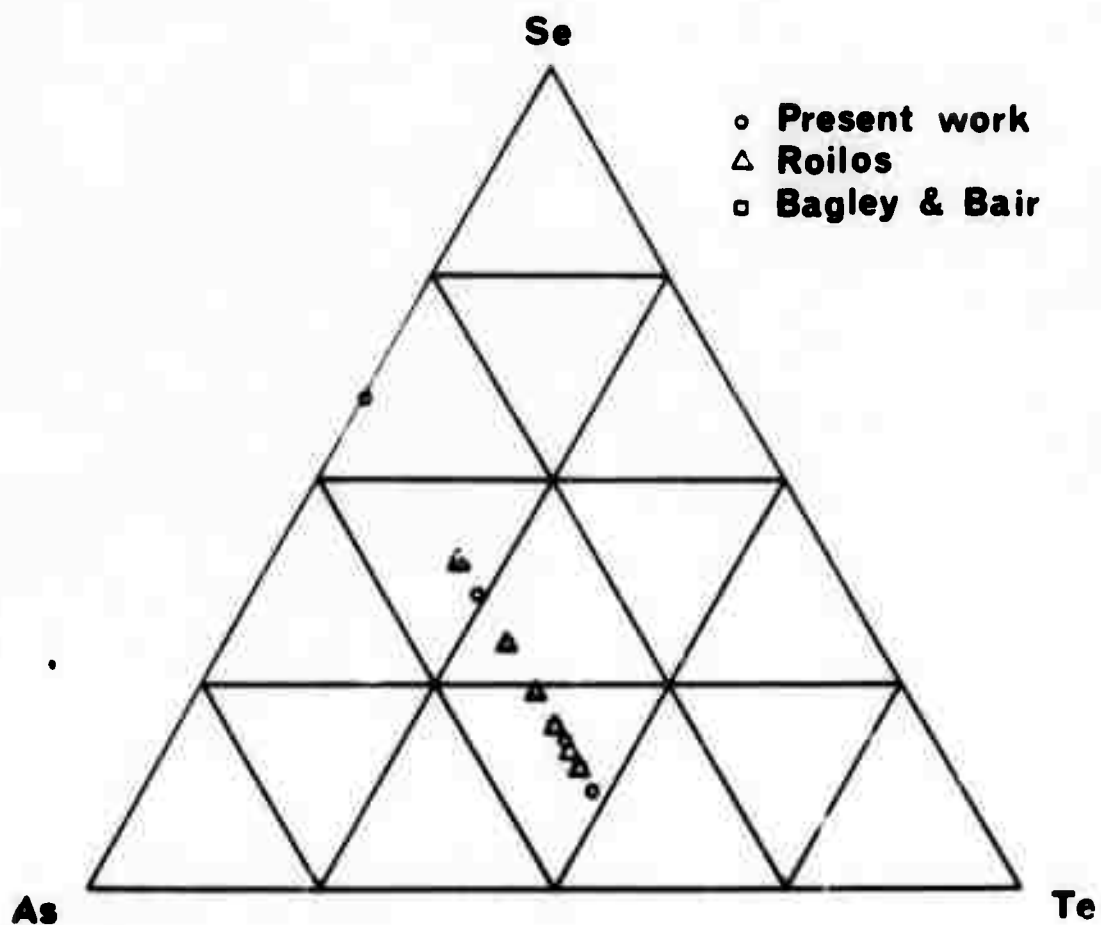
Figure 1. Arsenic-selenium-tellurium ternary phase diagram.

TABLE 1

HIGH PURITY MATERIALS

Te: American Smelting and Refining Co., Special
High-Purity, Semiconductor Grade (99.999%) Tellurium

Se: American Smelting and Refining Co., Special High
Purity (99.999+%) Selerium

As: United Mineral and Chemical Corp., Arsenic Powder,
99.9999% Pure

as described above and showed no variation in properties from samples made with the reagent grade materials. It is also well established in the literature[13,14,15] that amorphous semiconductors in general are not sensitive to impurities. However, Mackenzie[16] did note some marked effect by oxygen impurities to heat treated selenium samples.

Studies conducted consisted of measurement of the electrical properties, replica electron microscopy (E.M.), Guinier-de Wolff x-ray analysis, differential thermal analysis (DTA) and dilatometric analysis.

Samples of the bulk glasses were powdered and studied in a Guinier-de Wolff powder camera to verify that the materials were indeed non-crystalline. Crystals of 0.1 weight per cent can be detected by this method.

Electrical specimens in platelet form were prepared by briefly softening a sufficient quantity of the bulk glass on a graphite plate and pressing with a second graphite plate. All samples had an area of approximately one square centimeter and a thickness of about 2 millimeters. All samples had similar thermal histories. No samples were subjected to further thermal treatment. Conductivity measurements were made through silver conductive paste, Walso #36-1 Silver Print, in a guard ring configuration. The applied fields were approximately five volts per centimeter. This is much less than that required to switch these glasses. Electrical measurements were divided into D.C. and A.C. segments, with the A.C. segment being further split into audio and radio frequency regions. The same sample was used for both A.C. and D.C. measurements. The specially constructed sample holder consisted of a shielded configuration (Figure 2), with an Iron-Constantan thermocouple

Figure 2a. Sample holder, without shield.

Figure 2b. Sample holder, with shield.

148

mounted adjacent to the sample. Electrical measurements on the As_2Se_3 composition were considered unreliable and electrical data on this composition was generally not included in this paper.

The D.C. conductivity measurements were taken over a range of temperatures from room temperature to about $115^{\circ}C$. Sample temperature control was facilitated by use of a heating tape and variable transformer. A Keithley high speed picoammeter was used to measure current in conjunction with a Hewlett Packard constant voltage source. Current readings were taken at approximately $10^{\circ}C$ intervals. The heating rate was determined by calibration of the variable transformer and heating tape system. The rate chosen was as close to equilibrium heating as practical without causing annealing of the sample at the higher temperatures and to minimize differences in sample/thermocouple temperature.

The A.C. conductivity and capacitance measurements were taken at room temperature. The audio frequency measurements, from 200 Hz to 50 kHz, utilized a Hewlett Packard 615 B oscillator coupled with a Wayne Kerr B221 audio frequency bridge, which had an internal null detector. A Wayne Kerr B601 radio frequency bridge and General Radio external null detector were used for the radio frequency measurements. Due to limitations of the null detector, an oscillator and a diode radio frequency mixer were used to mix a beat frequency with the output of the radio bridge for the measurements using frequencies greater than 100 kHz.

Dilatometric studies were undertaken to determine the softening point of the glasses. This was to establish a safe temperature limit for the D.C. measurements and an annealing temperature for later experiments.

Differential thermal analyses (DTA) were conducted to determine the ease of devitrification and the presence of glass transitions. The DTA data was taken using powdered samples, with a modified Fisher Differential Thermalyzer, Model 260P. Heating rates of 5, 10, and 25°C per minute were used on all compositions.

Electron microscopic studies were made of fresh fracture surfaces and etched fracture surfaces using two stage, platinum-palladium shadowed, carbon replicas. The etchant was a dilute solution of potassium hydroxide and water. The microscope was a Philips E.M. 300.

151

CHAPTER III

EXPERIMENTAL RESULTS

Guinier-de Wolff x-ray analysis showed no evidence of crystallization in any of the initially prepared glasses. Results of the DTA studies are summarized in Table 2. Two clearly defined exothermic reactions were noted for the 80/20 and 70/30 glasses. The 60/40 and 50/50 glasses each exhibited only one reaction. The glasses with higher Se/Te ratios showed very broad and diffuse peaks which made the accurate determination of reaction temperatures difficult. No reaction could be determined for the 40/60 glass nor for the As_2Se_3 glass. High selenium glasses are generally difficult to crystallize, and any reaction probably would proceed too slowly to be noticeable in our experiments. The results indicate that the crystallization temperature of the glasses increases as the Se/Te ratio increases. Our equipment was too insensitive to show any reactions which involve small heats of reaction. Thus reactions such as glass transitions were not detectable in our studies. The experiments were not continued to melting. Devitification in all samples except arsenic triselinide was confirmed by x-ray analysis. The author was unable to identify the crystalline phases.

The softening points determined by the dilatometric studies are listed in Table 3. The softening point, or softening temperature, as determined by the dilatometric studies is that maximum temperature at

10

TABLE 2

DTA DATA

	Heating Rate :	Observed Exothermic Reaction Temperature			
As_2Te_3/As_2Se_3		$5^{\circ}C/min$	$10^{\circ}C/min$	$25^{\circ}C/min$	$40^{\circ}C/min$
80/20		150,210	172,230	180,235	------
* 75/25		------	------	------	137,262
70/30		196	22C,255	225,247	------
* 66/33		------	------	------	136,266
60/40		213	255	250	------
50/50		220	260	270	------
40/60		N.O.	N.O.	N.O.	------
* 33/66		------	------	------	158,N.O.
0.100		N.O.	N.O.	N.O.	------

* Indicates data from Bagley and Bair.

------ Indicates no observations taken at noted heating rate.

TABLE 3

DILATOMETER DATA: SOFTENING POINTS

As_2Te_3/As_2Se_3	Softening Temperature $^{o}C \pm 2^{o}$
80/20	$100^{o}C$
70/30	$110^{o}C$
60/40	$125^{o}C$
50/50	$135^{o}C$
40/60	$145^{o}C$
0/100	$185^{o}C$

which the glass can hold its shape and resist deformation due to small applied forces. It can be viewed as that temperature, or range of temperatures, at which the viscosity of the glass is lowered to the point that the material is no longer rigid, but assumes more of the character of a liquid. The term actually has varied definitions and values, depending on the method of measurement, heating rates, and magnitude of force. The Orton dilatometer measures the linear expansion or contraction of the sample while it is being heated. A slight compressive pressure is maintained on the sample by a small spring. As can be seen from the dilatometer curve of Figure 3, there is a point, actually a 3° to 5° range, where the thermal expansion levels off and drops suddenly to zero. The minimum temperature of this range we defined as the softening point. The data indicates that the softening temperature rises with increased selenium content.

Electrical

Data from the D.C. experiments are plotted in Figures 4 through 9 as log conductivity versus inverse absolute temperature. These plots are combined in Figure 10. The samples behave as expected of electronically conducting semiconductors, with the conductivity increasing according to

$$\sigma = \sigma_0 \exp\left(-\Delta E/kT\right) .$$

A.C. electrical measurements were interpreted in terms of the loss tangent, $\tan \delta = G/\omega C$. This function is equivalent to the tangent of
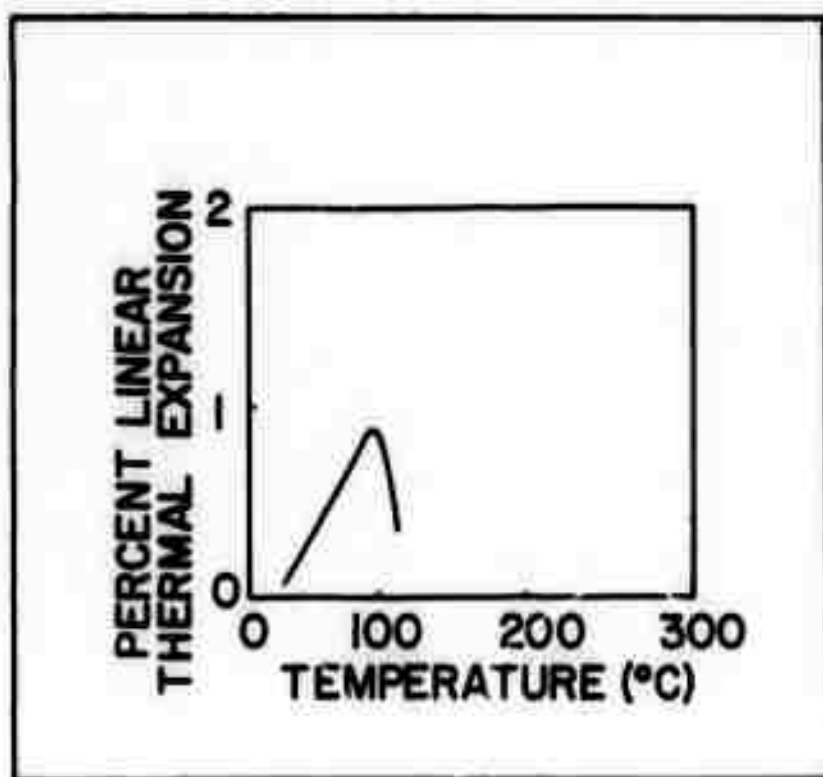
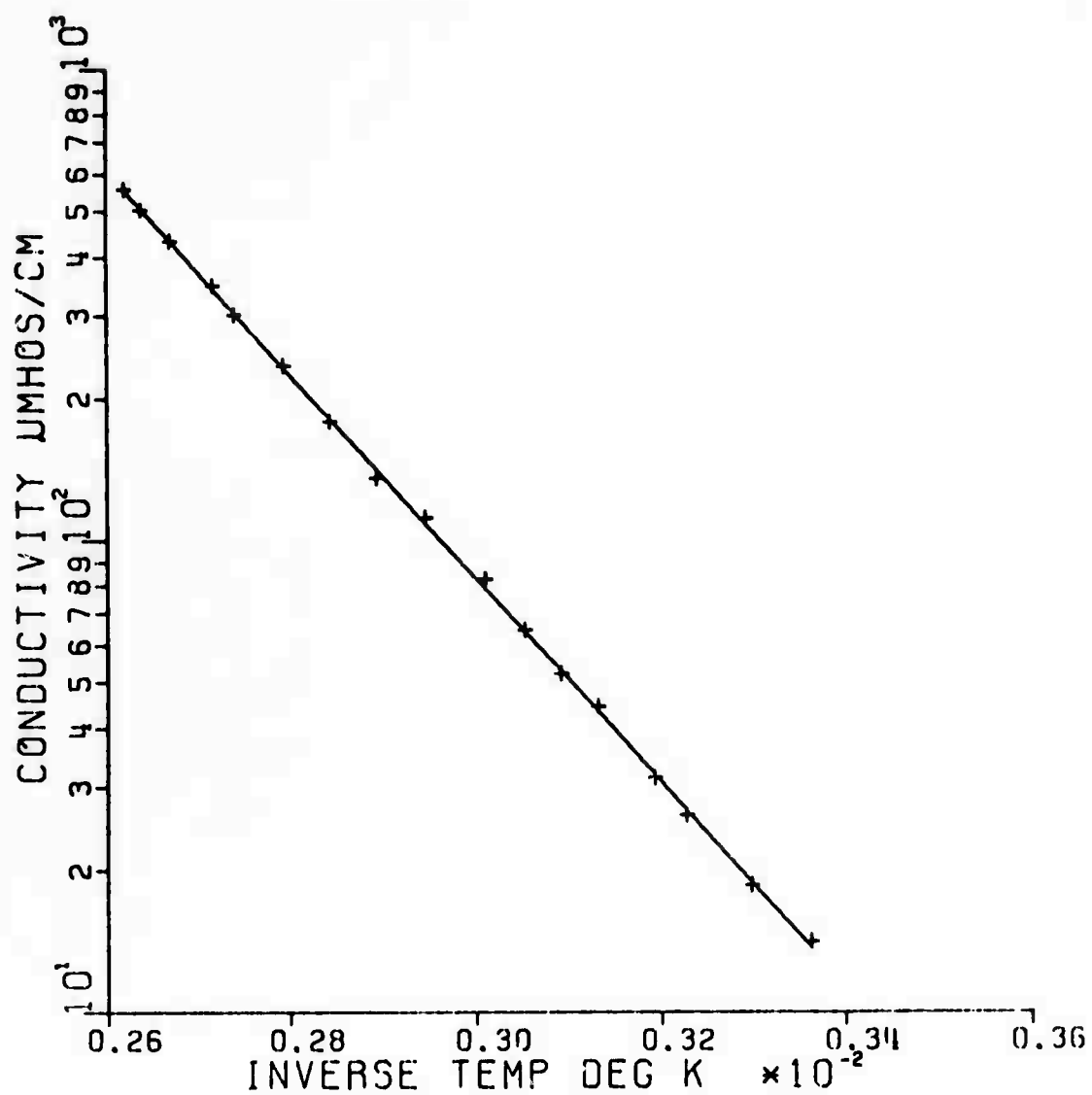Figure 3. Dilatometer curve.

Figure 4. Log conductivity versus inverse temperature,
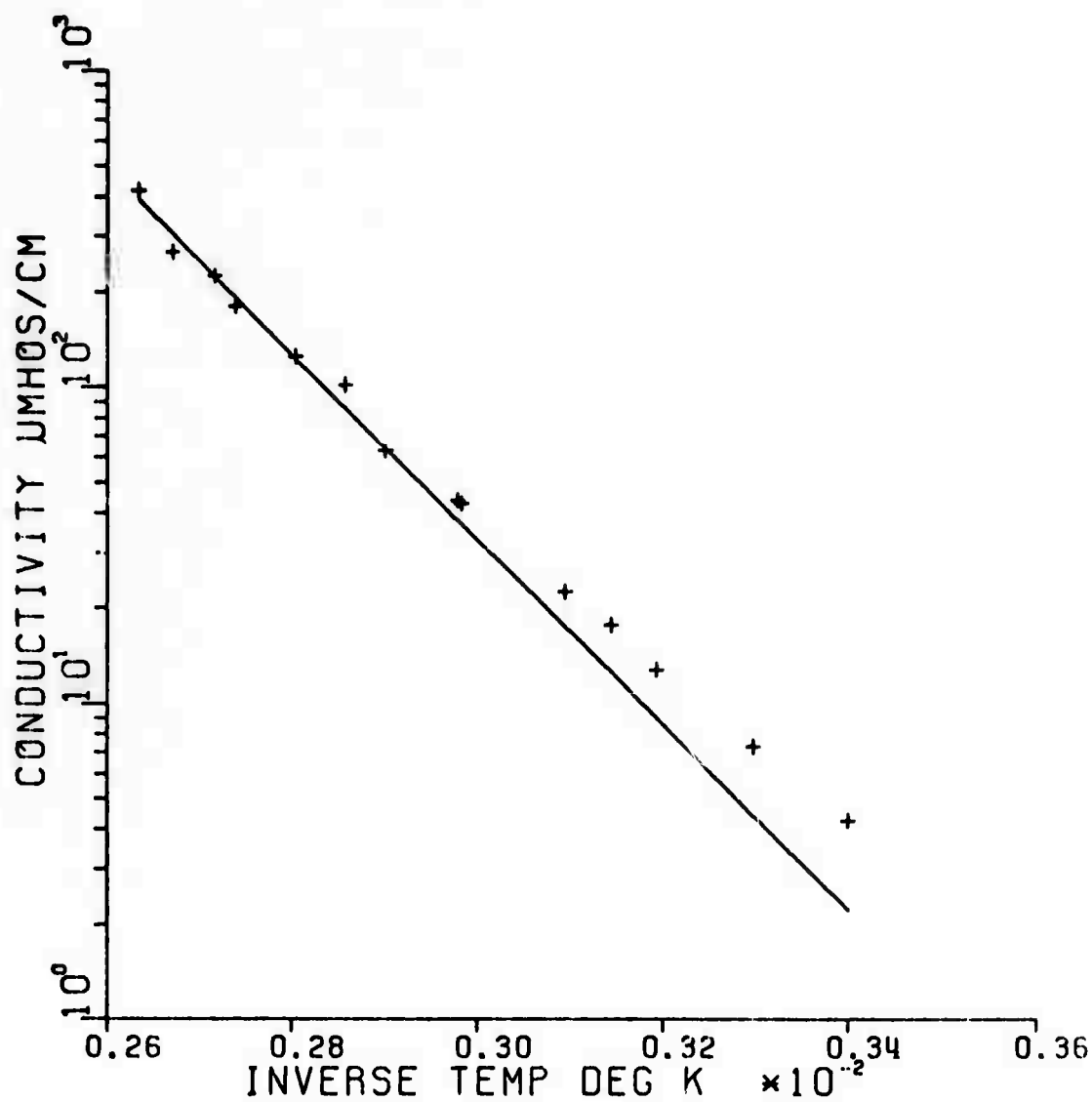80/20 glass.

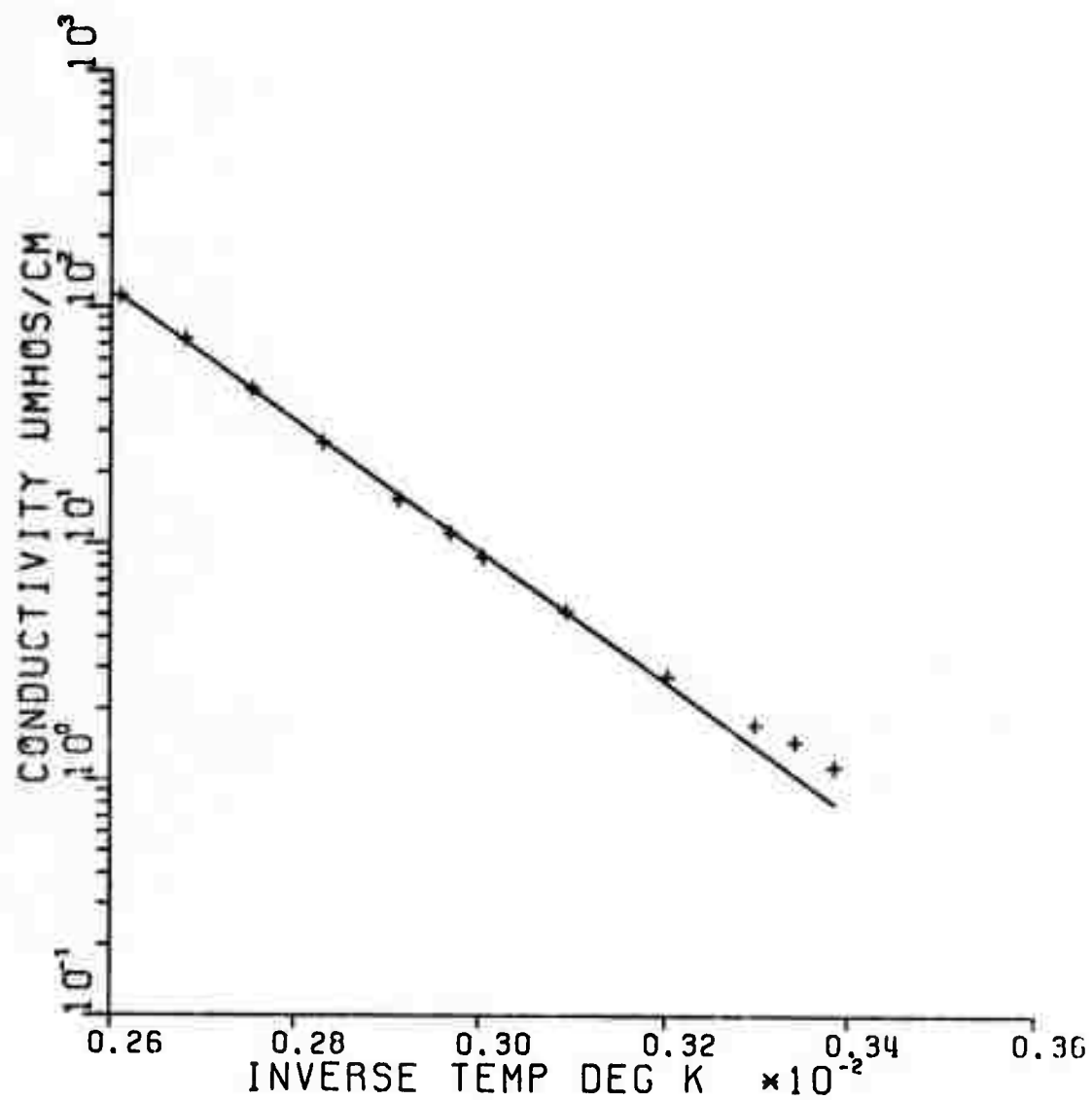Figure 5. Log conductivity versus inverse temperature,
          70/30 glass.

Figure 6. Log conductivity versus inverse temperature, 60/40 glass.
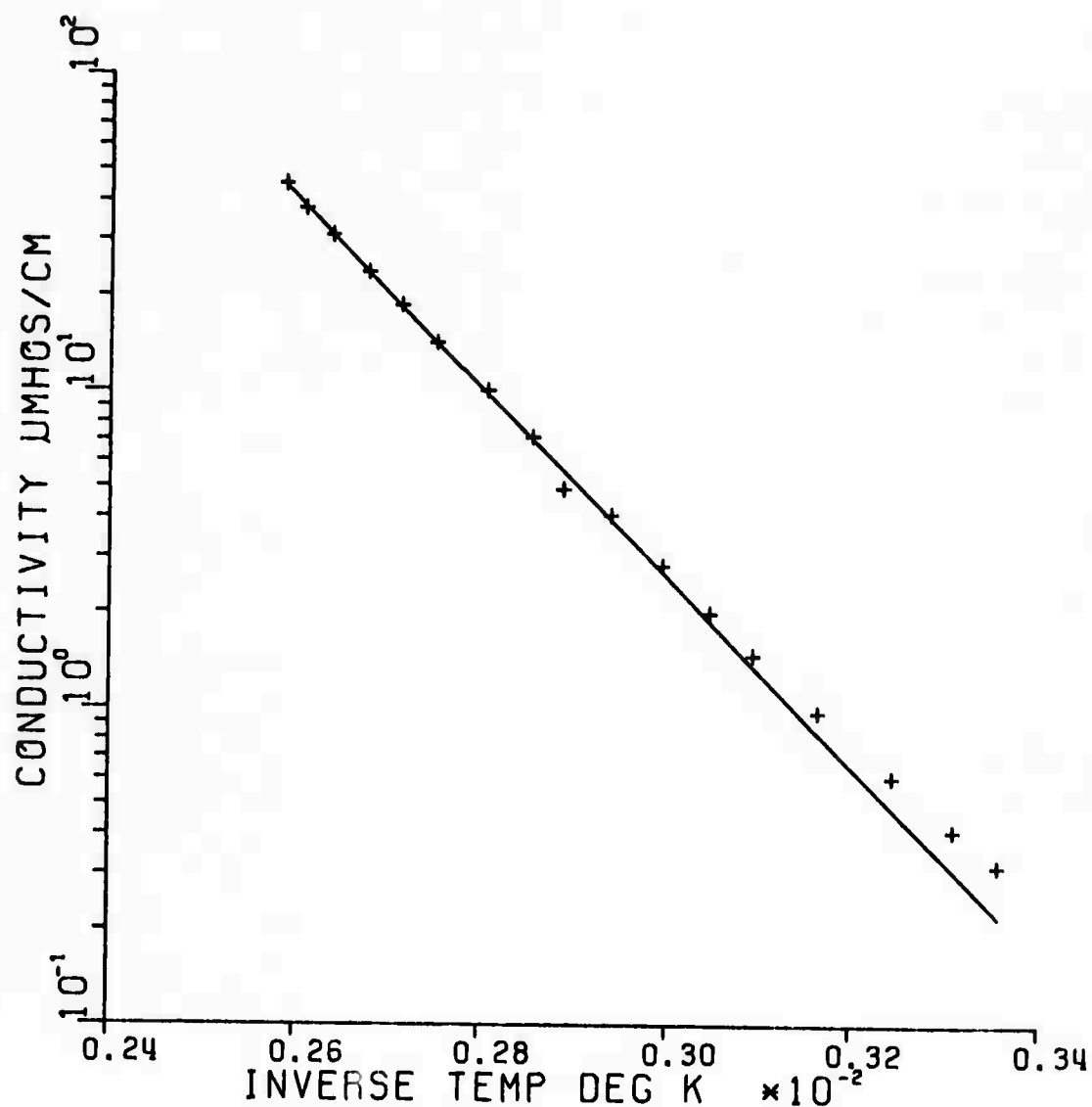
Figure 7. Log conductivity versus inverse temperature,
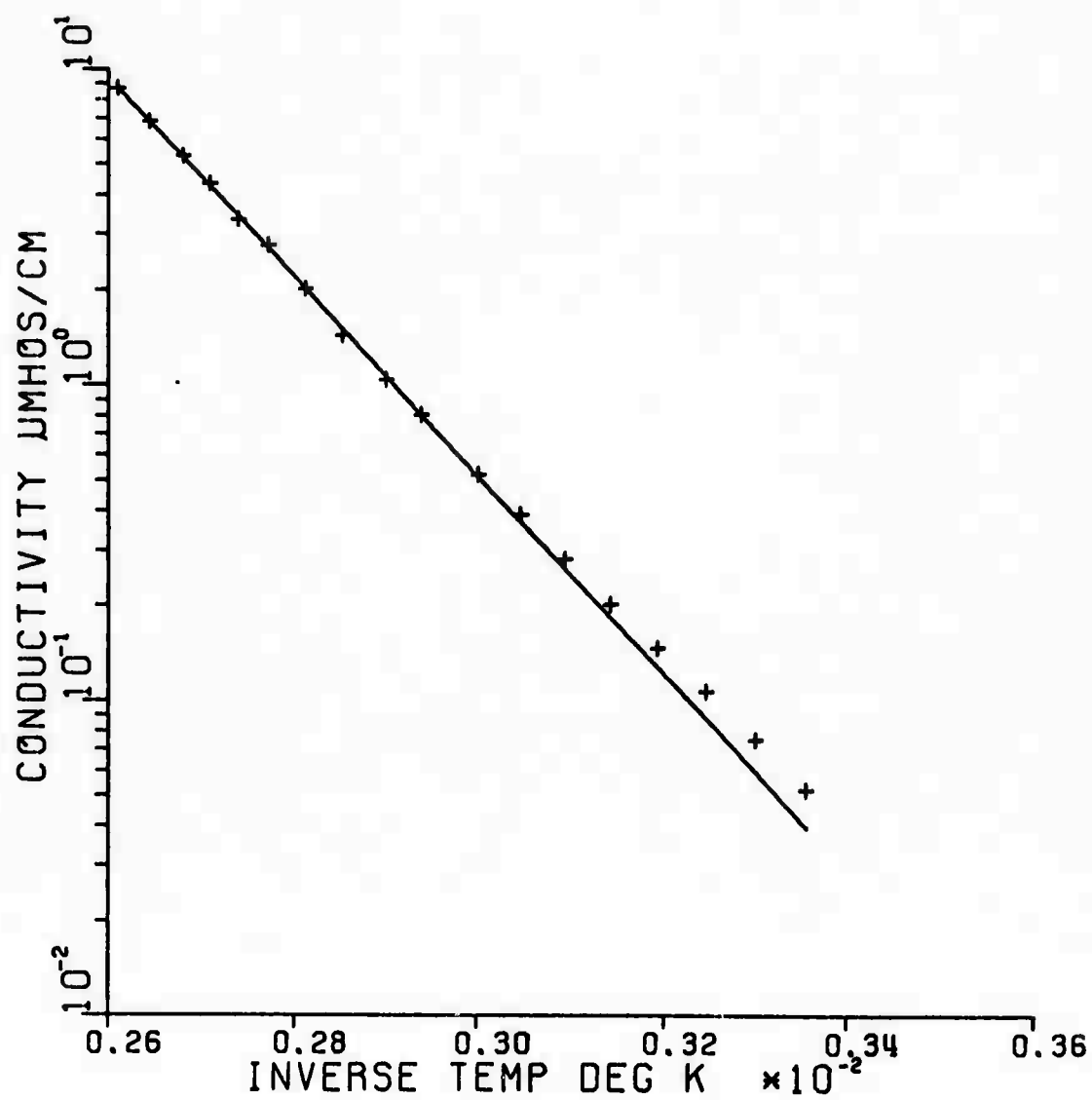50/50 glass.

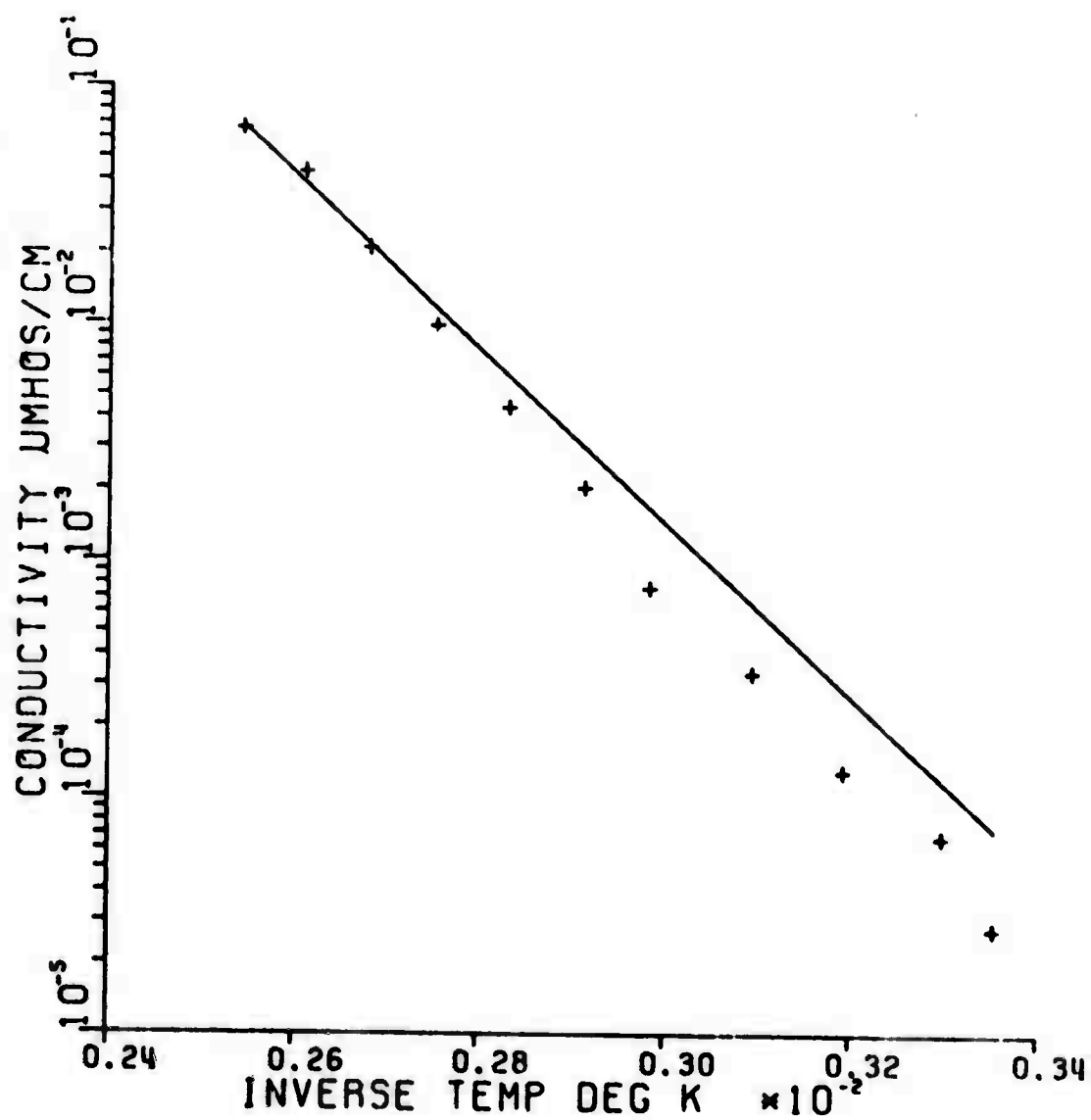Figure 8. Log conductivity versus inverse temperature, 40/60 glass.

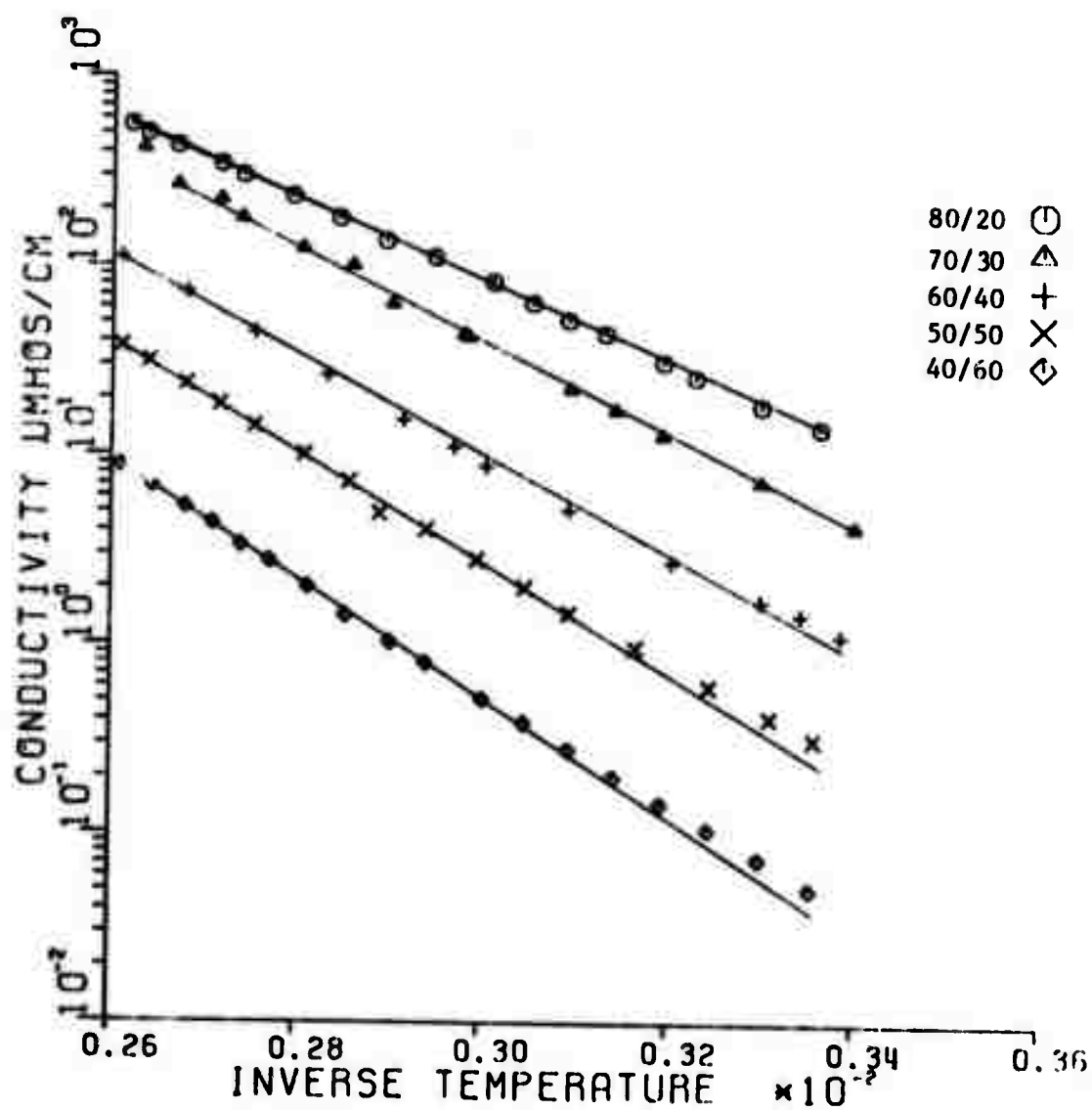Figure 9. Log conductivity versus inverse temperature, As$_2$Se$_3$ glass.

Figure 10. Log conductivity versus inverse temperature.

ϵ'/ϵ'', the ratio of the loss factor, ϵ', to the permittivity, ϵ''. Tan del can be considered to be composed of two components, an A.C. frequency dependent component, and a D.C. component. Thus

$$\tan \delta_{Total} = \tan \delta_{A.C.} + \tan \delta_{D.C.}$$

The loss at low frequency is higher and the D.C. component overwhelms the effect of the A.C. component. Thus, to examine the frequency dependence, we must subtract the D.C. component, based on the room temperature D.C. measurements, from the total value of the tan del function computed from the A.C. measurements. Thus

$$\tan \delta_{A.C.} = \tan \delta_{Total} - \tan \delta_{D.C.}$$

A full discussion on the tan del function can be found in van Beck.[17]

This tan del function, with the D.C. component subtracted, is plotted versus log frequency for each composition in Figures 11 through 15. These same plots are combined in Figure 16. All samples exhibited at least one loss peak and corresponding dielectric dispersion. This indicates that conditions for Maxwell-Wagner-Sillars heterogeneous losses are present in these glasses.

The activation energies and the corresponding pre-exponential term, σ_o, were calculated from the equation
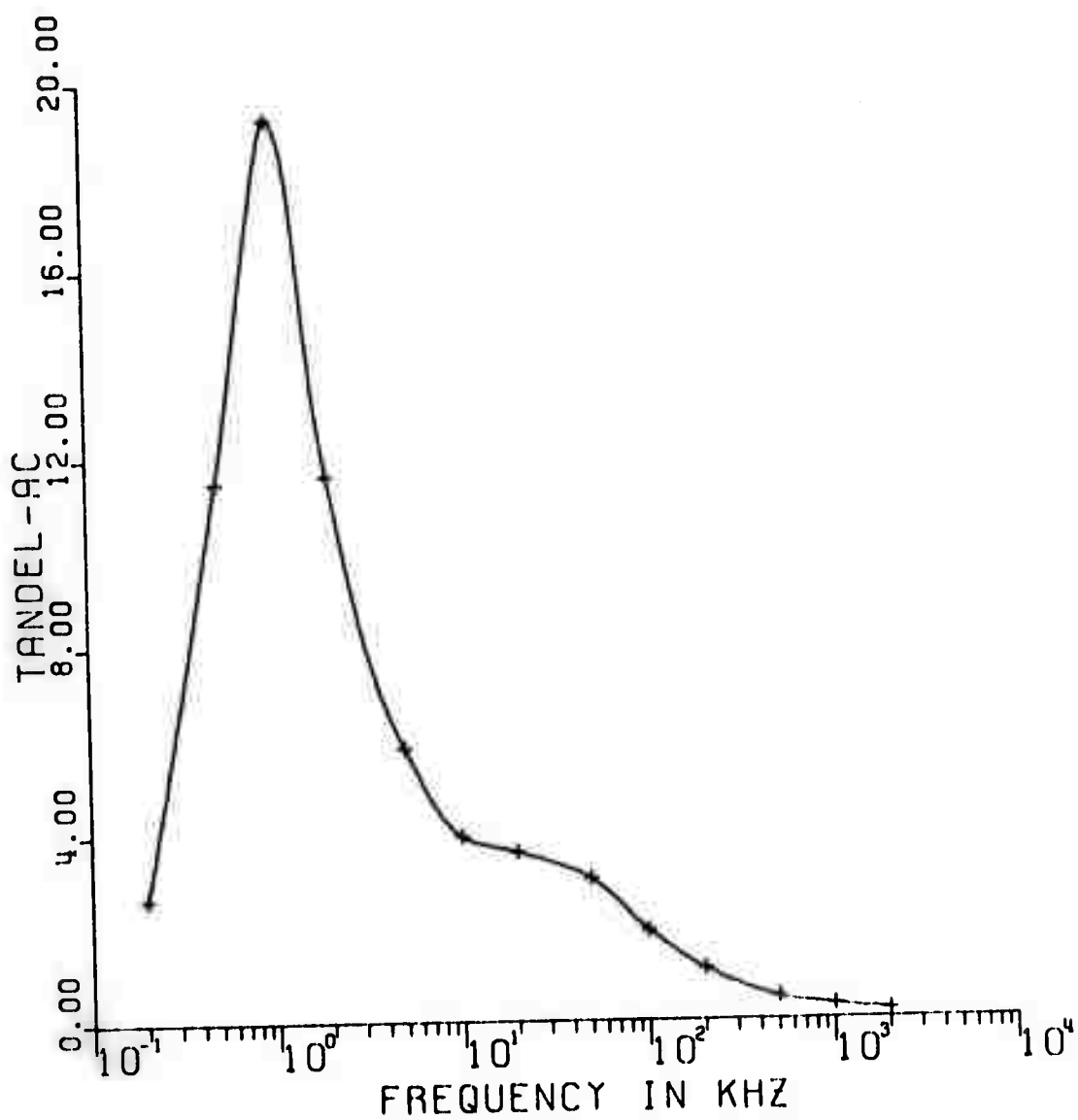
Figure 11. Tan del versus log frequency, 80/20 glass.
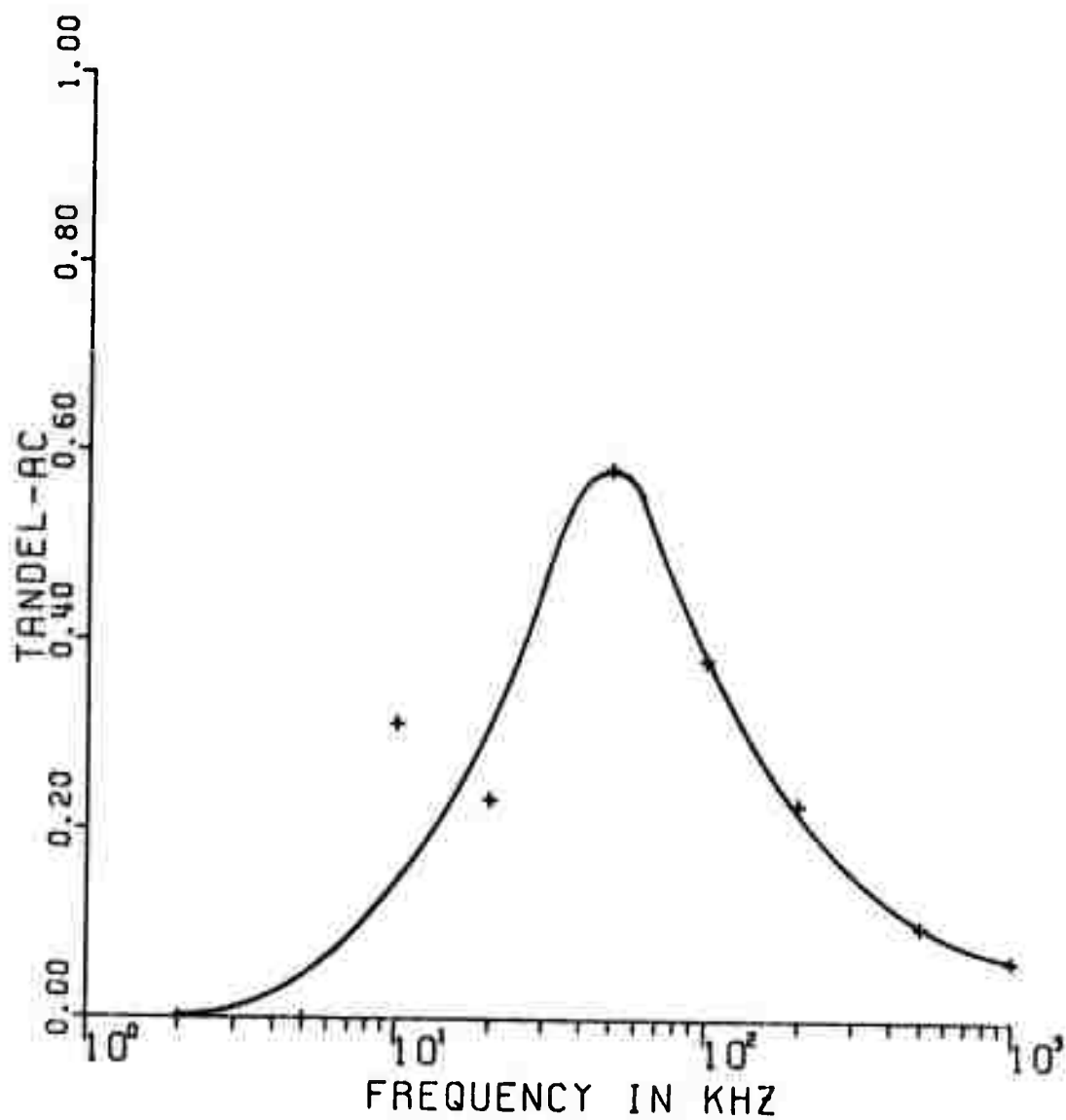
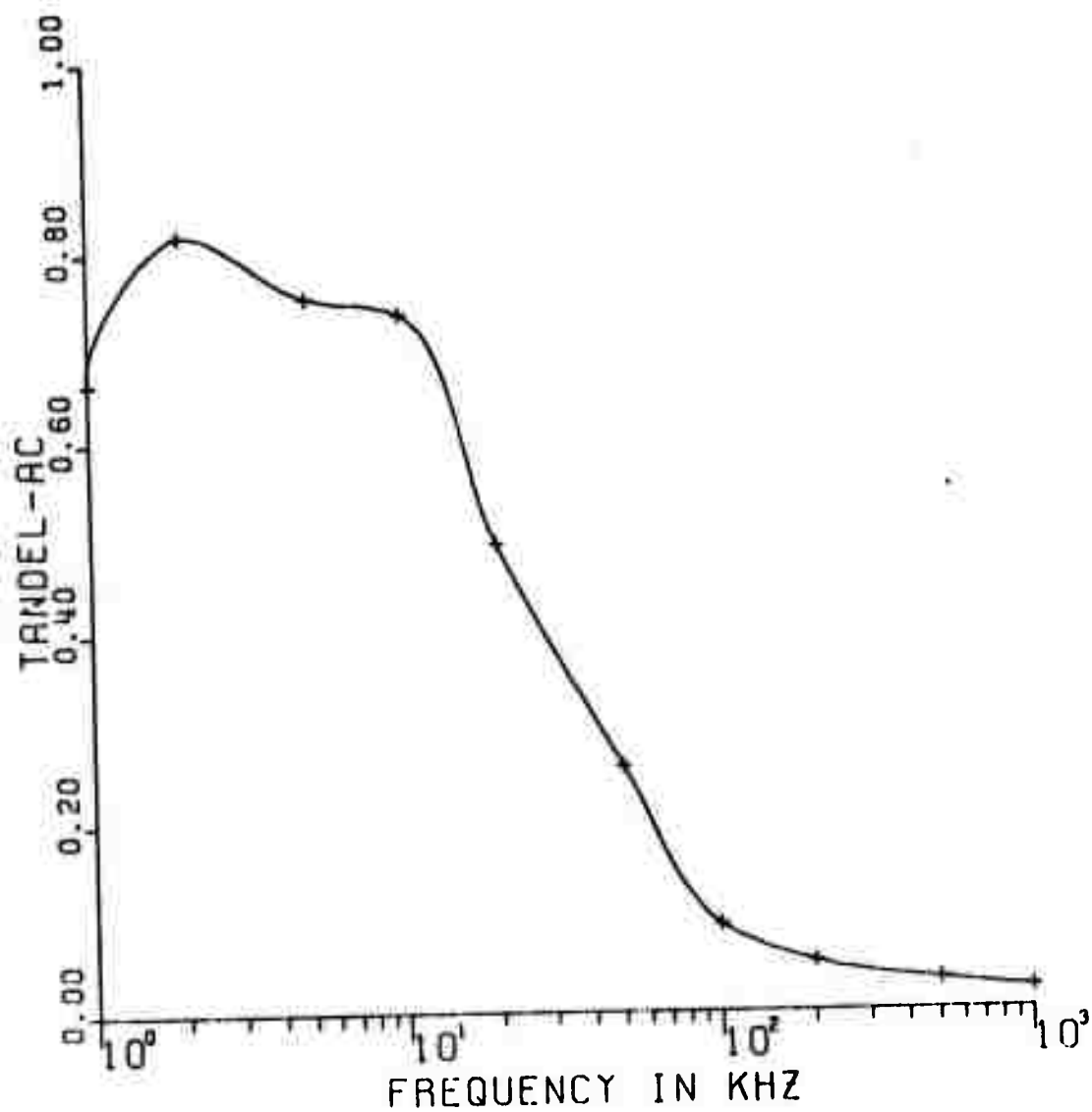Figure 12. Tan del versus log frequency, 70/30 glass.

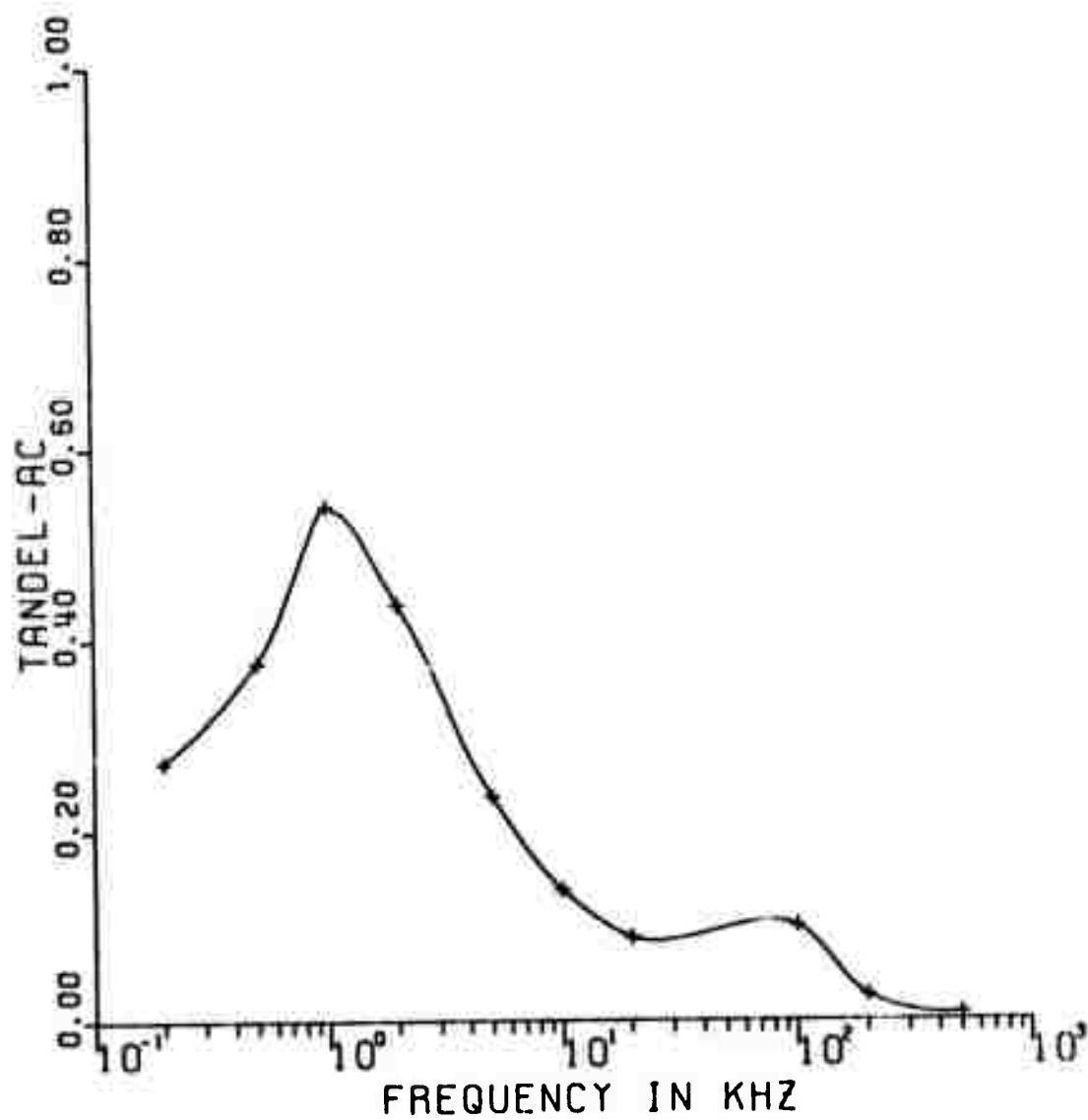Figure 13.   Tan del versus log frequency, 60/40 glass.

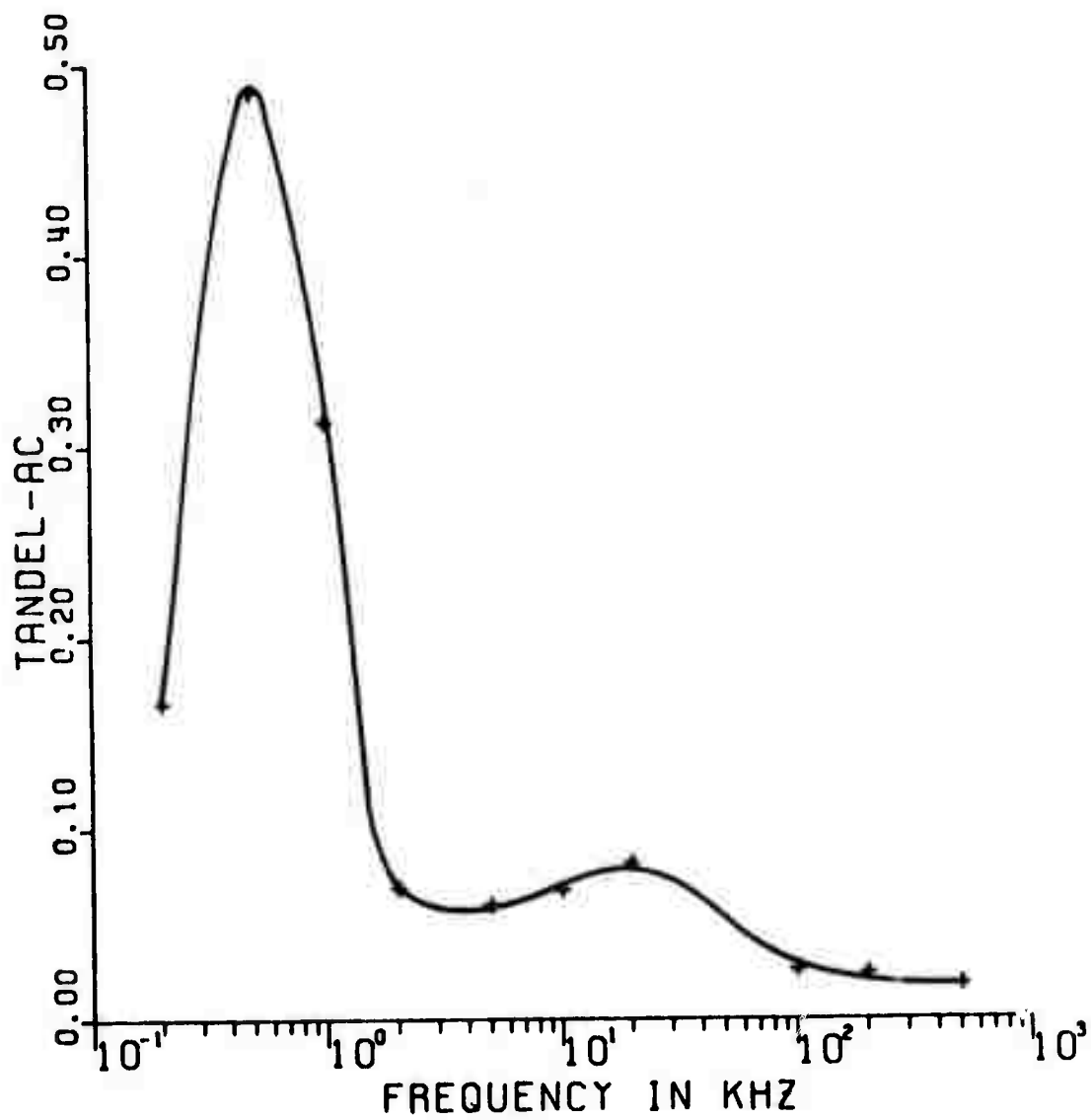Figure 14.   Tan del versus log frequency, 50/50 glass.
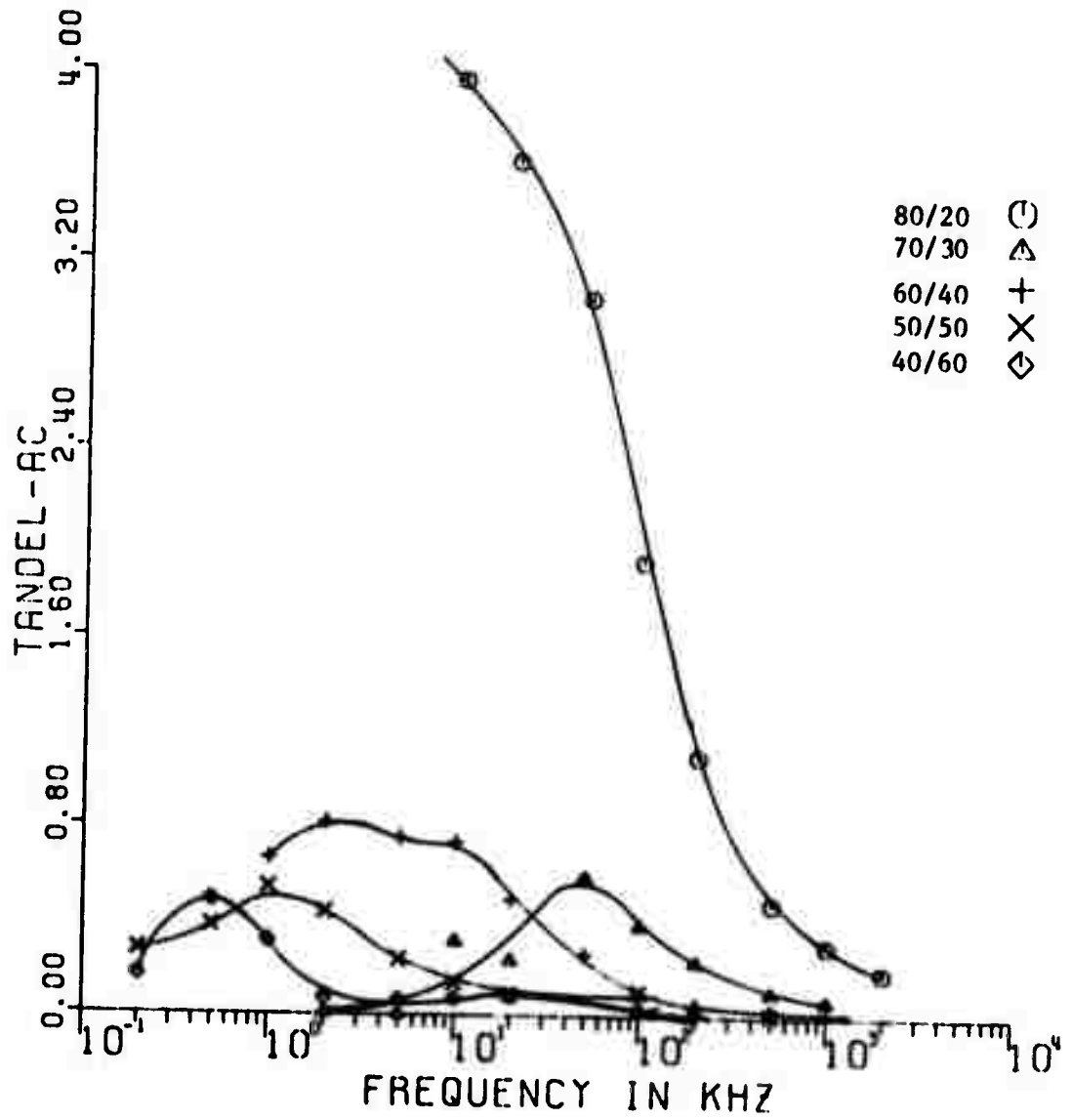
Figure 15. Tan del versus log frequency, 40/60 glass.

Figure 16. Tan del versus log frequency.

$$\sigma = \sigma_o \exp \left(\frac{-\Delta E}{kT} \right)$$

using a non-linear least squares fit.[18] This data is shown in Table 4, along with the data of Roilos.[19] Roilos' data was adjusted by a factor of one half due to a difference in the equations used by the two experimenters.

It was noted that surface conductivity is significant in these glasses. Measurements with unguarded samples resulted in conductivities approximately double those of the guarded samples. A guard ring configuration as was used was necessary.

The computations and plotting of the electrical results were by computer. The programs are included as an appendix.

E.M.

EM studies clearly indicate that liquid-liquid phase separation occurs in all the glasses studied, including arsenic triselinide. In all the compositions the droplike structure characteristic of nucleation and growth type of phase separation is apparent, while some also show a structure characteristic of a spinodal decomposition process. These processes are explained in the following chapter. Some of the droplets in the glasses have "tails," as shown by the arrow in Figure 17. These tails are formed as the fracture front passes around a drop and changes its plane of fracture. They are proof that the droplets are a part of the structure of the fracture surface, and not simply artifacts from the replicating procedure. The conchoidal mode of fracture and the

TABLE 4

ACTIVATION ENERGY

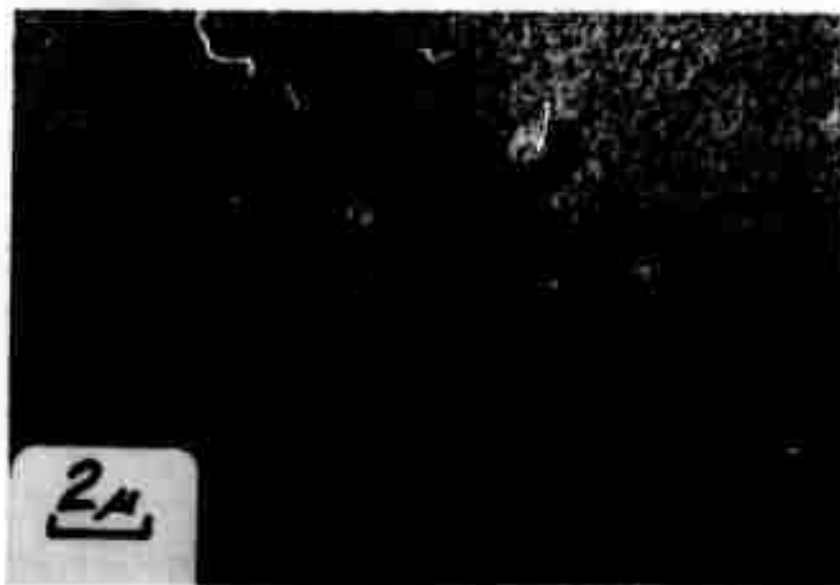| As_2Te_3/As_2Se_3	Activation Energy (ΔE) (e.v.)	σ_o $(x 10^3)$ $(\Omega \cdot cm)$
80/20	0.43	0.31
*75/25	0.49	
*71/29	0.51	
70/30	0.52	3.14
*66/33	0.515	
60/40	0.55	7.3
*60/40	0.53	
50/50	0.60	3.1
*50/50	0.575	
40/60	0.62	1.25
*33/66	0.64	

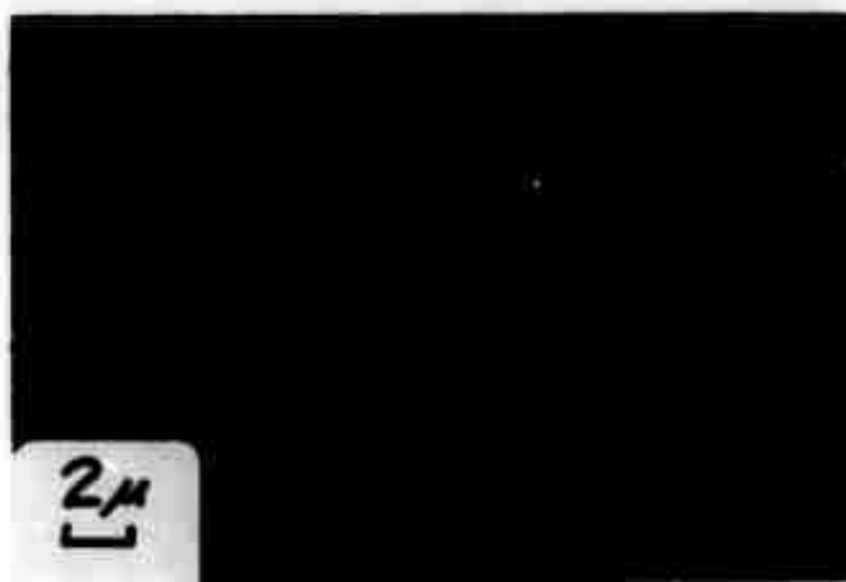Figure 17.   Electron micrograph showing droplet "tail."

Figure 18.   As$_2$Se$_3$ fracture surface.

x-ray results indicate that both phases are non-crystalline.

The electron photomicrographs of arsenic triselinide. Figures 18, 19, and 20 show the droplike structures. The drops are about one micron in diameter and are well formed. They occupy approximately a ten per cent volume fraction. A spinodal structure is not apparent in this glass. Note also, in Figure 20, that the fracture front has passed through the drops. This is indicated by the fracture pattern in the drops and the lack of relief in the surface. This implies that the drop and the matrix have similar mechanical properties and are probably of similar composition.

Micrographs of the 40/60 glass, Figures 21, 22 and 23 show large sized drops, primarily about three microns in diameter, but with some smaller drops apparent. Also apparent is an interesting structure within the drops not seen in the other glasses which may be indicative of a secondary segregation occurring in the primary separated phase.[20] The volume fraction of the large drops is less than ten per cent. No attempt was made to determine the amount of secondary segregation. The fracture "tails" are evident in this composition.

The 50/50 glass shows the droplet structure and also the spinodal structure, see Figure 24. The drop volume fraction is somewhat less than ten per cent, but the second phase, due to the spinodal decomposition, is much larger.

The 60/40 composition exhibits 1 to 1½ micron sized drops in a spinodal matrix. See Figure 25. Volume fraction of the drops is about 20%.

Micrographs of the 70/30 glass show a large quantity, approximately
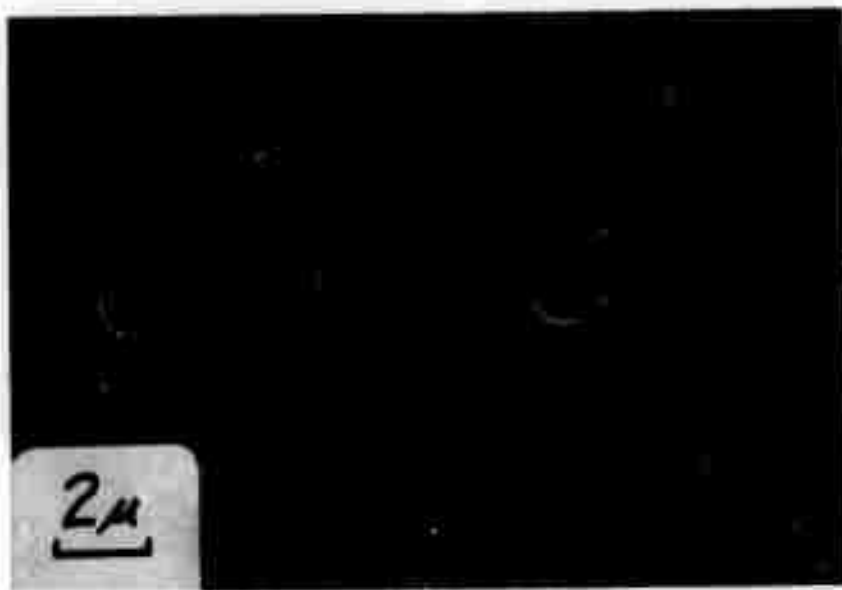
Figure 19. As_2Se_3 fracture surface.

Figure 20. As_2Se_3 fracture surface.

Figure 21.   40/60 glass fracture surface.

Figure 22.   40/60 glass fracture surface.

Figure 23. 40/60 glass fracture surface.

Figure 24. 50/50 glass, etched fracture surface.

176
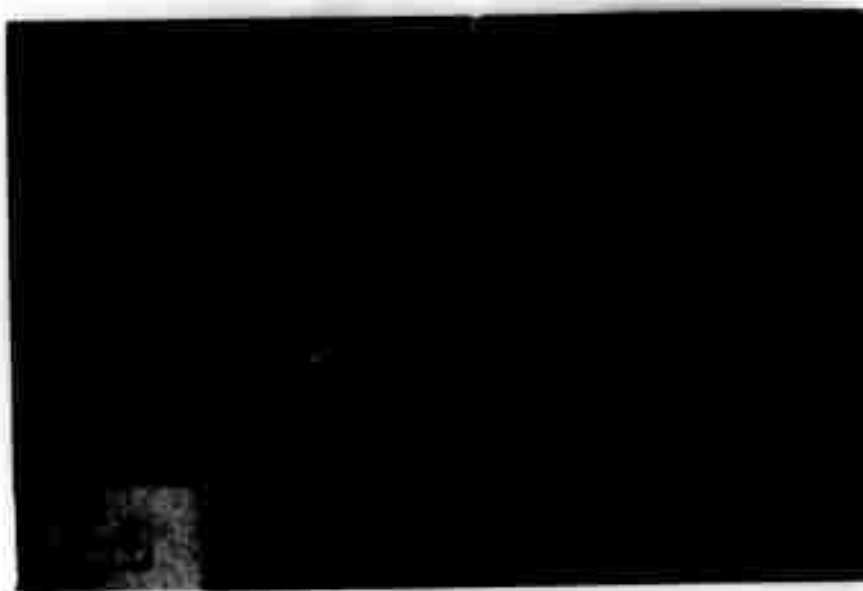
Figure 25. 60/40 glass, etched fracture surface.
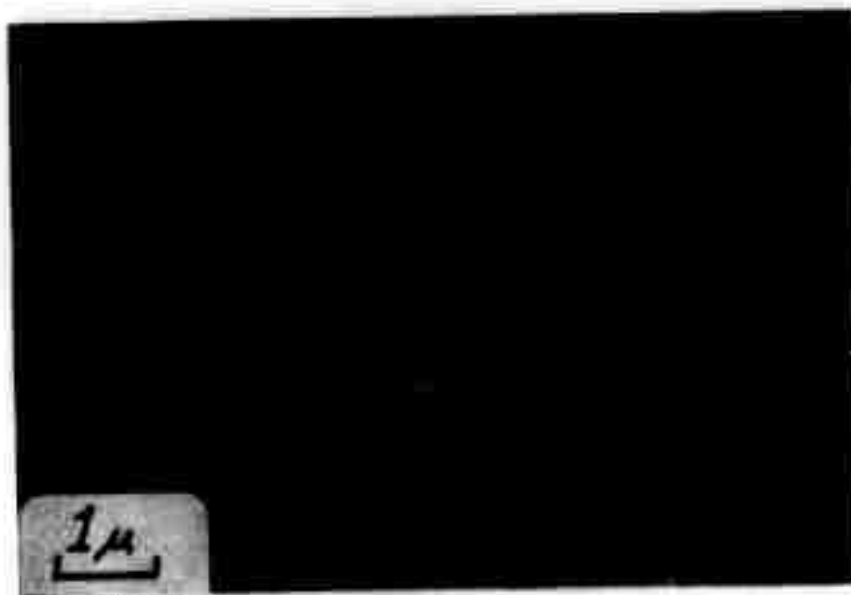
Figure 26. 70/30 glass fracture surface.

40% volume fraction, of small droplets. The majority are less than one micron in diameter. Many of the droplets are combining or are connnected. In Figures 26 through 28, the droplet morphology is clearly apparent, and is distinguishable from a spinodal structure.

The 80/20 glass shows a structure indicative of a spinodal decomposition process. The droplet morphology is discernable, but the structure is primarily that of two interconnected continuous phases. The volume fraction of the second phase is about 30%. Figures 29 and 30 are of the 80/20 glass.
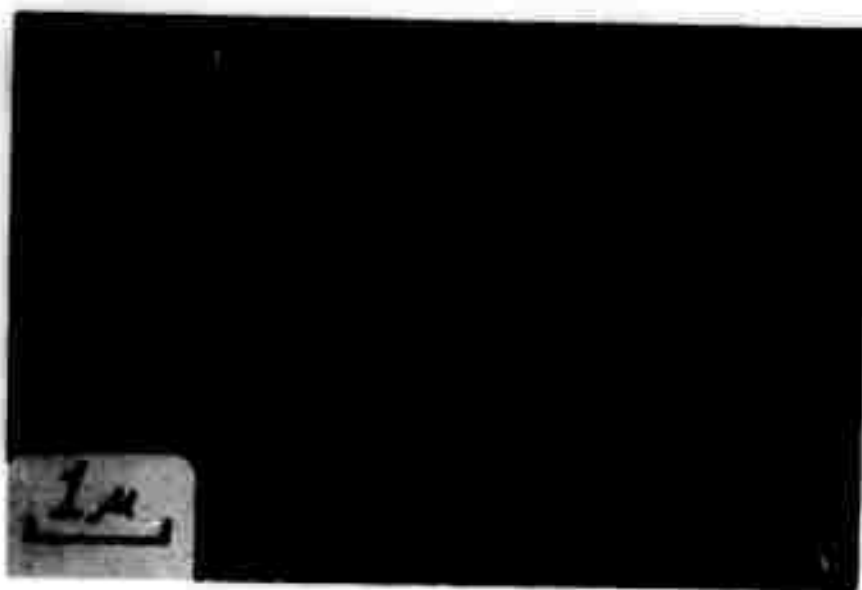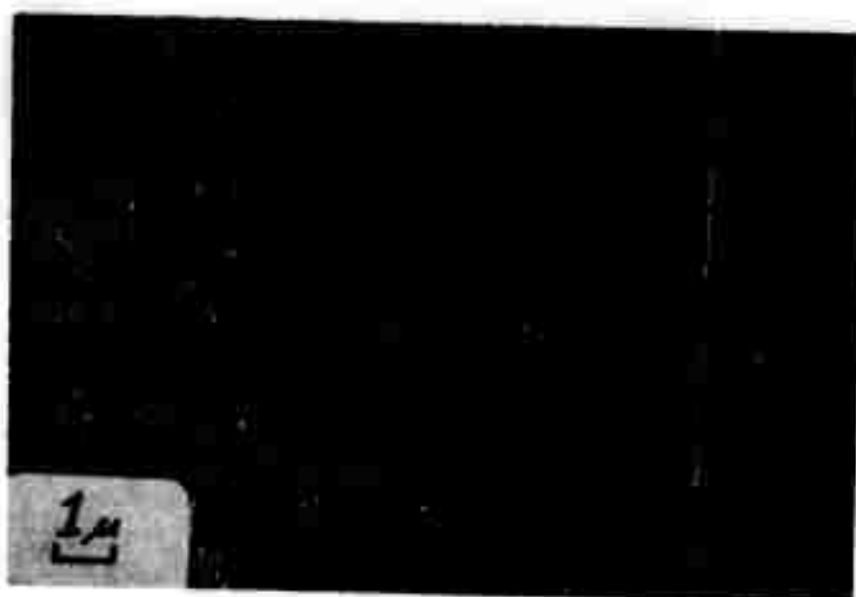
Figure 27. 70/30 glass, etched fracture surface.

Figure 28. 70/30 glass, etched fracture surface.

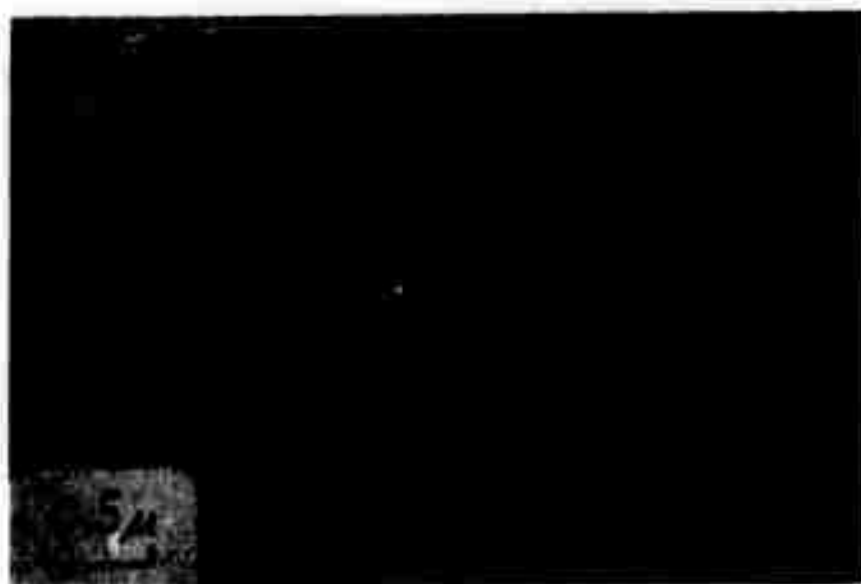Figure 29. 80/20 glass, etched fracture surface.

Figure 30. 80/20 glass, etched fracture surface.

CHAPTER IV

DISCUSSION

The results of the x-ray studies indicate that there are no crystal phases of greater than 0.1 weight per cent present. The DTA studies verify that the material is amorphous, by the occurrence of a crystallization reaction. These studies also indicate that the glasses with higher selenium content are better glass formers, as expected. A set of sample DTA curves showing the compositional dependence is given in Figure 31. The reaction temperature observed for each sample were dependent on the heating rate, indicating a kinetically limited process. Figure 32 shows the heating rate dependence of the reaction temperatures in the 80/20 glass. The occurrence of double crystallization peaks in the 80/20 and 70/30 glasses indicates that there are two crystalline phases forming in these compositions. These phases may both crystallize from a single phase glass, but the structural studies indicate that there are two glass phases present. Crystallization of each phase would result in a DTA peak. No double peaks are observed in the other glasses even though our E.M. studies show evidence of phase separation. The lack of the double peak could be due to the second phase being present in only small quantities. This is supported by the trend toward larger amount of phase separation in the higher tellurium glasses which was noted in the E.M. studies.

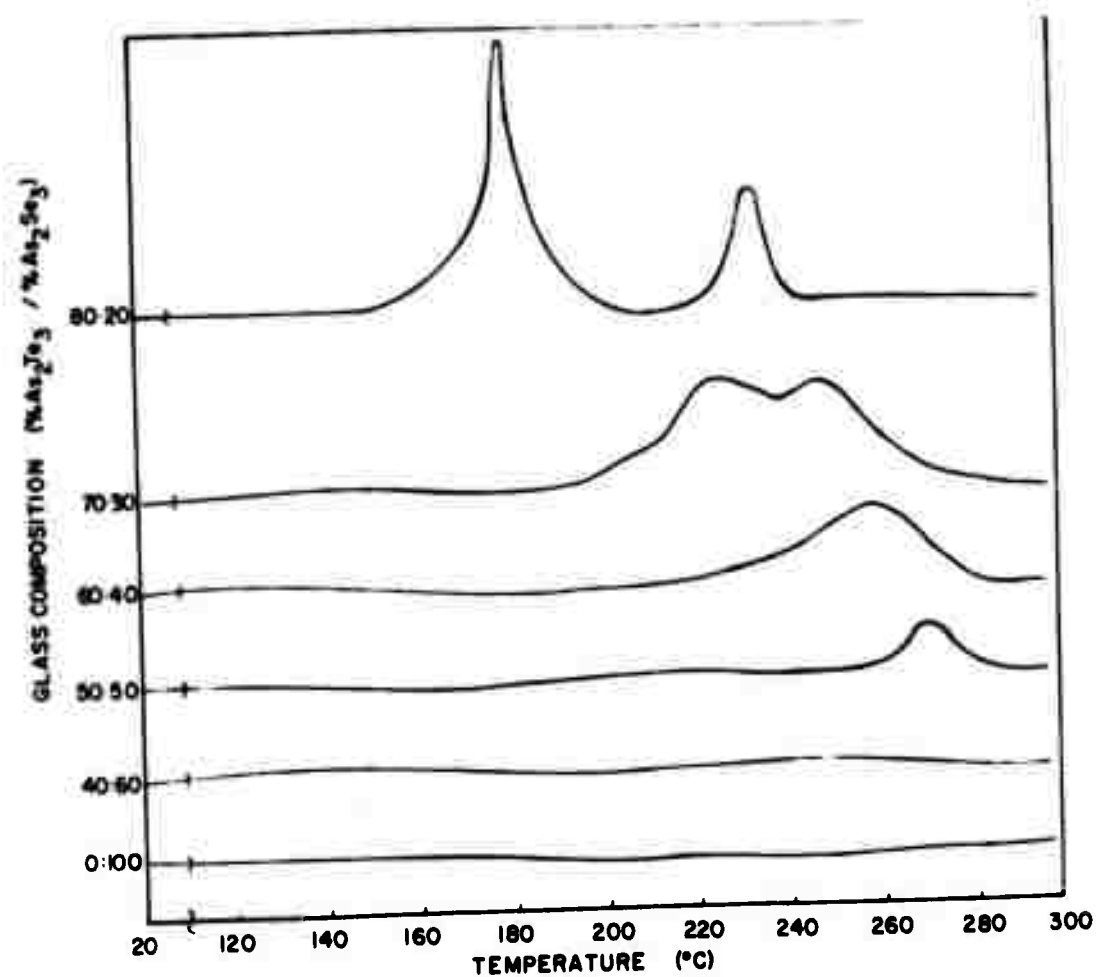Bagley and Bair[21] conducted differential scanning calorimetry on

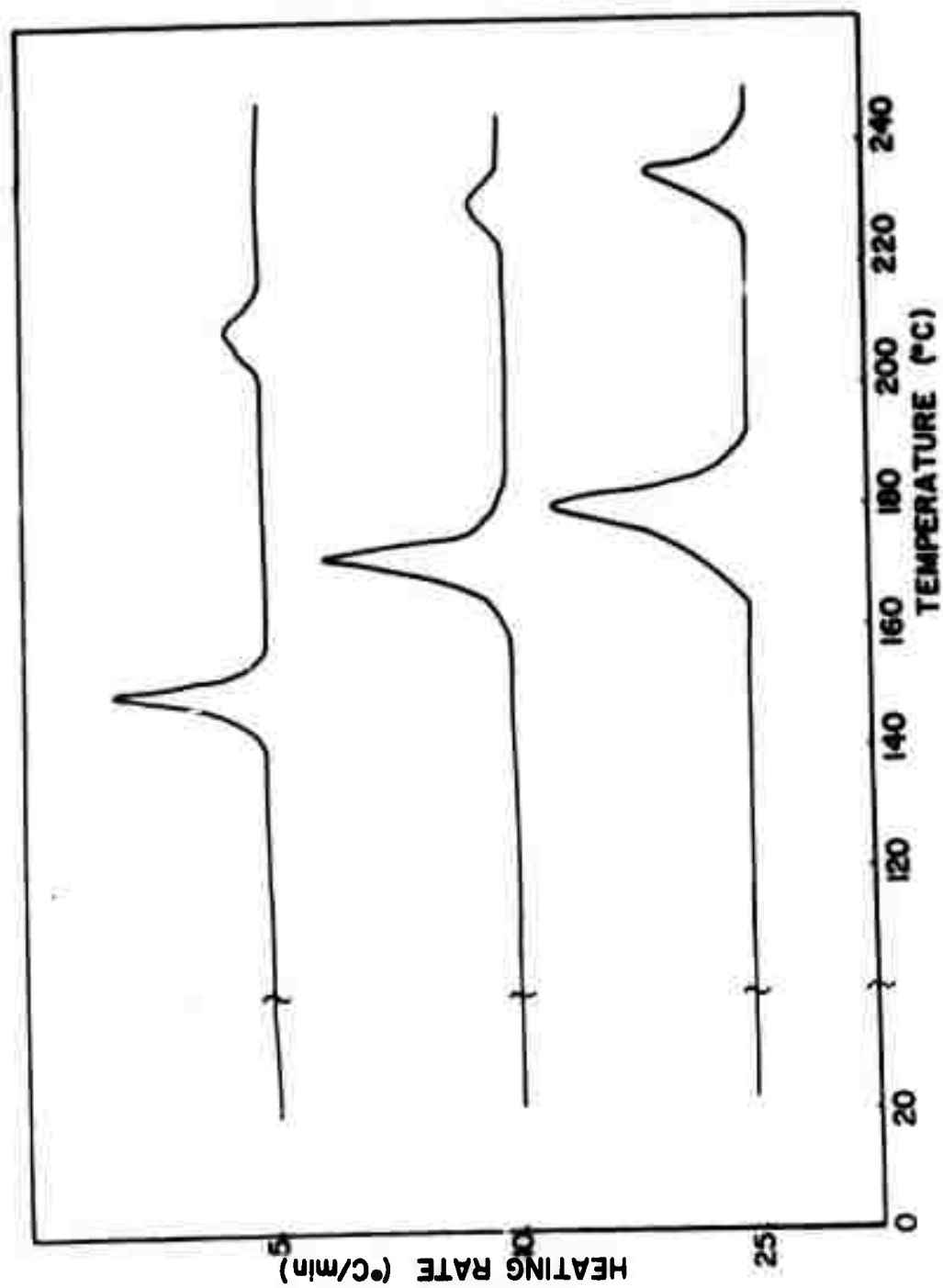Figure 31. Composition dependence in DTA curves.

Figure 32. Effect of heating rate in DTA curves.

183

arsenic triselinide-arsenic tritelluride glasses with As_2Te_3/As_2Se_3 ratios of 3/1, 2/1, and 1/2. The crystallization temperatures they determined (see Table 2) agree well with our data. However, they noted a small exothermic reaction preceding crystallization which they attributed to a glass transition. They also noted a doubly peaked endotherm at melting. They offered no explanation for the double peaks. In light of the phase separation our structural studies show is present in these glasses, it is reasonable to attribute the double peaks to a two phase melting occurring. Lack of a double peak at crystallization could be due to simultaneous crystallization of both phases.

Bagley and Northover[22] did not detect phase separation by electron microscopy in the glasses used by Bagley and Bair. However, they primarily used transmission microscopy on thin films, with some replica work on unetched, fracture surfaces. Phase separation is difficult to detect in specimens that have not been etched. If the electron densities of the separated phases are similar, then it is difficult if not impossible to detect phase separation in transmission. Also, a thin film of an amorphous material does not necessarily have the same structure as the bulk material.

The electron microscopic studies indicate the presence of separated phases in all the compositions studied. The DTA and x-ray data shows both (or all) of the phases to be amorphous. Since the phase separated glasses include both binary sides of the ternary phase diagram, it is likely that the phase separation, and therefore an immiscibility gap, extends across the entire arsenic tritelluride-arsenic triselinide join.

The morphology of the phases observed in the glasses indicate

that two phase separation processes are occurring: a nucleation and growth type of separation and a spinodal decomposition process. Nucleation and growth occurs by the classically accepted process of growth of a heterogeneously nucleated particle. Formation of well rounded spheriods or droplets is indicative of this type of diffusion controlled growth occurring in an amorphous material. The surface tension of the glassy-liquid controls the shape of the drop. This structure is similar to a suspension of water and oil.

Spinodal decomposition occurs spontaneously or homogeneously throughout the parent phase. It has more the appearance of a natural sponge parent phase, with the interconnected voids of the sponge filled with the second phase. Both new phases, of course, have a different composition than the original phase. A summary of the thermodynamic description of these processes by Cahn and Charles[13] is given here.

A necessary condition for stability of a phase with respect to infinitesimal composition or density fluctuations in that the chemical potential of each component increase with increasing density of that component. This condition, as will be seen, is not in conflict with the existence of a more stable phase, and thus metastability can and does occur commonly. In some systems there exists a temperature, which is a function of composition, where this necessary criterion for stability breaks down. This limit to the metastability has been called the spinodal. Beyond the spinodal a single phase is unstable with respect to infinitesimal composition fluctuation and begins to separate into two related phases differing only in composition. This occurs spontaneously, without the need for nucleation, since the phase is no longer metastable but unstable. The related phases that form may be the equilibrium phases, or they may in turn be only metastable with respect to still more stable phases and subject to further application of stability criteria.

In a binary system, Gibb's condition for metastability reduces to $\partial^2 F/\partial c^2 > 0$ where F is the molar free energy and c is the mole fraction. The spinodal is to be expected in every system that exhibits stable or metastable equilibrium between two related phases. It is

most commonly to be expected in systems having a consolute temperature. Consider a binary system with an upper consolute (sometimes called critical) temperature, T_c (Figure 33). At a constant temperature above the consolute temperature, the molar free energy F, as a function of composition must curve upward everywhere, Figure 33b. (Otherwise separation into two phases would reduce free energy). As the temperature is dropped the curve rises by an amount proportional to the molar entropy.

$$- \frac{\partial F}{\partial T} = S$$

Because the entropy is expected to be smallest for the two pure liquids (and for compounds) and greatest near the middle of the composition range, the free energy curve flattens as the temperature is dropped and, eventually, below the consolute temperature, a portion with negative curvature develops. If the composition lies between the compositions a and b, the lowest free energy is a two-phase mixture with one phase having composition a and the other b. Outside these limits a single phase is still stable.

In Figure 33b the inflexions in F occur at c and d and are the spinodal compositions for the temperature T_1, lying somewhere between a and b. If the free energy function exists and has no discontinuities in slope, the inflexions must exist at all temperatures below the upper consolute temperature. Therefore, the unstable region, beneath the spinodal, is shown in Figure 33a to extend to the consolute temperature.

The metastable region exists between the spinodal and the phase boundary. If the single phase is cooled from above the phase boundary into this region, it would be metastable and would only decompose into the two phases if the second phase can nucleate. Any attempt by the system to separate into regions differing only slightly in composition will raise the system free energy. If, however, the single phase is brought within the unstable region (between c and d) the system can continuously lower its free energy by continuous compositional changes until it reaches the two phases of equilibrium composition at a and b..... In the region where $\partial^2 F/\partial c^2 > 0$, the single phase liquid is metastable to infinitesimal composition fluctuations, and the second liquid phase must form by nucleation. In the unstable region, where $\partial^2 F/\partial c^2 < 0$, the single phase liquid is unstable to infinitesimal composition fluctuations, and phase separation proceeds without nucleation..... The characteristics of phase separation by nucleation and growth are the appearance of recognisable and distinctly separated particles of the new phase which in time grow in size and may coalesce.

When a single phase liquid is cooled through the metastable region rapidly enough to prevent appreciable phase separation, the mode of phase separation changes radically after it crosses the spinodal into
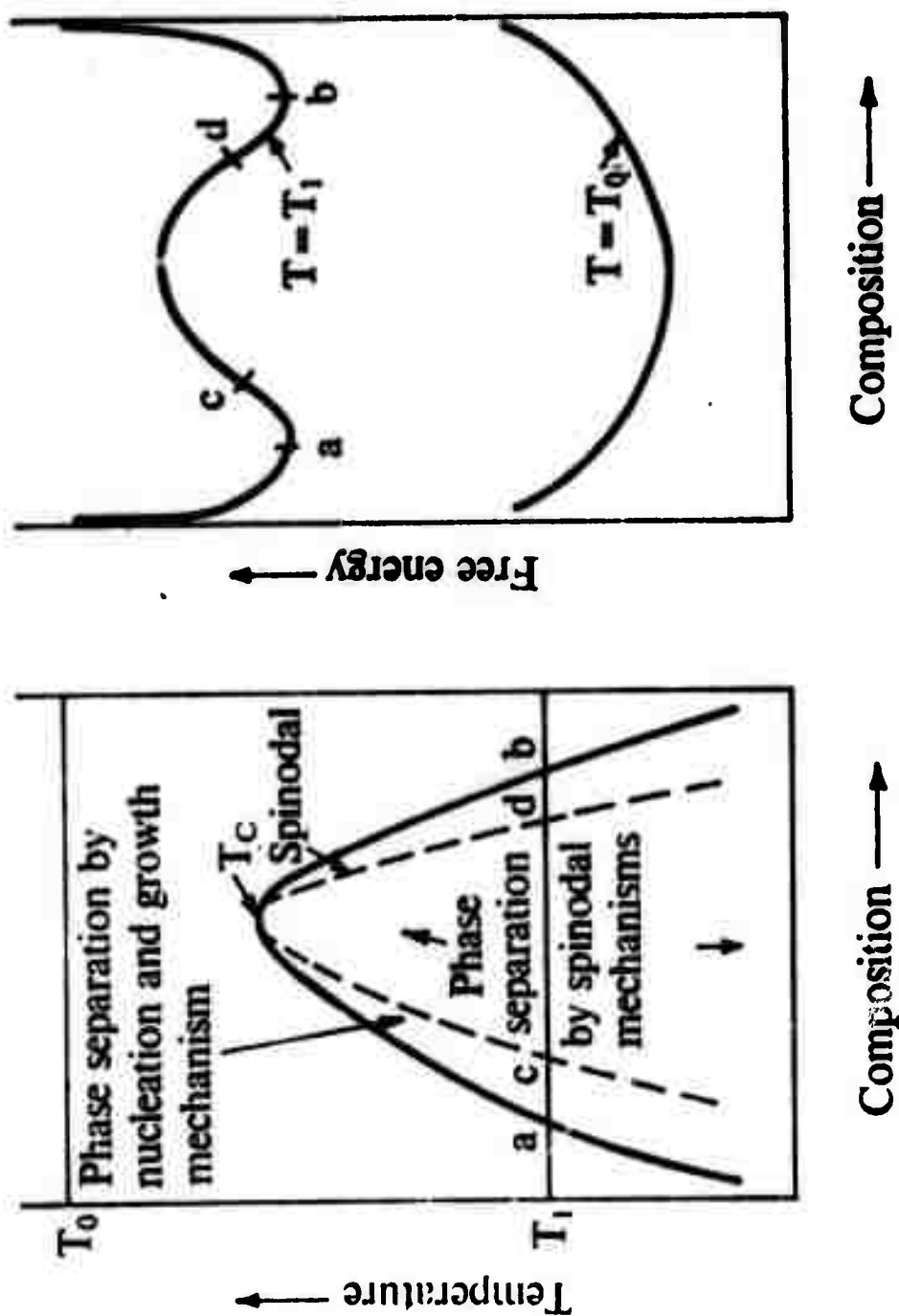
186

Figure 33. Schematic phase diagram showing the phase boundary and spinodel of a two-liquid immiscibility region; (b) free energy composition diagrams for the temperatures given in (a). (From Cahn and Charles)

the unstable region. Particles which had nucleated and were growing, now stop growing and become centres from which sinusoidal composition variations spread outward..... Two completely interpenetrating phases are formed from an initially homogeneous single phase. Each phase has a high degree of connectivity. The geometry of this two-phase structure initially remains unaltered, while the difference in composition between the two phases changes with time. Table 5 lists some of the factors which differentiate between the mechanisms.

The variation in the stages of phase separation in the samples studied makes it difficult to accurately correlate the amount of phase separation with composition. Generally the glasses with a higher selenium content tend to be more stable and exhibit less phase separation. This is significant in light of the concurrent switching studies being done by Sanders[24] in this laboratory. Sanders' results indicate that the higher selenium glasses have higher breakdown voltages and are more stable switches than the high tellurium glasses. This indicates a correlation between switching and the structure due to phase separation. Careful electron microscopic studies of heat treated glasses are needed to determine the extent of the phase separation and the compositions of the separated phases. Further switching studies of these heat treated glasses would allow any correlation to be verified.

The results of the electrical studies are conclusive. The conductivity-temperature behavior is typical of an intrinsic semiconductor. The D.C. conductivity data generally agree well with the results of Roilos.[25] Slight variations are probably due to thermal history differences.[26] The D.C. data as plotted in Figure 10 is repeated in Figure 34 with the data of Roilos. The activation energies are compared in Table 4. The room temperature conductivity also agrees well with that of Mott and Davis.[26] This data is graphed in Figure 35. As noted

TABLE 5

SOME FACTORS WHICH DIFFERENTIATE BETWEEN NUCLEATION AND GROWTH AND SPINODAL MECHANISMS DURING ISOTHERMAL PHASE SEPARATION. (From Cahn and Charles)

| Nucleation and Growth	Spinodal Decomposition
Invariance of second phase composition to time at constant temperature	Continuous variation of both extremes in composition with time until equilibrium compositions are reached
Interface between phases is always some degree of sharpness during growth	Interface between phases initially is very diffuse eventually sharpens
Tendency for random distributions of particle sizes and positions in matrix	Regularity of second phase distribution in size and position characterized by a geometric spacing
Tendency for separation of second phase spherical particles with low connectivity	Tendency for separation of second phase, non-spherical particles with high connectivity
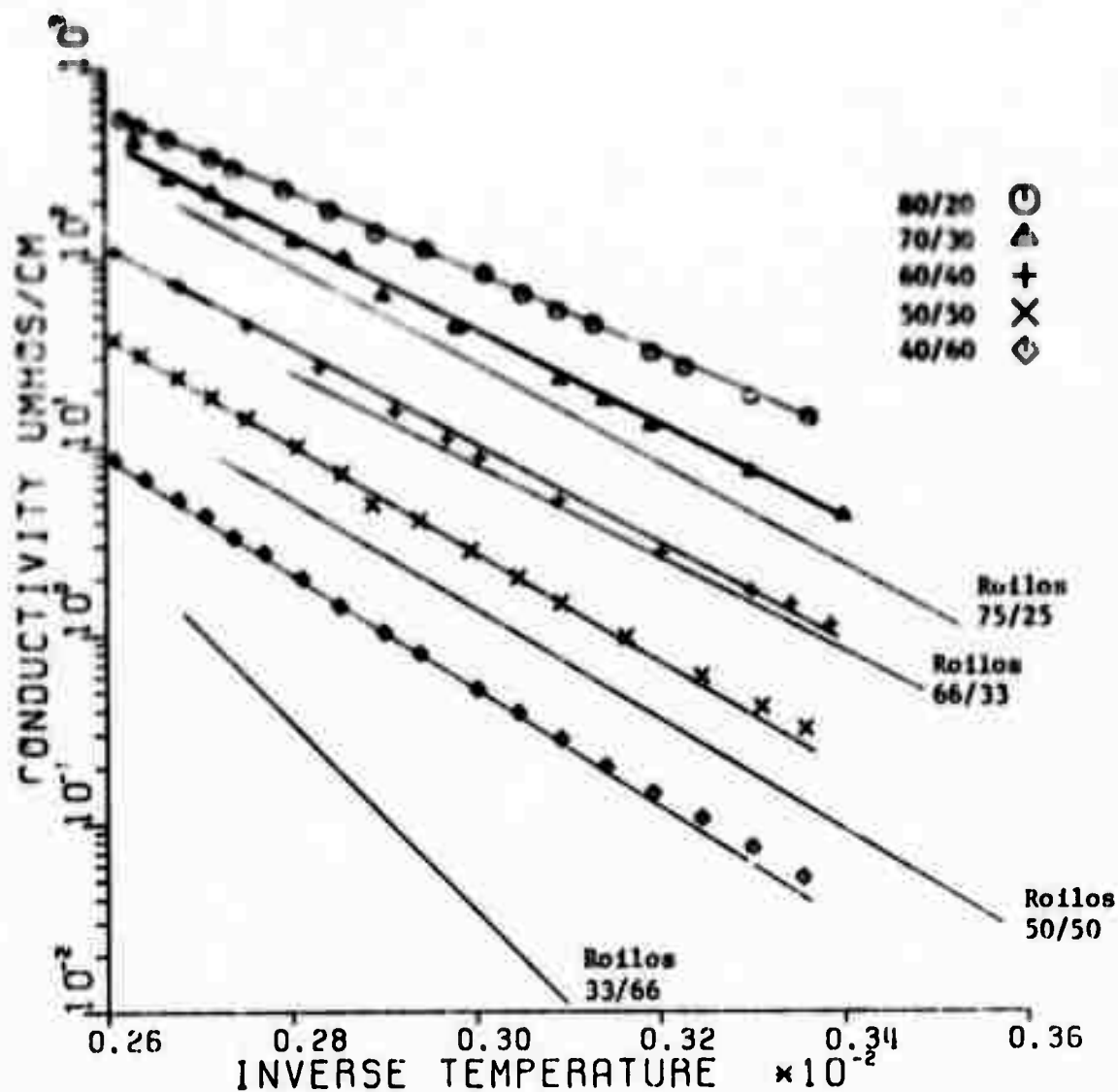
Figure 34.   Log conductivity versus temperature with Roilos'
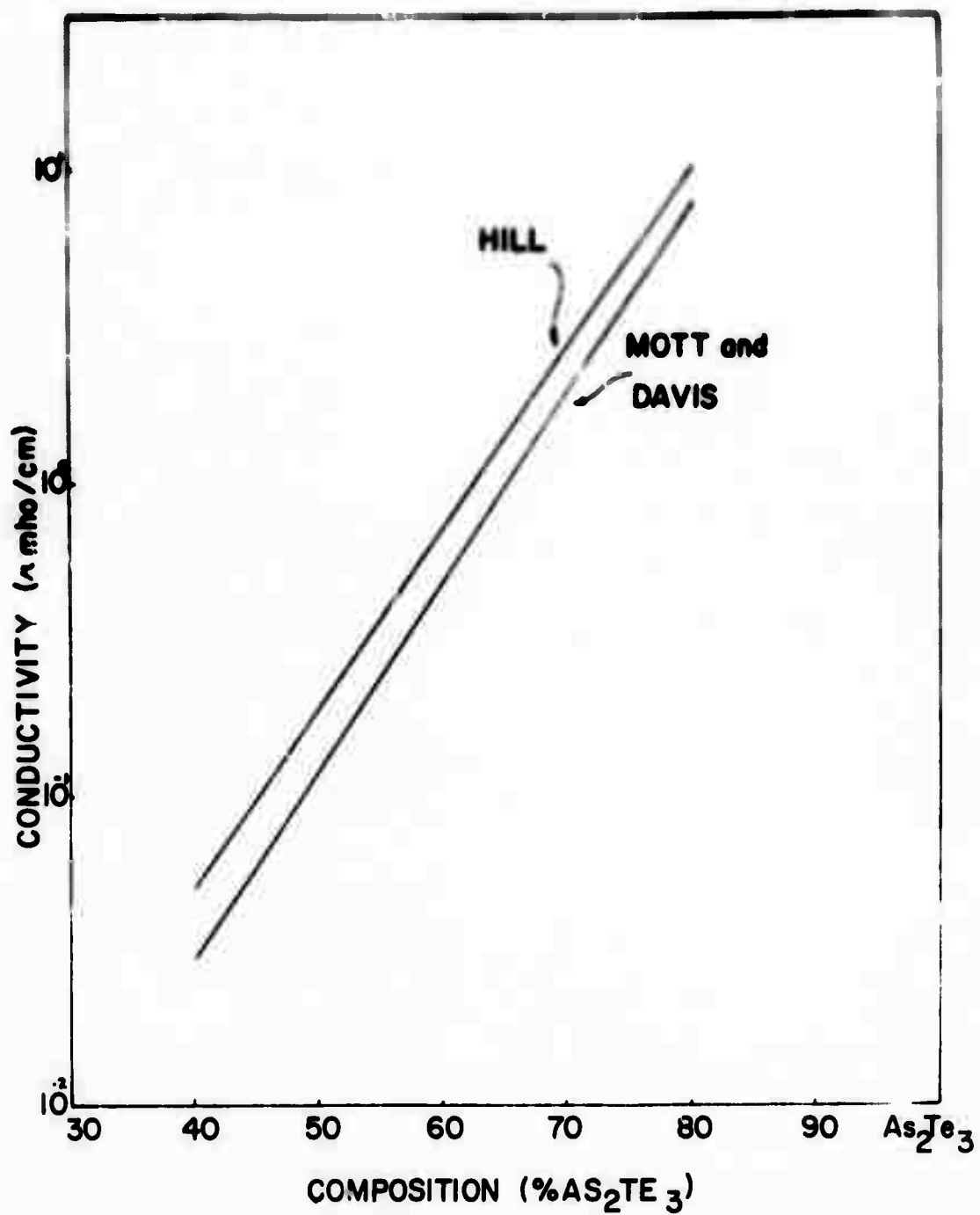   data.

Figure 35. Room temperature D.C. conductivity with data from Mott and Davis.

191

In Table 4, there is a variation in the pre-exponential term, σ_0, with a maximum at the 60/40 composition. It appeared to Mott and Davis[20] that the pre-exponential term "remained essentially constant." The variation in the D.C. electrical properties with composition is probably due to the interstitial substitution of selenium by the heavier tellurium atom. Structural rearrangements may also play a role, but it is felt that it would be a minor role in this case.

The dispersions in the tan del versus frequency curves indicate that Maxwell-Wagner-Sillars heterogeneous loss conditions are present. These losses result from the presence of structural inhomogeneities, such as crystallites or other large particles with distinct boundaries.

There can be some doubt that the dispersions in the curves are valid. By varying the value of the D.C. component subtracted in the tan del calculations and observing the changes in the curves, one can determine if the loss peaks are real. If, as the D.C. value is increased, the dispersions straighten out and the curves go smoothly through zero to negative tan del values, then the peak is not a real representation of the dielectric loss. However, if the peaks remain in the curves as they go negative, and the curves only smooth out with very large or very small D.C. values, then the dispersions are real and are due to actual losses within the system. All the samples behaved in the latter manner. An example is given in Figure 36. Thus, there is a definite loss effect in these glasses. In light of the microstructural studies, these losses are logically due to the structural inhomogeneities which are a result of the phase separation processes occurring in the glasses. The variation in the frequency at which the
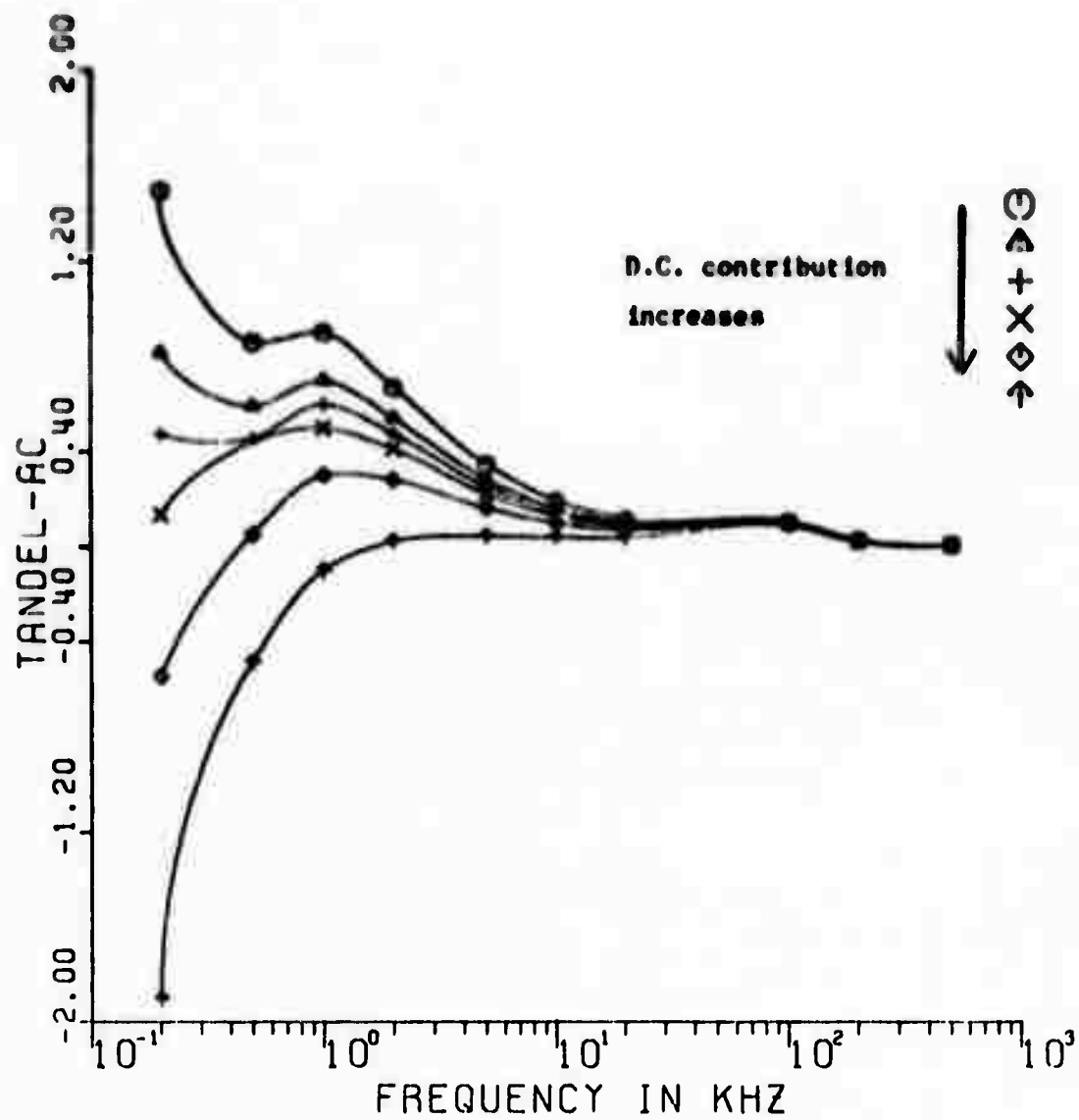
Figure 36. Effect of D.C. contribution on tan del.

193

dispersions occur for the different compositions results from changes in the microstructure. These changes are due to the variation in the amount of phase separation in the glasses.

The relationship between the structure and electrical properties of these glasses cannot yet be fully defined. It is possible that they are related solely through a compositional dependence. This author feels that the structural dependence is predominant, but additional studies with heat treated glasses are needed to correlate the structural and compositional variables. These studies are needed to fully characterize the system.

CHAPTER V

CONCLUSIONS

All of the arsenic triselinide-arsenic tritelluride glasses $xAs_2Te_3(1-xAs_2Se_3)$ studied from $x = 0$ to $x = 80$ are phase separated. This indicates that there exists a miscibility gap across the entire ternary phase diagram of the arsenic-selenium-tellurium system. The structure appears to be related to and vary with composition, but without further study the relationship cannot be defined. Analogous phase separation has been noted by other authors in related chalcogenide systems.

The electrical properties of these glasses vary with composition. D.C. conductivity increases with tellurium content. Activation energy decreases with tellurium content and σ_o has a maximum near the middle of the composition range. The variation in the D.C. properties may be due to structural changes, compositional changes, or a combination of both. Structural inhomogeneities resulting from glass-glass phase separation appear to be responsible for the occurrence of Maxwell-Wagner-Sillars heterogeneous losses in these glasses.

CHAPTER VI

RECOMMENDATIONS FOR FURTHER STUDY

Electrical and structural studies equivalent to those described
in this thesis need to be conducted using heat treated samples. The
use of annealed electrical specimens would allow any compositional
influence on the electrical properties to be defined. Correlations
between the dielectric losses and the phase separated structure would
result from careful structural analysis of these same heat treated
glasses. Extreme care should be exercised in the annealing process
and subsequent handling of these glasses as their structure is extra-
ordinarily sensitive to variations in heat treatment. Ideally, E.M.
samples should be taken from the actual electrical specimens. Finally
close contact with the switching studies should be maintained, as it
appears there are important correlations in this area.

APPENDIX

```
C
C
C
C             TANDEL
C    A PROGRAM TO CALCULATE CERTAIN
C    ELECTRICAL PROPERTIES OF
C    SEMICONDUCTING GLASSES
C        WRITTEN BY
C      GLENN A. MITCHELL
C          FOR
C    MATERIALS SCIENCE DEPARTMENT
C    VANDERBILT UNIVERSITY
C
      REAL INVTEM(20)
      DIMENSION SIGMA(30),F(30),CAPAC(30),TANDEL(30),TEMP(30),
     CAMPS(30),TANTOT(30),G(30),TITLE(10),GO(30),SIGAC(30)
     C,TITLE1(10),TITLE2(10),TITLE3(10)
      DATA TITLE/' CON','DUCT','IVIT','Y VS',', IN','VERS','E TE','MP,'
     C,' ',' '//,TITLE1/'FREC',', VS',', TA','NDEL',' TOT','AL',' ',' ',
     C' ',' '//,TITLE2/'FREQ',', VS',', TA','NDEL',',-AC',' ',' ',' ',
     C' '//,TITLE3/'FREQ',', VS',', CU','NDUC','TIVI','TY(A','C)',' ',' ',
     C,' '/
      READ(5,5)NDC
      READ(5,2)THICK,DIAM,VOLTS
      TA=THICK/((3.14159*DIAM*DIAM)/4.)
      DO 1 I=1,NDC
      READ(5,10)TEMP(I),AMPS(I)
      INVTEM(I)=1000./(TEMP(I)+273.16)
      GO(I)=AMPS(I)/VOLTS
    1 SIGMA(I)=TA*AMPS(I)/(VOLTS-.001*AMPS(I))
      CALL PLOT(SIGMA,INVTEM,1,NDC,TITLE,30)
      CALL PLOT(SIGMA,INVTEM,-1,NDC,TITLE,30)
      READ(5,5)NRF
      DO 2 I=1,NRF
      READ(5,8)F(I),CAPAC(I),R
      G(I)=1000./(R)
    2 SIGAC(I)=G(I)*TA
      READ(5,5)NAB
      NAC=NRF+NAB
      K=NRF+1
      DO 3 I=K,NAC
      READ(5,8)F(I),CAPAC(I),G(I)
    3 SIGAC(I)=G(I)*TA
      READ(5,17)GOC
      DO 4 I=1,NAC
      TANTOT(I)=G(I)*1000./(3.14159*2.*F(I)*CAPAC(I))
    4 TANDEL(I)=(G(I)-GOC)*1000./(3.1410559*2*F(I)*CAPAC(I))
```

197

```
     [illegible faded code lines]

C
C
C
11
        [illegible]
        [illegible]

14       [illegible]

16       [illegible]

18       [illegible]

20       [illegible]

C C C   PLOT IS A GENERALIZED SUBROUTINE WRITTEN BY RICHARD MANNING
C C C   OF THE ELECTRICAL ENGINEERING DEPARTMENT, VANDERBILT UNIVERSITY
C
        SUBROUTINE PLOT(A,B,D,STEP,RTYPE,N,TITLE,MAX)
        DIMENSION A(100),B(100),TA(9),LN(9),TITLE(10),LNUM(9),C(9),
       &R(50),ATEMP(1),BTEMP(1)
        LOGICAL LT1,LT2
        DATA HA/' ',...,'*'/,...,/LBLANK,LZERO/' ','0'/,LNUM
       &,LASK/'1','2','3','4','5','6','7','8','9','0'/
        ITYPE=RTYPE
        DO1000I=2,50
 1000   LN(I)=LN1
        DO 1005 I=1,N
        A(I)=ATEMP(I)
 1005   B(I)=BTEMP(I)
        LN(I)=LN26
        LN(51)=LN1
C***    THE NEXT 12 STATEMENTS ORDER THE DATA FOR PLOTTING
        M=N-1
        DO 1030 I=1,M
        JJ=I+1
        DO 1030 J=JJ,N
        IF (A(I).LE.A(J)) GO TO 1030
        R1=A(I)
```

198

LIST OF REFERENCES

1. B. T. Kolomiets and N. A. Goryunova, _Zhur. Tek. Fiz. SSSR_, 25 (1955), 984; from A. David Pearson, "The Glass Industry," January 1965, p. 18.

2. A. I. Gubanov, _Quantum Electron Theory of Amorphous Conductors_, Consultants Bureau, New York, (1963).

3. H. L. Uphoff and J. H. Healy, _J. Appl. Phys._, 32, (1961) p.950.

4. J. F. Dewald, A. D. Pearson and W. R. Northover and W. F. Peck, Jr., _J. Electrochem. Soc._ 109 (1962) p.243C.

5. M. H. Cohen, H. Fritzsche and S. R. Ovshinsky, _Phys. Rev. Lett._, 22 (1969) p.1065.

6. R. W. Vass and R. M. Anderson, _Electro-Optical Effects in Amorphous Solids_, Purdue University, 1970.

7. A. C. Warren, _Electron. Lett._, 5 (1969) p.461.

8. A. C. Warren, _J. Non-Crystalline Sol._, 4 (1970) p.613.

9. H. J. Stocker, C. A. Barlow, Jr., and D. F. Weirauch, _J. Non-Crystalline Sol._, 4 (1970) p.523.

10. A. D. Pearson, _J. Non-Crystalline Sol._, 2 (1970) p.1.

11. W. Haller, D. H. Blackburn, F. E. Wagstaff and R. J. Charles, _J. Am. Cer. Soc._, 53 (1970) p.34.

12. A. D. Pearson, _J. Electrochem. Soc._ 111 (1964) p.753.

13. N. S. Platakis, V. Sadagopan and H. C. Gatos, _J. Electrochem. Soc._, 116 (1969) p.1436.

14. A. D. Pearson, _The Glass Industry_ (1965) p.18.

15. B. T. Kolomiets and T. F. Nazarova, _Soviet Physics, Solid State_, 2 (1960) p.159.

16. J. D. Mackinzie, _J. Non-Crystalline Sol._, 2 (1970) p.19.

17. L. K. H. van Beek, _Progress in Dielectrics_, 7 (1967) p.69.

18. J. B. Scarborough, _Numerical Mathematical Analysis_, The John Hopkins Press, Baltimore, 1966, p.545.

19. M. Roilos, _J. Non-Crystalline Sol_., $\underline{6}$ (1971) p.10.

20. W. Vogel, _Structure and Crystallization of Glasses_, Pergamon Press, Germany, 1965, p.61.

21. B. G. Bagley and H. E. Bair, _J. Non-Crystalline Sol._, $\underline{2}$ (1970) p.155.

22. B. G. Bagley and W. R. Northover, _J. Non-Crystalline Sol._, $\underline{2}$ (1970) p.161.

23. J. W. Cahn and R. J. Charles, _Physics and Chemistry of Glasses_, $\underline{6}$ (1965) p.181.

24. H. Sanders, "Electrical Switching Phenomenon in the A_2Te_3-As_2Se_3 Glass System," to be published.

25. M. Roilos, p.8.

26. D. L. Kinser, D. J. Hill, H. R. Sanders and L. K. Wilson, _J. Non-Crystalline Sol._, $\underline{8\text{-}10}$ (1972) p.823.

27. N. F. Mott and E. A. Davis, _Electronic Processes in Non-Crystalline Materials_, Oxford University Press, 1971, p.362.

28. Ibid.

U.H.F. AND MICROWAVE DIELECTRIC PROPERTIES OF
A CLASS OF AMORPHOUS SEMICONDUCTORS

JOHN DAVID PEARSON

<u>Thesis under the direction of Professor Larry Kittrell Wilson</u>

Recent interest in amorphous semiconductors has focused primarily on the electrical switching behavior of these materials. Very little work has been directed, however, toward characterizing their dielectric properties at radio frequencies, especially in the U.H.F. and microwave range.

This paper considers the compositional variation in the dielectric properties of the glass system $(x)As_2Te_3(1-x)As_2Se_3$ for $x=0.4, 0.5, 0.6, 0.7,$ and 0.8 over the frequ range 100-18,000 Mhz, at room temperature ($25^{\circ}C$).

The materials were prepared by $\qquad$ the mixtures of As_2Te_3 and As_2Se_3 in a rocking furnace. After he for several hours, the molten material was quenched in water.

Complex permittivity measurements were made by three techniques. For the frequency range 100-500 Mhz, the materials were shaped into circular disks and placed in an air-filled coaxial line. A Thurston Bridge was used to determine the complex impedance of the sample, which was used to calculate the dielectric constant and loss tangent. In the range 500-2,000 Mhz, a slotted coaxial line was used to measure null shift and VSWR, which led to the calculation of the sample impedance and the dielectric properties. In the range 12,000-18,000 Mhz,

rectangular shaped samples were used in conjunction with a K_u-band slotted waveguide. The dielectric properties were obtained by measuring VSWR, wavelength, and position of the voltage minimum and using the Von Hippel Standing Wave Method to calculate the proper order solution to a complex transcendental equation.

The average dielectric properties measured over the entire frequency range are as follows:

Composition	ϵ'	tan δ
80%As$_2$Te$_3$-20%As$_2$Se$_3$	10.0	0.055
70%As$_2$Te$_3$-30%As$_2$Se$_3$	9.3	0.049
60%As$_2$Te$_3$-40%As$_2$Se$_3$	7.9	0.042
50%As$_2$Te$_3$-50%As$_2$Se$_3$	7.2	0.030
40%As$_2$Te$_3$-60%As$_2$Se$_3$	7.0	0.020

The dielectric properties of the samples were found to be essentially frequency independent over the frequency range studied, with slight variations attributed to differences in experimental techniques. By increasing the Tellurium composition, it was found that the dielectric constant can be varied from approximately 7.0 to 10.0. The loss tangent was also found to increase with increasing Te content and varied between approximately 0.02 and 0.06. The dielectric properties of this glass system compare favorably with those of dielectric materials used for microwave substrates, such as YIG, Silicon, or AlSIMag.

Approved _____ Date _____
                    Advisor

U.H.F. AND MICROWAVE DIELECTRIC PROPERTIES OF

A CLASS OF AMORPHOUS SEMICONDUCTORS

By

John David Pearson

Thesis

Submitted to the Faculty of the

Graduate School of Vanderbilt University

in partial fulfillment of the requirements

for the degree of

MASTER OF SCIENCE

in

Electrical Engineering

May, 1972

Nashville, Tennessee

Approved: Date:

_____   _____

_____   _____

ACKNOWLEDGMENTS

TABLE OF CONTENTS

LIST OF ILLUSTRATIONS

CHAPTER I

INTRODUCTION

Amorphous semiconductors are disordered materials in which atoms
have local organization or short-range order, but lack the periodic
structure of crystals, for distances greater than a few atomic radii.
The atomic positions in the nearest and next nearest neighbors are thus
essentially the same in the amorphous and crystalline states [1].
Elements which can be formed into amorphous compounds exhibiting these
characteristics include germanium and silicon (Group IV), antimony,
arsenic, and bismuth (Group V), and selenium, sulfur, and tellurium
(Group VI) [2]. The present study centers around examining some
properties of a class of these amorphous materials, $As_2Te_3-As_2Se_3$.

Amorphous semiconductors are probably most well known for their
switching and memory effects. In 1958 S. R. Ovshinsky began research on
these devices and in 1961 filed a patent on an amorphous device, 48%Te-
30%As-12%Si-10%Ge, which was insensitive to polarity in switching
operations [3]. Later in 1961, A. D. Pearson, J. F. Dewald, W. R.
Northover, and W. F. Peck discovered switching and memory phenomena in
As-Te-I glass. However its reset properties were subject to polarity
[4,5]. D. L. Eaton reported the same phenomena in this glass in 1964
[6]. In 1963 switching behavior was found in glasses of the class
$TlAs(Se,Te)_2$, by Kolomiets and Lebedev [7]. Later W. R. Eubank found
switching behavior in Sb-S-I glass [8]. Since this time considerable

1

efforts have been spent in studying the switching properties of other amorphous materials [9].

A threshold switch is a two terminal device which can be in an off (almost nonconducting) state or in an on (conducting) state. When the applied voltage is greater than the threshold value, the system switches to the conducting state and produces a "negative resistance" effect. However if the current is reduced below its critical "holding" value, the glass will switch back to its original high resistance state. Threshold switching has been seen to occur in 250 picosecond, with a one microsecond delay before switching [10].

The memory switch is similar to the threshold switch, but has a stable "on" state, and thus is a bistable device. When a high voltage pulse is applied to the switch when "off," heating and structural changes occur in the device with a partial ordering of its structure, and the device is permanently switched to the "on" state. It will remain there even if the current is completely removed. It is believed that the voltage pulse results in the growth of a crystal filament or pathway between anode and cathode, resulting in a low resistance path for the current [1]. The switch can be restored to the off state by applying a threshold pulse of either polarity [5]. Switching times for memory switches have been observed to be on the order of a few milliseconds [1C].

In addition to examining the switching properties of amorphous semiconductors, many researchers have studied various electrical and physical properties of these materials. Properties considered in the last several years include the optical absorption spectrum [11], the

variation of conductivity in the audio and high frequency range, the temperature dependence of the d.c. conductivity [12,13,14] and the thermal switching properties [15]. A general overview of research in the field is given in a recent National Materials Advisory Board report [11].

At Vanderbilt University the switching properties of the glass system $(x)As_2Te_3(1-x)As_2Se_3$ have recently been studied [16,32]. The electrical, thermal, and structural properties of this system have also been extensively investigated [17]. The dielectric properties of the glass in the frequency range from d.c. to 10 Mhz have been studied as a function of microstructure by Hill [18]. The only known research characterizing the high frequency dielectric properties of this glass system was published recently by this writer and others [19].

The purpose of the research presented in the present paper is to examine the U.H.F. and microwave dielectric properties of the glass system $(x)As_2Te_3(1-x)As_2Se_3$ for $x=0.4,0.5,0.6,0.7$, and 0.8, and in particular to note their range of variation as a function of tellurium content.

CHAPTER II

EXPERIMENTAL

Introduction

Dielectric constant and loss tangent measurements were made on the glass samples by three techniques. In the frequency range 100-500 Mhz a Thurston Bridge was used to determine the complex admittance of a circular sample placed at the end of a shorted air-filled coaxial line. This data was used with the field equations of a parallel plate capacitor to calculate the dielectric constant and loss tangent of its dielectric sample.

For the range 500-2,000 Mhz a slotted coaxial line, terminated in the sample and a variable short, was used to measure null shift and VSWR. This data was substituted into the transmission line equations for input admittance to yield the sample admittance, which was used with the capacitance equations, as above, to calculate the dielectric constant and loss tangent.

In the range 12,000-18,000 Mhz a K_u-band slotted waveguide was used, terminated with the sample and a variable short circuit. Measurements taken were wavelength, position of the voltage minimum, and VSWR. A graphical technique given by Von Hippel was used to solve the equation for the wave impedance in the sample, which led to the dielectric constant and loss tangent of the sample.

The materials were prepared by fusing the appropriate mixture of

4

As_2Te_3 and As_2Se_3 in evacuated Vycor ampoules at $800°C$ in a rocking furnace. After heating for one hour the molten material was quenched in water. The samples were then shaped and polished with wetted 60 and 90 grit carborundum paper, into circular disks and rectangles for the frequency ranges 100-2,000 Mhz and 12,000-18,000 Mhz respectively.

100-500 Mhz

In this frequency range the admittance of a sample positioned at the end of an air-filled coaxial line was measured by a Thurston bridge. Using this value in the equations for a parallel plate capacitor, the dielectric constant and loss tangent of its dielectric sample was calculated. The parallel plate capacitor arrangement of the sample is shown in Figure 1 and its electrical equivalent is shown in Figure 2.

A is the area of the sample face and T is the sample thickness. T is exaggerated in Figure 1 for clarity. However a very thin sample was used to avoid fringing effects. I_g and I_c are the dissipative and reactive currents in the sample, respectively. The derivation of the permittivity below follows the treatment given by Harrington [20].

The voltage-current relationship for a capacitor is

$$I = I_g + I_c = YV = (G + j\omega C)V \tag{1}$$

and the field strength and current density are, respectively, given by

$$E = \frac{V}{T} \tag{2}$$

and

$$J = \frac{I}{A} \tag{3}$$

The constitutive relation for the field in the dielectric is

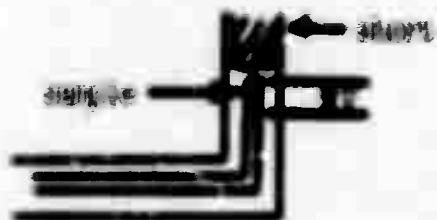$$J = (\sigma + \omega\varepsilon'' + j\omega\varepsilon')E \tag{4}$$

213

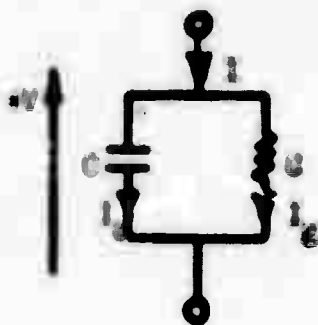FIGURE 1. Sample placement in capacitor arrangement.

FIGURE 2. Electrical equivalent of sample in circuit.

where σE represents the conduction current component and $(\omega\varepsilon'' + j\omega\varepsilon')E$ represents the displacement current components. Substituting Equations (2) and (3) into (4),

$$I = [(\sigma + \omega\varepsilon'' + j\omega\varepsilon')(\tfrac{A}{T})]V \tag{5}$$

Comparing (5) with (1) we find

$$Y = G + j\omega C = (\sigma + \omega\varepsilon'' + j\omega\varepsilon')\tfrac{A}{T} \tag{6}$$

or

$$G = (\sigma + \omega\varepsilon'')\tfrac{A}{T} \tag{7}$$

and

$$C = (\varepsilon')\tfrac{A}{T} \tag{8}$$

Substituting $C = \dfrac{B}{\omega}$ in Equation (8), and dropping σ from (7) because it is small for the glasses considered, and dividing both equations by ε_0 to give relative values, we can solve for the complex permittivity:

$$\varepsilon' = \frac{BT}{\varepsilon_0 \omega A} \tag{9}$$

$$\varepsilon'' = \frac{GT}{\varepsilon_0 \omega A} \tag{10}$$

Dividing Equation (10) by Equation (9) we obtain the loss tangent

$$\tan\delta = \frac{\varepsilon''}{\varepsilon'} = \frac{G}{B} \tag{11}$$

The computer program COMP given in Appendix I uses the above equations with the admittance data from the Thurston Bridge to calculate the relative dielectric constant and loss tangent of the sample.

The experimental setup used a G.R. 1602-B Thurston Bridge or admittance meter, to obtain the complex admittance of the sample which was placed at the end of a shorted air-filled coaxial line. The samples were circular disks, approximately 0.246" in diameter and ranged in thickness between 0.029" and 0.042". Figure 3 shows a block diagram of

the setup used.

The rf source was set to the operating frequency and the local rf source was set to a frequency 30 Mhz below this. A 30 Mhz amplifier and meter were used to adjust the airline and stub tuner by detecting the difference component between the two sources, so that the sample admittance appeared at the bridge's input. By adjusting the conductance and susceptance lever arms of the bridge for a null meter reading, the sample admittance was read directly in millimhos. The frequency was read by detecting a harmonic with a Transfer Oscillator and a 10 Mhz Electronic Counter. The technique used in this frequency range was not repeated for higher frequencies because of the unavailability of two stable rf sources covering frequencies greater than 500 Mhz.

A 90° coaxial bend was placed at the end of the air-line with the sample holder and variable short placed vertically into this. This is detailed in Figure 4. The sample was placed atop the brass rod which extended up from the bottom of the sample holder. The sample and rod had approximately the same diameter. The short, a solid brass cylinder glued to the micrometer drive rod, was carefully lowered until it made contact with the sample. Admittance measurements were then taken with data treated according to the program COMP given in Appendix I.

500 Mhz-2,000 Mhz

In this frequency range a slotted coaxial line, terminated in a circular sample and a variable short, was used in measuring the null shift and VSWR. This data was used to calculate the sample admittance,
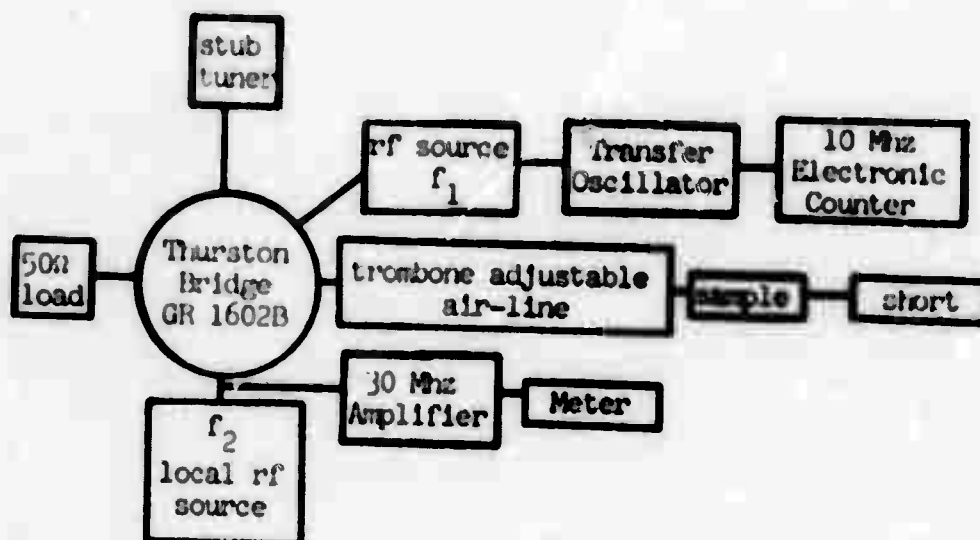
FIGURE 3. Equipment setup for measuring dielectric constant and loss tangent in the range 100-500 Mhz.
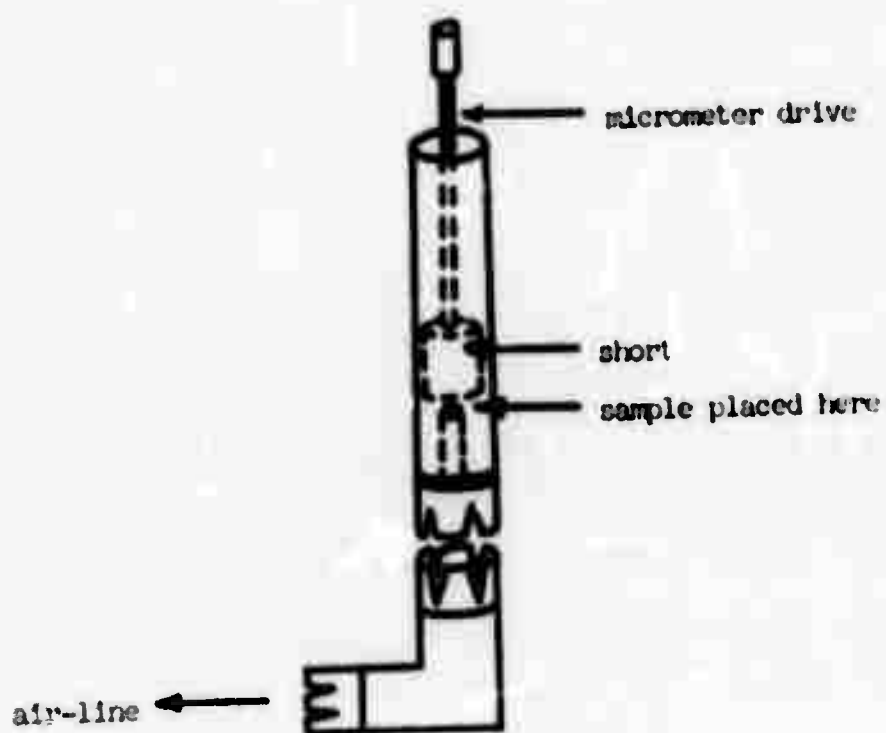
FIGURE 4. Sample holder assembly.

which was used with the parallel plate capacitance relations to calculate the dielectric constant and loss tangent of the sample.

The derivation of the transmission line admittance equation is given below. It is similar to that given for impedance by Collin [21]. Figure 5 shows a transmission line, terminated in a load Y_L, and with incident and reflected voltages V^+ and V^- respectively. The incident and reflected waves interfere to form a sinusoidal standing wave pattern. Thus the voltage at any point on the line can be written as

$$V = V^+ e^{j\beta\ell} + V^- e^{-j\beta\ell} \qquad (12)$$

where $\beta = \frac{2\pi}{\lambda}$ is the propagation constant at some frequency, and $\ell > 0$. Similarly the current at any point is

$$I = I^+ e^{j\beta\ell} - I^- e^{-j\beta\ell} \qquad (13)$$

The normalized input admittance is

$$\bar{Y}_{in} = \frac{Y_{in}}{Y_c} = \left(\frac{1}{Y_c}\right)\left(\frac{I}{V}\right) = \frac{(I/Y_c)}{V} = \frac{V^+ e^{j\beta\ell} - V^- e^{-j\beta\ell}}{V^+ e^{j\beta\ell} + V^- e^{-j\beta\ell}} \qquad (14)$$

where Y_c is the characteristic admittance of the line. By definition the reflection coefficient at the load is $\Gamma_L = \frac{V^-}{V^+}$. Thus (14) can be rewritten as

$$\bar{Y}_{in} = \frac{e^{j\beta\ell} - \Gamma_L e^{-j\beta\ell}}{e^{j\beta\ell} + \Gamma_L e^{-j\beta\ell}} \qquad (15)$$

Γ_L can also be written as $\Gamma_L = \frac{Z_L - Z_c}{Z_L + Z_c}$, a well known identity derived by Collin [21]. This identity can be rewritten as

$$\Gamma_L = \frac{Y_c - Y_L}{Y_c + Y_L} = \frac{1 - \bar{Y}_L}{1 + \bar{Y}_L} \qquad (16)$$

Now replacing $e^{\pm j\beta\ell}$ by $(\cos \beta\ell \pm j\sin \beta\ell)$ and substituting Equation (16)
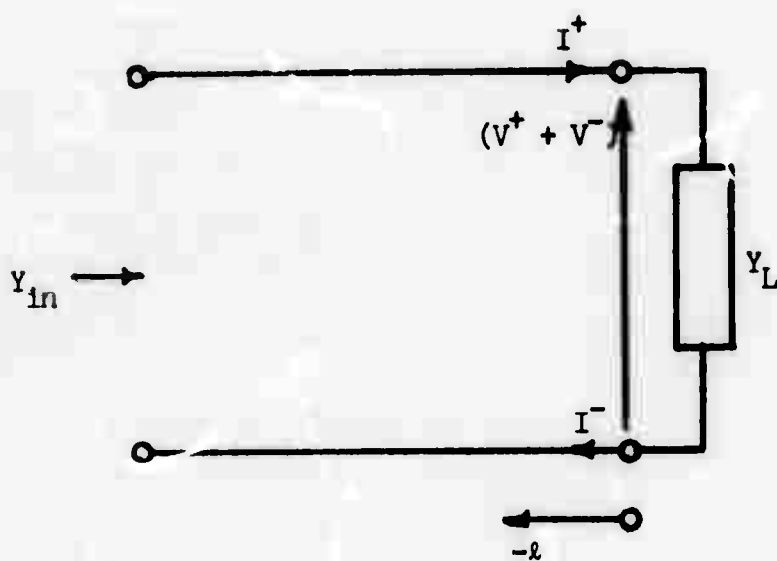
FIGURE 5. Transmission line with load Y_L.

into (15) we obtain

$$\bar{Y}_{in} = \frac{\bar{Y}_L \cos \beta l + j \sin \beta l}{\cos \beta l + j \bar{Y}_L \sin \beta l} \qquad (17)$$

This can be solved for $\bar{Y}_L$, the sample admittance,

$$\bar{Y}_L = \frac{\bar{Y}_{in} \cos \beta l - j \sin \beta l}{\cos \beta l - j \bar{Y}_{in} \sin \beta l} \qquad (18)$$

At the voltage minimum the value $\bar{Y}_{in}$ is real and in magnitude equals the VSWR, as proved in Appendix II. The computer program SLOT shown in Appendix II uses Equation (18) for admittance with Equations (9) and (11) to calculate values of dielectric constant and loss tangent for the samples.

The equipment used for this frequency range included a slotted coaxial line (G.R. Type 900-LB) which was used for measuring null shift and VSWR. The same disk-shaped samples used in the frequency range 100-500 Mhz were used in this range and the sample holder of Figure 4 was used at the end of the slotted line. The setup used is shown in Figure 6. The frequency was measured by using a transfer oscillator and a 10 Mhz Electronic Counter to observe a harmonic of the fundamental frequency.

The slotted line scale was calibrated in millimeters so that readings were accurate to 0.001 meter. The VSWR was read from this scale by the two point method, since high VSWR values were encountered [22]. This method involves finding the position of a standing wave voltage minimum along the slotted line using a square law detector and a 1000 Hz meter. Then the positions of points on each side of the minimum
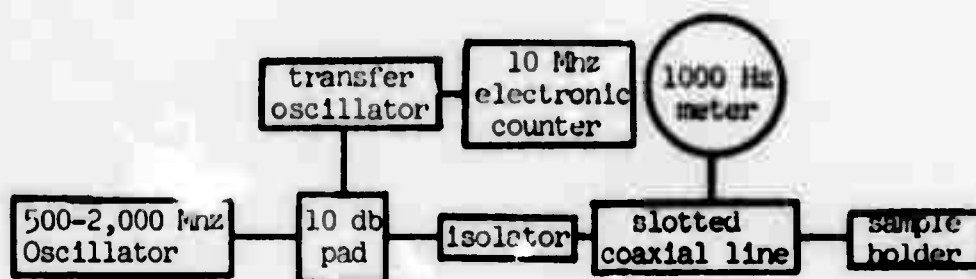
FIGURE 6. Equipment setup for measuring dielectric constant and loss tangent in the range 500-2,000 Mhz.

were read, which had exactly twice the power detected as that at the minimum. The VSWR was then computed by the two-point formula

$$VSWR = \frac{\pi(\Delta X)}{\lambda} \qquad (19)$$

where ΔX is the distance between the twice power points and λ is the wavelength in the slotted line. In this frequency range, the two-point method is valid for VSWR's greater than ten, but a correction can be applied for smaller values [22]. The null shift or difference in null position, for the sample in and out of the circuit, was measured near the center of the slotted line. These three pieces of data, null shift, wavelength (from frequency), and VSWR, were read for each frequency of interest in the range 500-2,000 Mhz. The data was treated according to the program SLOT given in Appendix II. This technique was not used above 3,000 Mhz be ause the sample arrangement could ther. no longer be considered to be a lumped capacitance [23]. This capacitance technique was used successfully by Daly, et al [24] up through che frequency 2,500 Mhz, but they suggest 3,000 Mhz as the upper limit for obtaining useful data by this method.

12,000 Mhz-18,000 Mhz

For this frequency range, a K_u-band slotted waveguide, terminated with the sample and a variable short circuit was used. The rectangular sample, slightly smaller than waveguide dimensions (0.622" x 0.311"), was placed just inside the variable waveguide short. A tightly fitting styrofoam spacer held the sample erect in the guide. The sample thickness was approximately 0.22". The setup used is shown in Figure 7.
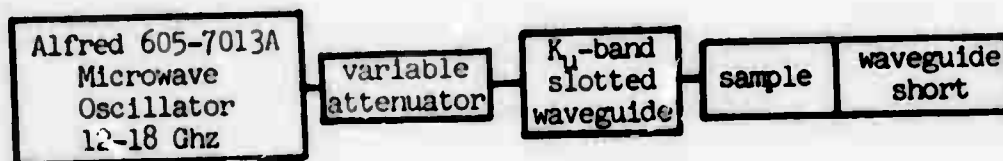
FIGURE 7. Equipment setup for measuring dielectric constant and loss tangent in the range 12,000–18,000 Mhz.

A variable attenuator was used to decrease the reflected signal from the short, a K_u-band isolator not being available at the time of testing. A vernier scale allowed readings to 0.1 mm, but table and waveguide vibration caused by the oscillator fan, caused the probe position to move slightly, resulting in an accuracy of about 0.5 mm.

Measurements taken for this method were wavelength, position of the voltage minimum, and VSWR. The two point method was again used to obtain the VSWR, readings being taken near the center of the waveguide to avoid end effects. A broadband probe was used to detect the signal. The voltage minimum of the VSWR pattern was made to appear on the lowest scale of the 1000 Hz meter by shortening the probe depth. Before any measurements were taken for glass samples, a number of teflon strips were used as a sample. These strips were slightly smaller than the waveguide dimensions and were pressed together by the strofoam spacer. Measured values of the teflon's dielectric constant averaged within 6% of known values.

The method used for this frequency range is derived in complete form by Roberts [25] and by Von Hippel [22]. It involves equating the wave impedance of the air-filled waveguide with that of the sample filled section of waveguide, at the air-sample interface. By using charts [22] which gave solutions to the resulting complex transcendental equations, the propagation constant in the sample was calculated. This then led to the complex permittivity of the sample,

$$\epsilon^* = \frac{(\frac{1}{\lambda_c})^2 - (\frac{\gamma_2}{2\pi})^2}{(\frac{1}{\lambda_c})^2 + (\frac{1}{\lambda})^2} \tag{20}$$

where λ_c is the cut-off wavelength and equals twice the width of the waveguide. The dielectric constant and loss tangent are then given by

$$\epsilon' = Re[\epsilon^*] \tag{21}$$

$$\tan \delta = \frac{Im[\epsilon^*]}{Re[\epsilon^*]} \tag{22}$$

The computer program HIPELKU given in Appendix III uses Von Hippel's equations to determine the wave impedance at the air-sample interface. This value was used with the available charts [22] and allowed the determination of γ_2, the propagation constant in the sample, and the complex permittivity, in the computer program FINALKU of Appendix III.

CHAPTER III

RESULTS

As described in Chapter II, dielectric constant and loss tangent
data were taken in three frequency bands, 100-500 Mhz, 500-2,000 Mhz,
and 12,000-18,000 Mhz. The data thus obtained for dielectric constant
is combined together on one continuous graph as a function of frequency
in Figure 8. Figure 9 shows the combined data for loss tangent versus
frequency. The average values of data for the entire frequency range,
100 Mhz-18,000 Mhz, are indicated in these figures by a dashed line for
each composition.

The variation of dielectric constant with composition of the
material is more clearly indicated in Figure 10. This figure shows the
average value of dielectric constant taken over the entire frequency
range, plotted against the five compositions of As_2Te_3-As_2Se_3 glass. By
increasing the tellurium content of the glass, it was found that the
dielectric constant can be varied from approximately 7.0 to 10.0, for
the compositions studied. The values for dielectric constant found here
compare favorably with data recently given for As_2Se_3 by Taylor, et al
[26], by Crevecoeur, et al [27], and by Lakatos, et al [28], who give a
microwave dielectric constant ranging between 9.0 and 9.7 for this
material.

Figure 11 shows the average value of loss tangent over the entire
frequency range, plotted against the five compositions of As_2Te_3-As_2Se_3

19
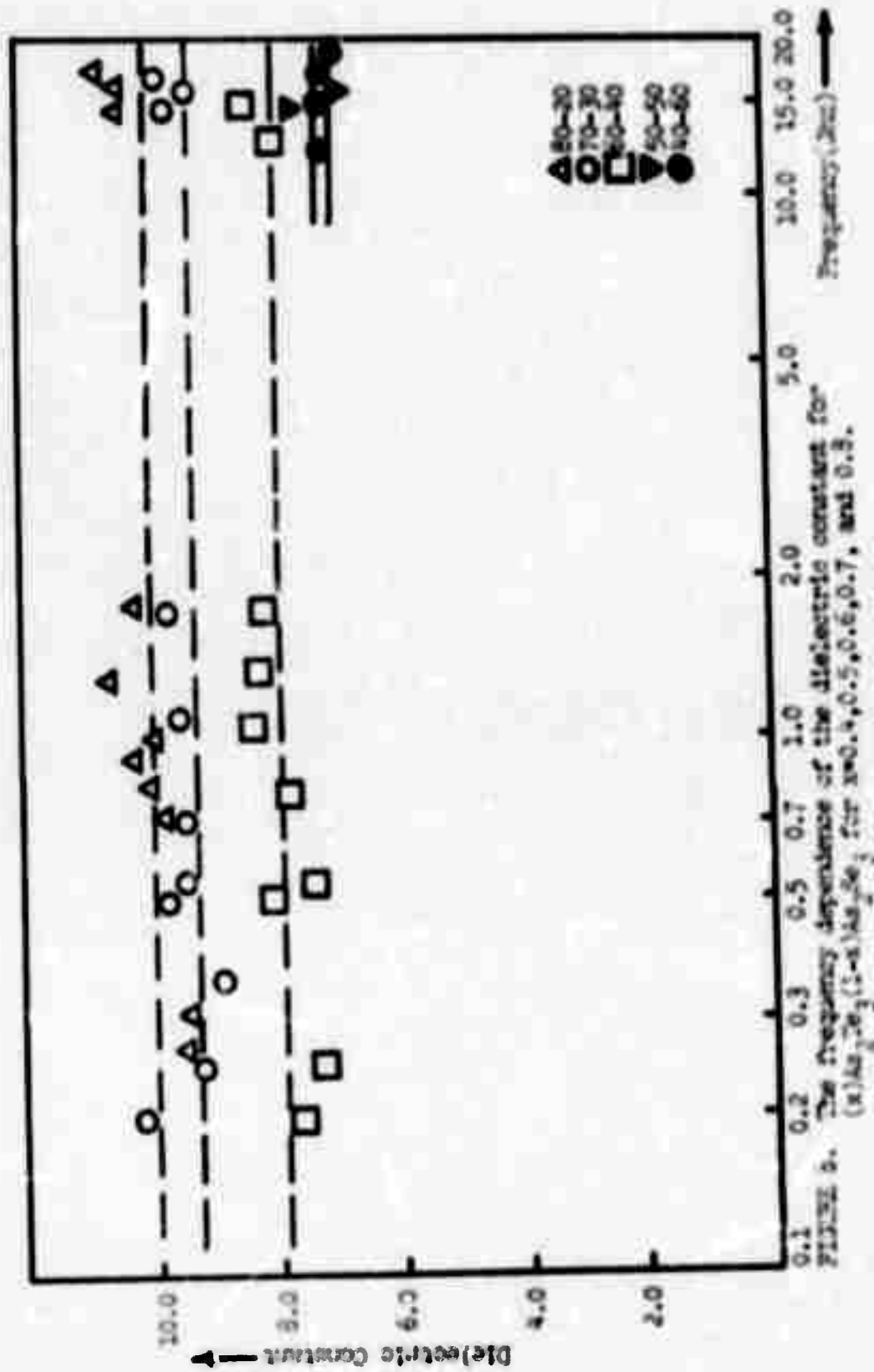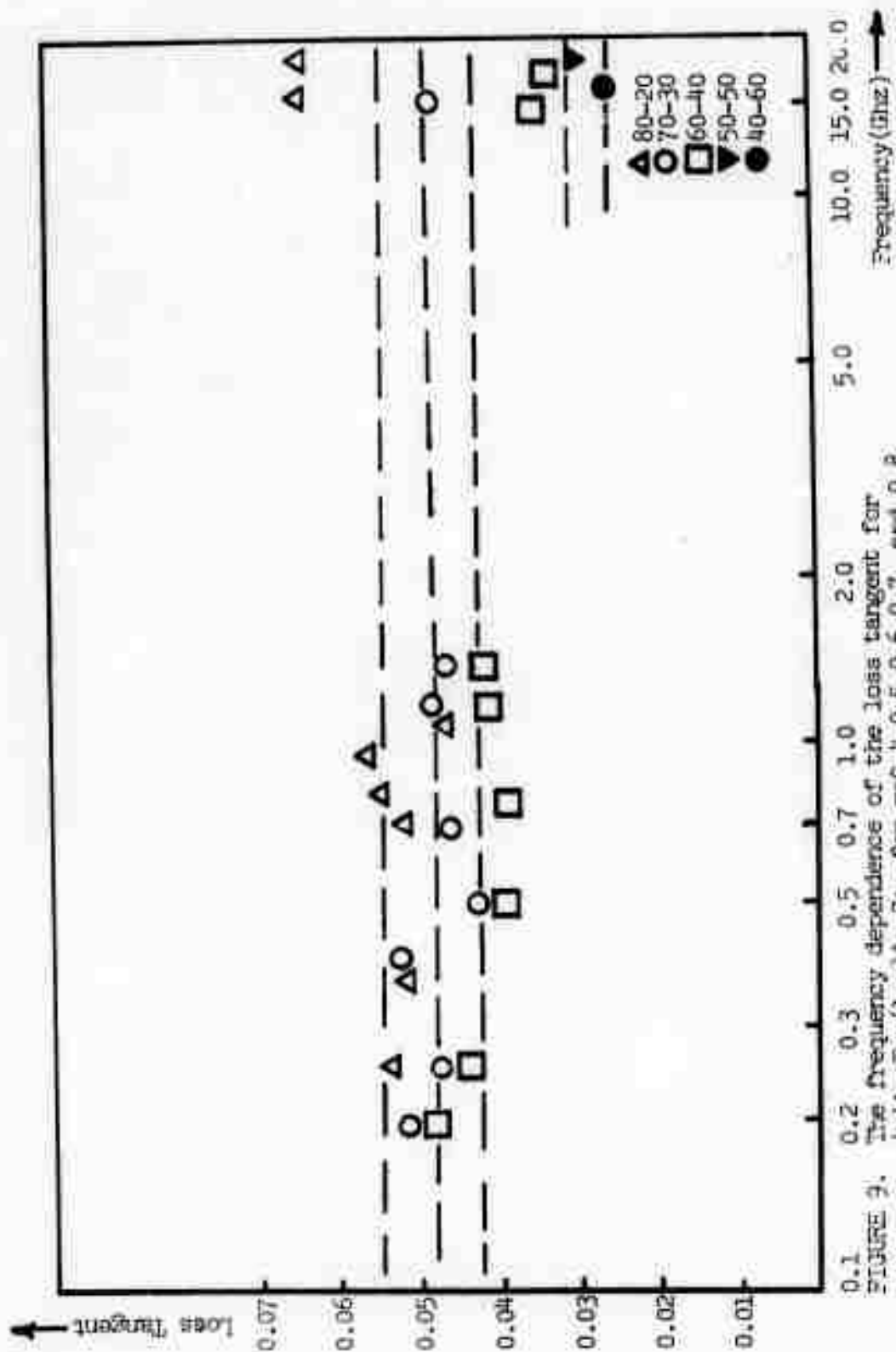
FIGURE 3. The frequency dependence of the dielectric constant for $x=0.4, 0.5, 0.6, 0.7,$ and 0.8.

Dielectric Constant

Frequency (Hz)

FIGURE 9. The frequency dependence of the loss tangent for $(x)As_2Te_3(1-x)As_2Se_3$ for $x=0.4, 0.5, 0.6, 0.7$, and 0.8.
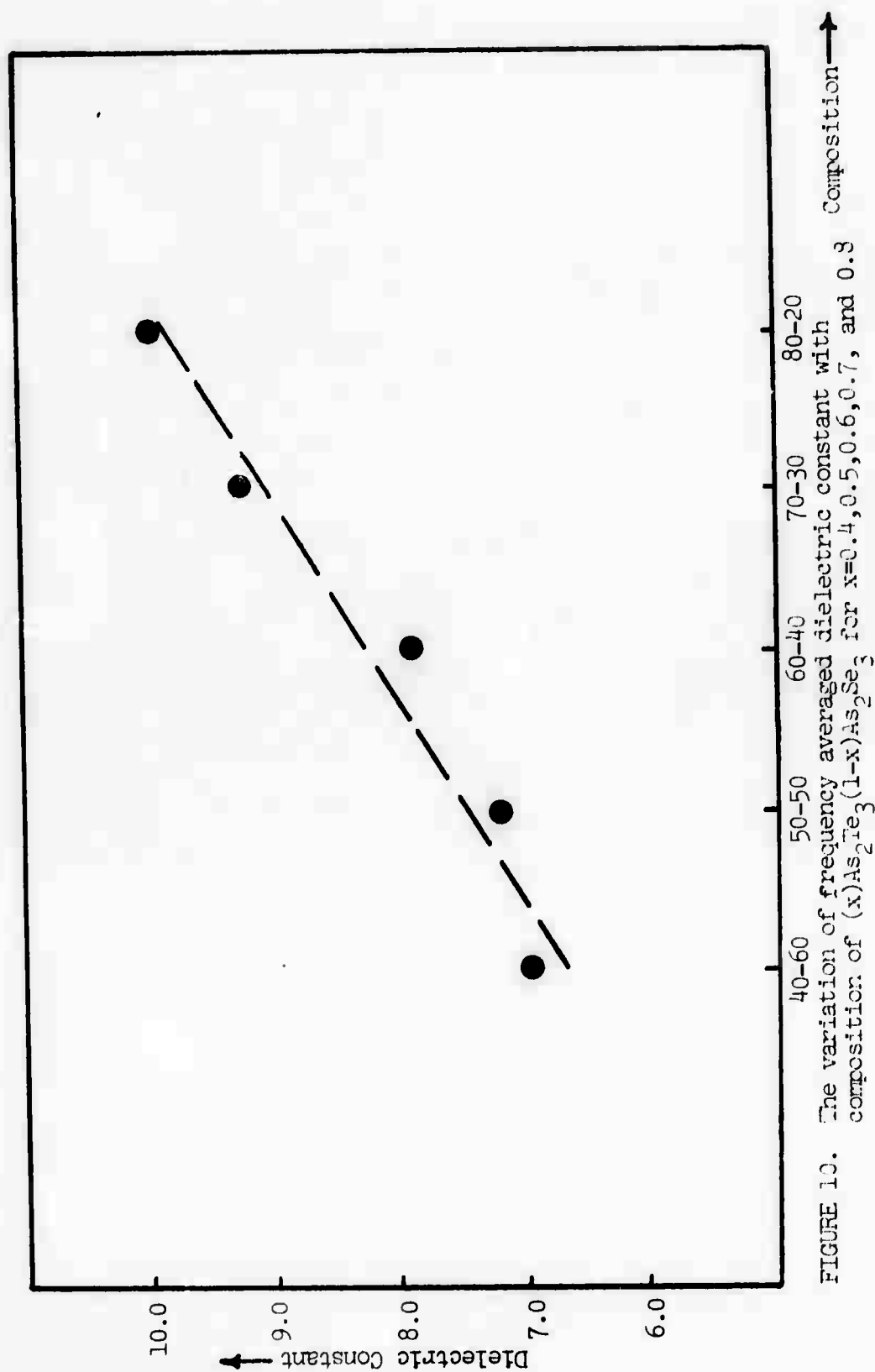
FIGURE 10. The variation of frequency averaged dielectric constant with composition of $(x)As_2Te_3(1-x)As_2Se_3$ for $x=0.4,0.5,0.6,0.7$, and 0.8

FIGURE 11. The variation of frequency averaged loss tangent with composition of $(x)As_2Te_3(1-x)As_2Se_3$ for $x=0.4,0.5,0.6,0.7,$ and 0.8 composition.

231

23

glass. The loss tangent was found to also increase with increasing tellurium content, and varied between approximately 0.02 and 0.06. Crevecoeur and de Wit [27] have presented the loss tangent of As_2Se_3 glass over 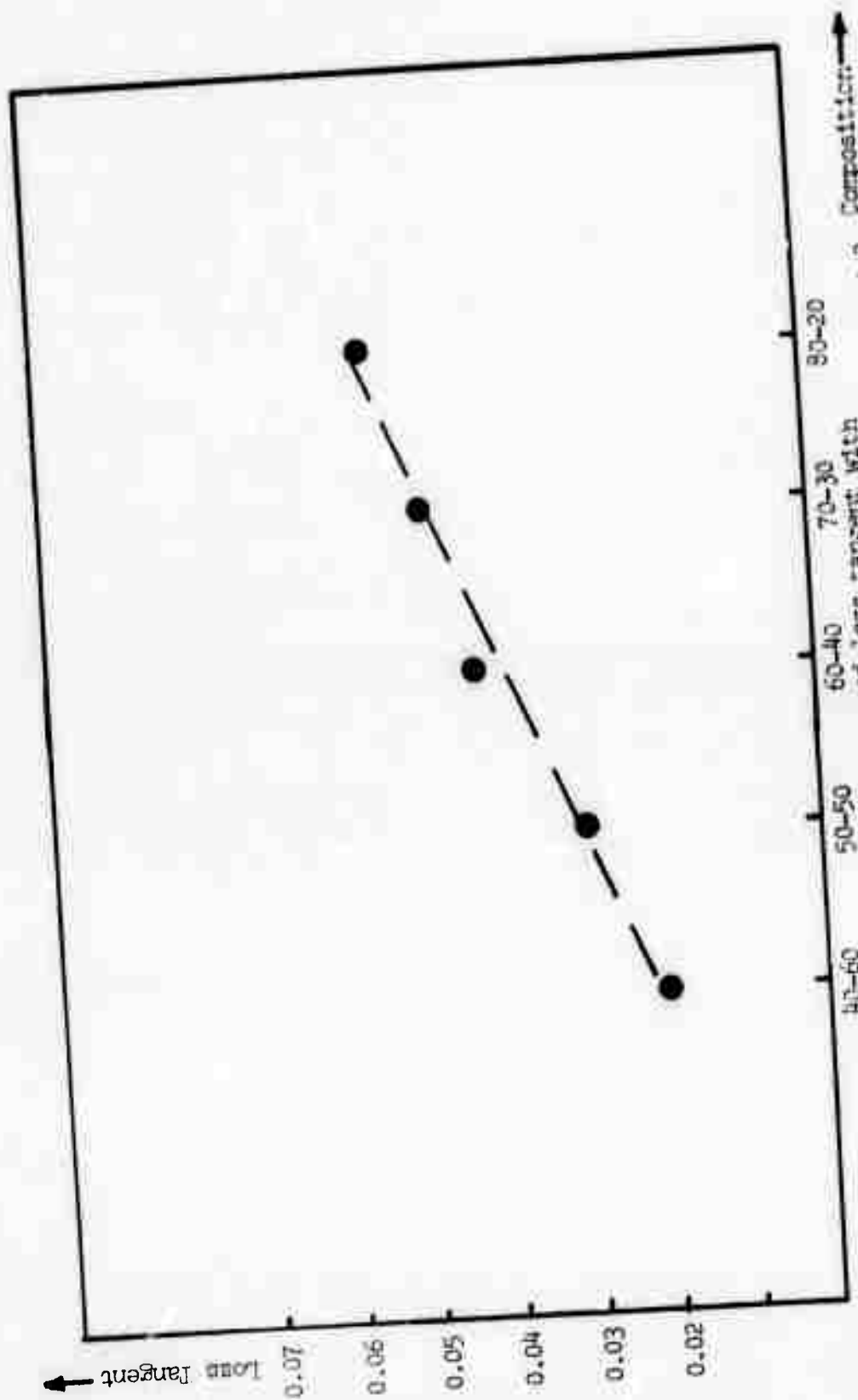the frequency range 10^2 to 10^{10} Hz. In the U.H.F. and microwave regions, they give an average loss tangent of 10^{-4}. However other investigators [29,30] give loss tangents for this material averaging between 10^{-2} and 10^{-3}. These values may be considered as a low limit to the data for loss tangent given in the present study, since they represent glass having no tellurium content.

The dielectric constants and loss tangents of the samples were found to be essentially frequency independent over the frequency range studied. Slight variations can be attributed to certain measurement errors and to differences of method and equipment used in the three frequency ranges. Measurement errors included errors in slotted line null readings caused by oscillator and waveguide vibration produced by the oscillator fan, errors in VSWR measurements, and slight errors in sample height and position. These led to a statistical error of about $\pm$ ten percent.

232

CHAPTER IV

CONCLUSION

This paper has presented the U.H.F. and microwave dielectric properties of the glass system $(x)As_2Te_3(1-x)As_2Se_3$ for $x=0.4, 0.5, 0.6,$ 0.7, and 0.8. Future research performed on this glass should include the determination of the behavior of the dielectric properties as a function of temperature, and under switching conditions. This could help to clarify our understanding of the basis of the switching mechanism in amorphous thin films.

A possible use for the glass system is an a dielectric substrate material for microstrip transmission lines. Within a given range, one may choose the composition of the glass for specified dielectric properties, since the dielectric constant can be varied from 7.0 to 10.0, and the loss tangent and from 0.02 to 0.06. The loss can be reduced further by reducing the tellurium content while still retaining the amorphous properties. Commonly used microwave substrates with dielectric properties in this region are Silicon (ϵ = 11.5, tan δ = 0.15), Yttrium Iron Garnet (YIG), and AlSiMag [30]. The glass system presently studied has several properties which are desirable in choosing a substrate material [31]. These include a fairly high dielectric constant, high resistivity [11], essentially constant permittivity over the U.H.F. and microwave regions, and a good surface smoothness with no surface ripples comparable to the size of the thin-film components. The

glass also exhibits a high dielectric strength, dependent on the magnitude of the threshold voltage required for switching.

APPENDIX I

COMP

Line

```
1       WRITE(6,200)
2     5 READ(5,100)G,B,FREQ,DIA,T
3       G=0.001*G
4       B=0.001*B
5       C=B/(6.2832*FREQ)
6       A=0.7854*((DIA)**2)
7       CAIR=(0.0254*A)/(113.0973*T)
8       EP=C/CAIR
9       TNDLT=G/B
10      WRITE (6,300)FREQ
11      WRITE(6,400)EP,TNDLT
12 100 FORMAT(9G)
13 200 FORMAT('G(MMHO),B(MMHO),FREQ(GHZ),DIA(IN),TH(IN)')
14 300 FORMAT('FREQ='F7.3,1X'GHZ')
15 400 FORMAT('EP='F10.5,5X'LOSS TANGENT='F10.5/)
16      END
```

The program COMP uses the admittance data from the Thurston Bridge to calculate the relative dielectric constant and loss tangent of the sample in the frequency range 100-500 Mhz. Values of G and B are entered in millimhos, the frequency in Gigahertz, and the sample dimensions in inches.

In deriving the equations for permittivity shown in the program, Equation (9) is first rewritten as

$$\varepsilon' = \frac{\frac{B}{\omega}}{\varepsilon_0 \frac{A}{T}} \tag{23}$$

This is seen to be the ratio of the capacitance measured with the sample in, to the capacitance calculated for the sample out (free space

dielectric), when the thickness T is equal in each case. The numerator of Equation (23) is shown on line 5 of the program. The denominator is multiplied by 0.0254 to change inches to meters. ϵ_o is normalized and is written as $\frac{1}{36\pi} = \frac{1}{113.0973}$. The factor 10^9 is dropped from ϵ_o and is also dropped from the frequency, which is expressed in Gigahertz. This eliminates very small numbers from computer program calculations. Note that the 10^9 factors would have cancelled in Equation (23) even if they were not dropped. The resulting equations used to calculate dielectric constant and loss tangent are shown on lines 7 and 8 of the program.

APPENDIX II

SLOT

Line

```
1       COMPLEX CJ,YL
2       WRITE(6,200)
3       READ(5,100)DIA,T
4       WRITE(6,300)
5       READ(5,100)FREQ,X1,X2,B0,B1
6       ELMG=30./FREQ
7       VSWR=ELMG/(3.1416*(X2-X1))
8       YIN=VSWR
9       BETA=6.2832/ELMG
10      ELL=(B0-B1)
11      A=BETA*ELL
12      C=SIN(A)
13      D=COS(A)
14      CJ=CMPLX(0.,C)
15      YL=0.02*(YIN*D-CJ)/(D-YIN*CJ)
16      G=REAL(YL)
17      B=AIMAG(YL)
18      C=B/(6.2832*FREQ)
19      A=0.7854**((DIA)**2)
20      CAIR=(0.0254*A)/(113.0973*T)
21      EP=C/CAIR
22      TNDLT=G/B
23      WRITE(6,400)EP,TNDLT
24 100  FORMAT(9G)
25 200  FORMAT('DIA(IN),T(IN)')
26 300  FORMAT('FREQ(GHZ),X1,X2,B0,B1(ALL IN CM)')
27 400  FORMAT('EP='F10.5,5X'LOSS TANGENT='F10.5/)
28      END
```

The program SLOT uses the data from slotted line measurements
and sample dimensions to calculate the relative dielectric constant and
loss tangent of the sample in the frequency range 500-2,000 Mhz. The
VSWR was obtained by the two-point method (line 7 of program) wherein
the position of the voltage minimum, B1, and its twice power points on

either side, X1 and X2, were observed. B0 is the position of the voltage minimum with the sample removed and the line short circuited, and (B0-B1) is the "null shift." Values of slotted line data were entered in centimeters, with the frequency entered in gagahertz and sample dimensions in inches.

The value $\overline{Y}_{in}$ of line 15 is the input admittance at the position of a voltage minimum. This value is therefore real and maximum and can be written $\overline{Y}_{in} = \overline{G}_{max}$. For the position of a null, Equation (16) for reflection coefficient can be rewritten

$$\Gamma = \frac{1 - \overline{G}_{max}}{1 + \overline{G}_{max}} \tag{24}$$

By definition the voltage standing wave ratio is

$$S = \frac{|V^+| + |V^-|}{|V^+| - |V^-|} = \frac{1 + |(V^-/V^+)|}{1 - |(V^-/V^+)|} = \frac{1 + |\Gamma|}{1 - |\Gamma|} \tag{25}$$

Substituting (24) into (25),

$$S = \frac{1 + \overline{G}_{max} + |1 - \overline{G}_{max}|}{1 + \overline{G}_{max} - |1 - \overline{G}_{max}|} \tag{26}$$

Since $\overline{G}_{max}$ is greater than 1, then $|1 - \overline{G}_{max}| = \overline{G}_{max} - 1$. Then (26) may be rewritten

$$S = \overline{G}_{max} \tag{27}$$

which states that the VSWR equals the magnitude of the normalized input conductance (or admittance) at a null. This result is shown on line 8 of the program.

The load admittance is calculated on line 15 and is denormalized by multiplying by 0.02 mho. Lines 16-22 of the program, which calculate

the relative dielectric constant and loss tangent of the sample in a capacitor arrangement, are identical in form and method to those given in Appendix I in the program COMP.

APPENDIX III

HIPELKU AND FINALKU

Hipelku

Line

```
1        COMPLEX B1,CEJZ,ELMG1
2        READ(5,100)D1
3        D=2.54*D1
4        READ(5,100)X1,X2,X11,X22
5        AL2=(X11+X22)/2.
6        AL1=(X1+X2)/2.
7        ELMG=2.*(AL1-AL2)
8        X0=AL2+0.56-D
9        VSWR=ELMG/(3.]4]6*(((X1-X2)+(X11-X22))/2.))
10       RECIP=1./VSWR
11       A=6.2832*X0/ELMG
12       B=SIN(A)/COS(A)
13       B1=CMPLX(0.,B)
14       ELMG1=CMPLX(0.,ELMG)
15       CEJZ=(-ELMG1/(6.2832*D))*(RECIP-B1)/(1.-(RECIP*B1))
16       C=CABS(CEJZ)
17       RECPC=1./C
18       F=REAL(CEJZ)
19       G=AIMAG(CEJZ)
20       ZRA=ATAN2(G,F)
21       Z=ZRA*180./3.1416
22       WRITE(6,200)C,Z,RECPC
23 100   FORMAT(9G)
24 200   FORMAT('C='F9.4,5X'Z(DEGREES)='F12.3,5X'ONE OVER C='F9.4/)
25       END
```

The program HIPELKU uses the experimental data for the frequency range 12,000-18,000 MHz, with line 15 of the program, to calculate the parameters C and Z of the complex number Ce^{jZ}. The sample thickness D1 is entered in inches, while the slotted waveguide readings are entered in centimeters. The readings X1 and X2 are twice power points on either side of the null AL1, the same being true for X11, X22, and AL2. In line 8 the position of the voltage null (X0) with respect to the sample

face is calculated. The quantity (0.56-D) centimeter is added to this line because the shorting plunger was fixed at a position 0.56 centimeter inside the mouth of the waveguide short, and the sample, of thickness D, was placed in this space. The VSWR was calculated by the two-point method as shown on line 9.

The values C and Z, calculated on lines 16 and 21, are entered into tables which allow one to read T and τ, the parameters of the complex number $Te^{j\tau}$. T and τ are then entered in the program FINALKU shown below, which calculates the dielectric constant and loss tangent.

Finalku

Line

```
1       COMPLEX TAURC,GAM2,EPSLN
2       READ(5,100)H,D
3       READ(5,100)AL1,AL2,T,TAU
4       TAUR=TAU*3.14159/180.
5       TAURC=CMPLX(0.,TAUR)
6       DCM=2.54*D
7       GAM2=(T*CEXP(TAURC))/DCM
8       A=0.622
9       B=0.311
10      ACM=2.54*A
11      FLIP=1./(4.*ACM*ACM)
12      ELMG=2.*(AL1-AL2)
13      EPSLN=(FLIP-(GAM2/6.2832)**2)/(FLIP+(1./ELMG)**2)
14      EMP=REAL(EPSLN)
15      EMPP=AIMAG(EPSLN)
16      TNDLM=EMPP/EMP
17      ECP=EMP*B/(B-((B-H)*EMP))
18      TNDLC=TNDLM*B/(B-((B-H)*EMP))
19      WRITE(6,200)ECP,TNDLC
20      WRITE(6,300)EMP,TNDLM
21 100  FORMAT(9G)
22 200  FORMAT('DIELECTRIC CONSTANT(CORR)='F11.7,5X,'LOSS TANG(CORR)='
        F11.7/)
23 300  FORMAT('DIELECTRIC CONSTANT(MEAS)='F11.7,5X,'LOSS TANG(MEAS)='
        F11.7/)
24      END
```

The input data for this program include sample height and thickness, H and D, which are entered in inches, slotted line measurements in centimeters, are values for T and ι obtained from charts and the program HIPHLKU. The dielectric constant and loss tangent are calculated using equations (20) through (22), in lines 13-16 of FINALKU. These values are then corrected by using formulas given by Ward and Rapaport [33] which correct ε' and tan δ for the air gap between the sample and the broadwall of the waveguide. The corrected values for dielectric constant and loss tangent are calculated on lines 17 and 18.

LIST OF REFERENCES

1. E. A. Davis, Endeavour 30, 55 (1971).

2. M. H. Cohen, Physics Today 24, 26 (1971).

3. S. R. Ovshinsky, Physical Review Letters 21, 1450 (1968).

4. A. D. Pearson, W. R. Northover, J. F. Dewald, and W. F. Peck, Advances in Glass Technology. New York: Plenum Press, 1962.

5. H. K. Henisch, Scientific American 221, 30 (1969).

6. D. L. Eaton, Journal of The American Ceramic Society 47, 554 (1964).

7. B. T. Kolomiets and E. A. Lebedev, Radiotechnika i Electronika 8, 2097 (1963).

8. "Glassy Semiconductors Show Switching and Memory Effects," Physics Today 22, 63 (1969).

9. Journal of Non-Crystalline Solids 4, 1 (1970).

10. N. J. Kreidl, The Glass Industry 51, 264 (1970).

11. National Materials Advisory Board, Fundamentals of Amorphous Semiconductors. Washington, D. C.: National Academy of Sciences, 1971.

12. M. Roilos, Journal of Non-Crystalline Solids 6, 5 (1971).

13. Proceedings of the 4th International Amorphous Semiconductor Conference, Ann Arbor, Michigan, August 1971. To be published in Journal of Non-Crystalline Solids.

14. N. J. Kreidl, The Glass Industry 52, 396 (1971).

15. A. C. Warren, Journal of Non-Crystalline Solids 4, 613 (1970).

16. H. R. Sanders, D. L. Kinser, and L. K. Wilson, "Low-Field Switching and Memory Phenomena in an Amorphous Semiconductor," in Proceedings of the 9th Annual (1971) IEEE Region III Convention. Charlottesville, Virginia: Central Virginia Section, Institute of Electrical and Electronics Engineers, 1971.

17. D. L. Kinser, L. K. Wilson, H. R. Sanders, and D. J. Hill, "Electrical, Thermal, and Structural Properties of As_2Te_3-As_2Se_3 Glasses." To be published in Journal of Non-Crystalline Solids.

18. D. J. Hill, "Structural and Electrical Properties of As_2Se_3-As_2Te_3 Glass System." M. S. Thesis, Vanderbilt University, Nashville, Tennessee, 1972.

19. J. D. Pearson, G. T. O'Reilly, and L. K. Wilson, "U.H.F. and Microwave Dielectric Properties of an Amorphous Semi-Conductor," in Southeastcon 1972 Proceedings of the 10th Annual IEEE Region 3 Convention. Knoxville, Tennessee: Institute of Electrical and Electronics Engineers.

20. R. F. Harrington, Time-Harmonic Electromagnetic Fields. New York: McGraw-Hill, 1961.

21. R. E. Collin, Foundations for Microwave Engineering. New York: McGraw-Hill, 1966.

22. A. R. Von Hippel, Dielectric Materials and Applications. New York: Technology Press of M.I.T., 1954.

23. H. E. Bussey, Proceedings of the IEEE 55, 1046 (1967).

24. D. A. Daly, S. P. Knight, M. Caulton, and R. Ekholdt, IEEE Transactions on Microwave Theory and Techniques MTT-15, 713 (1967).

25. S. Roberts and A. R. Von Hippel, Journal of Applied Physics 17, 610 (1946).

26. P. C. Taylor, S. G. Bishop, and D. L. Mitchell, Solid State Communications 8, 1783 (1970).

27. C. Crevecoeur and H. J. de Wit, Solid State Communications 9, 445 (1971).

28. A. I. Lakatos and M. Abkowitz, Physical Review B 3, 1791 (1971).

29. M. Kitao, F. Araki, and S. Yamadi, Physica Status Solidi 37, 119 (1970).

30. Sperry Rand, Summary of Microwave Integrated Circuit Investigations. Clearwater, Florida: Sperry Microwave Electronics Division, 1968.

31. F. Z. Keister, IEEE Transactions on Microwave Theory and Techniques MTT-16, 469 (1968).